COMPARATIVE STUDY OF HYBRID SUPPORT VECTOR REGRESSION DROUGHT FORECASTING MODELS FOR LANGAT RIVER BASIN

By

FUNG KIT FAI

A dissertation submitted to the Department of Civil Engineering,
Lee Kong Chian Faculty of Engineering and Science,
Universiti Tunku Abdul Rahman,
in partial fulfillment of the requirements for the degree of
Master of Engineering Science
September 2018

ABSTRACT

COMPARATIVE STUDY OF HYBRID SUPPORT VECTOR REGRESSION DROUGHT FORECASTING MODELS FOR LANGAT RIVER BASIN

Fung Kit Fai

Drought is one of the most harmful but least understood natural hazard and thus, accurate forecasting is essential for drought risk management. Although Malaysia is located in the heavy rainfall region, droughts happened in 1991 (Malacca), 1998 (Klang Valley) and 2014 (Selangor) showed that Malaysia is also vulnerable to drought occurrences. This study aimed to develop hybrid support vector regression drought forecasting models with the Standardized Precipitation Evapotranspiration Index (SPEI) of different time scales and lead times as the drought barometer, for the Langat River Basin, Malaysia. Multi-Input Wavelet Fuzzy Support Vector Regression (M-W-FSVR), Weighted Wavelet Fuzzy Support Vector Regression (W-W-FSVR) and Wavelet Boosting Support Vector Regression (W-BS-SVR) models were developed to predict the SPEI-1, SPEI-3 and SPEI-6 on 1-month, 3-month and 6-month lead times. The homogeneity of rainfall data for years 1976 – 2015 were tested before combining with temperature data to develop the SPEI series, with the sensitivity of series being described using the Average Moving Range. The SPEIs were de-

noised through wavelet transformation, with decompositions executed up to the maximum level. The W-BS-SVR models were developed by boosting the wavelet transformed SPEIs, then trained using SVR with data partitioned into 90% and 10% for training and validation respectively. For the M-W-FSVR and W-W-FSVR models, fuzzy membership values for each wavelet transformed SPEIs were estimated and used as additional input or weightage to reduce outlier effects during the training of SVR. Models' performance were evaluated using Mean Absolute Error (MAE), Root Mean Square Error (RMSE) and Bias. For 1-month lead time, the results showed that the M-W-FSVR and W-W-FSVR models performed the best for cases of SPEI-1 and SPEI-3 through their ability in reducing outlier effects but however the W-BS-SVR model was the better for the SPEI-6 case. For 3-month and 6-month lead times, the performance of the models deteriorated due to the increase in training difficulties. With the increases in training difficulties, the W-BS-SVR model created more ensembles and increased the complexity of the regression, causing it deteriorated most among the three models. On the other hand, the deterioration in fuzzy-based models are less due to the outliers reducing effect algorithm itself that does not further burden the training process even when the training process became more difficult, with the W-W-FSVR model deteriorated least, performing the best for most of the cases. The major challenge of this study is the way to improve prediction accuracy SVR models against the effects from changing SPEI time scales and prediction lead time. This study proved that fuzzy-based models are effective in improving the prediction accuracy when the variations in SPEI and prediction lead time increases.

ACKNOWLEDGEMENTS

First of all, I would like to express my sincere appreciation to my supervisor, Ir. Dr. Huang Yuk Feng for his precious advices, guidance and help throughout this study. He always motivates me and give me suggestions when I faced problems during the study. Besides, I would like to thank my co-supervisor, Ir. Dr. Koo Chai Hoon, who has always helped me with throughout my studies. Patience, suggestions and reminders given by her are important for me to finish my study. In addition, I would like to thank Dr. Ling Lloyd for his comments to help me understand and solve the statistical problems in my study.

This research was funded by UTAR Research Fund and thus, I would also like to express my appreciation to UTAR for the financial support for making this research study a success.

Finally, I would like to thank my family and friends for their permanent support and encouragement during my master study.

APPROVAL SHEET

This dissertation entitled "**COMPARATIVE STUDY OF HYBRID SUPPORT VECTOR REGRESSION DROUGHT FORECASTING MODELS FOR LANGAT RIVER BASIN"** was prepared by FUNG KIT FAI and submitted as partial fulfillment of the requirements for the degree of Master of Engineering Science at Universiti Tunku Abdul Rahman.

Approved by:

_____
(Ir Dr Huang Yuk Feng)
Date:……..
Supervisor
Department of Civil Engineering
Lee Kong Chian Faculty of Engineering Science
Universiti Tunku Abdul Rahman

_____
(Ir Dr Koo Chai Hoon)
Date:……..
Co-supervisor
Department of Civil Engineering
Lee Kong Chian Faculty of Engineering Science
Universiti Tunku Abdul Rahman

LEE KONG CHIAN FACULTY OF ENGINEERING AND SCIENCE

UNIVERSITI TUNKU ABDUL RAHMAN

Date: _____

SUBMISSION OF DISSERTATION

It is hereby certified that ***__Fung Kit Fai__*** (ID No: ***16UEM06209***) has completed this dissertation entitled "*COMPARATIVE STUDY OF HYBRID SUPPORT VECTOR REGRESSION DROUGHT FORECASTING MODELS FOR LANGAT RIVER BASIN*" under the supervision of Ir Dr Huang Yuk Feng (Supervisor) from the Department of Civil Engineering, Lee Kong Chian Faculty of Engineering and Science, and Ir Dr Koo Chai Hoon (Co-Supervisor) from the Department of Civil Engineering, Lee Kong Chian Faculty of Engineering and Science.

I understand that University will upload softcopy of my dissertation in pdf format into UTAR Institutional Repository, which may be made accessible to UTAR community and public.

Yours truly,

_____

(*Fung Kit Fai)*

DECLARATION

I FUNG KIT FAI hereby declare that the dissertation is based on my original work except for quotations and citations which have been duly acknowledged. I also declare that it has not been previously or concurrently submitted for any other degree at UTAR or other institutions.

_____

(FUNG KIT FAI)

Date _____

TABLE OF CONTENTS

		Page
ABSTRACT		**ii**
ACKNOWLEDGEMENTS		**iv**
APPROVAL SHEET		**v**
SUBMISSION SHEET		**vi**
DECLARATION		**vii**
TABLE OF CONTENTS		**viii**
LIST OF TABLES		**xi**
LIST OF FIGURES		**xiii**
LIST OF ABBREVATIONS		**xiv**

CHAPTER

1.0	INTRODUCTION		1
	1.1	Background	1
	1.2	Problem Statement	4
	1.3	Aim and Objectives	7
	1.4	Significance of Study	7
	1.5	Scope of Work	9
2.0	LITERATURE REVIEW		10
	2.1	Drought Indices (DI)	10
		2.1.1 Percent of Normal (PN)	10
		2.1.2 Palmer Drought Severity Index (PDSI)	12
		2.1.3 Crop Moisture Index (CMI)	13
		2.1.4 Effective Drought Index (EDI)	14
		2.1.5 Standardized Precipitation Index (SPI)	15
		2.1.6 Standardized Precipitation Evapotranspiration Index (SPEI)	17
	2.2	Drought Forecasting Models	19
		2.2.1 Time Series Analysis – Autoregressive Integrated Moving Average (ARIMA) and Seasonal Autoregressive Integrated Moving Average (SARIMA)	19
		2.2.2 Probability Model – Markov Chain (MC)	25
		2.2.3 Artificial Intelligence Based Models	30
		2.2.3.1 Artificial Neural Network (ANN)	30
		2.2.3.2 Fuzzy Logic (FL)	36
		2.2.3.3 Support Vector Regression (SVR)	40
	2.3	Wavelet Transformation	45
	2.4	Boosting Technique	47
	2.5	Hybrid Models	49
	2.6	Summary	55

3.0 METHODOLOGY 58
3.1 Workflow/Flowchart 58
3.2 Location of Study, Data Acquisition and Data Repairing 61
3.3 Test of Homogeneity 64
3.3.1 Standard Normal Homogeneity Test (SNHT) 65
3.3.2 Buishand Range Test (BR) 65
3.3.3 Pettitt Test (PeT) 66
3.3.4 Von Neumann Ratio (VNR) Test 67
3.3.5 Assessment of Results 68
3.4 Development of the SPEI 69
3.5 Wavelet Transformation of the SPEIs 72
3.6 Multi-Input Wavelet Fuzzy Support Vector Regression (M-W-FSVR) and Weighted Fuzzy Support Vector Regression (W-W-FSVR) 73
3.7 Wavelet-Boosting-Support Vector Regression (W-BS-SVR) 75
3.8 Performance Measures 77
3.8.1 Mean Absolute Error (MAE) 77
3.8.2 Root Mean Square Error (RMSE) 78
3.8.3 Bias 79

4.0 RESULTS AND DISCUSSIONS 80
4.1 Data Acquisition, Data Repairing and Homogeneity Tests 80
4.2 Development of SPEI 81
4.3 Wavelet Transformation of SPEIs 84
4.4 Fuzzy Membership Values of Wavelet Transformed SPEIs 87
4.5 Boosting Ensemble 88
4.6 Support Vector Regression 91
4.7 Model Performance 93
4.7.1 Selection of Optimum Wavelet Decomposition Level 94
4.7.2 Model Selection 95
4.7.2.1 Model performance under different time scales of SPEI 98
4.7.2.2 Model performance under different lead times 100

5.0 CONCLUSIONS AND RECOMMENDATIONS 108
5.1 Conclusions 108
5.2 Recommendations 111

REFERENCES 113

APPENDICES 126
APPENDIX A1 126
APPENDIX A2 129
APPENDIX A3 132
APPENDIX A4 135

APPENDIX A5 138
APPENDIX A6 141
APPENDIX B1 144
APPENDIX B2 149
APPENDIX B3 154
APPENDIX B4 159
APPENDIX B5 164
APPENDIX B6 169
APPENDIX C 174
APPENDIX D 178
APPENDIX E 198

LIST OF TABLES

Table		Page
2.1	Categories of SPEI	18
3.1	Details of the selected stations	63
3.2	The 5% Critical Values for the homogeneity tests.	64
4.1	Number of missing data for station s2815001, s2917001 and s48648	80
4.2	Homogeneity Test Results for station s2815001 and s2917001	81
4.3	Maximum Decomposition Levels for each SPEIs	85
4.4	Average moving range values of original SPEIs and their wavelet transformed series	85
4.5	Optimum number of learning cycles for station s2815001	89
4.6	Optimum number of learning cycles for station s2917001	90
4.7	Training and Validation Periods	92
4.8	Estimated model's parameters for station s2815001	93
4.9	Estimated model's parameters for station s2917001	93
4.10	Results of performance measures (MAE, RMSE and Bias) for the training of models at station s2815001	96
4.11	Results of performance measures (MAE, RMSE and Bias) for the validation of models at station s2815001	96
4.12	Results of performance measures (MAE, RMSE and Bias) for the training of models at station s2917001	97
4.13	Results of performance measures (MAE, RMSE and Bias) for the validation of models at station s2917001	97
4.14	Deterioration of models at s2815001 (Training)	102

4.15	Deterioration of models at s2815001 (Validation)	103
4.16	Deterioration of models at s2917001 (Training)	103
4.17	Deterioration of models at s2917001 (Validation)	103
5.1	Identified best models	111

LIST OF FIGURES

Figures		Page
2.1	Multilayer Perceptron with One Hidden Layer (Jalalkamali et al. 2015)	31
2.2	Fuzzy Logic Concepts (Mathworks, 2016)	36
2.3	Main Stages in Fuzzy Modeling (Sicat et al., 2005)	38
3.1	Overall Workflow/Flowchart	60
3.2	Map of Langat River Basin with the locations of meteorological stations, dams and land use	62
3.3	Four Quadrant Method	63
4.1	Developed SPEI-1, SPEI-3 and SPEI-6 of station s2815001	83
4.2	Developed SPEI-1, SPEI-3 and SPEI-6 of station s2917001	83
4.3	Average moving range of original and wavelet transformed SPEIs with different decomposition levels for station s2815001	86
4.4	Average moving range of original and wavelet transformed SPEIs with different decomposition levels for station s2917001	86

LIST OF ABBREVATIONS

AIC	Akaike Information Criterion
ANFIS	Adaptive Neuro-Fuzzy Inference System
AR(1)	First Order Auto-regressive Multivariate Model
AR(2)	Second Order Auto-regressive Multivariate Model
ARID	Agricultural Reference Index for Drought
ARIMAX	Multivariate Autoregressive Integrated Moving Average
BIC	Bayesian information criterion
BP-ANN	Back Propagation Artificial Neural Network
DMSGRNN	Direct Multi-Step Generalized Regression Neural Network
DMSMLP	Direct Multi-Step Multi-Layer Perceptron
DMSNN	Direct Multistep Neural Network
DMSRBF	Direct Multi-Step Radial Basis Function
EDI	Effective Drought Index
ELM	Extreme Learning Machine
ENSO	El Niño Southern Oscillation
FFNN	Feed Forward Neural Networks
GLM	Generalized Linear Model
GMSS	Gandin-Murphy Skill Score
HMM	Hidden Markov Chain
HSNNDA	Hybrid Stochastic Neural Network of Direct Approach
HSNNRA	Hybrid Stochastic Neural Network of Recursive Approach
IIS-W-ANN	Iterative Input Selection Wavelet Artificial Neural Network
MAE	Mean Absolute Error
MARE	Mean Absolute Relative Error

MCFO	First Order Markov Chain
MCSO	Second Order Markov Chain
ME	Mean Error
MLM	Multiple Linear Model
MLP-ANN	Multilayer Perceptron Artificial Neural Network
MODIS	Moderate Resolution Imaging Spectroradiometer
MSE	Mean Square Error
NADI	Nonlinear Aggregated Drought Index
NAO	North Atlantic Oscillation
NCEP	National Centers for Environmental Prediction
NDVI	Normalized Difference Vegetation Index
NSE	Nash–Sutcliffe Efficiency Coefficient
PDSI	Palmer Drought Severity Index
PI	Persistency Index
R	Coefficient of Correlation
R^2	Coefficient of Determination
R^2_{McF}	McFadden Pseudo- Coefficient of Determination
RCP	Representative Concentration Pathway
RMSD	Root Mean Square Difference
RMSE	Root Mean Square Error
RMSGRNN	Recursive Multi-Step Generalized Regression Neural Network
RMSMLP	Recursive Multi-Step Multi-Layer Perceptron
RMSNN	Recursive Multistep Neural Network
RMSRBF	Recursive Multi-Step Radial Basis Function
ROC	Receiver Operating Characteristic

RPS	Ranked Probability Score
RRMSD	Relative Root Mean Square Prediction
SARIMA	Seasonal ARIMA
SBC	Schwarz Bayesian Criterion
SD	Standard Deviation
SDI	Streamflow Drought Index
SHI	Standardized Hydrological Index
SLP	Sea Level Pressure
SPI	Standardised Precipitation Index
SOI	Southern Oscillation Index
SST	Sea Surface Temperature
SSTA	Sea Surface Temperature Anomalies
TLRN	Time Lagged Recurrent Network
VTCI	Vegetation Temperature Condition Index

CHAPTER 1

INTRODUCTION

1.1 Background

Conceptually, a drought is the short in precipitation for a prolonged period which usually resulting in massive calamities to mankind. Operationally, drought can be grouped into four scenarios: meteorological, agricultural, hydrological and socioeconomic (Eschooltoday.com, 2016). A meteorological drought is expressed in relation to the scale of dryness (compared to normal amount) and the duration of the dry period. Since weather conditions such as low precipitation, dry winds, high temperature and so on are highly variable from region to region, the definition of meteorological drought must be regionally specific. An agricultural drought happens when the moisture of surroundings is reduced to an extent where the soil moisture is affected. It affects evapotranspiration and brings negative effects to crops and animals. A hydrological drought is the deficiency of surface water and ground water supply as a result of deficient precipitation coupled with an over reliance of surface water for human needs. Normally, the occurrence and severity of hydrological drought is described on the watershed or river basin scale. On the other hand, a socioeconomic drought occurs when people starts to be affected by the water shortage or, in other terms, definitions of socioeconomic drought are accompanied with the supply and demand of an economic good.

Drought is one of the most damaging but least understood of all "natural" hazards (Pulwarty and Sivakumar, 2014). Drought are events with impacts span for ages but evolve slowly in time (Wilhite et al., 2014). These features enable possible drought mitigations but however, difficult. This is because it is difficult to be determined the onsets and offsets of droughts. In particular, some of the rare and extreme drought events differ greatly over time and extent (Burke et al., 2010). For such events, a thorough and challenging evaluation of changes in drought characteristics is required in order to improve drought adaptation (Mondal and Mujumdar, 2014). Nevertheless, drought management and mitigation are still commonly practiced as it is important and necessary. Forecasting and warning facilitation are commonly recognized as important aids in managing natural hazards. It can be defined as data collection, analysis, and reporting to develop information on current and future drought conditions. However, drought forecasting is difficult due to the inherent complexity of the spatial and temporal variability of meteorological and hydrological processes. This research is aimed at increasing the drought forecasting capability and subsequently improves the drought management practices.

Although Malaysia is located in the heavy rainfall region, it has large variability in rainfall amount and rain day. The variability of rainfall amount and rain day of wet and dry seasons can be extreme at times, caused difficulties to sustainable water storage and supply management, which main water sources are direct rain water and rain water stored in dams (Abdulah et al., 2014). Thus, droughts can happen in Malaysia when extreme weather hits. Some of the remarkable droughts that had happened in Malaysia are 1991 Malacca water

crisis, 1998 Klang Valley water crisis, 2014 Selangor water crisis (Abdulah et al., 2014). Given the adverse consequences of droughts, and the vulnerability of Malaysia to it, this research is conducted to improve the forecasting capability. The Langat River Basin, an area covering most of the important cities including Putrajaya, Petaling and Cheras, was the chosen study area.

In the past, many drought forecasting models have been developed to improve drought forecasting capability, such as Autoregressive Integrated Moving Average (ARIMA), Markov Chain, Artificial Neural Network (ANN), Support Vector Regression (SVR) and different hybrid models (Belayneh et al., 2014; Belayneh et al., 2016; Han et al., 2010; Masinde, 2014; Sun et al., 2016). However, droughts vary spatially, rendering changes in the accuracy of the models for the different locations where they are applied. To overcome this anomaly, in this research, artificial intelligence-based hybrid models were constructed to forecast future drought events in Langat River Basin. Three different hybrid models, the Multi-Input Wavelet Fuzzy Support Vector Regression (M-W-FSVR), the Weighted Wavelet Fuzzy Support Vector Regression (W-W-FSVR) and the Wavelet Boosting Support Vector Regression (W-BS-SVR) models were respectively constructed to determine the best forecasting model. The Standardized Precipitation Evapotranspiration Index (SPEI) have been proven to be an effective index in indicating droughts (Paulo et al., 2012; Potop, 2011; Wei-Guang et al., 2012) and is used as in this research. For the development of forecasting models, the variation in the series and the increase in lead time always post difficulties to modelers. Hence, this study

targeted to overcome these difficulties by exploring the combination of wavelet transformation, boosting technique and fuzzy concept with SVR.

1.2 Problem Statement

As aforementioned, Malaysia is vulnerable to droughts with the proof of several remarkable historical drought events. Among them, the most notable one was the Klang Valley water crisis occurred in February 1998 when the three reservoir dams supplying water to the Klang Valley, the Klang Gates Dam, the Batu Dam and the Semenyih Dam suffered a significant drop in water level during the period of the El Niño phenomenon which had impacted the whole world. The water shortage caused by the drought affected majority of the residents in the Klang Valley as the government had to execute water rationing before the 1998 Commonwealth Games in Kuala Lumpur. The water rationing lasted for five months, causing an estimated economic loss of USD 9 billion (Abdulah et al., 2014). The lengthy drought also caused forest fires and thick haze produced, inflicting poor vision to the traffic commuters and threatened the health of the people (Hussaini, 2007). Other cases of severe drought events in Malaysia include the terrible drought in the state of Malacca in 1991. It was so severe to the extent that the main water supply dam of the state, the Durian Tunggal Dam had run dried, causing water crisis problems in Malacca (Hussaini, 2007). There was also this lengthy dry meteorological condition across Peninsular Malaysia in 2014 that affected the 2 million of people in Kuala Lumpur and Selangor having to experience water rationing that lasted for 3

months (Leister, 2014). During this period, multi-million ringgits were lost especially in the sector of food and drinks processing industries, rubber manufacturing, chemical and electrical related industries, and tourism activities (Zachariah, 2014).

The Langat River Basin, being one of the more important basins in Malaysia, is also vulnerable to droughts. The two main dams in the basin are the Langat Dam and the Semenyih Dam. These dams serve Putrajaya, Hulu Langat, Kuala Langat, Sepang, Petaling and Cheras (Berita Harian, 2016). Putrajaya, being the federal administrative centre of Malaysia and Petaling as the district with most number of factories in Malaysia, are factors that make water resources planning in the Langat River Basin important so as to avoid severe impacts on the progress and development of the country's economy. However, the susceptibility to droughts continue at the basin. The most recent one being in April of 2016, leading to a suggestion for a 25% reduction of water consumption, as the Semenyih dam was depleting at a rate of 0.47% daily and was going to drop below the critical level of 40% if the droughts were to continue for another 43 days (Shazwan, 2016). Forest fires occurred and the Langat River had dried up, making them lacked of water to extinguish the fires. Air quality also worsened as five areas in the Klang Valley recorded unhealthy Air Pollutant Index readings and low visibility levels of 1.5km visible range (Today Online, 2016).

Until now, drought monitoring system in Malaysia was done by comparing current rainfall to the past, but not using forecasting methods. According to the Department of Irrigation Malaysia (2016), the percentage of difference from the long term mean (LTM) of the 3-month moving rainfall totals is used as barometer of the watershed condition to monitor droughts. When there is a negative difference from the LTM value, the particular region is said to be undergoing a dryer than normal condition or also known as drought. Although this had been practiced since the first circulation of the Standard Operating Procedure (SOP) in 2011 (Abdulah et al., 2014), the evidence of having more frequent droughts occurrences in Malaysia shows there is a need to have a better drought forecasting capability in order to improve the drought management practices.

Moreover, to the best knowledge of the author, drought forecasting model for Malaysia and the Langat River Basin in particular, has not been done by any researcher in the past. Thus, the Langat River Basin was chosen as the study area for this research, with the aim of increasing drought forecasting capability and subsequently improving the drought management practices.

1.3 Aim and Objectives

The aim of the study is to develop hybrid support vector regression drought forecasting models with the Standardized Precipitation Evapotranspiration Index (SPEI) of different time scales and lead times as the drought barometer, for the Langat River Basin, Malaysia. The specific objectives are:

i. To develop three hybrid models namely: The Multi-Input Wavelet Fuzzy Support Vector Regression (M-W-FSVR), Weighted Wavelet Fuzzy Support Vector Regression (W-W-FSVR) and the Wavelet Boosting Support Vector Regression (W-BS-SVR) models
ii. To enable prediction of drought events through implementing the Standardized Precipitation Evapotranspiration Index (SPEI) using the developed hybrid models, and
iii. To determine the best hybrid models for the SPEI of different time scales and lead times.

1.4 Significance of Study

According to reports, the boundaries of Metropolitan Kuala Lumpur in Malaysia will increase in the future and become a “Greater KL”. The Greater KL shall comprise of Kuala Lumpur, Putrajaya and all districts in Selangor with the exception of Kuala Langat, Kuala Selangor, Sabak Bernam and Hulu

Selangor. This makes the population of the area to grow from 6 million in 2010 to 10 million by 2020 (Economic Transformation Programme, 2012). By having the Greater KL located in the Langat River Basin, the growth in population makes the water resources planning in the basin more important in the future. To do so, there is a need to have better operation plans for the two main dams at the upstream of the basin. The development of the drought forecasting hybrid model in this research will come in handy. Apart from this, the Langat 2 Water Treatment Plant which aimed to give better and more consistent water supply in the basin is expected be completed in the 2019 (The Sun Daily, 2017). By using the developed drought forecasting model in this research, better operation planning for the plant can be implemented.

For agricultural activities, the downstream of the Langat River Basin has been actively used for oil palm plantations since 90s (Department of Agriculture, 1995). Even with the rapid development which caused rapid growth of the urban area, the oil palm plantations still occupied an area of 847 km^2 (estimated using latest Google Satellite image), which is a third of the whole basin area. Thus, the drought forecasting model would also be important for the crop yield production of oil palm plantation in Langat River Basin (e.g. estimate the appropriate seeding period using the predictions from the developed models to optimise the production).

1.5 Scope of Work

The scope of this study is to develop, evaluate and compare hybrid models to forecast droughts in Langat River Basin. Stations s2815001 (rainfall - downstream), s2917001 (rainfall - upstream) and 48648 (temperature – nearest to the rainfall stations) were selected for retrieval of raw data for this research. In this study, three hybrid models, M-W-FSVR, W-W-FSVR and W-BS-SVR are to be developed using MATLAB. They will be evaluated using different performance measures so that the best hybrid model can be determined.

The data collected on the Langat River Basin from the year 1974 to 2015 will be tested for homogeneity. Well known methods such as the Standard Normal Homogeneity Test (SNHT), the Buishand Range (BR) test, the Pettitt Test (PeT) and the Von Neumann ratio (VNR) test are used for the homogeneity test in this study. The performance of the models shall be evaluated using the mean absolute error (MAE), the root mean square error (RMSE) and the Bias parameters.

CHAPTER 2

LITERATURE REVIEW

2.1 Drought Indices (DI)

Drought indices are tools to determine and identify the characteristics of droughts. The application of drought indices relies on the study of interest in either the meteorological, hydrological or agricultural domains (Niemeyer, 2008) and also on the parameters provided. Hence, several of indicators of drought have been introduced to describe the many scales of drought.

2.1.1 Percent of Normal (PN)

The Percent of Normal PN, defines drought as the difference of precipitation from the normal or average value. Precipitation with a minimum 30 years historical period is the only input required. It is calculated by dividing actual precipitation by normal precipitation, which usually corresponds to the mean of the past 30 years and multiplying this by 100% (World Meteorological Organization, 2016). The PN can be computed for various time scales, from monthly to annual, depends on the objective of the user. Simplicity and transparency are the main advantages of this index and thus, it is favourable for communicating drought levels to the public (World Meteorological

Organization, 2016). However, the PN may not well represent the drought severity as no statistical method is used for the distribution of the recorded precipitation, the deviation between the median and the mean value can weaken its accuracy. Moreover, since the distributions varies temporally and regionally, PN cannot be used to compare drought through seasons and regions. As such, this method is not appropriate for operational use in planning and management.

In 2012, Dogan et al. (2012) conducted a study to compare several monthly rainfall-based drought severity indices. In the study, the author used monthly rainfall data of twelve spatially distributed stations to compare DIs for time-steps ranging from 1 month to 48 months. However, it was observed that the PN for variable time-steps is less consistent. Therefore, the author concluded that it may not be helpful in comparison studies if the aim is not decided. However, it was used in the same year by Nikbakht et al. (2012) for streamflow drought severity analysis. According to the author, the PN was used because it is easy to calculate and has simple definition which can be understood by general audiences easily. Gocic and Trajkovic (2013) also used the PN to define the spatiotemporal characteristics of drought in Serbia for the same reason. Nevertheless, the SPI was also used in that study based on the reason that it is not useful for making decisions when used alone. The PN once again proved to be unreliable as it tended to over forecast drought severity compared to other indices (Yacoub and Tayfur, 2016).

2.1.2 Palmer Drought Severity Index (PDSI)

It is the first comprehensive drought index developed in the United States (World Meteorological Organization, 2016). It is a well-known climatological tool in assessing long term meteorological drought. The index uses readily available precipitation and temperature data as their input parameters, as well as the local Available Water Content (AWC) of the soil. The objective for the PDSI is to measure the total duration and amount of intensity of the long-term drought-inducing the circulation patterns. The advantages of using the PDSI include a more comprehensive analysis such as considering the parameter of evapotranspiration and soil moisture as compare to precipitation-only indices such as the SPI, extremely efficient in measuring the effect of soil moisture sensitivity and providing excellent descriptions of historical droughts. However, it is less appropriate for areas with mountainous topography or frequent climatic extremes and its complexity of having an unspecified, built-in time scale that can be misleading making it become less popular to be used. The requirement of substantial input of meteorological data allows only places with advanced studies in meteorology to adopt this index, such as Rohli et al. (2016) and Mares et al. (2016) where studies were done in the south-central of USA and the Danube in Europe.

In 2015, Vicente-Serrano et al. (2015) explored the influence of precipitation and evapotranspiration to DIs under different climates using four different DIs, including the PDSI. The results showed that among the four indices, the PDSI was least sensitive to the variation in their climate inputs,

which may be caused by the process to standardize soil water budget anomalies. In another study (Rohli et al., 2016), PDSI were analysed to find its relationship to the drought damage and results showed a strong negative correlation exist between them.

2.1.3 Crop Moisture Index (CMI)

The Crop Moisture Index (CMI) applies a meteorological analysis in monitoring the growing of crop based on the weekly average temperature and average precipitation. It was proposed by Palmer from the calculation procedures of the PDSI. The CMI and PDSI both have the weakness where they consider the usage of the land and the soil characteristics are identical throughout the entire assessed region (Narasimhan and Srinivasan, 2005). The major difference of the PDSI and the CMI is the former analyses the long-term dry and wet seasons, while the latter was developed to analyse the short-term moisture across the main crop producing areas. Therefore, the CMI is suitable for use only during the crops growing season and it is not a good tool for monitoring of long-term drought as its high sensitivity to the changing of short-term conditions may lead to inaccurate results. Furthermore, during the time for seed germination and the starting spell for crop growing, the CMI was not appropriate for use as both of the conditions vary from the usual.

In 2011, the CMI was used to evaluate the Vegetation Temperature Condition Index (VTCI) by analysing the correlation between them (Patel et al. 2011). In another study, Li et al. (2014) assessed agricultural droughts in China using the CMI together with the Standardized Precipitation Index (SPI) and the Normalized Difference Vegetation Index (NDVI) by conducting correlation analysis between the indices and the final crop yield. Results showed both the CMI and NVDI positively correlated to the yield though in different period of time, but the SPI showed no correlation to the yield. Dhorde and Patel (2015) conducted a study to investigate how terminal drought varies spatially over western India using the CMI and the Temperature Vegetation Dryness Index (TVDI). The study revealed that the CMI was more sensitive than the TVDI to soil moisture in sparse vegetation canopies during drought period.

2.1.4 Effective Drought Index (EDI)

The concept of the Effective Drought Index (EDI) is a standardised daily difference between the accumulated weighted precipitation over a defined leading period and its multiyear mean value for each calendar day. It can determine the exact beginning and ending of a drought period more precisely and accurately. The EDI is computed using the daily time step unlike other available drought indices (Byun and Wilhite, 1999). In short, EDI is actually a measure of precipitation needed for the accumulated deficit to recover or return to normal conditions which in turn is correlated to the effective precipitation (EP).

In 2012, Arshad et al. (2012) conducted a study to monitor and forecast drought impact on dryland farming areas in Iran using four different DI, including the EDI. It was modelled using the Adaptive Neuro-Fuzzy Inference Systems (ANFIS) and concluded that the EDI showed better accuracy as the drought in question was a meteorological drought.

The EDI was used as the drought index to investigate the effectiveness of a proposed extreme learning machine to forecast drought in Eastern Australia (Deo and Sahin, 2015). Later, the daily EDI was again utilized to precisely and quantitatively forecast the future drought frequency in Korea for years 2014–2100 (Park et al, 2015). Li et al. (2016) also conducted a study to evaluate the importance of short-term relationship between drought and vegetation growth for drought monitoring and results showed that the EDI-NDVI correlation method is effective in identifying details of the drought-vegetation relationship.

2.1.5 Standardized Precipitation Index (SPI)

The drought index, Standardized Precipitation Index (SPI) was used to validate the shortfall in the rainfall for different time scales. This index is able to describe the effect of drought that causes the deficit in the continuous of water supply. The computation of the SPI is using the long-term rainfall data for a chosen period. This long-term data is modelled to form a probability distribution, and it is later converted into a normal distribution to ensure the mean SPI obtained for that chosen period at the location is zero (Edwards and McKee,

1997). The incident of drought is considered continuing if the SPI remains negative. In contrast, the drought event ceases if the SPI turn out to be positive. Every drought incident, thus, has a period described by its occurrence and cease, and the intensity for the event continues in each month.

One of the main benefits of applying the SPI is that only precipitation data is needed which provides relative simplicity. Besides, the SPI is very efficient for the drought analysis at different time scales and applicable for meteorological, agricultural and hydrological drought monitoring. Thus, it is the most commonly used index. However, this index loosely connected to soil conditions as potential evapotranspiration is an additional significance variable (Vicente-Serrano et al., 2010).

Huang et al. (2014) investigated the joint probabilities of combining dry and wet conditions in the Guanzhong Plain, China between adjoining seasons under the effect of global warming. The joint probabilities were computed based on the SPI for 1961–2010 using copulas functions. In the same year, Núñez, et al. (2014) analysed the applicability of the Standardized Streamflow Index (SSI), as an extension of the SPI to represent hydrological droughts under the influence of multidecadal climate variability and its connection with global recommendations for the appropriate use of Streamflow Drought Index (SDI). The study discovered that due to limitations caused by the probabilistic nature of the SPI, it is insufficient to define drought accurately even with global recommendations that were aimed at overcoming its limitations and these were supported by the study of long term SSI in the arid north-central region of Chile.

The SPI also came out in a few recent studies (Liu et al. 2016; Stagge et al, 2015; Venkataraman et al. 2016). However, the SPEI were also adopted in those studies to achieve better accuracy in defining the term, drought.

2.1.6 Standardized Precipitation Evapotranspiration Index (SPEI)

The drought index, the SPEI is identified as a very appropriate tool for researching and monitoring drought conditions under warming as some of the researchers had conducted the study of the SPEI drought analysis (Vicente-Serrano et al., 2010; Wang et al., 2014). The SPEI combines multi-scale nature of the SPI while considering the Palmer Index sensitivity with evapotranspiration (based on temperature variation) using simple computation. The SPEI takes the resultant effects of precipitation, temperature or evapotranspiration into account on developing of drought evolutionary stages (Beguería, et al., 2013; Vicente-Serrano, et al., 2012) that contrary to EDI and SPI that are solely assessed by rainfall data.

Unlike other drought indices such as the PDSI that is based on the water balance of a system (e.g. river, soil column, ecosystem, etc.), the SPEI does not assess the water balance deficit experienced by the particular system. However, the SPEI has an advantage that it can calculate for different time scales at which the drought response of the system is highest. In addition, the SPEI is able to identify different drought types that are induced by global warming context (Potop et al., 2012). Hence, the SPEI is widely accepted in drought forecasting

as it has a broader range of applications than the EDI, SPI and PDSI. Table below shows how drought severity is defined by the SPEI (Li et al., 2015).

Table 2.1: Categories of SPEI

Moisture Category	SPEI
Extremely Wet	2.00 and above
Very Wet	1.50 to 1.99
Moderately Wet	1.00 to 1.49
Near Normal	-0.99 to 0.99
Moderately Dry	-1.00 to -1.49
Severely Dry	*-1.50 to -1.99*
Extremely Dry	-2.00 and below

In 2010, Lorenzo-Lacruz et al. (2010) studied the influence of droughts and water management on different hydrological systems at the upstream of the Tagus River in central Spain. The DIs used were the SPI and the SPEI. Compared to SPI, the feedbacks in river discharge and reservoir storage were a little higher when SPEI was used. This showed that the effect from temperature was not negligible even precipitation played the major role in describing temporal variability in the analysed parameters. In another study, SPEI in different time scales were used to study the effects of climate variability to the hydrological system in Ebro Basin due to its capability to explain temporal variations in hydrological series in changing environments (López-Moreno et al., 2012). Liu et al, (2016) also used the SPEI to analyse multiscalar drought characteristics spatially and temporally on the Loess Plateau of China. The SPEI were compared with the SPI in the study and results showed that SPEI is a robust index to monitor and analyse regional drought, due to its multi-scale nature, simplicity in calculation, low data requirement, and the consideration of temperature effects on drought conditions. Due to the ability of identifying

effects from temperature, the SPEI once again proved its' mettle in the drought forecasting of Pearl River Basin, China which used the Markov Chain model that included climate indices in it (Xiao et al., 2016).

2.2 Drought Forecasting Models

There are many types of drought forecasting techniques use to forecast the future drought indices. Among these approaches, the artificial intelligence (AI) and the stochastic methods are widely adopted in the aspect of time series forecasting. Besides that, the wavelet transform is considered one of the powerful 'data pre-processors' as it can improve the performance of the models once it is coupled with the data driven approaches.

2.2.1 Time Series Analysis - Autoregressive Integrated Moving Average (ARIMA) and Seasonal Autoregressive Integrated Moving Average (SARIMA)

Time series models have been widely used for scientific applications, including analysing and modeling of the hydrologic time series. The advantages of time series models include better consideration on the serial linear correlation characteristic of time series; capable to search systematically for identification; estimation and diagnostic check for model development; and SARIMA requires only a few parameters to describe non-stationary time series for both within and

across seasons. Two important and popular classes of time series models are the ARIMA and the SARIMA (Mishra et al., 2007).

An ARIMA model contains three important parameters (*p,d,q*) which are respectively, an autoregressive order of *p*, the *d*th difference of the time series z_t and moving average order of *q*. In short notation, it is described as ARIMA (*p,d,q*) and may be written as

$$\phi(B)\nabla^{\mathrm{d}}Z_t = \theta(B)\mathrm{a_t} \qquad (2.1)$$

A seasonal SARIMA model is more appropriate when the time series is seasonal in which the statistics are not stationary across the year. Generally, SARIMA model is described as an ARIMA *(p,d,q)* $(P,D,Q)_s$, where (*p,d,q*) is the non-seasonal part of the model and $(P,D,Q)_s$ is the seasonal part of the model. It can also be written as

$$\phi_{\mathrm{P}}(B)\Phi_{\mathrm{P}}(B^s)\nabla^{\mathrm{d}}\nabla_{\mathrm{s}}^{\mathrm{D}}Z_t = \theta_{\mathrm{q}}(B)\Theta_{\mathrm{s}}(B^s)\mathrm{a_t} \qquad (2.2)$$

where $\phi(B)$ and $\theta(B)$ are polynomials of order *p* and *q*, respectively; $\Phi(B^s)$ and $\Theta(B^s)$ are polynomials in B^s of degrees P and Q, respectively; *p*=order of non-seasonal autoregression; *d*=number of regular differencing; *q*=order of the non-seasonal moving average; *P*=order of seasonal autoregression; *D*=number of seasonal differencing; *Q*=order of seasonal moving average; *s*=length of season.

Abebe and Foerch (2008) had carried out a study to identify a time series forecasting model for mathematical description, simulation and short-term forecasting of hydrological drought severity at the Wabi Shebele river basin, Ethiopia. Prominent homogeneous pools were developed using the parameters mean rainfall, temperature, normalized digital vegetation index and stream flow. Thereafter, forecasting using SARIMA models were carried out and the results showed that the $(0, 1, 1)\ (0, 1, 1)^{12}$ was the best among the candidate models. Durdu (2010) used ARIMA and SARIMA to predict the SPI at the Büyük Menderes river basin. The results suggested that the linear stochastic models were suitable to predict multiple time scales of the SPI time series for the Büyük Menderes river basin and other basins with similar hydrometeorology characteristics. Han et al. (2010) used ARIMA to forecast VTCI in the Guanzhong Plain. 36 pixels of VTCI were first studied for their model fitting, and then a first order auto-regressive multivariate model, AR(1) was chosen as the best model to be used in each pixel of the whole area. The forecasts were done in 1-2 steps and the results showed that the forecasting ability of 1 step was better than 2 steps after comparing the simulating data with the historical data. Yet, most of the simulating errors were small and with that, it was concluded that AR(1) model created for VTCI series is suitable to forecast drought in the Guanzhong Plain.

Fernández-Manso et al. (2011) also developed the SARIMA for drought prediction in the areas of Castile and Leon, Spain. A 10-day maximum value composite (MVC) bands of the NDVI was analysed using stochastic processes and then, NDVI in the following 10-day periods was forecasted using the

developed SARIMA model. The results showed that the MVC-NDVI with climatic variables as regressors can improve the accuracy of forecasting models if the species considered depends on summer water stress. In the following year, Chun et al. (2012) investigated and modeled the drought severity indices of six catchments in UK using ARIMA models and GLM. The ARIMA was used to identify the autocorrelation structures for the drought indices and to establish empirical relationships between climate variables and drought. Then, GLM was used to simulate the incidents and quantities of rainfall with the conditioning on climate variables. The results showed that ARIMA underestimated the magnitude of drought severity but it provided good short-term forecast fit. The GLM was concluded as being suitable for the local drought assessment at seasonal scale but needs improvement for rainfall simulations of more than six months.

Chen et al. (2012) also used ARIMA for drought forecasting at the Haihe river basin, China. The performance of ARIMA with Random Forest (RF) in predicting SPI was the subject of interest. Accordingly, the RF-based models have the advantages of doing nonparametric forecasting, flexible to capture the basic relationship of time series and able to generate ensemble of drought forecast instead of mean prediction. The results also showed that RF-based model was more reliable than ARIMA for both short and long term drought forecasting. Han et al. (2013) developed ARIMA models to forecast the SPI at the Guanzhong Plain, China. The forecast results showed that the ARIMA models are efficient in forecasting all SPI series with 1-month lead time and SPI-9, SPI-12, SPI-24 with 6-month lead time. In other words, the ARIMA

models were reflected as more convincing for the short-term forecasting. Over the same year, Shatanawi et al. (2013) used the Markov Chain to support ARIMA in forecasting the SPI for the Jordan River Basin in the Middle East. It was observed that the ARIMA models were not able to produce exact predictions for the SPI series, and that the Markov chain models can give only the likely condition based on the precursor condition of the one or two previous seasons. Hence, both models were used to support each other in order to get better drought predictions. The results showed that ARIMA models can be used to forecast long term future drought trends and with the aids from Markov transitional probabilities, and early warning of developing droughts can also be deduced.

Two years later, the ARIMA was used to assess the meteorological drought severity at the Bundelkhand, Central India (Alam et al. 2014). The SPI series at 3-month, 6-month, 9-month, 12-month and 24- month time scales had been used, and the statistical analysis revealed that the non-seasonal ARIMA model was suitable for the 3-month SPI series, while seasonal ARIMA models had been found assuring for the other longer SPI time scales. Then, the forecasted data from the best ARIMA model was compared to the observed data in which the forecasted data corresponded well with the observed data. Mossad and Alazba (2015) developed a linear ARIMA models to forecast the hyper-arid climate based on the SPEI. The few statistical parameters including the R^2, MAE, RMSE, AIC and SBC were used to evaluate the performance of different ARIMA models. The results demonstrated that the ARIMA models can accurately predict the drought event for a longer time scale, like the SPEI-24.

On the other hand, the performance was less reliable over a shorter time scale such as the SPEI-3. Bazrafshan et al. (2015) assessed the efficiency of ARIMA and SARIMA for monthly and seasonal hydrologic drought forecasting, as well as determined the amount lead time for effective forecasting, in the Karkheh Basin, Iran. The SRI in the study was generated using monthly and seasonal discharges from ten hydrometric stations of years 1974 to 2013. The results showed that the ARIMA model performed better for the two months and one season lead-time forecasts. For the SRI values forecasts, the SARIMA model performed better over the monthly time scale than seasonal time scale.

Tian et al. (2016) explored the effectiveness of AR(1) and SARIMA forecasting VTCI at the Guanzhong Plain of China. In the study, VTCI of the first 10 days of March 2000 to last ten days of March 2009 was used as input to develop the models. The results showed that the SARIMA has better performance compared to AR(1) as it can predict both no-drought grades and drought grades, unlike AR(1) which can only predict no-drought grades although it has lower absolute errors compared to the SARIMA. Mahmud et al. (2016) also adopted the SARIMA for drought forecasting in the same year. Rainfall data from thirty stations in Bangladesh was used as input to forecast monthly rainfall of twelve months ahead in the region. Based on R^2, RMSE and normalized BIC criteria, it was found that the SARIMA can predict monthly rainfall with reasonable accuracy and was concluded as a suitable model to forecast year-long rainfall for Bangladesh.

Karthika et al. (2017) used ARIMA models for short-term annual forecast on meteorological drought at the Lower Thirumanimuthar Sub-basin, India. 1-year to 3-years lead-time of forecasting was considered and the results showed that the developed model can be used to design a drought preparedness plan for the region, ensuring sustainable water resources planning in the sub-basin. However, this well-known and widely used model had been slowly but surely, being replaced by artificial intelligence models which have dominances of inborn nonlinear property and flexibility for modeling (Mishra et al. 2007). Furthermore, traditional model identification techniques with complicated computations which are difficult to understand are required to identify the correct model from the class of possible models. Thus, the reliability of the chosen model is subjected to the skills and experience of the user.

2.2.2 Probability Model – Markov Chain (MC)

MC is a memoryless random process in which if a present state has been known or given, the future and the past are independent of each other (Chen and Yang 2012). It is a mathematical technique to obtain the probabilities of the system using a set of transitions probabilities from one state to another. Generally, when the transitional probability is depending on the conditions in the previous *m* time periods, it is called an *m*th order Markov Chain, which can be expressed as (Avilés et al., 2016):

$$\text{Transitional Probability} = P\left\{X_{tn} \middle| X_{tn-1}, X_{tn-2}, X_{tn-3,} \dots, X_{tn-m}\right\} \quad (2.3)$$

Using the First Order Markov Chain as an example, the transitional probability, p_{ij}, of a stochastic process, $X(t)$, can be obtained as:

$$p_{ij}=\mathrm{P}\{X_{tn}=j|X_{tn-1}=i\} \tag{2.4}$$

where p_{ij} is the transition probability that X_{tn} is equal to category j given X_{tn-1} is equal to category i. The approximate of the transition probabilities ($\hat{p}_{ij}$) can be computed to comprise the conditional relative frequencies of transitions (n_{ij}):

$$\hat{p}_{ij}=\frac{n_{ij}}{\sum_{i=1}^{s} n_{ij}} \tag{2.5}$$

where n_{ij} is the frequency that X is equal to the category i at time t_{n-1} and equal to category j at the time t_n. The value of s represents the number of states of the system. The numerator stands for the number of transitions of category i to category j, and the denominator represents the total number of transitions of category i to any other category. For the Second Order Markov Chain, the value of m will be equal to 2 and the same for the Markov chain with higher orders.

Paulo and Pereira (2007) investigated the efficacy of non-homogeneous formulation for the Markov Chain model. 67 years of monthly SPI from Alentejo, southern Portugal were utilized for model development. The authors predicted drought class transitions up to 3 months ahead and the results showed that the non-homogeneous Markov Chain model has the advantage for distinguishing among months when drought is computed, compared to the

homogeneous Markov Chain model. Jiang and Chen (2009) developed a new model named weighted Markov SCGM(1,1)c for the prediction of drought crop area. This model combined the advantages of cloud grey system and Markov Chain to improve drought prediction accuracy. By using data from China as an example, it was proven that this model can predict drought crop area with high precision. Sharma and Panu (2012) used Markov Chain to forecast hydrological drought durations for the case of the Canadian prairies. Modeling was done using the SHI series derived from annual, monthly and weekly streamflow series. The results showed that the first-order Markov chain was suitable for the forecasting of annual drought lengths, while the second-order was found to be satisfactory on monthly and weekly time scales. Subsequently, Chen and Yang (2012) predicted regional drought using weighted Markov Chain model, with SPI as the drought index. In the study, monthly precipitation data from Anhui Province of Huaihe River in China was used to compute the SPI series which was used for model development. Based on the outcomes, it was concluded that the model is a useful method to predict drought and can be helpful for regional drought disaster management. Alam et al. (2014) used a Markov Chain model to analyse long-term rainfall data of 12 rainfall stations at the semiarid Barind region. The results were tested with hypothesis testing (χ^2 test) and the model was termed as statistically satisfactory.

Another Markov Chain study was done by Avilés et al. (2015). Unlike other studies, the performance of Markov Chain based drought forecasts were evaluated using skill scores, namely the RPS and the GMSS. The results indicated that drought events with greater severity were more accurately

forecasted. Yeh et al. (2015) also adopted a Markov Chain model for drought forecasting for the Lanyang River and Yilan River basins in Taiwan. Precipitation and streamflow data were used to compute the SDI as input to the model. The results showed that the Markov Chain model can produce reliable drought frequency and occurrence probabilities using short-term data. Nnaji et al. (2016) used a semi-Markov Chain model which can preserve longer memory persistence than the simple Markov process to predict monthly streamflow series for Apalachicola–Chattahoochee–Flint, USA. The results demonstrated that the model can accurately predict streamflow near drought and critical drought conditions. Khadr (2016) also investigated the use of the homogeneous HMM to forecast SPI for Blue Nile river basin, Egypt. A set of procedures for meteorological drought forecasting using homogeneous HMM to predict the SPI with multiple timescales with lead-time of more than 1-month was produced.

Chen et al. (2016) proposed a new approach called the HMM aggregated with the RCP 8.5 precipitation projection (HMM-RCP). A probabilistic forecast of the SPI-3 with the inference on the model parameters through reversible jump Markov Chain Monte Carlo algorithm and weight-corrected post-processing on the RCP precipitation projection transformed SPI (RCP-SPI) was the subject of investigation. The proposed approach showed good results of accurately predicting 71.19 % of drought events, and forecasted the mean duration with an error of less than 1.8 months and a mean severity error of less than 0.57. Avilés et al. (2016) produced another paper comparing the performances of the Markov Chain and Bayesian Network models. Monthly rainfall and streamflow data from the Chulco River basin, located in Southern Ecuador were used to develop

the models. From the results of the RPSS, the authors concluded that the MC-based models have higher prediction accuracy for wet and dry periods, and the BN-based models forecast better for extreme droughts.

A Markov Chain model was also used to forecast short-term droughts in Victoria, Australia (Rahmat et al., 2016). The estimated drought probabilities and drought forecasts up to three months lead time using a non-homogeneous Markov Chain model were analysed. The results showed that the model developed, forecasted drought situations one month ahead reasonably well, but further development was required to forecast drought situations of two and three months ahead. Sun et al. (2016) also evaluated the efficiency of Markov Chain models in forecasting two drought indices, SPEI and SRI. The MCFO and MCSO were developed in the study and the results showed that the first-order Markov chain model was acceptable for the modeling practice of the SPEI–SRI integrated drought events. Recently, a weighted Markov Chain model also evaluated by Zhang et al. (2017). The performance of the model was compared to the Volterra adaptive filter model and the 3D loglinear model, based on the accuracy in forecasting SPI and SRI series. The results showed that the 3D loglinear model can forecast drought class but limited to within one month, and the precision decreases with timescales. For the weighted Markov Chain, it is suitable for drought early warning as the precision is the highest for Non-drought, followed by the Moderate and then Severe/Extreme, and lowest for the Near-normal. The Volterra adaptive filter model is capable in forecasting long-term drought. Although the Markov Chain gives good results, even when dealing with complex distributions of data however, it is computationally

lengthy and expensive. The use of the Markov Chain may be limited by the performance of the researchers' computers and thus this further led to more newer approaches to achieve better overall efficiency.

2.2.3 Artificial Intelligence Based Models

In recent years, the use of artificial intelligence (AI) for the time series drought forecasting approach has manifested outstanding performance and accuracy. The flexibility and adaptability of AI models was found to be useful to forecast drought that has fluctuating durations, frequencies and intensities which cannot be determined effectively using empirical relations.

2.2.3.1 Artificial Neural Network (ANN)

Artificial neural networks are flexible nonlinear models that resemble the structure of a nerve system. It can adapt the data inserted and analyse and discover patterns from it. Theoretically, by giving an adequate amount of nonlinear processing units, neural networks are able to gain experiences and learn to estimate any complex functional relationship accurately (Mishra and Singh, 2011). Thus, ANNs have the advantage of not needing to define the procedures or processes between the inputs and outputs. The Multilayer perceptron feed forward model is the most popular neural network architecture (Djerbouai and Souag-Gamane, 2016).

Generally, a three-layer model consisting of input layer, hidden layer, output layer and nodes are used for forecasting purposes (Mishra and Singh 2011). The Input layer is the first layer of the framework, and it will receive external information. Then the hidden/intermediate layers with neuron-like processing will process the received information and finally, the forecasted results for different lead times can be obtained from the output layer. On the other hand, the nodes in neighbouring layers are normally connected by acyclic arcs (synapses), like a neural network, from the input layer to the output layer (Djerbouai and Souag-Gamane, 2016). Figure 2.1 illustrates the structure of a multiperceptron ANN model.

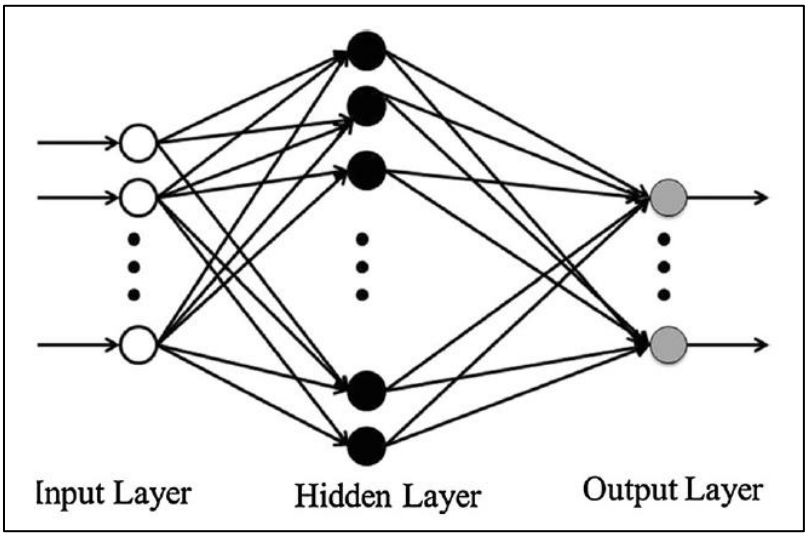

Figure 2.1: Multilayer Perceptron with One Hidden Layer (Jalalkamali et al. 2015)

Ochoa-Rivera (2008) investigated the performance between ANN and AR(2) in generating streamflows for the Alto Tajo River Basin in Spain. The ANN architecture used was the popular multi-layer perceptron ANN model. Average values of the mean, standard deviation, and skewness coefficient, and

correlation function of the synthetic series were estimated to compare with the historical series to analyse the goodness of fit of the models developed, while the RRMSD was used for the comparison of models. The results showed that ANN performed better than AR(2) and according to the authors, was due to the nonlinear structure of the ANN models. Following closely, Cutore et al. (2009) also applied ANN models to carry out forecasts of Palmer Index series in Sicily, Italy. The aim of the study was to investigate influence of the NAO and European Blocking (EB) indices on Palmer index series. The results showed that there was a significant improvement during the winter and autumn forecasts when NAO and EB were included in the ANN models. Dastorani et al. (2010) evaluated the applicability of ANN and ANFIS to predict dryland precipitation in Yazd, Central Iran. Different architectures of ANN were constructed to compare with ANFIS. The best architecture Time Lagged Recurrent Network ANN were then chosen as the best ANN model, and used to compare with ANFIS. The results showed that both models have similar efficiency in the dryland precipitation prediction and were efficient to predict precipitation 12 months advance.

Marj and Meijerink (2011) also conducted a study on drought forecasting for the Ahar-chay Basin, Iran. A feed-forward multiple neural network was used in the study to forecast the NDVI. The SOI and NAO was adopted as the input for ANN model and the results showed that the predicted NDVI has R^2 of 0.79, RMSE of 0.011 and the discrepancies are less than 1 SD compared to the observed NDVI. Barua et al. (2012) conducted a study to evaluate the effectiveness of an artificial neural network based model in

forecasting NADI. Two ANN forecasting models, namely the RMSNN and DMSNN, were developed in the study. Forecasted data from these two models were compared with ARIMA, and the results demonstrated that both RMSNN and DMSNN models had better performance than the ARIMA model. It was also found that the RMSNN model forecasted slightly more accurate than the DMSNN model for 2–3 months lead times, while the DMSNN model produced forecasts with higher accuracy than the RMSNN model for forecast 4–6 months lead times. ANN also used by Masinde (2014) to overcome the drawbacks of old drought forecasting approaches in Kenya that were unable to provide short and long-term forecasts and severity of the drought. The EDI was combined with ANN in the study, and accuracies as high as 98% were achieved, concluding that ANN can be a great enhancement to the old approaches practised in Kenya.

Apart from forecasting the NADI and EDI, the SPEI were also forecasted using ANN by Deo and Sahin (2015). In their study, the feasibility of the ANN was tested to predict the monthly SPEI for eight stations in eastern Australia. Different architectures of ANNs were tested and the structure with 18 input neurons, 43 hidden neurons and 1 output neuron was concluded as the best architecture. In addition, the results from performance measures of R^2, MAE and RMSE revealed that the Artificial Neural Network model was a useful data-driven method to forecast the monthly SPEI in the region. Hosseini-Moghari and Araghinejad (2015) also used ANN to forecast short-, mid-, and long-term droughts at the Gorganroud basin (northern Iran). Different architectures of ANN including the RMSMLP, DMSMLP, RMSRBF, DMSRBF, RMSGRNN,

and DMSGRNN were used to forecast SPI on 3, 6, 9, 12, and 24-month time scales. The results showed that recursive models performed better with the smaller time scales, whereas direct models have better performance at longer time scales. Rezaeianzadeh et al. (2016) compared the performance of ANN and Markov Chain models in drought forecasting for the Doroodzan reservoir dam, Iran. The 1-month lead time inflow volume using current reservoir inflow volumes and other hydroclimatic variables were forecasted. The results showed that ANN model performed better than Markov Chain model and it was concluded that simultaneous application of both models can reduce both the uncertainty and error of the models.

Maca and Pech (2016) also used ANN models for the forecasting and analysis of SPI and SPEI. The models they used are a feed forward multilayer perceptron based ANN and an integrated neural network model. Datasets from two different areas in USA were used, and they are the Leaf River in Collins Mississippi and the Santa Ysabel Creek in Ramona California. For data performance evaluation, the results of four from five performance measures showed that the integrated neural network model outperformed the feed forward multilayer perceptron based ANN. Deo and Sahin (2016) used ANN as a benchmark to interpret the predictive accuracy of ELM model for prediction of streamflow water levels. The streamflow water levels were predicted from a set of nine variables for three hydrological catchments in eastern Queensland, namely Gowrie Creek, Mary River and Albert River. The authors carried out correlation analysis for the selection of inputs in the training process of both

models. The results showed that ANN was outperformed by ELM. However, both models performed better when the selection of variables were done.

Ali et al. (2017) applied the MLP-ANN model to forecast the SPEI for seventeen climatology stations in the Northern Area and Khyber Pakhtunkhwa of Pakistan. Based on the outcomes, it was reported that the ANNs were able to learn the fluctuations in SPEI with a one-month time scale. The results from the MAE, R and RMSE also showed that the MLP-ANN has the potential capability for the SPEI forecasting. Kousari et al. (2017) also explored the potential of ANN in forecasting drought. They forecasted SPI in 3, 6, 9, 12, 18 and 24 monthly series for the Fars Province of Iran. It was reported that increasing the lead-time of forecasting leads to decreasing accuracy of the models. In order to achieve accurate drought forecasting, a set of procedures to be followed was given. Seibert et al. (2017) also used ANN to forecast seasonal hydrological drought at the Limpopo Basin, Africa. Streamflow data, climatic indices and gridded sea surface temperature anomalies were used as predictands for the models and the SPI with lead-time up to 12 months were the outcomes of the models. The performance of ANNs was compared with MLMs and RFORs and the results showed that MLMs is the best while ANNs and RFORs were likely to suffer from overfitting. With the advantages of less statistical training and its nonlinear property, ANN has the major disadvantages of being of a 'black-box' nature, computationally expensive, prone to overfitting and, with an empirical nature for model development.

2.2.3.2 Fuzzy Logic (FL)

Fuzzy logic was conceptualised by Zadeh (1965) and is defined in Mathworks (2016) as a handy way to map an input space to an output space. Among the several advantages of using fuzzy logic; the most relevant for our subject matter is the fact that it can model imprecise data and nonlinear functions of arbitrary complexity and that it is based on a natural language. The general concept behind fuzzy logic is that a set of pre-defined rules (if-else-statements) are applied in parallel to interpret some values in the input vector and then assign values to the output vector. Figure 2.2 explains this concept, while Figure 2.3 illustrates the three main stages of Fuzzy Modeling.

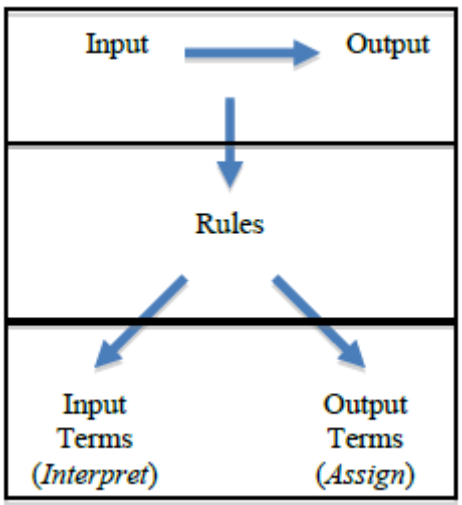

Figure 2.2: Fuzzy Logic Concepts (Mathworks, 2016)

Classically (Boolean or crisp set theory), membership of an element x in a set *A*, is defined by value of either 1 (true) or 0 (false) to each individual in the universal set X. That it is to say "*every proposition is either true or false*". But, Fuzzy Logic violates both "excluded middle" and "contradiction" laws

(Klir and Yuan, 2008). Fuzzy Logic is based on fuzzy sets in that, unlike classical sets, their membership is not a "true-false" but "not-quite-true-or-false" answer. A fuzzy set *A* is made up of ordered pairs and is defined as follow,

$$A = \{x|\mu_A(x)|x \epsilon X\} \tag{2.6}$$

where X is the universe of discourse with elements represented by x and $\mu_A(x)$ is the Fuzzy Membership Function (FMF) of x in A. This is a value in the unit interval [0,1], where 0=complete non-membership in a fuzzy set; 1=complete membership in a fuzzy set; grades between 0 and 1 mean partial membership in a fuzzy set.

An FMF is a function to assign membership value (or degree/grade of membership) between 0 and 1 to every points in the input space (universe of discourse). The choice of a FMF to be used is determined by the domain of the application as well as its simplicity, convenience, speed, and efficiency (Mathworks, 2016). Most standard membership functions can be categorized as either open (decreasing and with values between 0 and 1 only within a bounded interval) or closed category that allows nonzero values only in a bounded interval (Robinson, 2003). The two main classes under the open category are linear (usually left or right trapezoid function) and S-shape (left or right open shoulder) membership functions. Examples of functions under the closed category are: triangular (in general, the most commonly used category), trapezoidal, Gaussian, sigmoidal and generalised bell functions. Gaussian and sigmoidal are two S-Shaped membership mirror-image functions that open to

the right and are based on polynomial curves and are suitable for modeling indigenous knowledge because they have been proven to be appropriate and robust for linguistic variables (Sicat et al., 2005).

The three stages of fuzzy modeling (Sicat et al., 2005; Mathworks, 2016) are:

i. *Fuzzification*: generation of FMFs for input to a degree of membership between 0 and 1
ii. *Logical Inference procedures*: fuzzy set operations that combine fuzzy sets into a synthesised fuzzy set.
iii. *Defuzzyfication*: transformation of synthesised fuzzy set back to a crisp sets. It involves assigning an entire fuzzy set to the output based on the consequence of a fuzzy rule.

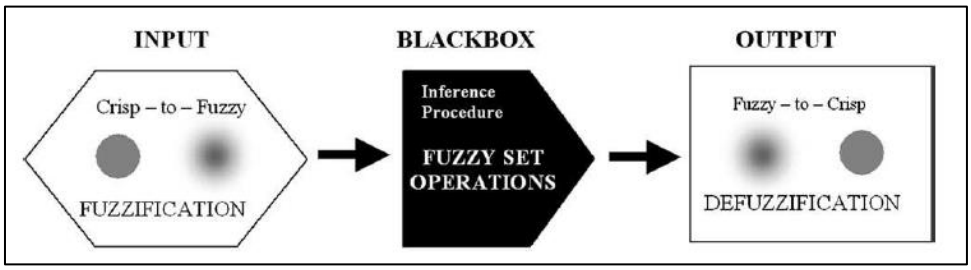

Figure 2.3: Main Stages in Fuzzy Modeling (Sicat et al., 2005)

Compared to the ANN which incorporates the humanlike thinking process to solve problems, Fuzzy Logic allows definite decision makings based on imprecise or ambiguous data. Both try to exploit the scope of using "Tolerance towards Uncertainty and imprecision", but the approaches used by each are starkly different. Whilst the Fuzzy logic is based on mathematical

modeling to incorporate imprecision and tolerance towards uncertainty, the Artificial Neural Network follows the human brain's biological model to solve the same problem. Thus, there is a possibility of Evolution and Learning for ANN whereas Fuzzy Logic is pure calculative logic taking into its faction (wherever possible), the scope of tolerance for imprecision and uncertainty and does not evolve by itself.

Keskin et al. (2009) applied FL models to analyse meteorological droughts at nine stations surroundings the Lakes District, Turkey. Analyses were performed on SPI of 3, 6, 9 and 12 months long. The simulated data from FL models were compared with data sets from ANFIS and the results showed that R^2 values of ANFIS models were higher than those of the FL models, especially for SPI-12. It was concluded that ANFIS models were effective for extreme point predictions. However, the advantage of FL models of not requiring the model structure to be known a priori can be used for hybrid models in the future. Agboola et al. (2013) investigated the ability of fuzzy rules/logic in modeling the precipitation of South Western Nigeria for better drought management. The model predicted outputs were compared with the observed rainfall data and it was concluded that fuzzy ruled based models were flexible, suitable for modeling of ill-defined scattered data. FL has also been proven to be useful in forming hybrid models for drought forecasting. Firstly, Ozger et al. (2011) combined wavelet transformation and fuzzy logic (W-FL) to forecast PDSI for the ten climate divisions in Texas and continued further studies the hybrid models by adopting the wavelet fuzzy logic (W-FL) and wavelet artificial neural network (W-ANN) to predict future long term drought events

in Texas (Ozger et al., 2012). The results showed that W-FL was more accurate for drought forecasting as compared to W-ANN. Although FL can model imprecise data and able to read "natural language" rules applied by the users, the limitation of increase in computational time when the set of fuzzy rules increases, making it less popular.

2.2.3.3 Support Vector Regression (SVR)

In 1997, Vapnik (Vapnik, 1997) introduced support vector machines (SVM) to describe properties of learning machines so that they were able to simplify unseen data (Kisi and Cimen, 2011). The learning process is unresponsive to the relative number of training cases in positive and negative classes. Unlike other Empirical Risk Minimization based learning algorithms (eg. ANN) that minimize the error over the training data set (training error), the SVM minimizes the model's generalisation error in high dimensional space, so-called Structural Risk Minimization. SVMs can be categorized into two types: support vector classification (SVC) and support vector regression (SVR).

SVR is a way of using SVMs to describe regression (Vapnik, 1997). In SVR, the functional dependency $f(\vec{x})$ between a set of sampled points $X = \{\overrightarrow{x_1}, \overrightarrow{x_2}, \overrightarrow{x_3}, \dots, \overrightarrow{x_i}\}$ taken from R^n and target values $Y = \{y_1, y_2, y_3, \dots, y_i\}$ with $y_i \in$ R will be estimated. Supposing that these samples were created separately from probability distribution function $P(\vec{x}, y)$ and a group of functions (Vapnik, 1997):

$$F = \{\mathrm{f}|\mathrm{f}(\vec{x}) = (\overrightarrow{W}, \vec{x}) + B_s : \overrightarrow{W} \in R^n, R^n \to R\} \quad (2.7)$$

where $\overrightarrow{W}$ and B_s are coefficients approximated from the input data. The aim is to obtain a function $f(\vec{x}) \in$ F that minimizes a risk functional (Cimen, 2008):

$$R[f(\vec{x})] = \int l(y - f(\vec{x}), \vec{x}) dP(\vec{x}, y) \quad (2.8)$$

where l is a loss function measuring the deviation between the target, y, and estimate $f(\vec{x})$, values. Although the risk functional cannot be minimized directly due to the reason that the distribution function $P(\vec{x}, y)$ is unidentified, the empirical risk function can be computed as (Cimen, 2008):

$$R_{emp}[f(\vec{x})] = \frac{1}{N} \sum_{i=1}^{N} l(y_i - f(\overrightarrow{x_i})) \quad (2.9)$$

where N is the number of samples. Since it is unwise to minimize empirical risk without any processes of structural control or regularization, a regularized risk function was introduced (Cimen, 2008):

$$R_{reg}[f(\vec{x})] = R_{emp}[f(\vec{x})] + \gamma \left\| \overrightarrow{W} \right\|^2 \quad (2.10)$$

where γ is a constant ($\gamma \geq 0$). By adding this term, the model space is reduced and thus the complexity of the solution is controlled, lead to the transformation of the expression into (Cimen, 2008):

$$R_{reg}[f(\vec{x})] = C_C \sum_{x_i \in X} l_{\epsilon}\left(y_i - f(\vec{x_i})\right) + \frac{1}{2}\left\|\vec{W}\right\|^2 \qquad (2.11)$$

where C_C is a pre-decided positive constant that influences a balance between an approximation error and the regression (weight) vector $\left\|\vec{W}\right\|$, which is a design parameter. ε-insensitive loss function (l_ε) is the loss function of this expression. By using it, not all the input data are required to describe the regression vector$\left\|\vec{W}\right\|$. It can be written as (Cimen, 2008):

$$l_{\varepsilon}\left(y_i - \mathrm{f}(\vec{x_i})\right) = \begin{cases} 0, \text{if } |y_i - \mathrm{f}(\vec{x_i})| < \varepsilon \\ |y_i - \mathrm{f}(\vec{x_i})|, \text{otherwise} \end{cases} \qquad (2.12)$$

This function can be used to estimate bias by combining with the regularization term ($\gamma\left\|\vec{W}\right\|^2$). When the difference between the forecasted and observed value is less than the loss function, the loss is equals to zero. The nonlinear regression function is given as (Cimen, 2008):

$$f(x) = \sum_{i=1}^{N} (\alpha_i^* - \alpha_i) K(x, x_i) + B_s \qquad (2.13)$$

where $\alpha_i{}^*, \alpha_i \geq 0$ are the Lagrange multipliers, B_s is a bias term, and $K(x, x_i)$ is the Kernel function which is based upon Reproducing Kernel Hilbert Spaces (Kisi and Cimen, 2011). The kernel function enables operations to be done in the input space as opposed to the potentially high dimensional feature space. Thus, an inner product in the feature space has an equivalent kernel in input space. Different types of functions are given by SVR, including polynomial functions, Gaussian radial basis functions, multi-layer perception functions, functions with splines, etc. (Kisi and Cimen, 2011).

Deng et al. (2011) used the Least Squares Support Vector Machine (LS-SVM) to simulate the daily soil water content of Hunan Province, southern China. Compared to the conventional SVM, LS-SVM is an improved algorithm using equality type constraints instead of inequalities. The model's performance was compared with BP-ANN and ANFIS in terms of MARE, R and MRSE. The results showed that LS-SVM was more stable and superior at soil water simulation compared to the BP-ANN and ANFIS. Chiang and Tsai (2012) compared the performance of the SVM model to three other models (ANN, maximum likelihood classifier, Bayesian classifier). The models were used to forecast reservoir drought conditions of Tsengwen Reservoir with the lead time of 10-90 days. The results showed that SVM had better performance than the other three approaches in drought forecasting. Even with the evidence of reduced accuracy for longer lead time, the accuracy of forecasting the next 50 days was still high with percentages of about 85% both in training and testing data set by SVM. Hence, SVM was concluded to have high accuracy in drought forecasting.

Chiang and Tsai (2013) improved the SVM model into a two-stage SVM model. The improved version of SVM (two-stage SVM) outperformed the original SVM and the three other approaches (ANN, maximum likelihood classifier, Bayes classifier), that were used for evaluation through comparisons. Ganguli and Reddy (2014) also applied SVM for drought forecasting over Western Rajasthan, India. Two variants of SPI-based drought forecast models were developed to simulate SPI up to 3 months lead time, which were the SVM-copula approach without seasonal partition and the SVM-copula approach with seasonal partition. It was found that the developed SVM–copula approach improved the drought prediction capability for the combined seasonal model as compared with the model without seasonal partition. Jalili et al. (2014) also explored the use of SVM in drought forecasting comparing the SVM with other models, namely the MLP-ANN and RBF-ANN in the study. The SPI drought index was used in the study but the results showed that MLP-ANN was the best performing model. The advantages of SVM were utilised by Belayneh et al. (2016) to combine with wavelet, bootstrap and boosting techniques, forming different hybrid models. The performance measures results showed that all SVM based hybrid models outperformed the ANN-based hybrid models in drought forecasting.

Borji et al. (2016) also explored the usage of SVR in drought forecasting and compared its performance with ANNs. Runoff data from Jajrood River, Iran was used to predict SDI for hydrological drought analysis. The conclusion was that the SVR has better efficiency in forecasting long-term droughts compared to ANNs due to the reason that the SVR does not fall into the trap of local errors.

Compared to ANN, SVR has the advantage of avoiding overfitting and no local minima. However, it has the same weakness shared among models with nonlinear property, and that is, it is just as computationally inefficient.

2.3 Wavelet Transformation

Wavelet transformation is the process to produce time-scale representation of a time series using mathematical functions for the purpose of non-stationaries analysis. Compared to other signal analysis techniques, wavelet transformation has the ability to uncover trends in the data such as breakdown points, discontinuities, local minima and maxima. Other than that, another popular use of wavelet analysis is to de-noise a particular data set. With the flexible choice of mother wavelet, wavelet analysis is applicable to time series of different characteristics (Adamowski and Sun, 2010). Given the advantages of wavelet transforms, it has been used a lot in drought forecasting studies, mainly coupled with AI machine learnings to produce hybrid models, and this is reviewed in Section 2.5.

There are two types of wavelet transform which are known as Continuous Wavelet Transform (CWT) and Discrete Wavelet Transform (DWT). The CWT is defined as the sum over all time of the signal multiplied by a scaled and shifted version of the wavelet function ψ (Nason and Von Sachs, 1999):

$$W(\tau, s) = \frac{1}{\sqrt{|s|}} \int_{-\infty}^{\infty} x(t)\psi^* \left(\frac{t-\tau}{s}\right) dt \qquad (2.14)$$

where s is the scale parameter; τ is the translation and * corresponds to the complex conjugate (Kim and Valdes, 2003). The CWT has been useful for processing images and signals. However, the problem of long computation time has stopped it from being popular in forecasting applications. Instead, DWT which requires less computation time and simpler to implement is more frequently used.

DWT is a simplified approach of the wavelet transform using an independent set of the wavelet scales and decomposes the time series into a mutually orthogonal set of wavelets, which is the major difference from the CWT. The original time series are decomposed into two components, high-frequency (details) component and low-frequency (approximation) component. Unlike the Fourier transform, the DWT localises a time series both in scaling and space and has some other favourable components where the wavelet function can be analysed more rapidly compare to the similar Fourier function (Kanika et al., 2012). DWT can be defined by modifying the wavelet representation to (Cannas et al., 2006):

$$\psi_{j,m}(m) = \frac{1}{\sqrt{|s_o^j|}} \sum_k \psi \left(\frac{k - m\tau_0 s_0^j}{s_0^j}\right) x(k) \qquad (2.15)$$

where j and m are integers that control the scale and translation respectively, while $s_o^j > 1$ is a fixed dilation step and τ_0 is a translation factor that depends on the dilation step.

2.4 Boosting Technique

Boosting is a technique which attempts to improve the performance of a given learning algorithm by producing a series of ensembles where each subsequent ensemble concentrates on the training cases that were not well forecasted by the previous one (Schapire, 1990; Freund and Schapire, 1996). Boosting technique able to produce satisfactory results although the weak learners (also known as "base classifiers") have slightly better accuracy than random guessing. With the accuracy of random guessing equal to 50%, a weak learner only required to achieve the accuracy of a little more than 50% (Sutton, 2005; Cordiner, 2009). Boosting was first used for classification applications, but it was "profitably extended to regression" by Hastie et al. (2009). Compared to other ensemble techniques such as bagging, boosting train the weak learners in sequence (Bishop, 2006). The training of the weak learners is done using weighted form of the data. The weighting coefficients are based on the performance of the previous weak learners where cases with poor results are given greater weight for the training of the next weak learner in the sequence.

Adaptive Boosting (Ada-Boost), one of the earliest and most famous boosting algorithms was introduced by Freund and Schapire (1997) and solved many of the previous practical difficulties of boosting algorithms (Freund and Schapire, 1999). Similar to the original boosting algorithms, Ada-Boost was designed for two-class classification tasks, with the concerns of its ability in reducing the training error. The capability of Ada-Boost algorithm has been verified empirically by many researchers (Freund and Schapire, 1999). For example, Freund and Schapire (1996) used a set of UCI benchmark datasets which aimed to find the best "decision stump" or single-best decision tree to verified the capability of Ada-Boost. Then, Schapire and Singer (2000) adopted boosting for text categorization tasks to classify a word or phrase as being either present or absent. Two years later after Ada-Boost being introduced, Friedman (1999) introduced another boosting method which fitted for regression of time series, named Least Squares Boosting (LS-Boost). The algorithms of LS-Boost differ with Ada-Boost by changing the exponential loss function to a least square loss function.

Adopting boosting technique for forecasting is a relatively new approach, thus literature review for its use in drought forecasting is limited. Based on the literature reviews done by the author, the only example of boosting technique in drought forecasting was done by Belayneh et al. (2016) to predict SPI-3, SPI-12 and SPI-24. The results also showed that using boosting ensemble technique can improve the accuracy of forecasted SPIs. Given the worth-to-explore and advantage of boosting technique, LS-Boost will be adopted in this study to produce hybrid model.

2.5 Hybrid Models

To the best understanding of the author, the first drought forecasting hybrid model used in the field of hydrology, was introduced by Mishra et al. (2007). They combined the advantages of both a linear stochastic model (ARIMA) and a nonlinear ANN model to forecast droughts in the Kansabati River basin in India using the SPI. Two kinds of hybrid ARIMA-ANN models were created in the study, namely HSNNRA and HSNNDA. The performance of the hybrid models were compared with individual ARIMA and ANN models, and the results showed that the hybrid models were able to forecast droughts with greater accuracy. Two years later, another hybrid model ANFIS was tested for its applicability for SPI forecasting in Central Anatolia, Turkey by Bacanli et al. (2009). The basic problems of fuzzy systems are the difficulties in defining the membership function parameters and the design of fuzzy if–then rules. To overcome this, the authors utilized the learning capability of ANN to generate fuzzy rule and optimize parameter automatically. Therefore, a hybrid model combining the advantages of fuzzy system and ANN, the so-called ANFIS was developed in the study. Monthly mean precipitation was used to compute the values of SPI for different time scales of 1 month to 12 months. The FFNN was used to compare with ANFIS for their performance. The results demonstrated that ANFIS was more accurate and reliable for drought forecasting. The findings described the ANFIS model as a suitable approach for drought forecasting as it combined the advantages of neural network and fuzzy logic methods.

In 2010, ANFIS were compared with ANN for their applicability in forecasting droughts for the Yazd meteorological station in Central Iran (Dastorani et al., 2010). Different architectures of ANN and ANFIS models together with various combinations of meteorological conditions were applied in the study. The results showed that both the ANN model with structure of TLRN and ANFIS were efficient tools to forecast droughts in that area. In another study (Farokhnia et al. 2011), ANFIS was once again adopted as drought forecasting tool. The study intended to examine the utility of SST and SLP global data to forecast the trend of drought events compared to EDI by using them as inputs to the ANFIS model. It was found that in all the cases, those that had applied SST/SLP datasets, had a higher accuracy. Woli et al. (2013) also used ANFIS to predict ARID for five locations in the south-eastern United States. The performance of ANFIS were compared with other approaches namely ANN, ARMA, Linear Regression and ENSO based approach (the ARID values were separated into three ENSO phases and averaged by phase). However, the results showed that ANFIS performed poorly, in general, due to the limited availability of the input data.

To further study the application of hybrid model in drought forecasting, Nguyen et al. (2015) applied the ANFIS model for forecasting the drought event at the Cai River basin in Vietnam. The precipitation, temperature and SSTA were used as the input for ANFIS to predict the SPI and SPEI. The results showed that the ANFIS model provided a satisfactory forecasted result, and it was further concluded that the SPI was more suitable in predicting the short-term drought event (1 and 3-month models) than the SPEI, whilst the SPEI was

found to be more suitable in predicting the long-term drought event (6 and 12-month models). Jalalkamali et al. (2015) applied several artificial intelligence models including ANN, SVM and ANFIS to compare with the performance of the ARIMAX model for drought forecasting at Yazd Province, Iran. The past monthly precipitation for 51 years' period was used to calculate the SPI values. All the performance of the models was evaluated by R^2 and RMSE. All the models showed good performance in forecasting drought, with the ARIMAX was slightly better for the 9-month SPI prediction, followed by ANFIS, ANN and SVM.

Further on, a hybrid model that combined wavelet transformation and fuzzy logic (W-FL) was applied to ten climate divisions in Texas to forecast the PDSI (Ozger et al., 2011). The performance of the model was compared with the traditional fuzzy logic (FL) model. Better results from the W-FL model were obtained, where the annual cycle of precipitation was dominant. They concluded that using wavelet transformation to combine with FL model can improve the performance significantly in forecasting PDSI as W-FL was capable of modeling more complex problem. Ozger et al. (2012) further studied hybrid models by adopting the wavelet fuzzy logic (W-FL) and wavelet artificial neural network (W-ANN) approaches to forecast the long lead drought event in Texas. The results showed that W-FL was more accurate for drought forecasting. Belayneh and Adamowski (2012; 2013) also compared among W-ANN, ANN and SVR using data from the Awash River Basin of Ethiopia. SPI was chosen as the drought index to represent drought in the basin, and the results indicated that the forecasted SPI values over multiple lead times had the highest

accuracy when W-ANN models were used. Belayneh et al. (2014) increased the number of model comparisons by developing a new W-SVR model for the same river basin as the previous studies. Accordingly, it was the first time that W-SVR models had been studied and verified for long-term SPI forecasting. However, the results of the RMSE, MAE and R^2 showed that W-ANN had better performance compared to W-SVR. Mehr et al. (2014) also developed a new hybrid model called wavelet–linear genetic programing (W-LGP), for long lead-time drought forecasting. The results were promising, showing that W-LGP can be effectively used for the forecasts of 3-, 6-, and 12-month lead times drought conditions. Additionally, they found that the W-LGP was slightly less precise than the W-FL and W-ANN models as the original time series in both W-FL and W-ANN models were decomposed prior to training.

The benefit of using the wavelet decomposition was further studied by Djerbouai and Souag-Gamane (2016), where the meteorological drought was forecasted in the western part of the Algerois Catchment. Similar to the previous studies, SPI-12 for all the models were considered the best parameter to model the drought event for all the lead times (1-month to 6-month). Additionally, the hybrid model W-ANN was better than the other two models (ARIMA and ANN) for all the time scales and lead times. It was found that the wavelet transform had the ability to reduce the complexity of a given time series, thus managed to reduce the number of hidden neurones and saved the computation time. The extent of adopting the wavelet transform with the extreme machine learning was studied by Deo et al. (2016). A wavelet-based extreme learning machine (W-ELM) was proposed to forecast the monthly EDI for three hydrological stations

in Australia. The performance of the W-ELM was compared with the ANN, LS-SVR and their wavelet-equivalent models (W-ANN and W-LS-SVR). The results showed that W-ELM was the best among the models. Moreover, W-ELM model was found computationally efficient as running time was faster, and most of the predicted errors were considered low.

In spite of the fact that these hybrid models, with the combination of two models, showed satisfactory prediction accuracy, many researchers however attempted to improve the hybrid models using a combination of three models. Shirmohammadi et al. (2013) came up with a three-layer hybrid model, Wavelet-ANFIS (W-ANFIS) by combining wavelet transformation with the existing hybrid model, ANFIS. The capability of this model was evaluated by comparing with W-ANN, ANN and ANFIS. The results showed that ANFIS models forecasted more accurately than ANN models, and also demonstrated that wavelet transform can improve meteorological drought modeling. This showed that the performance of wavelet-hybrid models is quite promising. This was further proven by Shabri (2014) through his study on W-ANFIS model in Malaysia. W-ANFIS was once again proven to be outperforming the traditional ANFIS and ARIMA models. Other than combining ANFIS model with the wavelet transform, Memarian et al. (2016) further improved the performance of ANFIS by integrating fuzzy inputs with modular neural network to increase the accuracy in estimating complex functions, namely the co-active neuro-fuzzy inference system (C-ANFIS). The results showed that C-ANFIS succeeded in predicting drought events in Birjand climate region with the advantage of requiring less inputs compared to statistical models.

Belayneh et al. (2016) explored the ability of wavelet transforms, bootstrap and boosting ensemble techniques in developing reliable ANN and SVR models for drought forecasting. The bootstrap artificial neural network (BS-ANN), bootstrap support vector regression (BS-SVR) and their wavelet coupled bootstrap ensemble (W-BS-ANN and W-BS-SVR) models were used to forecast the SPI-3, SPI-12 and SPI-24. The results showed that using boosting ensemble technique can improve the accuracy of forecasted SPIs. Besides, wavelet analysis also enhanced the performance of all models though its capability in de-noising. Thus, the wavelet boosting SVR (W-BS-SVR) model provided better forecast accuracies compared to other assessed models. A year later, Prasad et al. (2017) evaluated the capability of iterative input selection (IIS) method in aiding W-ANN, benchmarking with the M5 Tree model. The area selected in the study was the Murray-Darling Basin, Australia and monthly streamflow water levels of the basin were used as input to develop the models. The results showed that the IIS-W-ANN model outperformed W-ANN models and the IIS-W-ANN model accuracy outweighed the IIS-W-M5 model. Hence, iterative input selection was concluded as a useful model enhancing method for streamflow forecasting models. Given the ability of increasing the performance by combining multiple models or methods, this type of forecasting method seemed to be the trend currently.

2.6 Summary

In summary, the PN is a robust index to show and explain to public but it is not ideally operational in use for planning and management due to its lack of statistical transformation. The PDSI is an extremely efficient index in measuring the effect of soil moisture sensitivity and providing excellent descriptions of historical droughts as it includes the parameter of evapotranspiration and soil moisture. However, complex computations and requirement of substantial data limited it its use. The same goes for the CMI as the major difference of the PDSI and the CMI is the former analyses the long-term dry and wet seasons, while the latter was developed to analyse short-term moisture across the main crop producing areas. The EDI is one of the simplest DI available as it requires only rainfall data to be computed. It is normally used to calculate daily drought severity, and with its advantages of quick detection and detailed measurement of short term drought, it is always used to define meteorological droughts.

The SPI is the most commonly used index for drought monitoring and forecasting due to its simplicity of only requiring rainfall data as input and variability of being able to be calculated in different time scales. However, the effect of potential evapotranspiration was not considered in the SPI and it was not negligible. Hence, the SPEI which correlates better with hydrological (rainfall) and ecological (temperature) variables while having advantage of being able to be calculated for different time scales was chosen as the drought indicator in this study. The limitation of the data availability of only having

rainfall and temperature data at the basin, is also a reason for not choosing other indices such as the PDSI or the CMI which requires soil moistures records.

As for the drought forecasting models, they can be grouped in to three different categories, which are the time series analysis or stochastic models, the probability models and the artificial intelligence-based models. For stochastic models, the most well-known model is ARIMA. It was the most popular model being used for drought forecasting before the AIs models outperformed them with the innate nonlinear property and flexibility for modelling. Then, another type of model named Markov Chain which uses mathematical technique to obtain the probabilities of the system using a set of probabilities of transitions from one state to another. Studies show that it is a good forecasting model with high accuracy. However, this approach is not the focus of this study.

For the third group of models – AIs, they are the most popular models in recent years. This is due to their flexibility and adaptability in forecasting the occurrence of drought that poses varying durations, frequencies and intensities. In the group, there are three main type of models: ANN, FL and SVR. Artificial Neural Networks (ANN) are flexible nonlinear models that resemble the structure of a nerve system. It forecast droughts by adapting into the data inserted and discover patterns from it without involving any mathematical techniques. Fuzzy Logic (FL), in contrast with ANNs, is based on mathematical modelling to incorporate imprecision and tolerance towards uncertainty, causing it unable to evolve by itself. While for the Support Vector Regression (SVR), it's like ANNs it forecast drought by learning from the inserted data, but

however, the learning processes are done by Structural Risk Minimization which is insensitive to the relative number of training examples, unlike that of ANNs which does not adhere to Empirical Risk Minimization.

Two other model improving techniques which are popular in recent years were also reviewed in this study. The two techniques are the wavelet transformation and the boosting technique. Wavelet transform reveals trends in the time series by giving the data a time-scale representation. Then, boosting technique boost the performance of a model by producing a series of ensembles where each subsequent ensemble concentrates on the training cases that were not well forecasted by the previous one

With the advantages of the SVR not limited by the time series size, it was chosen as the base model for the hybrids being proposed in this study. Other than that, the FSVR which have never been explored for its capability in drought forecasting, will be adopted in this study as well. Wavelet transforms and boosting technique which were suggested by the reviewed papers to be useful in improving models' performance, is also proposed to be combined with the SVR.

In this study, three different hybrid models namely, the Multi-Input Wavelet Fuzzy Support Vector Regression (M-W-FSVR), the Weighted Wavelet Fuzzy Support Vector Regression (W-W-FSVR) and the Wavelet Boosting Support Vector Regression (W-BS-SVR) models will be the focus on drought forecasting modelling.

CHAPTER 3

METHODOLOGY

3.1 Workflow/Flowchart

The workflow (Figure 3.1) of this study is summarized as follows. First, the raw input data, rainfall and temperature from the year 1976 to 2015, were collected from respective departments. After that, the homogeneity tests including the Standard Normal Homogeneity Test (SNHT), the Buishand Range Test (BR), the Pettitt Test (PeT) and the Von Neumann Ratio Test (VNR) were performed to check the homogeneity of the rainfall data based on 95% confidence interval. Thereafter, the rainfall data were combined with temperature data to develop SPEI with time scales of 1-month (SPEI-1), 3-month (SPEI-3) and 6-month (SPEI-6).

For model development, the Discrete Wavelet Transformation were conducted on the developed SPEIs, using Daubechies as the mother wavelet and decomposed up to the maximum allowable level in MATLAB. Then, the transformed SPEI series were used as the inputs for the next stage. For the development of the Multi-Input Wavelet Fuzzy Support Vector Regression (M-W-FSVR) model and the Weighted Fuzzy Support Vector Regression (W-W-FSVR) model, fuzzy membership values for each data points of wavelet tranformed SPEIs were estimated using fuzzy membership function Equation (3.21) . Then, the fuzzy membership values were used as an additional training

input (for the M-W-FSVR) or as the weightage of each data points of the input (for the W-W-FSVR). The algorithm, 'fitensemble' function in MATLAB was used to boost the wavelet transformed data for the Wavelet Boosting Support Vector Regression (W-BS-SVR) model, using Mean Absolute Error (MAE) to estimate the optimum number of learning cycles. After that, respective results were used to train and validate in the Support Vector Regression (SVR) stage. For SVR, the input data were partitioned into 90% for training and 10% for validation, with the two important parameters C and Epsilon estimated using Equation (3.22) and Equation (3.23) respectively.

Thereafter, the performance of the M-W-FSVR, W-W-FSVR and W-BS-SVR models were evaluated using commonly used performance measures, including MAE, RMSE and Bias. Finally, the best model was determined based on the conditions of (i) the MAE and RMSE of lowest value, and (ii) the Bias of lowest magnitude (prioritizing positive values as overpredictions are favourable over underpredictions), but priority will be given to the first condition.

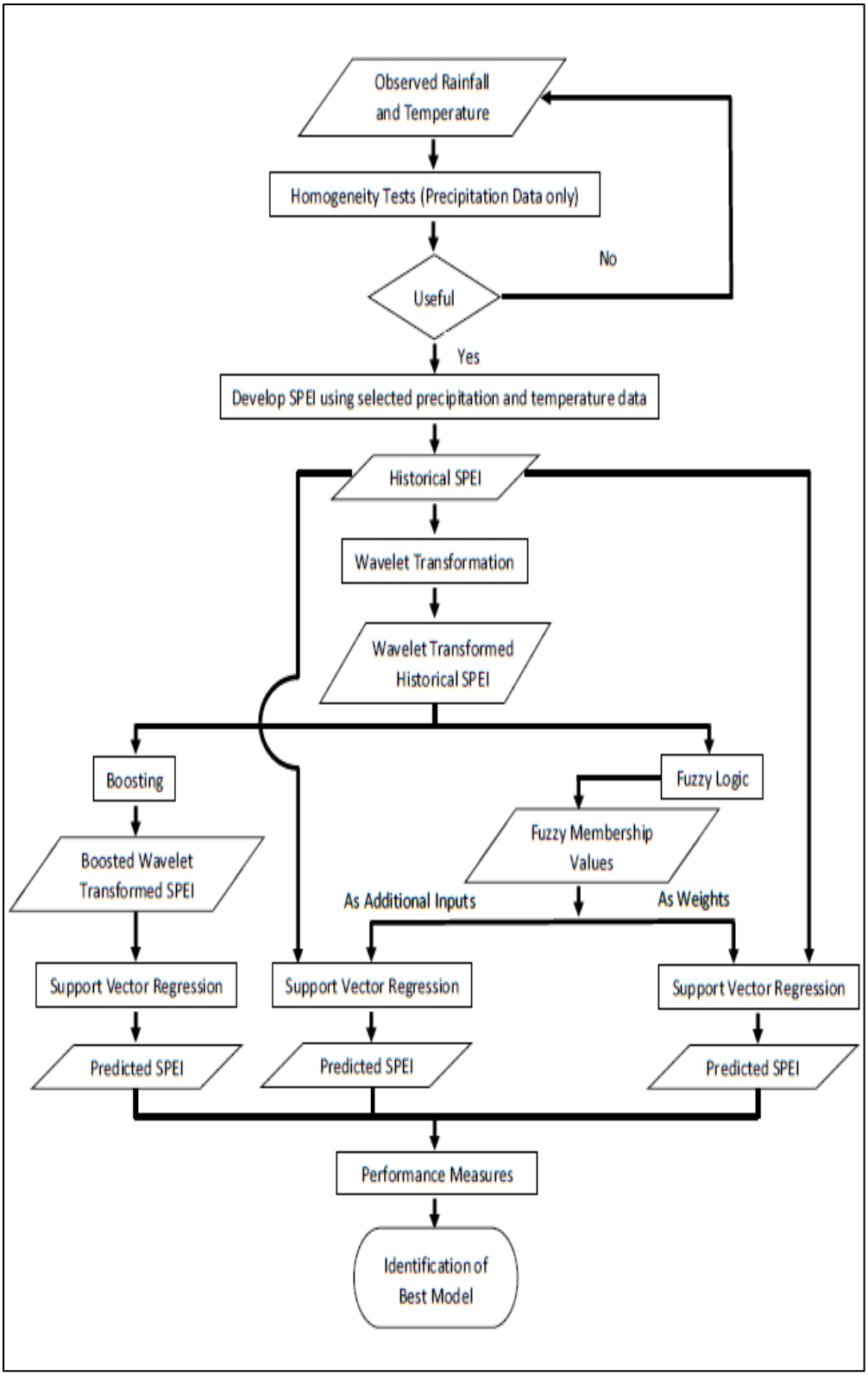

Figure 3.1: Overall Workflow/Flowchart

3.2 Location of Study, Data Acquisition and Data Repairing

The study area for this research is the Langat River Basin which located in the states of Selangor and Negeri Sembilan, within latitudes 2^{o} 40’ 152” to 3^{o} 16’ 15” and longitudes 101^{o} 19’ 20” to 102^{o} 1’ 10” (Juahir et al., 2011). It has a total area of approximately 2,400 km^{2} and has two dams, the Langat Dam and the Semenyih Dam both located upstream. These two dams supply water to the households and the industrial areas, which are Putrajaya, Hulu Langat, Kuala Langat, Sepang, Petaling and Cheras. Meanwhile, the Langat Dam also serves as a hydro-power plant with a limited energy capacity for the population within the Langat River Basin. Langat Dam and Semenyih Dam were built in 1981 and 1982 repectively. The length of the main river is about 141 km, located at 40 km east from Kuala Lumpur. The Langat River has a few tributaries, namely the Semenyih River, the Beranang River and the Labu River (Juahir et al., 2011). An estimated area of 847 km^{2} oil palm plantations (through QGIS and Google Satellite images) were located at the downstream section of the Langat River Basin. Figure 3.2 shows the locations of the Langat River Basin, rainfall stations, temperature station, dams, landuse and tributaries.

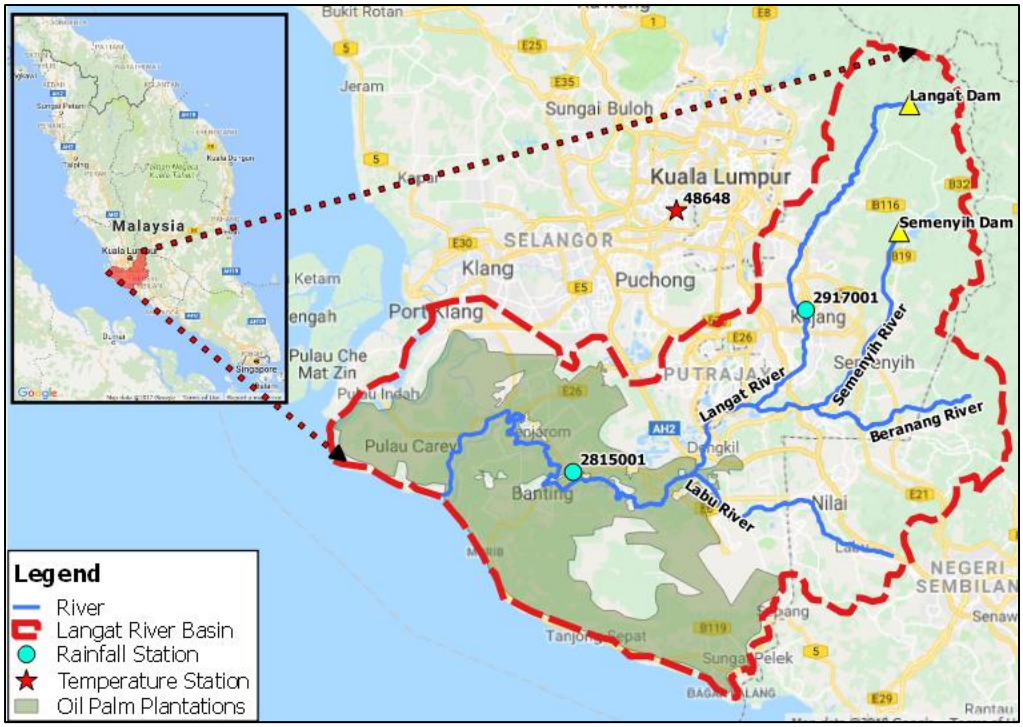

Figure 3.2: Map of Langat River Basin with the locations of meteorological stations, dams and land use

As shown in Figure 3.2, rainfall stations s2815001 (downstream) and s2917001 (upstream) together with temperature station s48648 were selected to retrieve data for this study. The rainfall data were retrieved from the Department of Irrigation and Drainage (DID) Malaysia while the temperature data were from the Malaysian Meteorology Department (MMD). The location of selected stations in Langat River Basin are illustrated in Figure 3.2 and the detailed characteristics of these stations are tabulated in Table 3.1. After obtaining the historical data from the rainfall and temperature stations, data repairing procedure was carried out to obtain the missing rainfall data. The method used was Four Quadrant Method (Sharp and Sawden, 1984), as illustrated in Figure 3.3 where “h” represents rainfall data and “d” represents distance between stations.

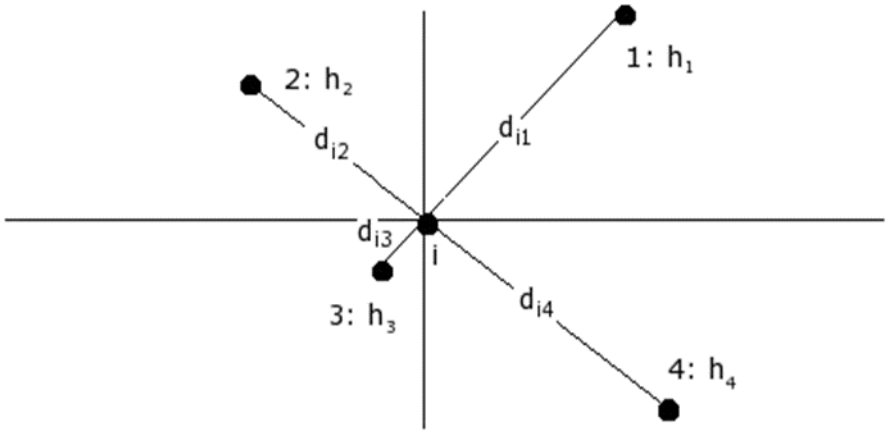

Figure 3.3 Four Quadrant Method

Table 3.1: Details of the selected stations

Station Code	Station Name	Latitude	Longitude	Elevation above sea level (m)	Data Available	Record's Period
2815001	Pejabat JPS Sg. Manggis	2°49'35" N	101°32'30" E	3	Daily Rainfall	1976-2015
2917001	RTM Kajang	2°59'46" N	101°47'09" E	39	Daily Rainfall	1976-2015
48648	Petaling Jaya	3°06'00" N	101°39'00" E	45.7	Daily Temperature	1976-2015

3.3 Test of Homogeneity

For rainfall data, four different homogeneity tests; the Standard normal homogeneity test (SNHT), Buishand range (BR) test, Pettitt test (PeT) and Von Neumann ratio (VNR) test were used to test the homogeneity of the rainfall data.

For the tests, null hypothesis, H_0 assumed that the time series was independent and identically distributed (homogeneous) while alternative hypothesis, Ha assumed the series consists of breaks in the mean (inhomogeneous). All three tests were performed because SNHT is sensitive in indentifying the breaks near the beginning and the end of the series while BR and PeT were used to detect the break in the middle of the series. On the other hand, VNR test assumed the same null hypothesis (homogeneous) as the previous three tests but for alternative hypothesis it assumed that the series was not randomly distributed (inhomogeneous). Table 3.2 summarizes the 5% critical values for the four homogeneity tests as a function of n, number of years.

Table 3.2: The 5% Critical Values for the homogeneity tests.

n	T_0 (SNHT)	$R/\sqrt{n}$ (BR)	X_E (PeT)	N (VNR)
20	6.95	1.43	57	1.30
30	7.65	1.50	107	1.42
40	8.10	1.53	167	1.49
50	8.45	1.55	235	1.54

3.3.1 Standard Normal Homogeneity Test (SNHT)

Alexanderson (1986) developed Standard Normal Homogeneity Test which describes a statistic T_k to compare between the mean of the first k years and the last year (n - k) years. It is sensitive in detecting the breaks near the beginning and the end of the series.

$$T_k = k\overline{z_1^2} + (n-k)\overline{z_2^2}\,, k = 1,2,\dots,n \tag{3.1}$$

$$\overline{z_1} = \frac{1}{k}\sum_{i=1}^{k}\frac{(Y_i - \bar{Y})}{s} and\ \overline{z_2} = \frac{1}{n-k}\sum_{i=k+1}^{n}\frac{(Y_i - \bar{Y})}{s} \tag{3.2}$$

where s is the standard deviation of the series. T_k comes to a maximum near the year k=K when a break occurs at the year K. T_0 is defined as:

$$T_0 = \max_{1\le k\le n} T_k \tag{3.3}$$

The critical value of $\frac{R}{\sqrt{n}}$ is given by Alexanderson (1986) in Table 3.2.

3.3.2 Buishand Range Test (BR)

Buishand Range test detects dataset that break in the middle of the series. The adjusted partial sums are shown as below;

$$S_0^* = 0 \text{ and } S_i^* = \sum_{i=1}^{k} (Y_i - \bar{Y}), k = 1,2, \dots, n \quad (3.4)$$

where S_i^* is the cumulative deviations from the mean. The values will fluctuate around 0 when the series is homogeneous and reaches a maximum or a minimum near the year *k*= *K* if there is a break in year *K*. The significance shift in the series can be tested by 'rescaled adjusted range' R which can be obtained through:

$$R = \frac{\left(\max_{0 \le k \le n} S_k^* - \min_{0 \le k \le n} S_k^*\right)}{s} \quad (3.5)$$

where *s* is the standard deviation of the series. The critical value of $\frac{R}{\sqrt{n}}$ is given by Buishand (1982) in Table 3.2.

3.3.3 Pettitt Test (PeT)

Pettitt test is a non-parametric rank test which used to identify break in the middle of series. However, it has poorer sensitivity to outliers than other tests. The statistic was evaluated by

$$X_k = 2\sum_{i=1}^{k} r_i - k(n+1)\,, k = 1,2, \dots, n \quad (3.6)$$

where r_i is the rank of the observations. When breaks occur in the year E, the statistic reaches a maximum or a minimum near the year $k = E$:

$$X_E = \max_{1 \le k \le n} |X_k| \tag{3.7}$$

The critical values of X_E is given by Pettitt (1979) in Table 3.2.

3.3.4 Von Neumann Ratio (VNR) Test

Von Neumann Ratio test evaluated whether the series was randomly distributed. It is known as the ratio of the mean square successive difference to the variance (Von Neumann, 1941):

$$N = \frac{\sum_{i=1}^{n-1}(Y_i - Y_{i+1})^2}{\sum_{i=1}^{n}(Y_i - \bar{Y})^2} \tag{3.8}$$

N value determined the homogeneity of series, with the value of 2, it reflected the series was homogenous. N inclines to values lower than 2 if the dataset contains a break in the series and greater than 2 when the dataset has rapid variations in the mean. The significance level for N is given in Table 3.2.

3.3.5 Assessment of Results

The test results were tabulated and classified. There were three classes of classification, Class A, Class B and Class C. The details on how to carry out the classifications are shown below (Wijngaad et al., 2003).

Class A: Useful

One or none null hypothesis of the four tests was rejected at 5% significance level. If test results were categorized under this class, the series was concluded to achieve homogeneity and can be used for further analysis.

Class B: Doubtful

Any two null hypotheses of the four tests was rejected at 5% significance level. If test results were categorized under this class, the series was concluded as showing inhomogeneous signal and should be diagnostically reviewed before further analysis.

Class C: Suspect

Three or all null hypotheses of the four tests was rejected at 5% significance level. If test results were categorized under this class, the series was concluded as inhomogeneous series signal and cannot be used for further analysis.

3.4 Development of the SPEI

SPEI was calculated using the concept of deficit or surplus of water, which is the weekly or monthly difference between precipitation and potential evapotranspiration, as shown below:

$$D_i = P - PET \tag{3.9}$$

where D_i is the difference between precipitation and potential evapotranspiration, P is the total precipitation over a period of time and PET represents the potential evapotranspiration

It can be computed by different time scales such as 1-month, 3-month and 6-month, allowing the evaluation of the type of droughts affecting shortage of water resources. Based on the standard operating procedure mentioned in Malaysia Meteorological Department (2014), monitoring and management of droughts in Malaysia are done based on SPI index of time scales up to 6 months. Since SPEI has multi-scale nature that is similar with SPI, the time scales of SPEI adopted in this study are 1, 3 and 6 months and computed using the observed data from years 1976-2015. SPEI-1, SPEI-3 and SPEI-6 were selected to represents meteorological, agricultural and hydrological droughts (WMO, 2012).

Unlike the calculation of the SPI that adopts the probability distribution, the SPEI applies three-parameter distribution where the log-logistic distribution f(x) is given by:

$$f(x) = \frac{\beta}{\alpha}\left(\frac{x-\gamma}{\alpha}\right)^{\beta-1}\left[1+\left(\frac{x-\gamma}{\alpha}\right)^{\beta}\right]^{-2} \tag{3.10}$$

where α represents the scale, β represents the shape, γ represents the origin parameters, for D values in the range (γ>D<∞). They can be determined using the L-moment method (Ahmad et al., 1988) as:

$$\beta = \frac{2w_1 - w_0}{6w_1 - w_0 - 6w_2} \tag{3.11}$$

$$\alpha = \frac{(w_0 - 2w_1)\beta}{\Gamma\left(1+\frac{1}{\beta}\right)\Gamma\left(1-\frac{1}{\beta}\right)} \tag{3.12}$$

$$\gamma = w_0 - \alpha\Gamma\left(1+\frac{1}{\beta}\right)\Gamma\left(1-\frac{1}{\beta}\right) \tag{3.13}$$

where Γ is the gamma function of β and w_l(l=0, 1, 2…) can be computed by probability weighted moments (PWMs) through the L-moment method (Hosking and Wallis, 1997);

$$w_l = \frac{1}{n}\sum_{i=1}^{n} x_i \left(1 - \frac{i-0.35}{n}\right)^{l} \tag{3.14}$$

where x_i is the ordered random sample ($x_1 < x_2 \ldots < x_n$) of D and n represents the sample size. Then, the probability distribution function can be calculated as shown below:

$$F(x) = \left[1 + \left(\frac{\alpha}{x - \gamma}\right)^{\beta}\right]^{-1} \tag{3.15}$$

At last, the computed $F(x)$ are converted into Z-standardized normal values to obtain the SPEI values by using the classical approximation provided by Abramowitz and Stegun (1965).

$$SPEI = W - \frac{c_0 + c_1 W + c_2 W^2}{1 + d_1 W + d_2 W^2 + d_3 W^3} \tag{3.16}$$

$$W = \sqrt{-2\,ln(P)} \qquad \text{for P}\leq 0.5 \tag{3.17}$$

where P represents the probability of exceeding a determined D value,

$c_0 = 2.515517$, $c_1 = 0.8082853$, $c_2 = 0.010328$,

$d_1 = 1.432788$, $d_2 = 0.189269$, $d_3 = 0.001308$.

If P>0.5 then P will be replaced by 1-P and the sign of the resultant SPEI is reversed. With different time scales, the sensitivity of the SPEIs varies.

Thus, Average Moving Range (MR) was adopted to estimate the variations in the series (Montgomery and Runger, 2014), as shown in Equation (3.18):

$$MR = \frac{1}{m-1}\sum_{i=2}^{m}|X_i - X_{i-1}| \tag{3.18}$$

where *X* represents the values of SPEI and m represents the data size.

3.5 Wavelet Transformation of the SPEIs

When conducting wavelet analysis, optimum mother wavelet that is suitable for the time series must be chosen. There is no direct way to determine the optimum mother wavelet. However, according to Maheswaran and Khosa (2011), Daubechies (with vanishing moments of 2) showed better capability in forecasting hydrologic time series with long term features (eg. monthly). Therefore, it was adopted in this study. While for the optimum number of decomposition levels, maximum number of eight was allowed in MATLAB and hence, the wavelet transformations in this study was carried out to the decomposition level of eight. Equation (3.19) which was suggested by de Artigas, et al. (2006) to estimate the maximum decomposition level was also used as a guideline in this study.

$$max.L = \frac{log(\frac{N}{2v-1})}{log2} \tag{3.19}$$

where v is the number of vanishing moments or half of the starting filter length,

N is the number of samples

After decomposing the input signals to their low and high frequency components (approximation and details), the chosen series was fed into subsequent hybrid models. The chosen series was the approximation components as generalized models were desired and usually, the approximation series alone resulted in the best prediction results.

3.6 Multi-Input Wavelet Fuzzy Support Vector Regression (M-W-FSVR) and Weighted Fuzzy Support Vector Regression (W-W-FSVR)

After carrying out wavelet transformation for each SPEIs, fuzzy membership values were obtained through fuzzifying the series using the fuzzy membership function suggested by Lin and Wang (2002) to reduce the effects of outliers. Since the equations require the data sets to be separated into positive and negative classes, the SPEIs were separated into wet (SPEI>0) and dry (SPEI< or = 0) periods to carry out the tasks. Equation (3.20) show the radius of class and Equation (3.21) show the fuzzy membership functions.

$$r_+ = max|x_+ - x_i| \text{ for positive class}$$
$$r_- = max|x_- - x_i| \text{ for negative class} \quad (3.20)$$

where r_+ and r_- are the radius of positive and negative classes,

x_+ and x_- are the mean of positive and negative classes.

$$s_i = 1 - |x_+ - x_i|/(r_+ + \sigma) \textit{ for positive class}$$
$$s_i = 1 - |x_- - x_i|/(r_- + \sigma) \textit{ for negative class} \quad (3.21)$$

where s_i is the fuzzy membership values.

With these, the fuzzy membership values, s_i corresponding to each wavelet transformed SPEI data points were produced. Thereafter, fuzzy membership values, wavelet transformed historical SPEI and targeted historical SPEI with lead time of 1-month, 3-month and 6-month were imported to the 'fitrsvm' function in MATLAB for training and validation of SVR. For the M-W-FSVR model, the generated fuzzy membership values were used as additional inputs together with wavelet transformed SPEIs (two input variables) to transform training points from $\{(x_1, y_1), \dots, (x_i, y_i)\}$ to $\{(x_1, s_1, y_1), \dots, (x_i, s_i, y_i)\}$. For the W-W-FSVR model, the fuzzy membership values were used as weights for SVR training part, which is allowed in the 'fitrsvm' function of MATLAB and only available since year 2015.

As aforementioned, this study used the 'fitrsvm' function in MATLAB for training and validation of SVR. SPEIs of years 1976-2011 (90%) were used for subsequent mandatory training and years 2012-2015 for validation thereafter (10%). In the case of nonlinear regression, an SVM uses Radial Basis Function, rbf kernels due to its ability in parameters tuning to cope with different pattern

analysis (Kecman, 2001). Thus, two important parameters, parameters *C* and *Epsilon* have to be estimated in the study. According to Kisi and Cimen (2011), parameter C is responsible for the balance between the model complexity and the degree of deviations (from Epsilon) to be tolerated, whereas Epsilon determines the width of 'epsilon-insensitive zone' (for the fitting of trainnig data). As suggested by Cherkassky and Ma (2004), the parameters *C* and *Epsilon* for rbf kernel were estimated based on Equation (3.22) and Equation (3.23):

$$C = \max(|\bar{y} + 3\sigma_y|, |\bar{y} - 3\sigma_y|) \tag{3.22}$$

where $\bar{y}$ and σ_y are the mean and standard deviation of the y values of training data (targetted data).

$$\varepsilon = 3\sigma\sqrt{\frac{\ln n}{n}} \tag{3.23}$$

where σ is the standard deviation of noise and n is the data size.

3.7 Wavelet-Boosting-Support Vector Regression (W-BS-SVR)

The W-BS-SVR models were trained in exactly the same way as the M-W-FSVR model with the 'fitrsvm' function in MATLAB with the exception that it has only one input series called boosting ensembles, which is the wavelet

transformed SPEIs that was further processed through boosting ensemble technique.

All boosting ensembles in this study were developed in MATLAB using 'fitensemble' function. At every step, the ensemble creates a new learner by observing the difference between the observed response and the accumulated prediction of all learners created previously. The'fitensemble' function fits to minimize the mean absolute error. The 'fitensemble' function fits every new learner to:

$$y_n - \eta f(x_n) \tag{3.24}$$

where y_n is the observed response, $f(x_n)$ is the aggregated prediction from all weak learners created so far for observation x_n and η is the learning rate. Within this function, the appropriate ensemble function, the appropriate weak learner and the number of learning cycles had to be selected. The LS Boost ensemble function was chosen as this boosting technique is appropriate for regression and forecasting problems (Belayneh et al., 2015). For the appropriate weak learner, 'Decision Tree' which was recommended in MATLAB documentation (Mathworks, 2011) was chosen. In determining the number of learning cycles, balancing the need for accuracy and model development speed was important. Larger ensembles take longer to train and can become over trained when too large (Cordiner, 2009). Thus, the optimum number of learning cycles was determined using MAE, which was estimated from the difference between the boosted SPEIs and targeted SPEIs.

After that, the boosted SPEIs produced using optimum parameters were used for SVR with function ‘fitrsvm’ in MATLAB. Similar to SVR of Section 3.6, the data was partitioned into 90% for training and 10% for validation, while parameters *C* and *Epsilon* were determined using Equation (3.22) and Equation (3.23).

3.8 Performance Measures

The proposed hybrid models were evaluated based on the comparisons between predicted and historical values. The mean absolute error (MAE), root mean square error (RMSE) and Bias are the performance criteria used in this study.

3.8.1 Mean Absolute Error (MAE)

The MAE measures the average magnitude of the errors in a set of predictions, without considering their direction. It is the average of the absolute differences between prediction and actual observation where all individual differences have equal weight. In this study, the MAE measures how close predicted SPEI are to the historical SPEI. The lower the value of MAE, the lower the average absolute difference between predicted and historical SPEI, the better the performance of the model.

$$MAE = \sum_{i=1}^{N} \frac{|\hat{y}_i - y_i|}{N} \tag{3.25}$$

where $\overline{y_i}$ is the mean value taken over N,

y_i is the historical SPEI,

$\hat{y}_i$ is the predicted SPEI,

N is the number of samples.

3.8.2 Root Mean Square Error (RMSE)

The RMSE measures the variance of errors independently of the sample size. It is a quadratic scoring rule that also measures the average magnitude of the error. However, it is the square root of the average of squared differences between prediction and actual observation. Since the errors are squared before they are averaged, the RMSE gives a relatively high weight to large errors. Hence, the RMSE is more useful to detect large errors. Similarly, the lower the value of RMSE, the lower the average squared difference between predicted and historical SPEI, the better the performance of the model.

$$RMSE = \sqrt{\frac{\sum_{i=1}^{N}(\hat{y}_i - y_i)^2}{N}} \tag{3.26}$$

where the variables have been defined in the previous section.

3.8.3 Bias

Similar to the MAE, the Bias measure the average of the errors in a set of predictions. However, the Bias also consider the direction of the predictions, unlike the MAE which only consider the magnitude. Hence, it is able to indicate the condition of over or under prediction through positive or negative values of the average errors. Since the predictions are about drought (natural disaster) in this study, over prediction is preferable when the Bias does not equal to zero.

$$Bias = \sum_{i=1}^{N} \frac{\widehat{y_i} - y_i}{N} \tag{3.27}$$

where the variables have been defined in the previous section.

CHAPTER 4

RESULTS AND DISCUSSIONS

4.1 Data Acquisition, Data Repairing and Homogeneity Tests

Based on the data retrieved from DID and MMD, the number of missing data from each station were tabulated as Table 4.1. as shown in the table, there are 745 missing data for station s2815001 and 847 missing data for station s2917001. Hence, data repairing using Four Quadrant Method was carried out before proceeding to homogeneity tests.

Table 4.1: Number of missing data for station s2815001, s2917001 and s48648

Station	Number of Missing Data
s2815001	745
s2917001	847
s48648	0

After the repairing of data, homogeneity tests using the Standard Normal Homogeneity Test (SNHT), the Buishand Range (BR) test, the Pettitt (PeT) test and the Von Neumann Ratio (VNR) test on precipitation data of stations s2815001 and s2917001 were carried out and the results are shown in Table 4.2**.** Based on the results, the p-values of four tests of station s2815001 for the months Jan, Mar, Apr, May, Jun, Jul, Aug, Sep, Oct and Nov are more than 0.05. For Feb and Dec, each had one failed test (null hypothesis rejected) with results of 0.036 (PeT) and 0.003 (SNHT) respectively. For station s2917001, most of

the precipitation data passed all four tests with p-values of more than 0.05, except in Apr when the homogeneity test (VNR) failed with the p-value of only 0.001.

With the p-values acquired, both stations achieved Class A for the homogeneity tests for all the months (Wijngaard et al., 2003). Since Class A is the desired results for the homogeneity test, the precipitation data from s2815001 and s2917001 were combined with temperature data from station 48648 to generate the SPEI with different time scales, as shown and discussed in Section 4.2.

Table 4.2: Homogeneity Test Results for station s2815001 and s2917001

Station	Homogeneity Tests	Jan	Feb	Mar	Apr	May	Jun	Jul	Aug	Sep	Oct	Nov	Dec
s2815001	PeT	0.897	**0.036**	0.433	0.503	0.382	0.332	0.755	0.977	0.869	0.867	0.897	0.277
	SNHT	0.100	0.625	0.551	0.582	0.965	0.178	0.647	0.259	0.509	0.063	0.100	**0.003**
	BR	0.397	0.941	0.461	0.494	0.780	0.843	0.359	0.531	0.669	0.275	0.397	0.077
	VNR	0.807	0.746	0.252	0.319	0.425	0.579	0.409	0.066	0.679	0.101	0.196	0.148
Class	Class	A	A	A	A	A	A	A	A	A	A	A	A
s2917001	PeT	0.688	0.655	0.584	0.785	0.777	0.667	0.704	0.229	0.544	0.206	0.688	0.405
	SNHT	0.449	0.707	0.584	0.480	0.563	0.587	0.549	0.409	0.326	0.692	0.449	0.417
	BR	0.190	0.826	0.359	0.676	0.700	0.322	0.396	0.351	0.369	0.648	0.190	0.201
	VNR	0.964	0.312	0.401	**0.001**	0.262	0.877	0.732	0.500	0.290	0.532	0.393	0.123
Class	Class	A	A	A	A	A	A	A	A	A	A	A	A

4.2 Development of SPEI

As aforementioned, temperature data from station 48648 were combined with the precipitation data from station s2815001 and s2917001 respectively, to estimate the drought index SPEI. Next, the SPEI-1, SPEI-3 and SPEI-6 were

developed in this study and average moving range values were adopted as an indicator for their variations in the series/sensitivity toward changes. Figure 4.1 and Figure 4.2 show the SPEIs of s2815001 and s2917001 respectively, with their average moving range values being stated in the graphs.

Compared to SPEI-1, both SPEI-3 and SPEI-6 are longer term SPEIs and thus less sensitive to any changes in monthly precipitation and/or temperature within the long term record. Since SPEI-3 and SPEI-6 are longer cumulative indices than SPEI-1, the onset of drought only becomes obvious at longer timeframe, as shown in both Figure 4.1 and Figure 4.2. As expected, SPEI-1 which is most sensitive to changes acquired the highest average moving range values of 1.0942 for s2815001 and 1.1565 for s2917001, respectively. For SPEI-3 and SPEI-6 that are less sensitive, it is characterised with lower average moving range values of 0.6472(SPEI-3) and 0.5622(SPEI-6) for s2815001, and 0.6905(SPEI-3) and 0.4075(SPEI-6) for s2917001, respectively.

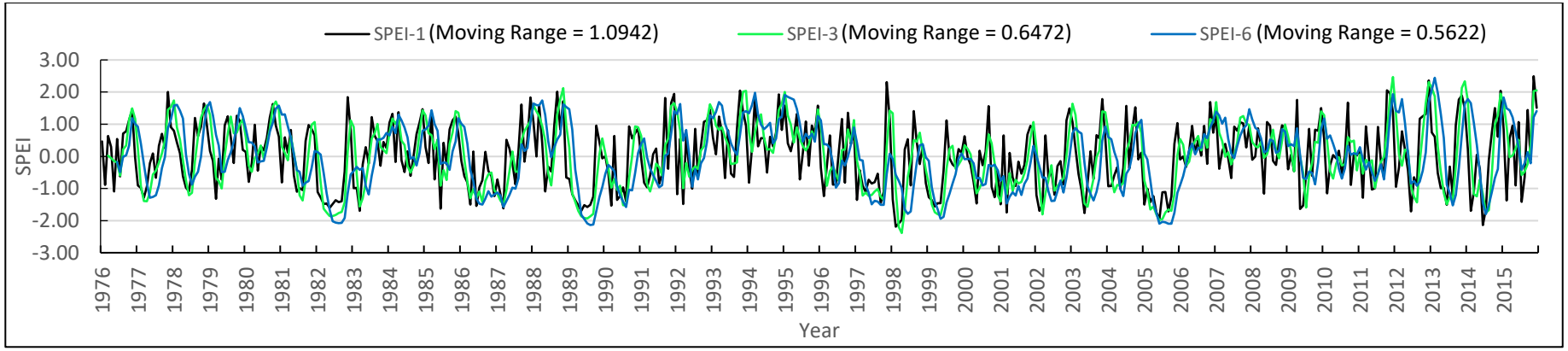

Figure 4.1: Developed SPEI-1, SPEI-3 and SPEI-6 of station s2815001

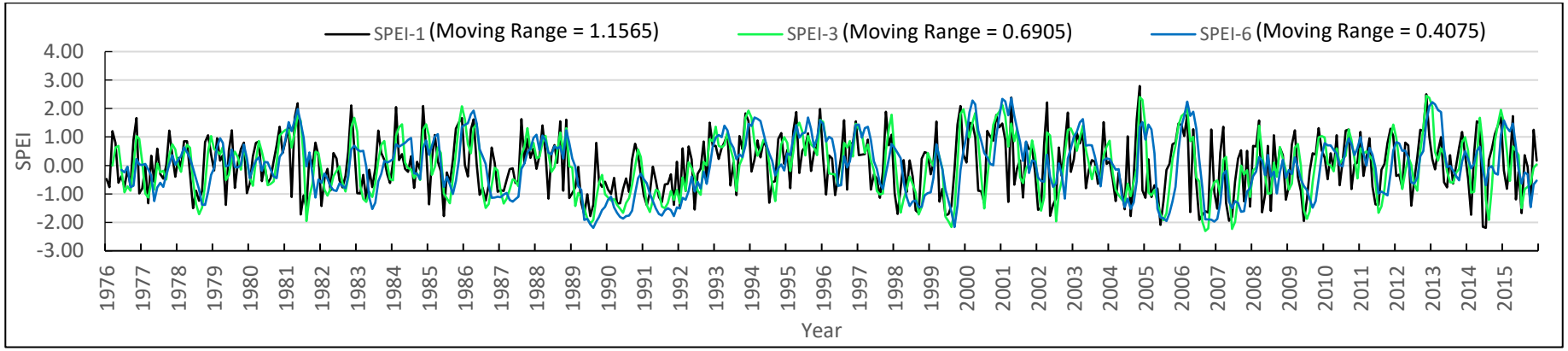

Figure 4.2: Developed SPEI-1, SPEI-3 and SPEI-6 of station s2917001

4.3 Wavelet Transformation of SPEIs

Wavelet transformation have been used as a pre-processing technique to de-noise and improve the quality of the data. In this study, each of the SPEIs has been decomposed into different levels of approximation and detail components. Since generalized models are desired, approximation components which show the general changes of a series were adopted as the inputs. With the maximum allowable decomposition level of eight in MATLAB (for the developed SPEIs in this study), the original SPEIs were wavelet transformed into eight different wavelet transformed series (a1, a2, a3, …, a8).

The wavelet transformed SPEIs of both stations, s2815001 and s2917001 were plotted in Appendix A1 to Appendix A6, with 'a1' representing approximation component of decomposed SPEIs at level one, 'a2' representing approximation component of decomposed SPEIs at level two and similarly, for 'a3' to 'a8'. It can be observed that each SPEIs was smoothened by the de-noising effect of wavelet decomposition, and the degree of de-noising effect increases when the decomposition level increases. Based on the plotted graphs, wavelet decomposition seemed to over de-noised the series when the decomposition above the level of six, as even the trend of the series was not shown in 'a7' and 'a8' for all the SPEIs of both stations. Furthermore, the maximum decomposition level estimated using Equation (3.19) also showed that the wavelet transformation process should be stopped at level seven, as shown in Table 4.3. Thus, the wavelet transformation process in this study should be sufficient as maximum decomposition level have been considered.

Table 4.3: Maximum Decomposition Levels for each SPEIs

SPEI	Number of Training Data	Max Level of Decompositions
1	426	7
3	425	7
6	422	7

Apart from that, it was observed that when the average moving range of the original series is high, wavelet decomposition tends to de-noise more compared to series with lower average moving range, even at the same decomposition level. For example, 'a2' of SPEI-1 visually differs more from original SPEI-1 (MR=1.0942) compared to 'a2' of SPEI-3 and original SPEI-3 (MR=0.6472), as referred to Appendix A1 and Appendix A2. In order to have better visualization on the changes of SPEIs throughout the wavelet transformation processes, the average moving range of each approximation components for both stations were calculated to estimate the variations in the series, then tabulated as Table 4.4 and plotted as Figure 4.3 and Figure 4.4.

Table 4.4: Average moving range values of original SPEIs and their wavelet transformed series

Station	SPEI	Original	a1	a2	a3	a4	a5	a6	a7	a8
	SPEI-1	1.0942	0.7204	0.4058	0.0759	0.0393	0.0249	0.0127	0.0056	0.0019
s2815001	SPEI-3	0.6472	0.6210	0.5390	0.1178	0.0370	0.0220	0.0117	0.0062	0.0020
	SPEI-6	0.5622	0.5344	0.5228	0.1463	0.0309	0.0211	0.0122	0.0081	0.0025
	SPEI-1	1.1565	0.7661	0.2165	0.0708	0.0181	0.0069	0.0069	0.0019	0.0003
s2917001	SPEI-3	0.6905	0.6157	0.3818	0.1325	0.0301	0.0165	0.0129	0.0008	0.0002
	SPEI-6	0.4075	0.3797	0.3232	0.1969	0.0416	0.0275	0.0201	0.0005	0.0005

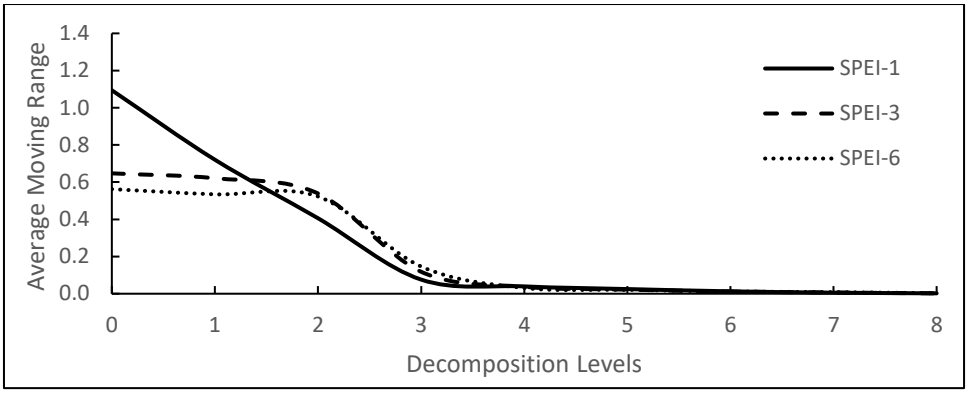

Figure 4.3: Average moving range of original and wavelet transformed SPEIs with different decomposition levels for station s2815001

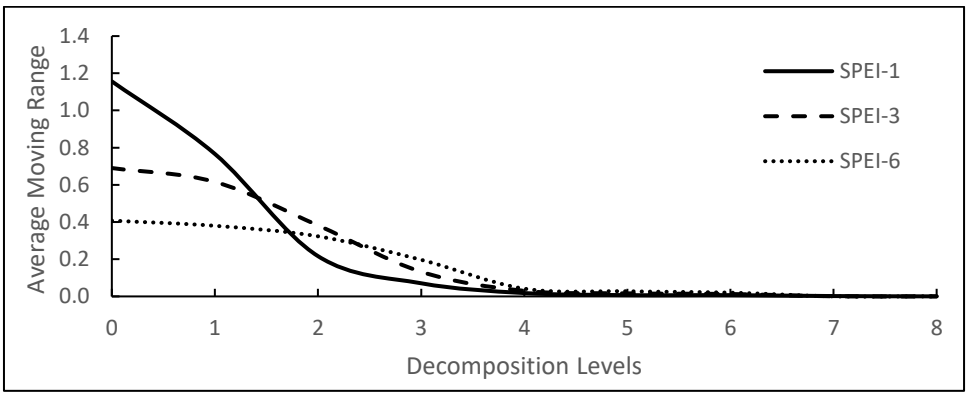

Figure 4.4: Average moving range of original and wavelet transformed SPEIs with different decomposition levels for station s2917001

By referring to Figure 4.3, the SPEI-1 of station s2815001 which has high variations in the original series, has a sharp decreased in average moving range values when the decomposition levels increased from one to four. On the other hand, SPEI-3 and SPEI-6 have gentler decrease as they have less variations in the original series compared to SPEI-1. For decomposition levels five to eight, the de-noising effects are similar, causing the decrease in average moving range values are small compared to decomposition levels of one to four and this happened to all three SPEIs. Similar observations were obtained from Figure 4.4 for station s2917001.

4.4 Fuzzy Membership Values of Wavelet Transformed SPEIs

The wavelet transformed SPEIs were then fuzzified using fuzzy membership functions to reduce the effects of outliers by giving the degree of importance for each point. As required, the SPEIs were separated into wet (SPEI>0) and dry (SPEI< or = 0) periods to carry out the tasks. The fuzzy membership values (Si) of all wavelet transformed SPEIs for both stations were then plotted as graphs in order to have better results visualisation, as shown in Appendix B1-B6. (Note: The positive and negative values of Si in the graphs are to indicate their classes, either wet or dry. All s_i were shown as positive values when it was used to train the models.)

Based on the graphs, it was observed that when the wavelet transformed SPEIs is closed to the mean value, it will acquire a high fuzzy membership value, or vice versa. For example, SPEI-1 (a1) of s2815001 with the value of -0.7513 at time step of 50, was closed to the mean value (-0.7447) of the negative class, so it has a high fuzzy membership value of 0.9975 (ranges from 0 to 1, where value 1 is the best), as shown in Figure B1.1 (Appendix B1). Contrary then, for SPEI-3 (a1) of s2917001 with the value of 2.9540 at time step of 346, which differed a lot from the mean value (0.7784) of positive class, it has a very low fuzzy membership value of 0.3041, as shown in Figure B2.1 (Appendix B2).

With these results, it was shown that the adopted fuzzy membership functions have the ability to estimate the degree of importance for each points. Thus, the fuzzy membership values were then used as extra inputs (M-W-FSVR)

or weightage of training points (W-W-FVSR), hoping to reduce the effects of outliers and produce models with higher accuracies.

4.5 Boosting Ensemble

Boosting is a technique to improve predictions by creating ensembles from weak learners. Hence, the number of learning cycles is an important parameter for, if the number is too low the model will be underfitted, while overfitting may happen when it is too high. In order to choose the appropriate number of learning cycles in the boosting procedure, the MAE between the targeted and boosted values were calculated, for both training and validation datasets. Thereafter, the number of learning cycles that have the lowest difference between the MAE of training and validation datasets was chosen, as generalized models are desired in this study. The results of optimum number of learning cycles for different scenarios were tabulated in Table 4.5 for station s2815001 and Table 4.6 for station s2917001.

Table 4.5: Optimum number of learning cycles for station s2815001

Lead Time	Time Scales	Process	Wavelet Decomposition Levels							
			1	2	3	4	5	6	7	8
1-Month	SPEI-1	Number of Learning Cycles	297	320	344	346	347	348	349	349
		Training MAE	0.593	0.554	0.656	0.688	0.715	0.765	0.760	0.751
		Validation MAE	0.835	0.708	0.995	1.025	1.032	1.010	1.034	1.034
		Difference in MAE	0.242	0.154	0.339	0.337	0.317	0.244	0.274	0.284
	SPEI-3	Number of Learning Cycles	183	186	200	203	203	204	204	204
		Training MAE	0.409	0.397	0.577	0.626	0.665	0.722	0.724	0.705
		Validation MAE	0.611	0.689	1.037	1.125	1.093	1.077	1.051	1.067
		Difference in MAE	0.203	0.292	0.460	0.499	0.428	0.355	0.326	0.362
	SPEI-6	Number of Learning Cycles	142	142	156	160	160	161	161	161
		Training MAE	0.310	0.343	0.500	0.535	0.623	0.650	0.640	0.665
		Validation MAE	0.575	0.607	0.960	1.115	1.152	1.078	1.136	1.085
		Difference in MAE	0.265	0.265	0.459	0.580	0.529	0.428	0.495	0.419
3-Month	SPEI-1	Number of Learning Cycles	319	358	399	403	405	407	408	408
		Training MAE	0.764	0.708	0.710	0.694	0.716	0.772	0.762	0.756
		Validation MAE	1.099	1.072	1.032	1.076	1.065	1.060	1.083	1.059
		Difference in MAE	0.335	0.364	0.322	0.382	0.349	0.288	0.320	0.303
	SPEI-3	Number of Learning Cycles	209	218	263	271	273	274	275	275
		Training MAE	0.733	0.689	0.660	0.636	0.662	0.707	0.715	0.705
		Validation MAE	1.128	1.185	1.054	1.131	1.166	1.125	1.062	1.057
		Difference in MAE	0.395	0.496	0.393	0.495	0.504	0.417	0.347	0.353
	SPEI-6	Number of Learning Cycles	165	166	206	218	219	220	220	221
		Training MAE	0.650	0.609	0.563	0.543	0.624	0.640	0.642	0.665
		Validation MAE	1.158	1.136	0.940	1.062	1.091	1.048	1.048	1.037
		Difference in MAE	0.508	0.527	0.377	0.518	0.468	0.408	0.407	0.371
6-Month	SPEI-1	Number of Learning Cycles	330	372	415	420	422	424	425	425
		Training MAE	0.783	0.792	0.784	0.714	0.744	0.768	0.768	0.766
		Validation MAE	1.076	1.053	1.100	1.077	1.078	1.088	1.187	1.101
		Difference in MAE	0.293	0.261	0.317	0.363	0.334	0.320	0.419	0.335
	SPEI-3	Number of Learning Cycles	219	228	277	286	288	289	297	290
		Training MAE	0.761	0.781	0.738	0.639	0.710	0.716	0.718	0.729
		Validation MAE	1.116	1.114	1.122	1.128	1.106	1.129	1.258	1.427
		Difference in MAE	0.355	0.334	0.384	0.489	0.396	0.413	0.541	0.699
	SPEI-6	Number of Learning Cycles	177	178	224	239	240	241	204	242
		Training MAE	0.783	0.773	0.665	0.591	0.661	0.677	0.677	0.675
		Validation MAE	1.159	1.247	1.160	1.017	1.098	1.051	1.056	1.049
		Difference in MAE	0.376	0.474	0.495	0.427	0.437	0.374	0.378	0.374

Table 4.6: Optimum number of learning cycles for station s2917001

Lead Time	Time Scales	Process	Wavelet Decomposition Levels							
			1	2	3	4	5	6	7	8
1-Month	SPEI-1	Number of Learning Cycles	306	354	367	371	372	372	373	373
		Training MAE	0.638	0.620	0.679	0.744	0.765	0.768	0.784	0.784
		Validation MAE	0.766	0.708	0.836	0.885	0.875	0.894	0.962	0.911
		Difference in MAE	0.128	0.088	0.157	0.141	0.110	0.126	0.179	0.128
	SPEI-3	Number of Learning Cycles	190	198	207	211	211	212	212	212
		Training MAE	0.474	0.445	0.611	0.679	0.697	0.739	0.765	0.754
		Validation MAE	0.705	0.621	0.775	0.829	0.866	0.866	0.835	0.845
		Difference in MAE	0.232	0.176	0.164	0.149	0.169	0.128	0.070	0.091
	SPEI-6	Number of Learning Cycles	135	143	162	184	186	187	190	190
		Training MAE	0.803	0.785	0.749	0.630	0.700	0.719	0.692	0.709
		Validation MAE	0.716	0.720	0.796	0.786	0.778	0.722	0.730	0.743
		Difference in MAE	-0.087	-0.065	0.047	0.156	0.078	0.003	0.038	0.034
3-Month	SPEI-1	Number of Learning Cycles	330	394	411	417	418	418	419	419
		Training MAE	0.807	0.736	0.729	0.757	0.766	0.763	0.771	0.771
		Validation MAE	0.891	0.884	0.863	0.879	0.886	0.899	0.997	0.892
		Difference in MAE	0.085	0.148	0.134	0.122	0.120	0.136	0.226	0.121
	SPEI-3	Number of Learning Cycles	213	236	261	271	272	273	274	274
		Training MAE	0.784	0.727	0.662	0.688	0.720	0.732	0.758	0.752
		Validation MAE	0.875	0.862	0.776	0.792	0.853	0.887	0.857	0.862
		Difference in MAE	0.091	0.134	0.114	0.104	0.132	0.156	0.099	0.110
	SPEI-6	Number of Learning Cycles	119	125	137	153	154	155	157	157
		Training MAE	0.653	0.608	0.603	0.598	0.700	0.705	0.661	0.688
		Validation MAE	0.748	0.743	0.659	0.764	0.785	0.697	0.698	0.757
		Difference in MAE	0.094	0.135	0.056	0.166	0.085	-0.008	0.036	0.069
6-Month	SPEI-1	Number of Learning Cycles	345	420	440	448	449	449	450	450
		Training MAE	0.796	0.799	0.781	0.764	0.779	0.784	0.783	0.781
		Validation MAE	0.885	0.936	0.861	0.861	0.889	0.858	0.954	0.890
		Difference in MAE	0.089	0.137	0.080	0.097	0.110	0.074	0.171	0.109
	SPEI-3	Number of Learning Cycles	225	254	284	296	298	298	300	300
		Training MAE	0.808	0.812	0.781	0.711	0.742	0.758	0.764	0.758
		Validation MAE	0.918	0.882	0.858	0.859	0.849	0.838	0.857	0.861
		Difference in MAE	0.110	0.070	0.077	0.148	0.107	0.079	0.093	0.103
	SPEI-6	Number of Learning Cycles	135	143	162	184	186	187	190	190
		Training MAE	0.803	0.785	0.749	0.630	0.700	0.719	0.692	0.709
		Validation MAE	0.716	0.720	0.796	0.786	0.778	0.722	0.730	0.743
		Difference in MAE	-0.087	-0.065	0.047	0.156	0.078	0.003	0.038	0.034

Based on Table 4.5 and Table 4.6, it can be observed that the number of learning cycles decreased when the time scales of the SPEI series increased whereas for lead time, the number of learning cycles increased when the lead

time increased. At every learning cycle, MATLAB trains one weak learner for every template object in learners. Thus, the increasing number of learning cycles to reach the optimum stage also indicate that the number of weak learners are increasing for the decreasing time scales and increasing lead time. Hence, the results of boosting ensembles are also showing that the training difficulties are getting higher when the time scales of SPEIs decreases or the lead time increases.

4.6 Support Vector Regression

For the development of each models, each SPEIs were partitioned into training and validation period, as shown in Table 4.7. As shown in the table, the period of validation data are different from the period of training data. Thus, the validation data are untouched data and hence, if the performance measures results are similar for both training and validation stage, the trained model can be considered as a well-trained generalized model.

Table 4.7: Training and Validation Periods

Time Scales	Process	Lead Time	Input	Target	Number of Data
SPEI-1	Training	1-Month	1976 Jan - 2011 Jun	1976 Feb - 2011 Jul	426
		3-Month	1976 Jan - 2011 Jun	1976 Apr - 2011 Sep	426
		6-Month	1976 Jan - 2011 Jun	1976 Jul - 2011 Dec	426
	Validation	1-Month	2012 Jan - 2015 Jun	2012 Feb - 2015 Jul	42
		3-Month	2012 Jan - 2015 Jun	2012 Apr - 2015 Sep	42
		6-Month	2012 Jan - 2015 Jun	2012 Jul - 2015 Dec	42
SPEI-3	Training	1-Month	1976 Mar - 2011 Jul	1976 Apr - 2011 Aug	425
		3-Month	1976 Mar - 2011 Jul	1976 Jun - 2011 Oct	425
		6-Month	1976 Mar - 2011 Jul	1976 Sep -2012 Jan	425
	Validation	1-Month	2012 Feb - 2015 Jun	2012 Mar - 2015 Jul	41
		3-Month	2012 Feb - 2015 Jun	2012 May - 2015 Sep	41
		6-Month	2012 Feb - 2015 Jun	2012 Aug - 2015 Dec	41
SPEI-6	Training	1-Month	1976 Jun - 2011 Jul	1976 Jul - 2011 Aug	422
		3-Month	1976 Jun - 2011 Jul	1976 Sep - 2011 Oct	422
		6-Month	1976 Jun - 2011 Jul	1976 Dec - 2012 Jan	422
	Validation	1-Month	2012 Feb - 2015 Jun	2012 Mar - 2015 Jul	41
		3-Month	2012 Feb - 2015 Jun	2012 May - 2015 Sep	41
		6-Month	2012 Feb - 2015 Jun	2012 Aug - 2015 Dec	41

For the training of each model, two most important parameters, which are the *Epsilon* and *C* were estimated using Equation (3.22) and Equation (3.23), then tabulated in Table 4.8 and Table 4.9. Based on the calculated values, it can be observed that both parameters have an inversely proportional relationship. Upon relating the average moving range of each SPEIs to epsilon values, it was found that the *Epsilon* parameters have larger values when the average moving range is high. To the author, this is reasonable as larger fitting zone (*Epsilon*) should be used when the training series has high variations (average moving range) so that the distribution of the training series can be captured and accurate predictions can be produced.

Table 4.8: Estimated model's parameters for station s2815001

Time Scales	Lead Time	Noise Variance	Noise SD	n	**Epsilon**	$\bar{y}$	σy	**C**
SPEI-1	1-Month	0.3733	0.6110	426	**0.2185**	-0.0245	0.9648	**2.9189**
	3-Month	0.3726	0.6104	426	**0.2183**	-0.0259	0.9639	**2.9177**
	6-Month	0.3520	0.5933	426	**0.2122**	-0.0127	0.9743	**2.9356**
SPEI-3	1-Month	0.0112	0.1058	425	**0.0379**	-0.0361	0.9595	**2.9145**
	3-Month	0.0113	0.1063	425	**0.0381**	-0.0338	0.9603	**2.9147**
	6-Month	0.0095	0.0975	425	**0.0349**	-0.0193	0.9737	**2.9404**
SPEI-6	1-Month	0.0035	0.0592	422	**0.0212**	-0.0470	0.9677	**2.9503**
	3-Month	0.0040	0.0632	422	**0.0227**	-0.0473	0.9681	**2.9516**
	6-Month	0.0024	0.0490	422	**0.0176**	-0.0402	0.9754	**2.9664**
SPEI-12	1-Month	0.0029	0.0539	417	**0.0194**	-0.0616	1.0311	**3.1550**
	3-Month	0.0029	0.0539	417	**0.0194**	-0.0619	1.0312	**3.1556**
	6-Month	0.0031	0.0557	417	**0.0201**	-0.0544	1.0335	**3.1551**

Table 4.9: Estimated model's parameters for station s2917001

Time Scales	Lead Time	Noise Variance	Noise SD	n	**Epsilon**	$\bar{y}$	σy	**C**
SPEI-1	1-Month	0.9770	0.9884	426	**0.3535**	-0.0181	0.9896	**2.9868**
	3-Month	0.9722	0.9860	426	**0.3526**	-0.0193	0.9871	**2.9808**
	6-Month	0.9776	0.9887	426	**0.3536**	-0.0116	0.9899	**2.9813**
SPEI-3	1-Month	0.0147	0.1212	425	**0.0434**	-0.0268	0.9967	**3.0170**
	3-Month	0.0146	0.1208	425	**0.0433**	-0.0313	0.9964	**3.0206**
	6-Month	0.0144	0.1200	425	**0.0430**	-0.0189	0.9998	**3.0184**
SPEI-6	1-Month	0.0018	0.0424	422	**0.0152**	-0.0355	1.0066	**3.0553**
	3-Month	0.0019	0.0436	422	**0.0157**	-0.0397	1.0088	**3.0660**
	6-Month	0.0020	0.0447	422	**0.0161**	-0.0342	1.0089	**3.0609**
SPEI-12	1-Month	0.0031	0.0557	417	**0.0201**	-0.0588	1.0147	**3.1028**
	3-Month	0.0028	0.0529	417	**0.0191**	-0.0590	1.0148	**3.1033**
	6-Month	0.0029	0.0539	417	**0.0194**	-0.0538	1.0130	**3.0929**

4.7 Model Performance

The performances of different models were evaluated using the commonly used performance measures, namely MAE, RMSE and Bias, for all three SPEIs of both stations with different lead times of 1-month, 3-month and

6-month. Appendix C shows the performance measures of the models for the various wavelet decomposition levels, SPEIs and lead times.

4.7.1 Selection of Optimum Wavelet Decomposition Level

For the analysis of results based on decomposition levels, the optimum decomposition levels of each of the models under different lead times and SPEIs were identified and bolded in Appendix C. Based on Appendix C, it was observed that the optimum wavelet decomposition have a general trend that increase when lead time increase. It was also found that cases of local and global minima happened during the identification of optimum decomposition levels. For better visualisation, graphs of MAE over decomposition levels for each SPEIs and lead times are plotted and shown in Appendix D (with local and global minima indicated using red and green circles, respectively).

From Appendix D, the graphs showed that the W-BS-SVR and M-W-FSVR models encountered local and global minima problems in this study. For example, M-W-FSVR model achieved a local minimum MAE of 0.107 at decomposition level two but achieved the global minimum value of 0.044 at decomposition level six, during the training stage for the prediction of 1-month lead time SPEI-1 at station s2815001. Similarly, for the W-BS-SVR model, the case of local minima (MAE=0.156) and global minima (MAE=0.116) are shown in Appendix D, during the validation stage for the prediction of 3-month lead time SPEI-3 at station s2917001. Based on the results, it seemed like the

exploration for the optimum decomposition level should not only be done for a certain level in view of the fact that local and global minimum exists.

For the maximum decomposition level to be carried out in this study, Equation (3.19) estimated that the maximum decomposition level should be seven. Based on the results in Appendix C which show the performance measures up to a decomposition level of eight, it was again proved that Equation (3.19) to be feasible as optimum performance of each models never occurred for level eight. The statement of "over de-noised the series when the decomposition over level of six" in Section 4.3 looks plausibly correct for this study as optimum decomposition level never happen for level seven or eight in this study.

4.7.2 Model Selection

With the optimum decomposition levels being identified, the performance of best performing models for both training and validation stages were tabulated as Table 4.10 to Table 4.13. (WL* = Optimum Wavelet Decomposition Level). The best performing model under each lead times and SPEIs were highlighted in the tables shown.

Table 4.10: Results of performance measures (MAE, RMSE and Bias) for the training of models at station s2815001

Time Scales	Model	LT1				LT3				LT6			
		WL*	MAE	RMSE	BIAS	WL*	MAE	RMSE	BIAS	WL*	MAE	RMSE	BIAS
SPEI-1	W-BS-SVR	1	0.074	0.090	-0.040	2	0.138	0.163	0.011	4	0.261	0.309	-0.006
	M-W-FSVR	6	**0.044**	**0.057**	**0.025**	3	0.099	0.117	0.002	4	0.116	0.135	-0.039
	W-W-FSVR	1	0.075	0.090	-0.037	3	**0.084**	**0.100**	**-0.062**	5	**0.106**	**0.125**	**-0.024**
SPEI-3	W-BS-SVR	2	0.030	0.037	-0.016	5	0.086	0.106	-0.044	4	0.113	0.140	-0.080
	M-W-FSVR	2	0.031	0.037	0.024	4	0.076	0.084	-0.076	4	0.081	0.101	-0.079
	W-W-FSVR	2	**0.016**	**0.019**	**0.015**	3	**0.050**	**0.058**	**-0.050**	5	**0.057**	**0.071**	**-0.036**
SPEI-6	W-BS-SVR	1	**0.006**	**0.007**	**-0.002**	4	0.045	0.054	0.007	4	0.053	0.065	-0.040
	M-W-FSVR	4	0.012	0.015	0.008	4	0.030	0.035	-0.014	5	0.046	0.057	-0.040
	W-W-FSVR	2	0.012	0.014	0.005	6	**0.019**	**0.023**	**-0.011**	6	**0.033**	**0.034**	**0.033**

WL* = Optimum Wavelet Decomposition Level

Table 4.11: Results of performance measures (MAE, RMSE and Bias) for the validation of models at station s2815001

Time Scales	Model	LT1				LT3				LT6			
		WL*	MAE	RMSE	BIAS	WL*	MAE	RMSE	BIAS	WL*	MAE	RMSE	BIAS
SPEI-1	W-BS-SVR	1	0.090	0.104	-0.026	2	0.180	0.205	0.028	4	0.350	0.398	0.066
	M-W-FSVR	6	**0.054**	**0.067**	**0.014**	3	0.129	0.147	-0.012	4	0.140	0.158	-0.025
	W-W-FSVR	1	0.090	0.104	-0.025	3	**0.086**	**0.106**	**-0.068**	5	**0.137**	**0.158**	**-0.015**
SPEI-3	W-BS-SVR	2	0.039	0.045	-0.011	5	0.114	0.129	-0.030	4	0.162	0.189	0.015
	M-W-FSVR	2	0.037	0.047	0.030	4	0.070	0.082	-0.068	4	0.094	0.113	-0.058
	W-W-FSVR	2	**0.018**	**0.021**	**0.013**	3	**0.058**	**0.066**	**-0.058**	5	**0.067**	**0.081**	**-0.066**
SPEI-6	W-BS-SVR	1	**0.008**	**0.009**	**0.001**	4	0.058	0.068	0.021	4	0.068	0.084	-0.059
	M-W-FSVR	4	0.016	0.019	0.012	4	0.035	0.041	-0.016	5	0.059	0.067	-0.012
	W-W-FSVR	2	0.016	0.019	0.010	6	**0.025**	**0.031**	**-0.019**	6	**0.035**	**0.036**	**0.035**

WL* = Optimum Wavelet Decomposition Level

Table 4.12: Results of performance measures (MAE, RMSE and Bias) for the training of models at station s2917001

Time Scales	Model	LT1				LT3				LT6			
		WL*	MAE	RMSE	BIAS	WL*	MAE	RMSE	BIAS	WL*	MAE	RMSE	BIAS
SPEI-1	W-BS-SVR	2	0.091	0.114	-0.048	3	0.245	0.294	-0.027	4	0.375	0.450	-0.042
	M-W-FSVR	2	0.048	0.057	0.002	6	0.077	0.092	-0.015	6	0.082	0.099	0.014
	W-W-FSVR	1	**0.035**	**0.044**	**-0.028**	3	**0.036**	**0.046**	**-0.024**	4	**0.073**	**0.089**	**-0.034**
SPEI-3	W-BS-SVR	2	0.038	0.045	0.015	5	0.118	0.143	-0.040	4	0.249	0.297	0.019
	M-W-FSVR	2	0.037	0.050	0.017	5	0.048	0.064	-0.037	5	0.051	0.064	-0.037
	W-W-FSVR	2	**0.033**	**0.034**	**0.033**	6	**0.031**	**0.037**	**-0.020**	5	**0.048**	**0.061**	**-0.001**
SPEI-6	W-BS-SVR	2	**0.013**	**0.016**	**-0.007**	4	0.067	0.082	-0.026	4	0.094	0.115	-0.015
	M-W-FSVR	4	0.019	0.025	-0.016	5	0.025	0.031	0.015	4	0.056	0.070	0.011
	W-W-FSVR	2	0.011	0.014	-0.007	5	**0.015**	**0.017**	**0.015**	4	**0.039**	**0.047**	**0.031**

WL* = Optimum Wavelet Decomposition Level

Table 4.13: Results of performance measures (MAE, RMSE and Bias) for the validation of models at station s2917001

Time Scales	Model	L1				L3				L6			
		WL*	MAE	RMSE	BIAS	WL*	MAE	RMSE	BIAS	WL*	MAE	RMSE	BIAS
SPEI-1	W-BS-SVR	2	0.087	0.112	-0.029	3	0.261	0.323	0.035	4	0.396	0.494	0.048
	M-W-FSVR	2	0.050	0.062	-0.007	6	0.083	0.101	-0.028	6	0.084	0.105	-0.001
	W-W-FSVR	1	**0.035**	**0.046**	**-0.026**	3	**0.052**	**0.064**	**-0.010**	4	**0.072**	**0.091**	**-0.022**
SPEI-3	W-BS-SVR	2	0.042	0.053	0.028	5	0.116	0.144	0.000	4	0.265	0.326	0.100
	M-W-FSVR	2	0.033	0.040	-0.014	5	0.051	0.072	0.039	5	0.055	0.066	0.017
	W-W-FSVR	2	**0.030**	**0.031**	**0.030**	6	**0.033**	**0.042**	**-0.032**	5	**0.046**	**0.064**	**-0.037**
SPEI-6	W-BS-SVR	2	**0.010**	**0.012**	**0.000**	4	0.055	0.068	0.004	4	0.079	0.103	0.029
	M-W-FSVR	4	0.022	0.027	-0.021	5	0.029	0.037	0.024	4	0.069	0.088	-0.005
	W-W-FSVR	2	0.013	0.016	-0.010	5	**0.018**	**0.021**	**0.018**	4	**0.047**	**0.056**	**0.046**

WL* = Optimum Wavelet Decomposition Level

Based on the results shown in Table 4.10 to Table 4.13, it was observed that each models achieved fairly high accuracy in both training and validation stages. The values of performance measures range from 0.006 to 0.396 for MAE, 0.007 to 0.494 for RMSE and 0.000 to 0.100 (magnitude) for Bias. The results of the models have a general trend to improve when the sensitivity of the SPEIs decreases (SPEI-1 to SPEI-3, SPEI-3 to SPEI-6). On the other hand, when the lead time increases, the general performance of the models deteriorated.

4.7.2.1 Model performance under different time scales of SPEI

Based on Table 4.10 to Table 4.13, it can be observed that the overall performance of the models improved over the increasing time scales of SPEIs. For SPEI-1, the M-W-FSVR model showed the highest accuracy at station s2815001 for 1-month lead time predictions, with the lowest performance measures values during the training and validation stages. As for station s2917001, the most accurate prediction for SPEI-1 also occurred for a 1-month lead time achieved by the W-W-FSVR model, also at both training and validation stages.

For SPEI-3, the general performances of the models have lower errors compared to SPEI-1. For both stations, the W-W-FSVR model has the most accurate results in training and validation stages for the prediction of SPEI-3 and occurred at 1-month lead time. As for SPEI-6, the prediction errors at both training and validation stages are the lowest among the three SPEIs. It was achieved with the W-BS-SVR model for both stations at a lead time of 1-month. Thus, the results showed that the fuzzy based models have the most accurate results for SPEI-1 and SPEI-3, while the W-BS-SVR model has the best prediction for SPEI-6. These results may be due to the variations in SPEI series.

According to Table 4.4, the SPEI-1 of station s2815001 has the highest variations in data (Average Moving Range = 1.0942) among the three SPEIs, followed by SPEI-3 (Average Moving Range = 0.6472) and SPEI-6 (Average Moving Range = 0.5622). Similar for station s2917001, SPEI-1 also has the

highest variations in data (Average Moving Range = 1.1565) among the three SPEIs, followed by SPEI-3 (Average Moving Range = 0.6905) and then SPEI-6 (Average Moving Range = 0.4075). Thus, fuzzy based models that are capable to reduce outlier effects achieved accurate predictions for SPEI-1 of all lead times, with the M-W-FSVR performing best at 1-month lead time and the W-W-FSVR best at 3 and 6 months lead time.

Similar for SPEI-3, fuzzy based models are still dominating the predictions at both stations, even the variations in the SPEI-3 series is lower compared to SPEI-1. However, it can be observed that the difference in performance measures between the fuzzy based models and the W-BS-SVR models are smaller compared to SPEI-1. Thus, the advantage of fuzzy based models to produce accurate prediction by reducing outlier effects is getting less significant over the increasing timescales of SPEI. As for SPEI-6 which has the lowest sensitivity to the changes in temperature and precipitation (lowest average moving range values), the W-BS-SVR performed better than the other two models, but only in the case of a lead time of 1-month. Hence, fuzzy based models seemed to be more accurate when the SPEI series has high sensitivity.

The idea of boosting in the W-BS-SVR is to create an ensemble from weak learners so that predictions with better accuracy can be obtained. However, when the training series has high average moving range, then the training process become harder and more ensembles will be created. With this, the complexity in the model increases resulting in the problem of overfitting. For example, the validation results of the W-BS-SVR models deteriorated most

from the training stage in the predictions of SPEI-1 (highest sensitivity). Compared to the W-BS-SVR models, the M-W-FSVR and W-W-FSVR models which reduce the effects from outliers without causing higher complexity in the model, the problem of overfitting is less likely to happen and the degree of overfitting is lower even if it does. Hence, the W-BS-SVR model is only suitable for the predictions of SPEI-6 with a 1-month lead time, which is the easiest training case, compared to the M-W-FSVR and W-W-FSVR models which in general are more suited for predictions for SPEI-1 and SPEI-3 for all lead times and SPEI-6 for 3 and 6 months lead times. As for the performances of models for different lead times (1-month, 3-month, 6-month), the best results for each of the SPEIs was also found to occur at 1-month lead time for SPEI-1, SEPI-3 and SPEI-6. For the changes in models' performance under different lead times, it will be discussed in the next sub-section.

4.7.2.2 Model performance under different lead times

Based on the results shown in Table 4.10 to Table 4.13, the W-W-FSVR seemed to be the most accurate model in predicting SPEI-1, SPEI-3 and SPEI-6 at both station s2815001 and s2917001 for longer lead time, which are 3-month and 6-month lead time. As for 1-month lead time, the best performing models varied for different SPEIs, as discussed in Section 4.7.2.1.

For 1-month lead time, the models' target period is the nearest future to the input period of the model, compared to 3-month and 6-month lead time. This

makes it the easiest training case in terms of lead time. Hence, the accuracy of the models are dominated by the variations of the SPEI series, which is indicated by average moving range values. Given the explanations in Section 4.7.2.1 on the behaviour of models' accuracy when average moving range of the SPEI series increase, fuzzy-based models outperformed in predicting SPEI-1, SPEI-3 and W-BS-SVR model outperformed in predicting SPEI-6, under 1-month lead time predictions.

For 3-month lead time, the accuracy of the models started to be dominated by the difficulties caused by the increased lead time period. Fuzzy-based models seemed to have the ability in reducing the training difficulties through reducing the outlier effects, as shown in the results of the fuzzy based models overtaking the W-BS-SVR models for all SPEIs in 3-month lead time prediction. The general trend that optimum decomposition level is increasing with the increased lead time (Appendix C) also showed that reducing the variations in the SPEI series is required when the lead time increases. Thus, fuzzy based models which were designed to reduce outlier effects, outperformed the W-BS-SVR models especially the W-W-FSVR models, and seemed to be more efficient in reducing the training difficulties and improving the prediction accuracy.

On a 6-month lead time premise, the accuracy of the models in SPEI-6 predictions were dominated by the difficulties caused by the increased lead time period, instead of the variations in the SPEI series. Hence, the W-W-FSVR models which seemed to be most capable in improving long lead time prediction

accuracy outperformed the other two models for all three SPEIs in 6-month lead time predictions.

Deterioration of models for longer lead times prediction

Although with the efforts of performing wavelet transformation, boosting ensemble and reducing outlier effects to improve models' accuracy, the overall performances of the models deteriorated when the lead time increased. In order to have better visualisation on the deterioration of models' performances over increasing lead time, Table 4.14 to Table 4.17 were produced by getting the changes of MAE, RMSE and Bias from LT1 to LT3 (Values in LT3 – Values in LT1) and LT1 to LT6 (Values in LT6 – Values in LT1). Thus, larger values in Table 4.14 to Table 4.17 indicate higher deterioration in models' accuracy.

Table 4.14: Deterioration of models at s2815001 (Training)

Drought	Model	Deterioration from LT1 to LT3			Deterioration from LT1 to LT6		
		MAE	RMSE	BIAS (Magnitude)	MAE	RMSE	BIAS (Magnitude)
SPEI-1	W-BS-SVR	**0.064**	**0.073**	**-0.029**	**0.187**	**0.219**	**-0.034**
	M-W-FSVR	0.055	0.060	-0.023	0.072	0.078	0.014
	W-W-FSVR	0.009	0.010	0.025	0.031	0.035	-0.013
SPEI-3	W-BS-SVR	**0.056**	**0.069**	**0.028**	**0.083**	**0.103**	**0.064**
	M-W-FSVR	0.045	0.047	0.052	0.050	0.064	0.055
	W-W-FSVR	0.034	0.039	0.035	0.041	0.052	0.021
SPEI-6	W-BS-SVR	**0.039**	**0.047**	**0.005**	**0.047**	**0.058**	**0.038**
	M-W-FSVR	0.018	0.020	0.006	0.034	0.042	0.032
	W-W-FSVR	0.007	0.009	0.006	0.021	0.020	0.028

Table 4.15: Deterioration of models at s2815001 (Validation)

Drought	Model	Deterioration from LT1 to LT3			Deterioration from LT1 to LT6		
		MAE	RMSE	BIAS (Magnitude)	MAE	RMSE	BIAS (Magnitude)
SPEI-1	W-BS-SVR	**0.090**	**0.101**	**0.002**	**0.260**	**0.294**	**0.040**
	M-W-FSVR	0.075	0.080	-0.002	0.086	0.091	0.011
	W-W-FSVR	-0.004	0.002	0.043	0.047	0.054	-0.010
SPEI-3	W-BS-SVR	**0.075**	**0.084**	**0.019**	**0.123**	**0.144**	**0.004**
	M-W-FSVR	0.033	0.035	0.038	0.057	0.066	0.028
	W-W-FSVR	0.040	0.045	0.045	0.049	0.060	0.053
SPEI-6	W-BS-SVR	**0.050**	**0.059**	**0.020**	**0.060**	**0.075**	**0.058**
	M-W-FSVR	0.019	0.022	0.004	0.043	0.048	0.000
	W-W-FSVR	0.009	0.012	0.009	0.019	0.017	0.025

Table 4.16: Deterioration of models at s2917001 (Training)

Drought	Model	Deterioration from LT1 to LT3			Deterioration from LT1 to LT6		
		MAE	RMSE	BIAS (Magnitude)	MAE	RMSE	BIAS (Magnitude)
SPEI-1	W-BS-SVR	**0.154**	**0.180**	**-0.021**	**0.284**	**0.336**	**-0.006**
	M-W-FSVR	0.029	0.035	0.013	0.034	0.042	0.012
	W-W-FSVR	0.001	0.002	-0.004	0.038	0.045	0.006
SPEI-3	W-BS-SVR	**0.080**	**0.098**	**0.025**	**0.211**	**0.252**	**0.004**
	M-W-FSVR	0.011	0.014	0.020	0.014	0.014	0.020
	W-W-FSVR	-0.002	0.003	-0.013	0.015	0.027	-0.032
SPEI-6	W-BS-SVR	**0.054**	**0.066**	**0.019**	**0.081**	**0.099**	**0.008**
	M-W-FSVR	0.006	0.006	-0.001	0.037	0.045	-0.005
	W-W-FSVR	0.004	0.003	0.008	0.028	0.033	0.024

Table 4.17: Deterioration of models at s2917001 (Validation)

Drought	Model	Deterioration from LT1 to LT3			Deterioration from LT1 to LT6		
		MAE	RMSE	BIAS (Magnitude)	MAE	RMSE	BIAS (Magnitude)
SPEI-1	W-BS-SVR	**0.174**	**0.211**	**0.006**	**0.309**	**0.382**	**0.019**
	M-W-FSVR	0.033	0.039	0.021	0.034	0.043	-0.006
	W-W-FSVR	0.017	0.018	-0.016	0.037	0.045	-0.004
SPEI-3	W-BS-SVR	**0.074**	**0.091**	**-0.028**	**0.223**	**0.273**	**0.072**
	M-W-FSVR	0.018	0.032	0.025	0.022	0.026	0.003
	W-W-FSVR	0.003	0.011	0.002	0.016	0.033	0.007
SPEI-6	W-BS-SVR	**0.045**	**0.056**	**0.004**	**0.069**	**0.091**	**0.029**
	M-W-FSVR	0.007	0.010	0.003	0.047	0.061	-0.016
	W-W-FSVR	0.005	0.005	0.008	0.034	0.040	0.036

It can be observed that the models deteriorated when the lead time increased, as most of the deterioration in terms of MAE and RMSE values have positive values in Table 4.14 to Table 4.17, showing that the prediction errors have increased when the prediction lead time increased from LT1 to LT3 and LT1 to LT6. Table 4.14 to Table 4.17 also showed that the W-BS-SVR models deteriorated most (indicated by highlighted values in the tables) among the three models for the training and validation stages of all SPEIs at both stations, followed by the M-W-FSVR and W-W-FSVR models.

a) 1-Month Lead Time to 3-Month Lead Time

For station s2815001, Table 4.14 and Table 4.15 showed that the accuracy of all three models deteriorated for a change from 1-month to a 3-month lead time prediction. It can be observed that the W-BS-SVR model always has the highest deterioration for all three SPEIs, while the fuzzy based models are less prone to the deterioration caused by the increase in lead time, with the W-W-FSVR models with the lowest deterioration for most of the cases. It was also found that the models seemed to have lower deterioration when the time scale of SPEIs increased. This may due to the lower effects of variations in the series when the time scales of SPEIs increase, as discussed in Section 4.7.2.1.

For station s2917001, Table 4.16 and Table 4.17 results also portrayed similar trends, wherein the accuracy of all three models deteriorated for a 1-month lead time increased to a 3-month lead time prediction, with the accuracy

of the W-BS-SVR models deteriorated most and fuzzy based models have less deterioration for all SPEIs, whilst the W-W-FSVR models deteriorated least. For predictions done by the W-BS-SVR models, the model's accuracy deteriorated most for SPEI-1 when the lead time increased from 1-month to 3-month. Similar to the trend shown in station s2815001, the deterioration of the W-BS-SVR models decreased over increasing time scales of SPEIs (SPEI-1, SPEI-3, SPEI-6). As for the M-W-FSVR and W-W-FSVR models, they have lower deterioration compared to W-BS-SVR, as shown in Table 4.16 and Table 4.17. Thus, fuzzy based models seemed to be less prone to deterioration over predictions with increasing lead times, with the W-W-FSVR being the least affected, similar to the trend shown in station s2815001.

b) 1-Month Lead Time to 6-Month Lead Time

Similarly in this case, the accuracy of the models also reduced for the prediction of SPEI-1, SPEI-3 and SPEI-6 with a jump to a 6-month lead time. Furthermore, the degree of deterioration of each models are higher than in 3-month lead time, making the 6-month lead time predictions of SPEIs having lowest accuracy among the three different lead times done in this study. The deterioration of models for 6-month lead time are also shown in Table 4.14 to Table 4.17.

For station s2815001, Table 4.14 and Table 4.15 showed that the accuracy of all three models deteriorated from 1-month to 6-month lead time prediction of SPEI-1. The deterioration of models have similar trends as with

the increase to a 3-month lead time case, including that the W-BS-SVR always deteriorate most and fuzzy based models less. However, the trend of decreases in deterioration when the time scale of SPEIs increased was not shown in 6-month lead time predictions. For station s2917001, the M-W-FSVR and W-W-FSVR models also showed lower deterioration compared to W-BS-SVR, as shown in Table 4.16 and Table 4.17. Thus again, fuzzy based models seemed to be less prone to deterioration over predictions with increasing lead times, similar to the trend shown in station s2815001.

Advantage of Fuzzy-Based Models over W-BS-SVR Models in Long Lead Time Predictions

Given the results showing that M-W-FSVR and W-W-FSVR models outperformed W-BS-SVR models in both 3-month and 6-month lead time predictions, it seemed that fuzzy-based models have advantage over the W-BS-SVR models in longer lead time predictions. The reason behind the W-BS-SVR models being not predicting well for longer lead times could lie with its algorithm in boosting the weak learners. Since the difference between training and targeted values increases when the lead time increases, this causes the models' training process become harder and the number of poorly trained cases also increases. This raises the number of boosting process to accumulate preceding learners for new ensemble, increasing the complexity of the regression. This condition may further burden the training process in SVR, in addition to the increase in difficulties from the difference between training and targeted values, and hence, the deterioration in performances increased.

On the other hand, fuzzy-based models incorporated the idea of reducing outlier effects by adding an extra parameter (M-W-FSVR) or giving weights (W-W-FSVR) to each training points. Compared to boosting, the nature of each training cases remains at point-to-point level even when the training cases become more difficult. The algorithm itself does not further burden the training process when lead time increases. Also, the outliers reducing effects of the fuzzy based models depend on the mean value of the positive and negative classes, the fuzzy membership values do not change even if the training cases become harder when lead time increases. These two reasons may explain the phenomena of the fuzzy-based models deteriorated less compared with the W-BS-SVR models.

In summing up, the complexity of the W-BS-SVR models increases when the training cases become harder due to the increase in lead time, which does not happen with the case of the fuzzy based models. Thus, compared to the W-BS-SVR models, the fuzzy based models especially the W-W-FSVR model, have less deterioration and better accuracy for 3-month and 6-month lead time predictions.

CHAPTER 5

CONCLUSIONS AND RECOMMENDATIONS

5.1 Conclusions

Three hybrid drought forecasting models namely the M-W-FSVR, the W-W-FSVR and the W-BS-SVR to predict the SPEI for different time scales and lead times, at the Langat River Basin, Malaysia were developed in this study. The SPEI-1, SPEI-3 and SPEI-6 were specifically developed and implemented in the models to describe and predict the moisture condition of the basin. Predictions were done for 1-month, 3-month and 6-month lead times and the performance measures such as MAE, RMSE and Bias were used to evaluate the accuracy of the three models developed.

For the development of SPEI-1, SPEI-3 and SPEI-6, three SPEIs showed different degree of variations in the series. The average moving range attribute was used to describe the series variations in this study. The estimated average moving range values showed that the variations of SPEIs were decreasing in the order of SPEI-1, then SPEI-3 and then SPEI-6. It was concluded that the SPEI with higher time scales are less sensitive to any changes in monthly precipitation and/or temperature.

For the wavelet transformation, it was found that it is an effective method to de-noise and reveal the trend of a series, especially for series with high variations. A practical way to determine the optimum wavelet decomposition level was not found, but it was observed that the series may get over de-noised when the decomposition level is too high. Hence, it was concluded that the maximum decomposition level is necessary if wavelet transformation were to be used for de-noising a series.

With respect to fuzzy membership values, it was found that the fuzzy membership function used in the study was effective in reducing the effect of outliers in a series. Based on the plotted results, each estimated fuzzy membership values successfully showed the importance of their corresponding data to the series, where the data nearer to the class mean have higher fuzzy membership values or vice versa. Hence, the estimated fuzzy membership values was concluded as suitable datasets to represent the importance of each data point and ready to be used as either additional input (M-W-FSVR) or weightage (W-W-FSVR) for the model training sessions.

The use of the boosting ensemble technique to improve the performance of weak learners was also explored in this study. Results showed that the number of learning cycles was increasing with decreasing time scales and at increasing lead time. With the number of learning cycles indicating the number of trained weak learners, it was concluded that the training difficulties were getting higher when the time scale of the SPEIs decreases or the lead time increases.

For the selection of the optimum wavelet decomposition level, the decisions were made based on performance measures after executing the training and validation of models up to the maximum decomposition levels. Based on the results of the varying optimum decomposition level between different models, time scales and lead times, it was again concluded that it was essential to carry out wavelet transformation to the maximum decomposition level.

As for the performance of the models over different time scales, all models have a general trend to improve when the variations of the SPEI series decreased. For SPEI-1, the M-W-FSVR (rainfall station: s2815001) and the W-W-FSVR (rainfall station: s2910771) outperformed at their respective station. For SPEI-3, the W-W-FSVR outperformed the other two models at both stations. However, the W-BS-SVR showed the best performance for SPEI-6 at both stations. Thus, it was concluded that fuzzy based models are capable in providing accurate predictions for SPEIs with high variations (SPEI-1, SPEI-3) through their ability in reducing outlier effects but become less significant when the series has low variations (SPEI-6).

The general performance of the models deteriorated when the lead time of the predictions was increased. For the 1-month lead time, the performance of the models were as mentioned in the previous paragraph as the accuracy of the models were dominated by the variations of the SPEI series. For the 3-month lead time, W-W-FSVR outperformed the other two models for the predictions for all three SPEIs but the accuracies were lower compared to the 1-month lead

time results. Similar to it was for the 6-month lead time scheme but with higher deterioration compared to the 3-month case. It was observed that the W-BS-SVR models deteriorated most among the three models for the training and validation stages of all the SPEIs at both stations. Thus, it was concluded that fuzzy based models have the advantage over the W-BS-SVR models at longer lead time predictions, especially the W-W-FSVR model which showed the best performance and least deterioration for most of the cases. With the performance of models under different time scales and lead times been analysed, the best models for each conditions were identified and concluded as in Table 5.1.

Table 5.1: Identified best models

Station	Time Scales	LT1		LT3		LT6	
		Model	WL	Model	WL	Model	WL
s2815001	SPEI-1	M-W-FSVR	6	W-W-FSVR	3	W-W-FSVR	5
	SPEI-3	W-W-FSVR	2	W-W-FSVR	3	W-W-FSVR	5
	SPEI-6	W-BS-SVR	1	W-W-FSVR	6	W-W-FSVR	6
s2917001	SPEI-1	W-W-FSVR	1	W-W-FSVR	3	W-W-FSVR	4
	SPEI-3	W-W-FSVR	2	W-W-FSVR	6	W-W-FSVR	5
	SPEI-6	W-BS-SVR	2	W-W-FSVR	5	W-W-FSVR	4

WL* = Optimum Wavelet Decomposition Level

5.2 Recommendations

This study focused on drought forecasting at the Langat River Basin, which is a tropical climate region. Considering the fact that this study has not found a clear relationship between a particular basin and performance of models, studies of regions with different climate and physical characteristics should be conducted in the future using similar approaches to explore the robustness of

the proposed models. The use of ground-truth dataset should also be included to the similar studies in the future to ensure the robustness of the models by measuring their accuracy on "unseen" data, such as k-fold cross validation, Monte Carlo cross-validation and etc.

The hybrid models in this study were developed using the SVR as the base model. Further studies can be done by coupling the wavelet, fuzzy and boosting approach in this study with other artificial intelligence machine learning method (e.g. ANN) or stochastic method (e.g. ARIMA) to investigate their performances compared to the hybrid models produced. Thereafter, analysis can be done to select the most suitable models for drought forecasting in Langat River Basin.

The SPEI was the only drought index adopted in this study. Further studies to compare the effectiveness of different drought index (e.g. SPI, PDSI) to predict and describe the drought conditions in Langat River Basin should also be explored for the better sake of water management in the basin. The time scales used for the development of SPEI in this study were 1-month, 3-month and 6-month. SPEIs with time scales other than these three should be done in the future so that a better description of the moisture condition in Langat River Basin can be produced for other uses, e.g. SPEI-2 for the plantations with two months lifespan.

REFERENCES

Abdulah, N., Juhaimi, J. and Abdul Rahman, K., 2014. *Capacity Development to support National Drought Management Policy: National Reports - Malaysia*. Hanoi: UN-Water Decade Programme on Capacity Development.

Abebe, A. and Foerch, G., 2008. Stochastic simulation of the severity of hydrological drought. *Water and Environment Journal*, 22, pp. 2–10.

Abramowitz, M. and Stegun, A., 1965. *Handbook of mathematical functions: with formulas, graphs, and mathematical tables*. Dover Publications: New York.

Adamowski, J. and Sun, K., 2010. Development of a coupled wavelet transform and neural network method for flow forecasting of non-perennial rivers in semi-arid watersheds. *Journal of Hydrology*, 390, pp. 85-91.

Agboola, A., Gabriel, A., Aliyu, E. and Alese, B., 2013. Development of a Fuzzy Logic Based Rainfall Prediction Model. *International Journal of Engineering and Technology*, 3, pp. 427–435.

Ahmad, M. I., Sinclair, C. D. and Werritty, A., 1988. Log-logistic flood frequency analysis. *Journal of Hydrology*, 98, pp. 205–224.

Alam, A.T.M.J., Rahman, M.S. and Sadaat, A.H.M., 2014. *Computational Intelligence Techniques in Earth and Environmental Sciences*. Netherlands, Dordrecht: Springer.

Ali, Z., Hussain, I., Faisal, M., Nazir, H.M., Hussain, T., Shad, M.Y., Shoukry, A.M. and Gani, S.H., 2017. Forecasting Drought Using Multilayer Perceptron Artificial Neural Network Model. *Advances in Meteorology*, 2017, pp. 1–9.

Alexandersson, H., 1986. A homogeneity test applied to precipitation data. *Journal of Climatology*, 6(6), pp. 661-675.

Arshad, S., Morid, S., Mobasheri, M.R., Alikhani, M.A. and Arshad, S., 2012. Monitoring and forecasting drought impact on dryland farming areas. *International Journal of Climatology*, 33(8), pp. 2068-2081.

de Artigas, M.Z., Elias, A.G., de Campra, P.F., 2006. Discrete wavelet analysis to assess long-term trends in geomagnetic activity. *Physics and Chemistry of the Earth*, 31 (1–3), pp. 77–80.

Avilés, A., Célleri, R., Paredes, J. and Solera, A., 2015. Evaluation of Markov Chain Based Drought Forecasts in an Andean Regulated River Basin Using the Skill Scores RPS and GMSS. *Water Resources Management*, 29, pp. 1949–1963.

Bacanli, U.G., Firat, M. and Dikbas, F., 2009. Adaptive Neuro-Fuzzy inference system for drought forecasting. *Stochastic Environmental Research and Risk Assessment*, 23, pp. 1143–1154.

Barua, S., Ng, A.W.M. and Perera, B.J.C., 2012. Artificial Neural Network – Based Drought Forecasting Using a Nonlinear Aggregated Drought Index. *Journal of Hydrologic Engineering*, 17, pp. 1408–1413.

Bazrafshan, O., Salajegheh, A., Bazrafshan, J., Mahdavi, M. and Marj, A.F., 2015. Hydrological Drought Forecasting using ARIMA Models (Case Study : Karkheh Basin). *Ecopersia*, 3, pp. 1099–1117.

Beguería, S., Vicente-Serrano, S.M., Reig, F. and Latorre, B., 2013. Standardized precipitation evapotranspiration index (SPEI) revisited: parameter fitting, evapotranspiration models, tools, datasets and drought monitoring. *International Journal of Climatology,* 34, pp. 3001-3023.

Belayneh, A. and Adamowski, J., 2012. Standard Precipitation Index Drought Forecasting Using Neural Networks, Wavelet Neural Networks, and Support Vector Regression. *Applied Computational Intelligence and Soft Computing*, pp. 1–13.

Belayneh, A. and Adamowski, J., 2013. Drought forecasting using new machine learning methods. *Journal of Water and Land Development*, 18, pp. 3–12.

Belayneh, A., Adamowski, J., Khalil, B. and Ozga-Zielinski, B., 2014. Long-term SPI drought forecasting in the Awash River Basin in Ethiopia using wavelet neural networks and wavelet support vector regression models. *Journal of Hyrology,* 508, pp. 418–429.

Belayneh, A., Adamowski, J., Khalil, B. and Quilty, J., 2016. Coupling machine learning methods with wavelet transforms and the bootstrap and boosting ensemble approaches for drought prediction. *Atmospheric Research,* 172–173, pp. 37–47.

Berita Harian, 2016. Gangguan Air Gugat Kemampuan Ekonomi. *Berita Harian*, [online] 28 Oct. Available at: <https://www.pressreader.com/malaysia/berita.../281642484719923> [Accessed 23 November 2016].

Bishop, C.M., 2006. *Pattern recognition and machine learning*. Springer: New York.

Borji, M., Malekian, A., Salajegheh, A. and Ghadimi, M., 2016. Multi-time-scale analysis of hydrological drought forecasting using support vector regression (SVR) and artificial neural networks (ANN). *Arabian Journal of Geosciences*, 9 (725).

Buishand, T., 1982. Some methods for testing the homogeneity of rainfall records. *Journal of Hydrology*, 58(1-2), pp. 11-27.

Burke, E., Perry, R. and Brown, S., 2010. An extreme value analysis of UK drought and projections of change in the future. *Journal of Hydrology,* 388(1-2), pp. 131-143.

Byun, H. and Wilhite, D., 1999. Objective Quantification of Drought Severity and Duration. *Journal of Climate*, 12(9), pp.2747-2756.

Cannas, B., A. Fanni, Sias, G., Tronci, S. and Zedda, M.K., 2006. *River flow forecasting using neural networks and wavelet analysis.* Proceedings of the European Geosciences Union.

Chen, J. and Yang, Y., 2012. SPI-based regional drought prediction using weighted Markov Chain model. *Research Journal of Applied Sciences, Engineering and Technology*, 4(21), pp. 4293–4298.

Chen, J., Li, M. and Wang, W., 2012. Statistical Uncertainty Estimation Using Random Forests and Its Application to Drought Forecast. *Mathematical Problems in Engineering,* pp. 1–12.

Chen, S., Shin, J.Y. and Kim, T.W., 2016. Probabilistic forecasting of drought: a hidden Markov model aggregated with the RCP 8.5 precipitation projection. *Stochastic Environmental Research and Risk Assessment,* 31, pp. 1061–1076.

Cherkassky, V. and Ma, Y., 2004. Practical selection of SVM parameters and noise estimation for SVM regression. *Neural Networks,* 17(2004), pp. 113-126.

Chiang, J.L. and Tsai, Y.S., 2012. Reservoir Drought Prediction Using Support Vector Machines. *Applied Mechanics and Materials*, 145, pp. 455–459.

Chiang, J.L. and Tsai, Y.S., 2013. Reservoir drought prediction using two-stage SVM. *Applied Mechanics and Materials*, 284–287, pp. 1473–1477.

Chun, K.P., Wheater, H. and Onof, C., 2012. Prediction of the impact of climate change on drought: an evaluation of six UK catchments using two stochastic approaches. *Hydrological Processes*, 27, pp. 1600–1614.

Cimen, M., 2008. Estimation of daily suspended sediments using support vector machines. *Hydrological Sciences Journal,* 53, pp. 656–666.

Cordiner, A., 2009. *Adaboost Toolbox: A Matlab Toolbox for Adaptive Boosting. Advanced Multimedia Research Lab Oratory Information Communications Technology Research Institute*. University of Wollongong: Australia.

Cutore, P., Mauro, G. and Cancelliere, A., 2009. Forecasting Palmer Index Using Neural Networks. *Journal of Hydrologic Engineering,* 14, pp. 588–595.

Dastorani, M.T., Afkhami, H., Sharifidarani, H. and Dastorani, M., 2010. Application of ANN and ANFIS models on dryland precipitation prediction (case study: Yazd in central Iran). *Journal of Applied Sciences*, 10(20), pp. 2387-2394

Deng, J., Chen, X., Du, Z. and Zhang, Y., 2011. Soil Water Simulation and Predication Using Stochastic Models Based on LS-SVM for Red Soil Region of China. *Water Resources Management*, 25, pp. 2823–2836.

Deo, R.C. and Sahin, M., 2015. Application of the Artificial Neural Network model for prediction of monthly Standardized Precipitation and Evapotranspiration Index using hydrometeorological parameters and climate indices in eastern Australia. *Atmospheric Research*, 161–162, pp. 65–81.

Deo, R.C. and Sahin, M., 2016. An extreme learning machine model for the simulation of monthly mean streamflow water level in eastern Queensland. *Environmental Monitoring and Assessment*, 188(90).

Deo, R.C., Tiwari, M.K., Adamowski, J.F. and Quilty, J.M., 2016. Forecasting effective drought index using a wavelet extreme learning machine (W-ELM) model. *Stochastic Environmental Research and Risk Assessment*, 31, pp. 1211–1240.

Department of Irrigation and Drainage, 2016. *Brief History on Development of Drought Information Website.* [online] Available at: < http://infokemarau.water.gov.my/about.cfm > [Accessed 2 December 2016].

Department of Agriculture, 1995. *Land use of Selangor and Negeri Sembilan*. Kuala Lumpur, Malaysia: Department of Agriculture (DOA).

Dhorde, A.G. and Patel, N.R., 2015. Spatio-temporal variation in terminal drought over western India using dryness Index derived from long-term MODIS data. *Ecological Informatics*, 32, pp.28-38.

Djerbouai, S. and Souag-Gamane, D., 2016. Drought Forecasting Using Neural Networks, Wavelet Neural Networks, and Stochastic Models: Case of the Algerois Basin in North Algeria. *Water Resources Management*, 30, pp. 2445–2464.

Dogan, S., Berktay, A. and Singh, V.P., 2012. Comparison of multi-monthly rainfall-based drought severity indices, with application to semi-arid Konya closed basin, Turkey. *Journal of Hydrology*, 470-471, pp. 255–268.

Economic Transformation Programme, 2012. *Greater Kuala Lumpur/Klang Valley.* [pdf] Malaysia: ETP. Available at: <http://etp.pemandu.gov.my/annualreport2011/upload/ENG_NKEA_Greater_KLKV.pdf> [Accessed 23 November 2016].

Edwards, D.C. and McKee, T.B., 1997. Characteristics of 20th century drought in the United States at multiple time scales. *Atmospheric Science Paper*, 634, pp. 1-30.

Eschooltoday.com., 2016. *Types of droughts*. [online] Available at: http://eschooltoday.com/natural-disasters/droughts/types-of-droughts.html [Accessed 21 May 2018].

Farokhnia, A., Morid, S. and Byun, H.R., 2011. Application of global SST and SLP data for drought forecasting on Tehran plain using data mining and ANFIS techniques. *Theoretical and Applied Climatology*, 104, pp. 71–81.

Fernandez-Manso, A., Quintano, C. and Fernandez-Manso, O., 2011. Forecast of NDVI in coniferous areas using temporal ARIMA analysis and climatic data at a regional scale. *International Journal of Remote Sensing*, 32, pp. 1595–1617.

Freund, Y. and Schapire, R.E., 1996. Proceedings of the Thirteenth International Conference: Experiments with a new boosting algorithm. *Machine Learning*, pp. 148–156.

Freund, Y. and Schapire, R.E., 1997. A decision-theoretic generalization of on-line learning and an application to boosting. *Journal of Computer and System Sciences*, 55(1), pp. 119-139.

Freund, Y. and Schapire, R.E., 1999. Adaptive game playing using multiplicative weights. *Games and Economic Behavior*, 29, pp.79-103.

Friedman, J.H., 1999. Greedy Function Approximation: A Gradient Boosting Machine. *The Annals of Statistics*, 29(5), pp. 1189-1232.

Ganguli, P. and JangaReddy, M., 2014. Ensemble prediction of regional droughts using climate inputs and the SVM-copula approach. *Hydrological Process*, 28, pp. 4989–5009.

Gocic, M. and Trajkovic, S., 2013. Spatiotemporal characteristics of drought in Serbia. *Journal of Hydrology*, 510, pp.112-123.

Han, P., Wang, P.X., Zhang, S.Y. and Zhu, D.H., 2010. Drought forecasting based on the remote sensing data using ARIMA models. *Mathematical and Computer Modelling*, 51, pp. 1398–1403.

Han, P., Wang, P.X., Tian, M., Zhang, S.Y., Liu, J.M. and Zhu, D.H., 2013. Application of the ARIMA Models in Drought Forecasting Using the Standardized Precipitation Index. *IFIP Advances in Information and Communication Technology*, 352–358.

Hastie, T., Tibshirani, R. and Friedman, J.H., 2009. *The elements of statistical learning: data mining, inference, and prediction*. Springer: New York.

Hosking, J.R.M. and Wallis, J.R., 1997. *Regional Frequency Analysis – An Approach based on L-Moments.* Cambridge University Press: Cambridge.
Hosseini-Moghari, S.M. and Araghinejad, S., 2015. Monthly and seasonal drought forecasting using statistical neural networks. *Environmental Earth Sciences,* 74, pp. 397–412.

Huang, S., Hou, B., Chang, J., Huang, Q. and Chen, Y., 2014. Copulas-based probabilistic characterization of the combination of dry and wet conditions in the Guanzhong Plain, China. *Journal of Hydrology,* 519, pp. 3204-3213.

Hussaini, H.A., 2007. *Flood and Drought Management in Malaysia*. 21 June, Ministry of Natural Resources and Environment, Malaysia, Kuala Lumpur.

Jalalkamali, A., Moradi, M. and Moradi, N., 2015. Application of several artificial intelligence models and ARIMAX model for forecasting drought using the Standardized Precipitation Index. *International Journal of Environmental Science and Technology,* 12, pp. 1201–1210.

Jalili, M., Gharibshah, J., Ghavami, S.M., Beheshtifar, M. and Farshi, R., 2014. Nationwide prediction of drought conditions in Iran based on remote sensing data. *IEEE Transactions on Computers,* 63, pp. 90–101.

Jiang, X. and Chen, S., 2009. Application of Weighted Markov SCGM(1,1)c Model to Predict Drought Crop Area. *Systems Engineering - Theory & Practice*, 29, pp. 179–185.

Juahir, H., Zain, S.M., Yusoff, M.K., Hanidza, T.I.T., Armi, A.S.M., Toriman, M.E. and Mokhtar, M., 2011. Spatial water quality assessment of Langat River Basin (Malaysia) using environmetric techniques. *Environmental Monitoring and Assessment*, 173(1-4), pp. 625-641

Kanika, E., Dhillon, N. and Sharama, E.K., 2012. Comparative Analysis of Discrete Wavelet Transform and Fast Wavelet Transform on Image compression. *International Journal of Engineering Research & Technology*, 1(5), pp. 1–7.

Karthika, K., Krishnaveni and Thirunavukkarasu, V., 2017. Forecasting of meteorological drought using ARIMA model. *Indian Journal of Agricultural Sciences*, 51, pp. 103–111.

Kecman, V., 2001. Learning and Soft Computing. MIT Press: London.

Keskin, M.E., Terzi, Ö., Taylan, E.D. and Küçükyaman, D., 2009. Meteorological drought analysis using data-driven models for the Lakes District, Turkey. *Hydrological Sciences Journal,* 54, pp. 1114–1124

Khadr, M., 2016. Forecasting of meteorological drought using Hidden Markov Model (case study: The upper Blue Nile river basin, Ethiopia). *Ain Shams Engineering Journal*, 7, pp. 47–56.

Kim, T. and Valdes, J.B., 2003. Nonlinear Model for Drought Forecasting Based on a Conjunction of Wavelet Transforms and Neural Networks. *Journal of Hydrologic Engineering*, 8, pp. 319-328.
Kisi, O. and Cimen, M., 2011. A wavelet-support vector machine conjunction model for monthly streamflow forecasting. *Journal of Hydrology*, 399, pp. 132–140.

Klir, G.J. and Yuan, B., 2008. *Fuzzy sets and fuzzy logic, theory and applications*. Prentice Hall PTR: Upper Saddle River, New Jersey

Kousari, M.R., Hosseini, M.E., Ahani, H. and Hakimelahi, H., 2017. Introducing an operational method to forecast long-term regional drought based on the application of artificial intelligence capabilities. *Theoretical and Applied Climatology*, 127, pp. 361–380.

Leister, E., 2014. *Drought Worsens in Malaysia and Thailand*. [online] Available at: <http://www.accuweather.com/en/weather-news/drought-worsens-in-malaysia-an/23698698> [Accessed 21 May 2018].

Li, B., Zhou, Wei., Zhao, Y.Y., Ju, Q., Yu, Z.B., Liang, Z.M. Archarya, M., 2015. Using the SPEI to Assess Recent Climate Change in the Yarlung Zangbo River Basin, South Tibet. *Water*, 7, pp. 5474-5486.

Li, R., Tsunekawa, A. and Tsubo, M., 2014. Index-based assessment of agricultural drought in a semi-arid region of Inner Mongolia, China. *Journal of Arid Land*, 6, pp. 3-15.

Li, R., Wang, J., Zhao, T. and Shi, J., 2016. Index-based evaluation of vegetation response to meteorological drought in Northern China. *Natural Hazards*, 84(3), pp. 2179–2193.

Lin, C.F. and Wang, S.D., 2002. Fuzzy Support Vector Machines. *IEEE Transactions on Neural Networks and Learning Systems*, 13(2), pp. 464-471.

Liu, Z., Wang, Y., Shao, M., Jia, X. and Li, X., 2016. Spatiotemporal analysis of multiscalar drought characteristics across the Loess Plateau of China. *Journal of Hydrology*, 534, pp. 281-299.

Lorenzo-Lacruz, J., Vivente-Serrano, S.M., Lopez-Moreno, J.I., Begueria, S., Garcia-Ruiz, J.M. and Cuadrat, J.M., 2010. The impact of droughts and water management on various hydrological systems in the headwaters of the Tagus River (central Spain). *Journal of Hydrology*, 386, pp. 13-26.

López-Moreno, J.I., Vicente-Serrano, S.M., Zabalza, J., Begueria, S., Lorenzo-Lacruz, J., Azorin-Molina, C. and Moran-Tejeda, E., 2012. Hydrological response to climate variability at different time scales: A study in the Ebro basin. *Journal of Hydrology*, 477, pp. 175-188.

Maca, P. and Pech, P. 2016. Forecasting SPEI and SPI Drought Indices Using the Integrated Artificial Neural Networks. *Computational Intelligence and Neuroscience*, 2016, pp. 1–17.

Maheswaran, R. and Khosa, R., 2011. Comparative study of different wavelets for hydrologic forecasting. *Computers and Geosciences,* 46, pp. 284-295.

Mahmud, I., Bari, S.H. and UrRahman, M.T., 2016. Monthly rainfall forecast of Bangladesh using autoregressive integrated moving average method. *Environmental Engineering Research*, 22, pp. 162–168.

Malaysia Meteorological Department, 2014. *Country Reports – Malaysia*. Selangor: MetMalayisa

Mares, C., Mares, I. and Mihailescu, M., 2016. Identification of extreme events using drought indices and their impact on the Danube lower basin discharge. *Hydrological Processes,* 30(21), pp. 3839-3854.

Marj, A.F. and Meijerink, A.M.J., 2011. Agricultural drought forecasting using satellite images, climate indices and artificial neural network. *International Journal of Remote Sensing,* 32, pp. 9707–9719.

Masinde, M., 2014. Artificial neural networks models for predicting effective drought index: Factoring effects of rainfall variability. Mitigation and Adaptation Strategies for Global Change 19, pp. 1139–1162.

Mathworks, Inc., 2016. *Fuzzy Logic Toolbox, for Use with MATLAB®, User's Guide*. Version 2. Natick, MA: The Mathworks.

Mathworks, 2011. *'fitensemble' - Fit ensemble of learners for classification and regression.* [online]. Available at: <https://www.mathworks.com/help/stats/fitensemble.html#bu_gvq1_sep_shared-Learners> [Accessed 26 May, 2016]

Mehr, A.D., Kahya, E. and Ozger, M., 2014. A gene-wavelet model for long lead time drought forecasting. *Journal of Hydrology,* 517, pp. 691–699.

Memarian, H., Bilondi, M.P. and Rezaei, M., 2016. Drought prediction using co-active neuro-fuzzy inference system, validation, and uncertainty analysis (case study: Birjand, Iran). *Theoretical and Applied Climatology,* 125, pp. 541–554.

Mishra, A.K., Desai, V. and Singh, V., 2007. Drought Forecasting Using a Hybrid Stochastic and Neural Network Model. *Journal of Hydrologic Engineering,* 12, pp. 626–638.

Mishra, A.K. and Singh, V.P., 2011. Drought modeling - A review. *Journal of Hydrology,* 403, pp. 157–175.

Mondal, A. and Mujumdar, P. P., 2014. Return levels of hydrologic droughts under climate change. *Advances in Water Resources*, 75, pp. 67-69.

Montgomery, D.C. and Runger, G.C., 2014. *Applied Statistics and Probability for Engineers.*Wiley: United States of America.

Mossad, A. and Alazba, A.A., 2015. Drought forecasting using stochastic models in a hyper-arid climate. *Atmosphere,* 6, pp. 410–430.
Narasimhan, B. and Srinivasan, R., 2005. Drought and Evaluation of Soil Deficit Index (SMDI) and Evapotranspiration Deficit Index (ETDI) for Agricultural Drought Monitoring. *Agricultural and Forest Meteorology,* 133, pp. 69-88.

Nason, G.P. and Von Sachs, R., 1999. Wavelets in time-series analysis. *Philosophical Transactions of the Royal Society A: Mathematical, Physical and Engineering Sciences* 357 (1760), pp. 2511-2526.

National Drought Mitigation Centre, 2016. Comparison of Major Drought Indices [online] Available at: <http://drought.unl.edu/Planning/Monitoring/ComparisonofDroughtIndices.aspx> [Accessed 5 Jun 2016].

Nguyen, L.B., Li, Q.F., Ngoc, T.A. and Hiramatsu, K., 2015. Adaptive Neuro-Fuzzy Inference System for drought forecasting in the Cai River basin in Vietnam. *Journal of the Faculty of Agriculture, Kyushu University* 60, pp. 405–415.

Niemeyer, S. 2008. New drought indices. *Options Méditerranéennes. Série A,* 80, pp. 267–274.

Nikbakht, J., Tabari, H. and Talaee, P.H., 2012. Streamflow drought severity analysis by percent of normal index (PNI) in northwest Iran. *Theoretical and Applied Climatology,* 112, pp. 565-573.

Nnaji, G.A., Clark, C.J., Chan-Hilton, A.B. and Huang, W., 2016. Drought prediction in Apalachicola–Chattahoochee–Flint River Basin using a semi-Markov model. *Natural Hazards*, 82(1), pp. 267-297.

Núñez, J., Rivera, D., Oyarzún, R. and Arumí, J. L., 2014. On the use of Standardized Drought Indices under decadal climate variability: Critical assessment and drought policy implications. *Journal of Hydrology,* 517, pp. 458-470.

Ochoa-Rivera, J.C., 2008. Prospecting droughts with stochastic artificial neural networks. *Journal of Hydrology,* 352, pp. 174–180.

Ozger, M., Mishra, A.K. and Singh, V.P., 2011. Estimating Palmer Drought Severity Index using a wavelet fuzzy logic model based on meteorological variables. *International Journal of Climatology,* 31, pp. 2021–2032.

Ozger, M., Mishra, A.K. and Singh, V.P., 2012. Long Lead Time Drought Forecasting Using a Wavelet and Fuzzy Logic Combination Model: A Case Study in Texas. *Journal of Hydrometeorology*, 13, pp. 284–297.

Park, C.K., Byun, H.R., Deo, R. and Lee, B.R., 2015. Drought prediction till 2100 under RCP 8.5 Climate Change Scenarios for Korea. *Journal of Hydrology*, 526, pp. 221-230.

Paulo, A.A. and Pereira, L.S., 2007. Prediction of SPI drought class transitions using Markov chains. *Water Resources Management*, 21, pp. 1813–1827.

Paulo, A.A., Rosa, R.D. and Pereira, L.S., 2012. Climate trends and behaviour of drought indices based on precipitation and evapotranspiration in Portugal. *Natural Hazards and Earth System Sciences*, 12, pp. 1481-1491.

Patel, N.R., Parida, B.R., Venus, V., Saha, S.K. and Dadhwal, V.K., 2011. Analysis of agricultural drought using vegetation temperature condition index (VTCI) from Terra/MODIS satellite data. *Environmental Monitoring and Assessment*, 184, pp. 7153-7163.

Pettitt, A., 1979. A non-parametric approach to the change-point problem. *Applied Statistics*, 28(2), pp. 126-135.

Potop, V., 2011. Evolution of drought severity and its impact on corn in the Republic of Moldova. *Theoretical and Applied Climatology*, 105, pp. 469-483.

Potop, V., Mozny, M. and Soukup, J., 2012. Drought evolution at various time scales in the lowland regions and their impact on vegetable crops in the Czech Republic. *Agricultural and Forest Meteorology*, 156, pp. 121-133.

Prasad, R., Deo, R.C., Li, Y. and Maraseni, T., 2017. Input selection and performance optimization of ANN-based streamflow forecasts in the drought-prone Murray Darling Basin region using IIS and MODWT algorithm. *Atmospheric Research*, 197, pp. 42–63.

Pulwarty, R.S. and Sivakumar, M.V.K., 2014. Information systems in a changing climate: Early warnings and drought risk management. *Weather and Climate Extremes*, 3, pp. 14–21.

Rahmat, S.N., Jayasuriya, N. and Bhuiyan, M.A., 2016. Short-term droughts forecast using Markov chain model in Victoria, Australia. Theoretical and Applied Climatology, 129, pp. 445–457.

Rezaeianzadeh, M., Stein, A. and Cox, J.P., 2016. Drought Forecasting using Markov Chain Model and Artificial Neural Networks. *Water Resources Management*, 30, pp. 2245–2259.

Robinson, V.B., 2003. A Perspective on the Fundamentals of Fuzzy Sets and their Use in Geographic Information Systems. *Transactions in GIS*, 7, pp. 3–30.

Rohli, R.V., Bushra, N., Lam N.S.N., Zou, L., Mihunov, V., Reams, M.A. and Argote, J.E., 2016. Drought indices as drought predictors in the south-central USA. *Natural Hazards*, 83(3), pp. 1567-1582.

Schapire, R.E., 1990. The strength of weak learnability. *Machine Learning*, 5, pp. 197–227.

Schapire, R.E. and Singer, Y., 2000. BoosTexter: a boosting-based system for text categorization. *Machine Learning.* 39(2-3), pp. 135-168.
Seibert, M., Merz, B. and Apel, H., 2017. Seasonal forecasting of hydrological drought in the Limpopo Basin: A comparison of statistical methods. *Hydrology and Earth System Sciences*, 21, pp. 1611–1629.

Shabri, A., 2014. A Hybrid Wavelet Analysis and Adaptive Neuro-Fuzzy Inference System for Drought Forecasting. *Applied Mathematical Sciences,* 8, pp. 6909–6918.

Sharma, T.C. and Panu, U.S., 2012. Prediction of hydrological drought durations based on Markov chains: case of the Canadian prairies. *Hydrological Sciences Journal*, 57, pp. 705–722.

Sharp, J.J. and Sawden, P., 1984. *Basic Hydrology*. London, England: Butterworth & Co. Ltd.

Shatanawi, K., Rahbeh, M. and Shatanawi, M., 2013. Characterizing , Monitoring and Forecasting of Drought in Jordan River Basin. *Journal of Water Resource and Protection*, 5, pp. 1192–1202.

Shazwan, M.K., 2016. Prepare action plan to face dry spell, DAP MP tells Selangor. *The Malay Mail Online*, [online] 21 Apr. Available at: < http://www.themalaymailonline.com/malaysia/article/prepare-action-plan-to-face-dry-spell-dap-mp-tells-selangor > [Accessed 23 November 2016].

Shirmohammadi, B., Moradi, H., Moosavi, V., Semiromi, M.T., Zeinali, A., 2013. Forecasting of meteorological drought using Wavelet-ANFIS hybrid model for different time steps (case study: Southeastern part of east Azerbaijan province, Iran). *Natural Hazards,* 69, pp.389–402.

Sicat, R.S., Carranza, E.J.M., Bhaskar, U., 2005. Fuzzy modeling of farmers ' knowledge for land suitability classification. *Agricultural Systems*, 83, pp. 49–75.

Stagge, V., Kohn, I., Tallaksen, L.M. and Stahl, K., 2015. Modeling drought impact occurrence based on meteorological drought indices in Europe. *Journal of Hydrology,* 530, pp. 37-50.

Sun, P., Zhang, Q., Singh, V.P., Xiao, M. and Zhang, X., 2016. Transitional variations and risk of hydro-meteorological droughts in the Tarim River basin, China. *Stochastic Environmental Research and Risk Assessment*, 31, pp. 1515–1526.

Sutton, C.D., 2005. *Handbook of statistics: data mining and data visualization.* Elsevier: Amsterdam.

The Sun Daily, 2017. Langat 2 water treatment plant to be ready by 2019. *The Sun Daily,* [online] 5 Nov. Available at: <http://www.thesundaily.my/news/2017/11/05/langat-2-water-treatment-plant-be-ready-2019> [Accessed 21 May 2018].

Tian, M., Wang, P. and Khan, J., 2016. Drought Forecasting with Vegetation Temperature Condition Index Using ARIMA Models in the Guanzhong Plain. *Remote Sensing,* 8, pp.690.
Today Online, 2016. M'sia warns of extended spell of hot, dry weather. *Today Online,* [online] 24 Apr. Available at: < http://www.todayonline.com/world/asia/malaysias-dry-spell-may-last-till-september-warns-govt > [Accessed 23 November 2016].

Vapnik, V.N., 1997. *The Nature of Statistical Learning Theory*. IEEE transactions on neural networks, Springer: New York.

Venkataraman, K., Tummuri, S., Medina, A. and perry, J., 2016. 21st century drought outlook for major climate divisions of Texas based on CMIP5 multimodel ensemble: Implications for water resource management. *Journal of Hydrology,* 534, pp. 300-316.

Vicente-Serrano, S.M., Beguería, S. and López-Moreno, J.I., 2010. A Multiscalar Drought Index Sensitive to Global Warming: The Standardized Precipitation Evapotranspiration Index. *Journal of Climate,* 23, pp. 1696-1718.

Vicente-Serrano, S.M., Begueria, S., Lorenzo-Lacruz, J., Camarero, J.J., Lopez-Moreno, J.I., Azorin-Molina, Z., Revuelto, J., Moran-Tejeda, E. and Sanchez-Lorenzo, E., 2012. Performance of Drought Indices for Ecological, Agricultural, and Hydrological Applications. *Earth Interactions,* 16(10).

Vicente-Serrano, S.M., Schrier, G.V.D., Beguería, S., Azorin–Molina, C. and Lopez–Moreno, Juan-I., 2015. Contribution of precipitation and reference evapotranspiration to drought indices under different climates. *Journal of Hydrology,* 526, pp. 42-54.

Von Neumann, J., 1941. Distribution of the ratio of the mean square successive difference to the variance. *Annals of Mathematical Statistics,* 12(4), pp. 367-395.

Wang, Q.F, Wu, J.J., Lei, T.J., He, B., Wu, Z.T., Liu, M., Mo, X.Y., Geng, G.P., Li, X.H., Zhou, H.K. and Liu, D.C., 2014. Temporal-spatial characteristics of severe drought events and their impact on agriculture on a global scale. *Quaternary International,* 349, pp. 10–21.

Wei-Guang L., Xue Y., Mei-Ting H., Hui-Lin Ch. and Zhen-Li Ch., 2012. Standardized precipitation evapotranspiration index shows drought trends in China. *Chinese Journal of Eco-Agriculture*, 20(5), pp. 643−649.

Wijngaard, J. B., Klein Tank, A. M. G. and Konnen, G. P., 2003. Homogeneity of 20th century European daily temperature and precipitation series. *International Journal of Climatology*, 23(6), pp. 679–692.

Woli, P., Jones, J., Ingram, K. and Paz, J., 2013. Forecasting Drought Using the Agricultural Reference Index for Drought (ARID): A Case Study. *Weather and Forecasting*, 28, pp. 427–443.

World Meteorological Organization, 2012. *Standardized Precipitation Index: User Guide.* Geneva: World Meteorological Organization (WMO) and Global Water Partnership (GWP).

World Meteorological Organization, 2016. *Handbook of Drought Indicators and Indices.* Geneva: World Meteorological Organization (WMO) and Global Water Partnership (GWP).

Wilhite, D.A., Sivakumar, M.V.K. and Pulwarty, R., 2014. Managing drought risk in a changing climate: The role of national drought policy. *Weather and Climate Extremes*, 3, pp. 4–13.

Xiao, M., Zhang, Q., Singh, V.P. and Liu, L., 2016. Transitional properties of droughts and related impacts of climate indices in the Pearl River basin, China. *Journal of Hydrology*, 534, pp. 397-406.

Yacoub, E. and Tayfur, G., 2016. Evaluation and Assessment of Meteorological Drought by Different Methods in Trarza Region, Mauritania. *Water Resources Management*, pp. 1-21.

Yeh, C.F., Wang, J., Yeh, H.F. and Lee, C.H., 2015. SDI and Markov Chains for Regional Drought Characteristics. *Sustainability*, 7, pp. 10789–10808.

Zachariah, E., 2014. Selangor water crisis caused millions in losses to industries. *The Malaysian Insider*, [online] 10 November. Available at: < http://www.themalaysianinsider.com/malaysia/article/selangor-water-crisis-caused-millions-in-losses-to-industries> [Accessed 23 June 2016].

Zadeh, L.A., 1965. Fuzzy sets. *Information and Control*, 8, pp. 338–353

Zhang, T., Li, J., Hu, R., Wang, Y. and Feng, P., 2017. Drought class transition analysis through different models: a case study in North China. *Water Science & Technology Water Supply*, 17, pp. 138–150.

APPENDICES

APPENDIX A1

(SPEI-1, s2815001)

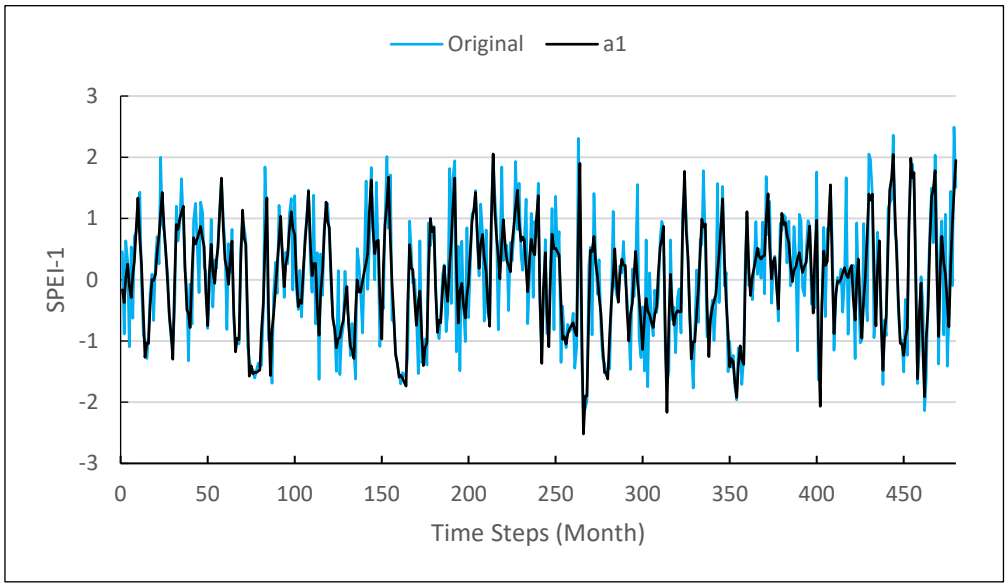

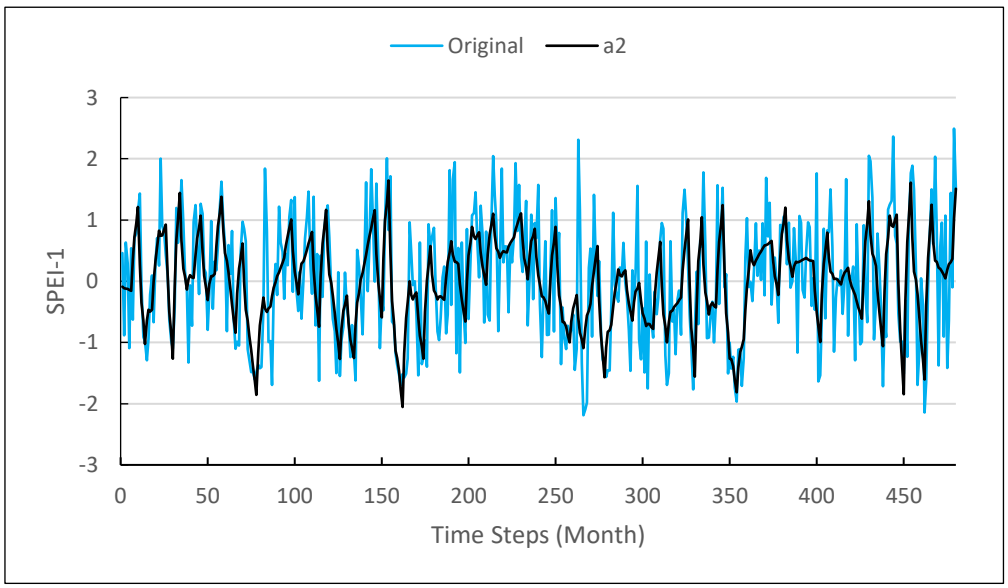

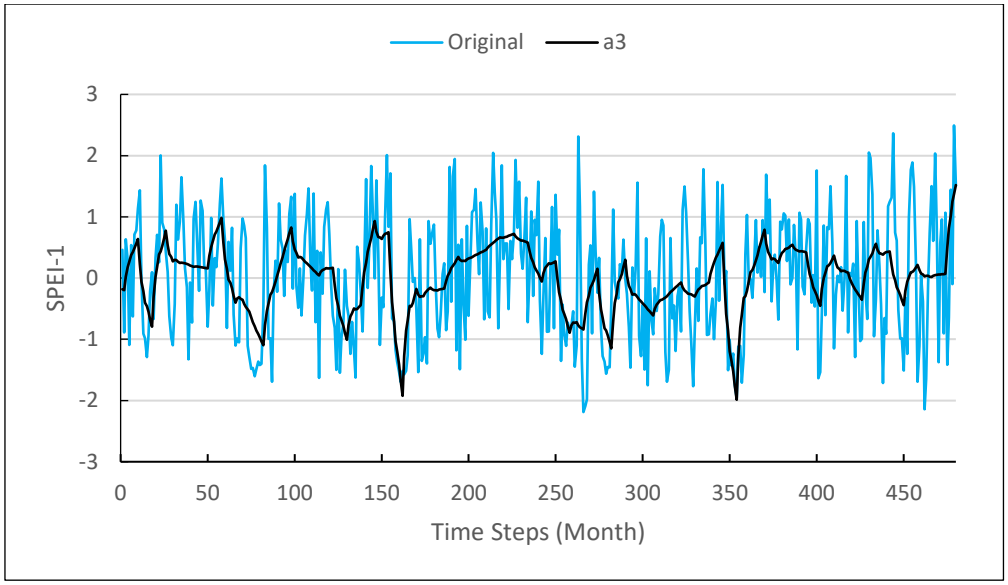
Original
a3
SPEI-1
3
2
1
0
-1
-2
-3
0
50
100
150
200
250
300
350
400
450
Time Steps (Month)

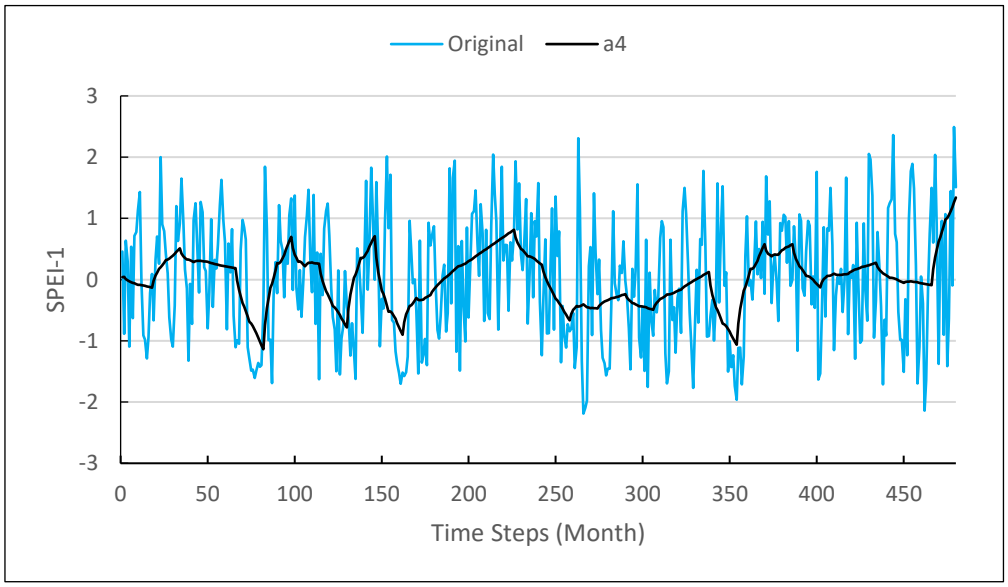
Original
a4
SPEI-1
3
2
1
0
-1
-2
-3
0
50
100
150
200
250
300
350
400
450
Time Steps (Month)

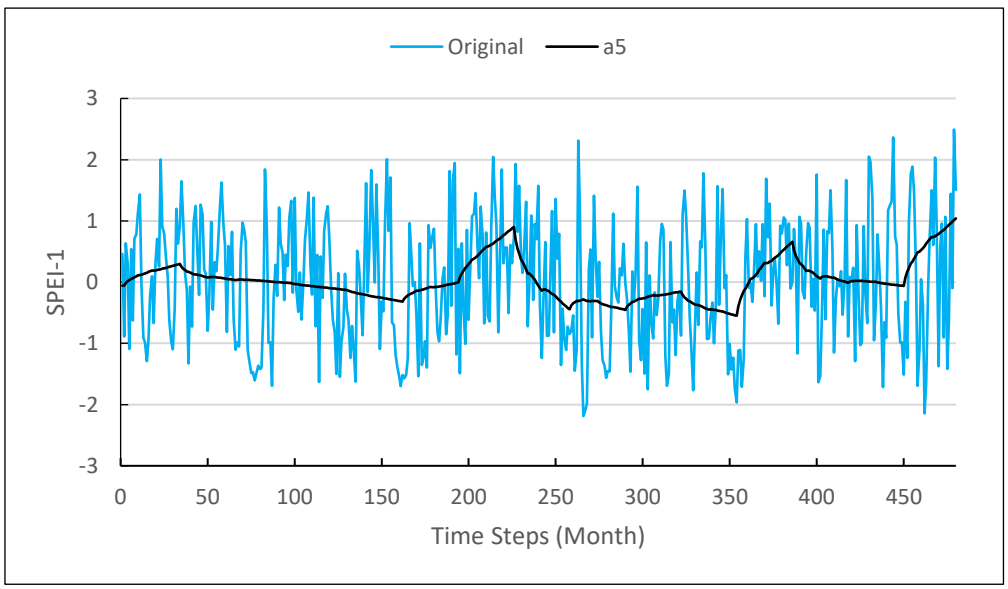
Original
a5
SPEI-1
3
2
1
0
-1
-2
-3
0
50
100
150
200
250
300
350
400
450
Time Steps (Month)

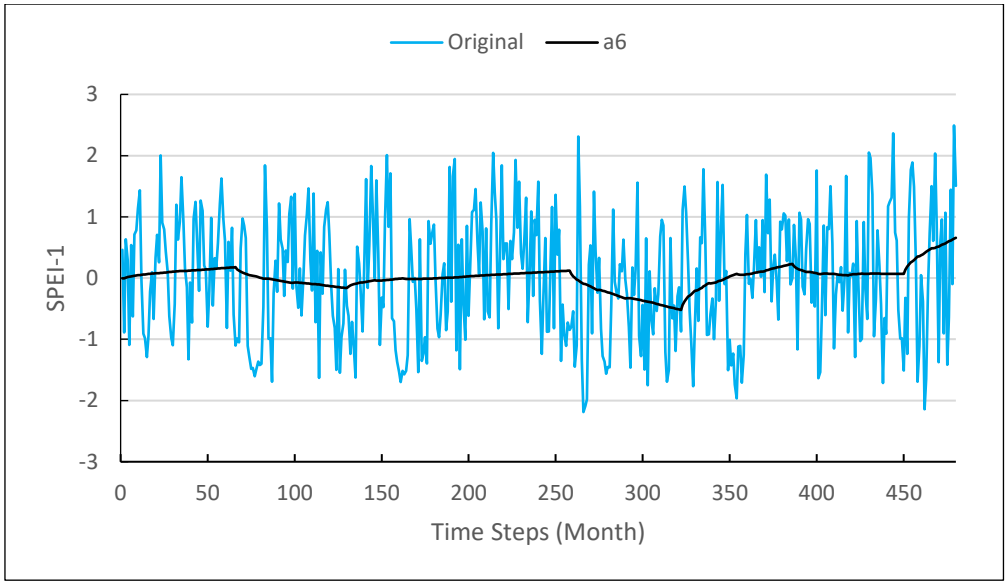
Original
a6
SPEI-1
3
2
1
0
-1
-2
-3
0
50
100
150
200
250
300
350
400
450
Time Steps (Month)

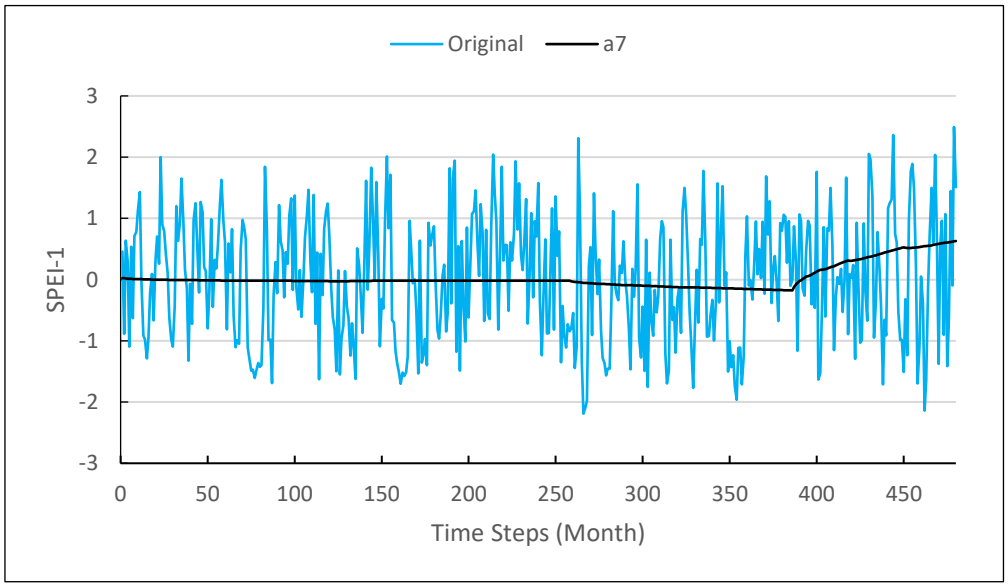
Original
a7
SPEI-1
3
2
1
0
-1
-2
-3
0
50
100
150
200
250
300
350
400
450
Time Steps (Month)

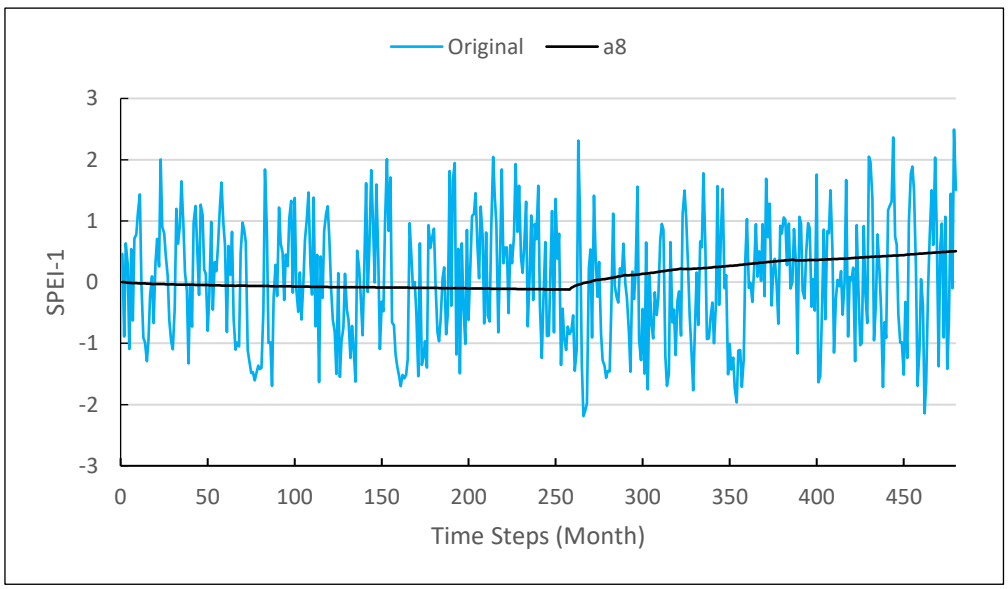
Original
a8
SPEI-1
3
2
1
0
-1
-2
-3
0
50
100
150
200
250
300
350
400
450
Time Steps (Month)

APPENDIX A2

(SPEI-3, s2815001)

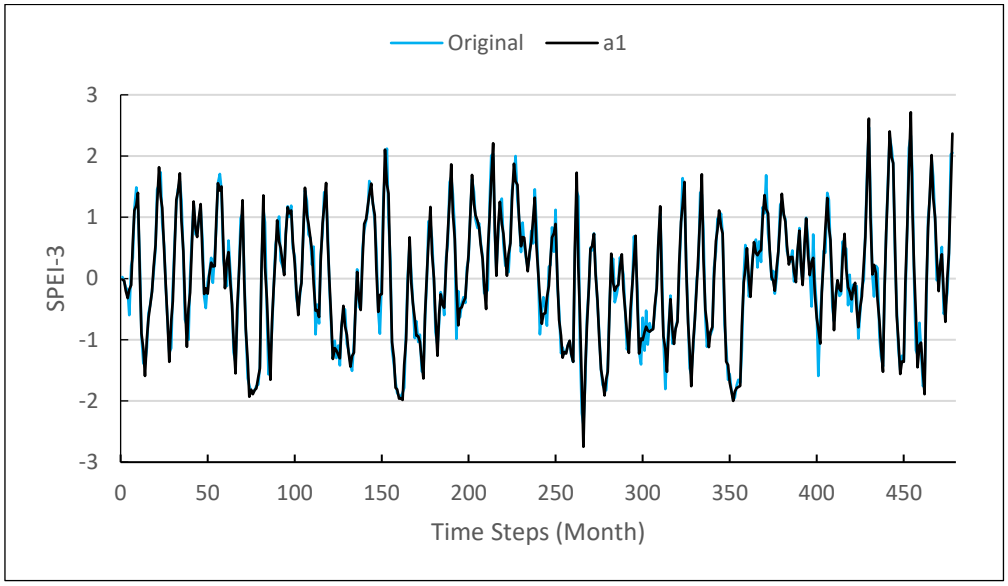

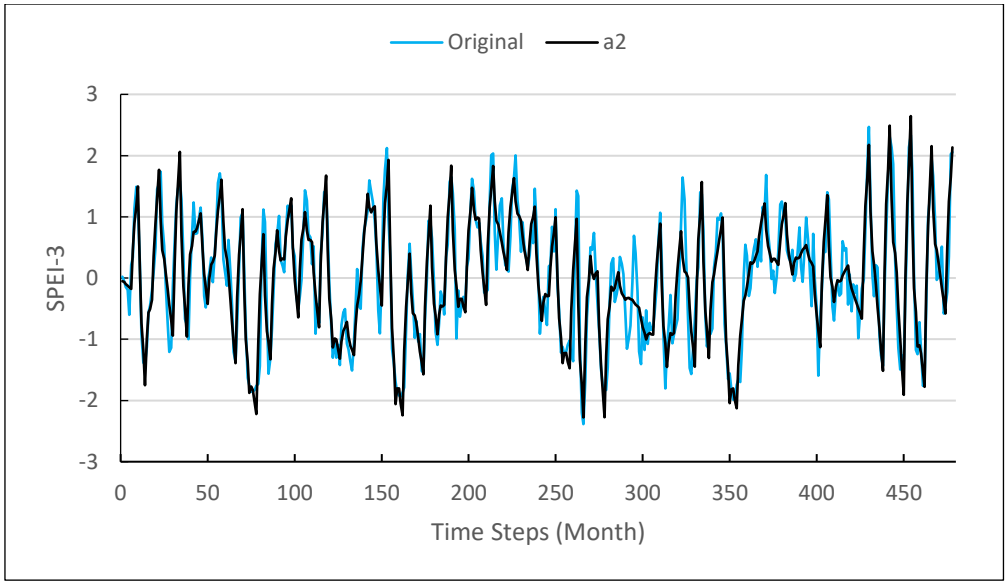

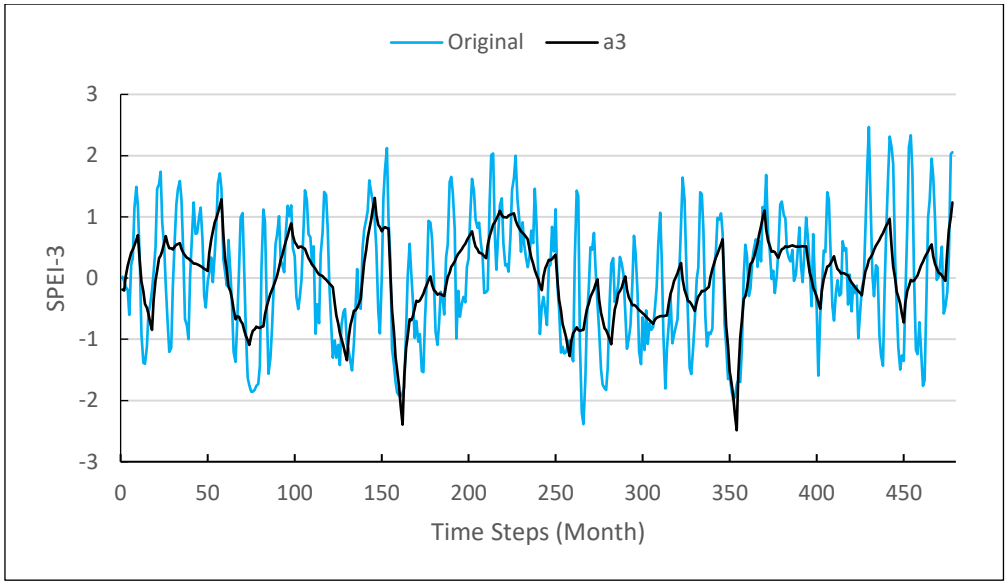
Original
a3
SPEI-3
3
2
1
0
-1
-2
-3
0
50
100
150
200
250
300
350
400
450
Time Steps (Month)

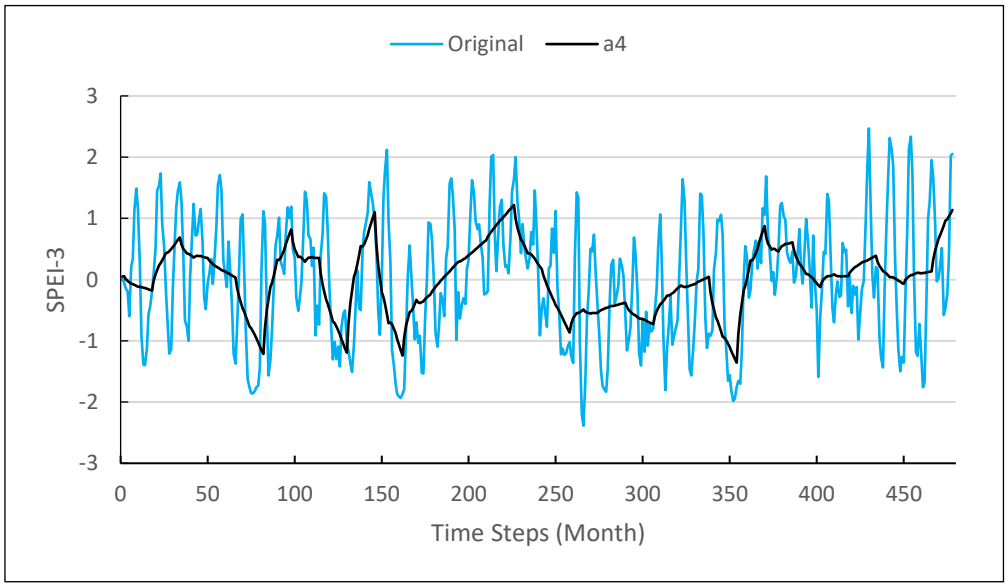
Original
a4
SPEI-3
3
2
1
0
-1
-2
-3
0
50
100
150
200
250
300
350
400
450
Time Steps (Month)

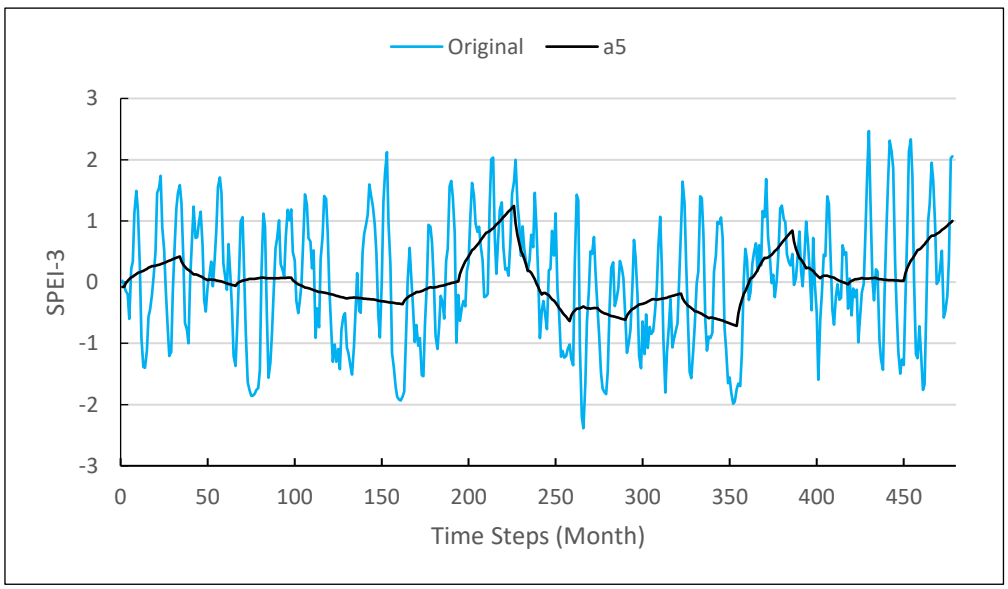
Original
a5
SPEI-3
3
2
1
0
-1
-2
-3
0
50
100
150
200
250
300
350
400
450
Time Steps (Month)

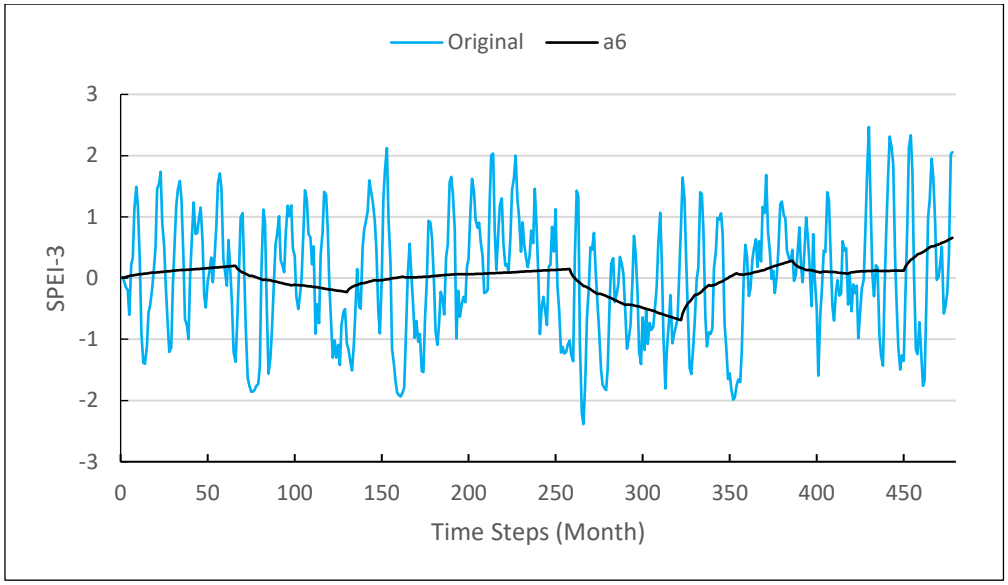
Original
a6
SPEI-3
3
2
1
0
-1
-2
-3
0
50
100
150
200
250
300
350
400
450
Time Steps (Month)

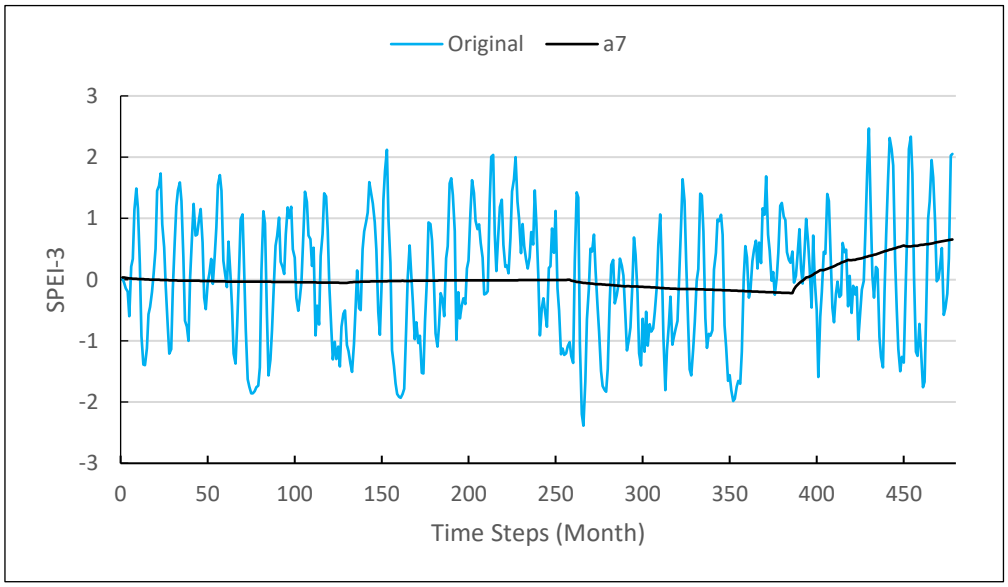
Original
a7
SPEI-3
3
2
1
0
-1
-2
-3
0
50
100
150
200
250
300
350
400
450
Time Steps (Month)

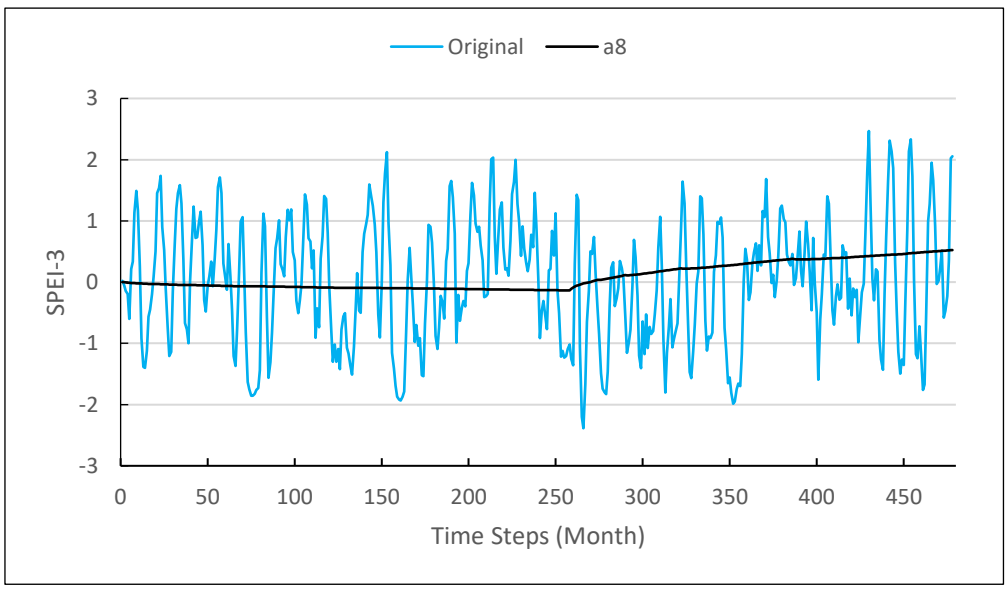
Original
a8
SPEI-3
3
2
1
0
-1
-2
-3
0
50
100
150
200
250
300
350
400
450
Time Steps (Month)

APPENDIX A3

(SPEI-6, s2815001)

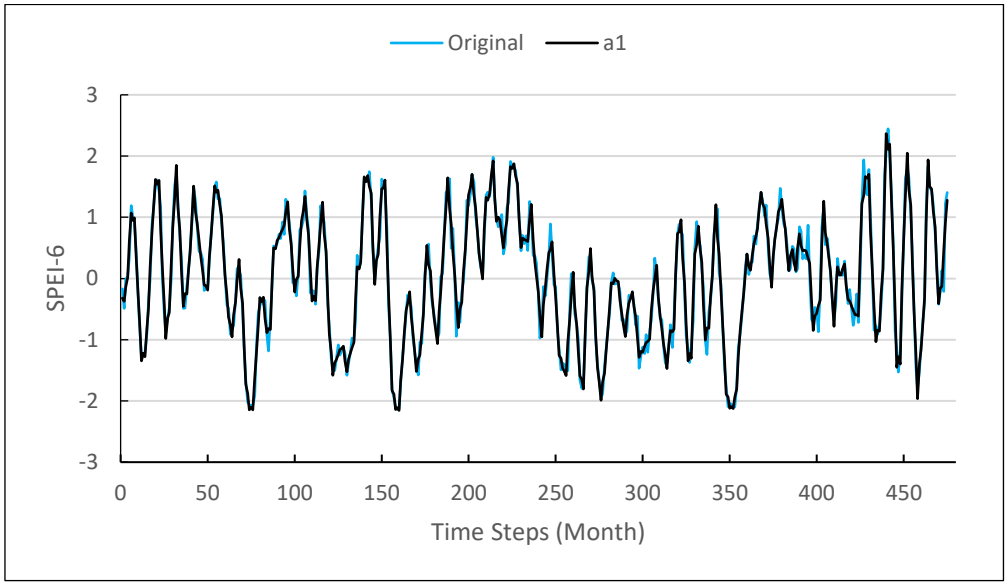

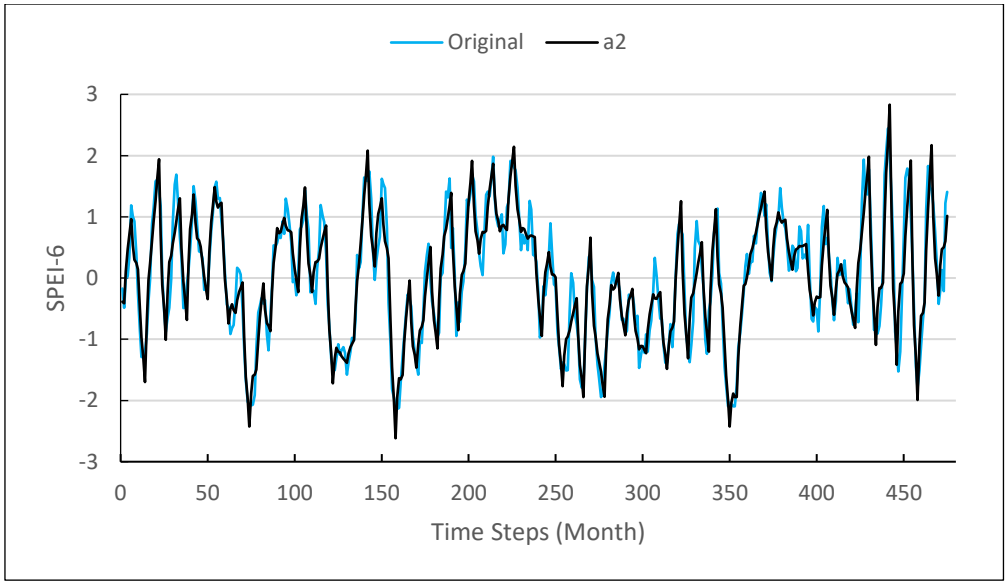

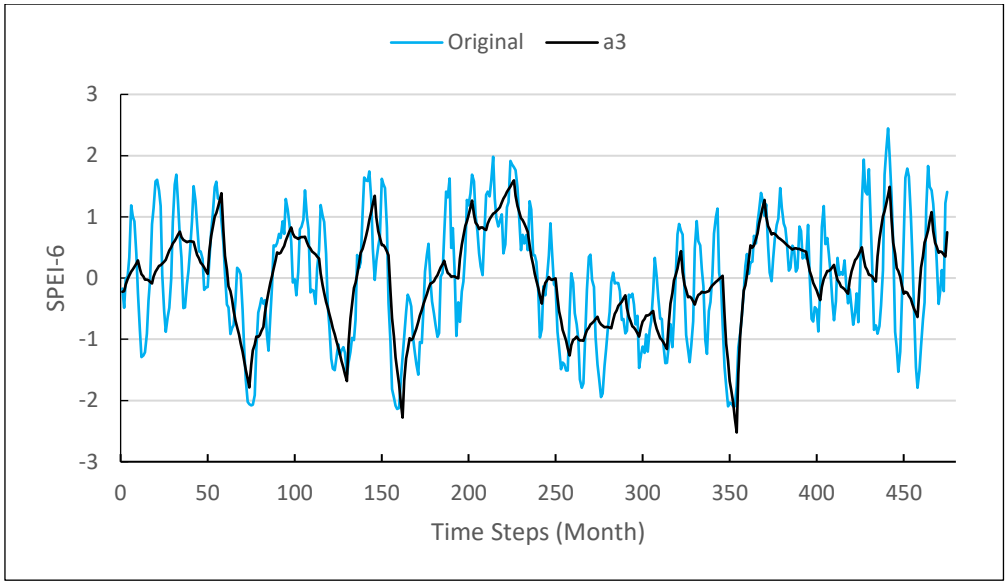
Original
a3
SPEI-6
Time Steps (Month)

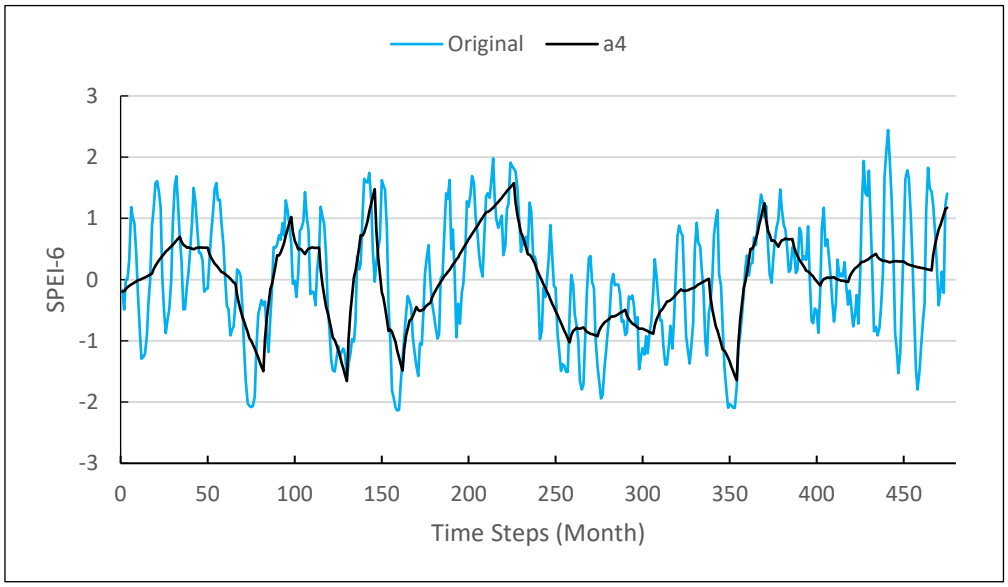
Original
a4
SPEI-6
Time Steps (Month)

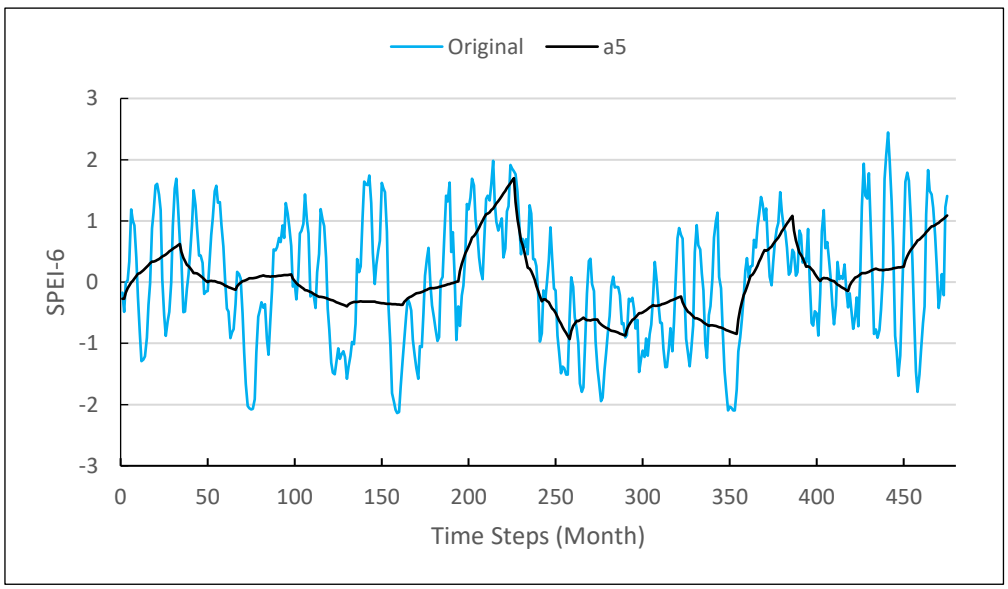
Original
a5
SPEI-6
Time Steps (Month)

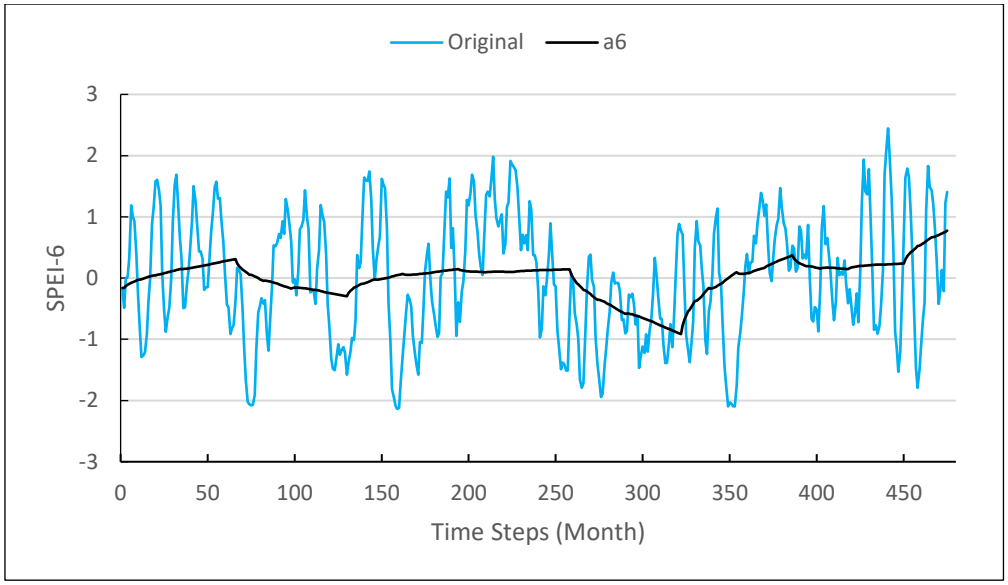
Original
a6
SPEI-6
3
2
1
0
-1
-2
-3
0
50
100
150
200
250
300
350
400
450
Time Steps (Month)

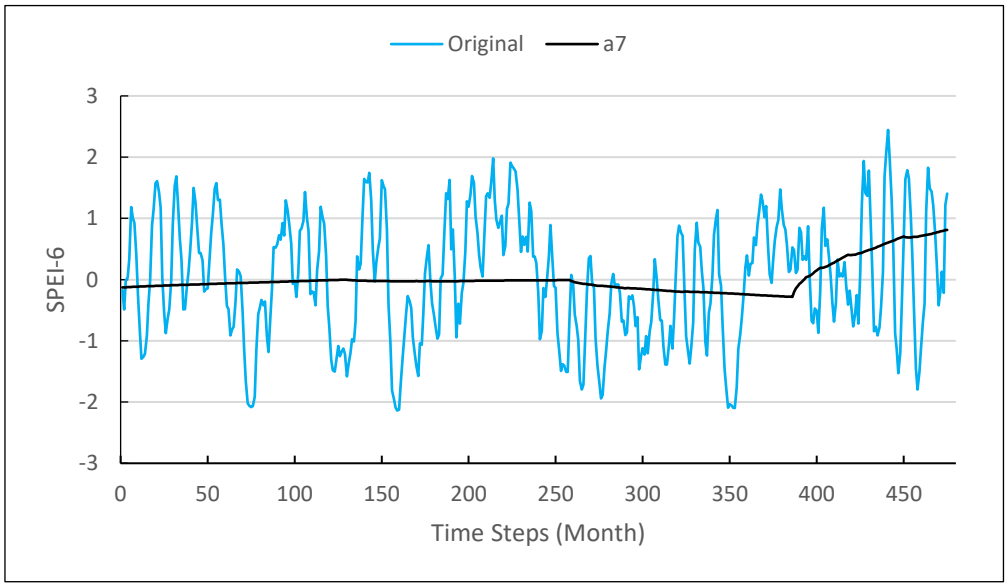
Original
a7
SPEI-6
3
2
1
0
-1
-2
-3
0
50
100
150
200
250
300
350
400
450
Time Steps (Month)

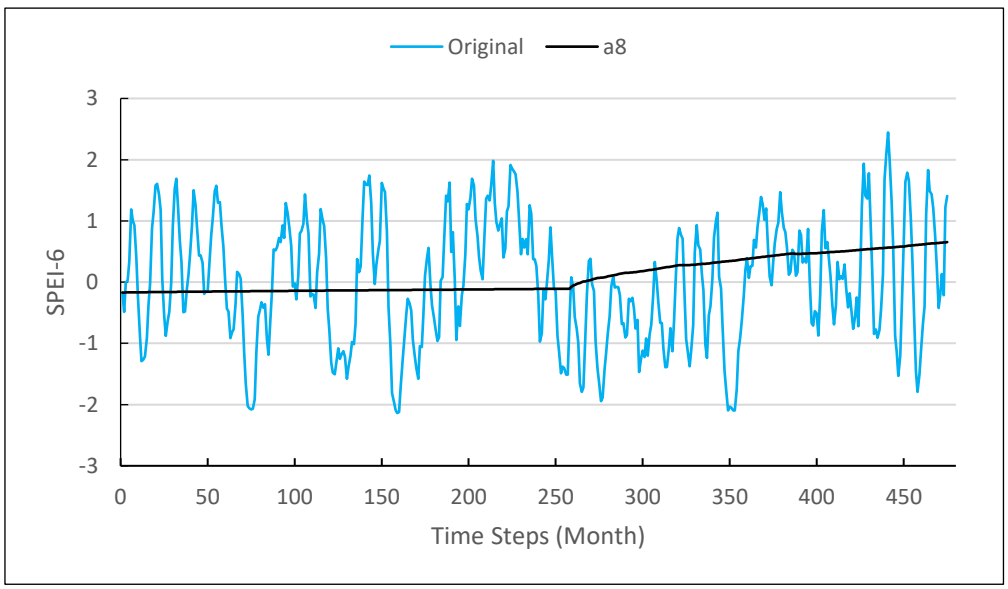
Original
a8
SPEI-6
3
2
1
0
-1
-2
-3
0
50
100
150
200
250
300
350
400
450
Time Steps (Month)

APPENDIX A4

(SPEI-1, s2917001)

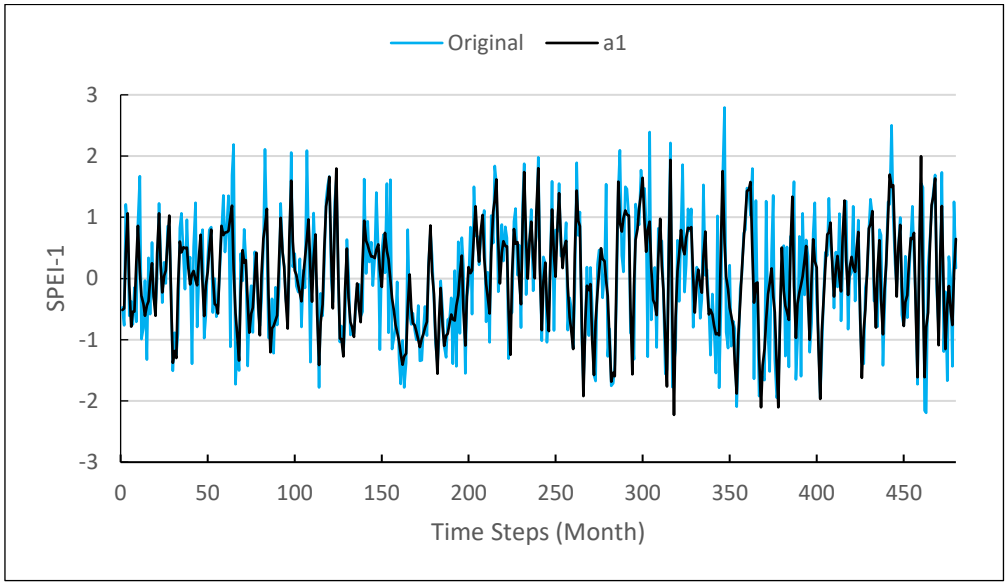

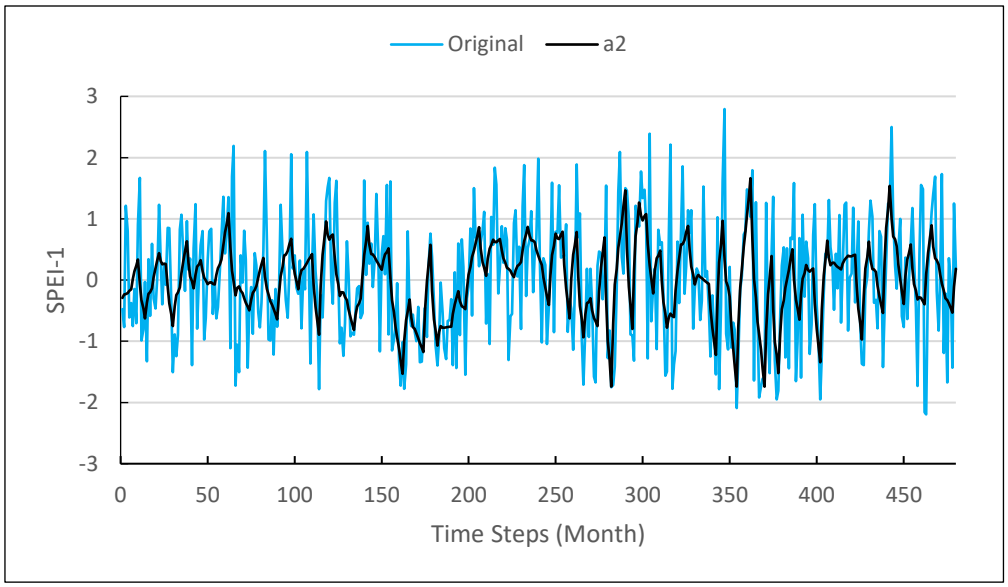

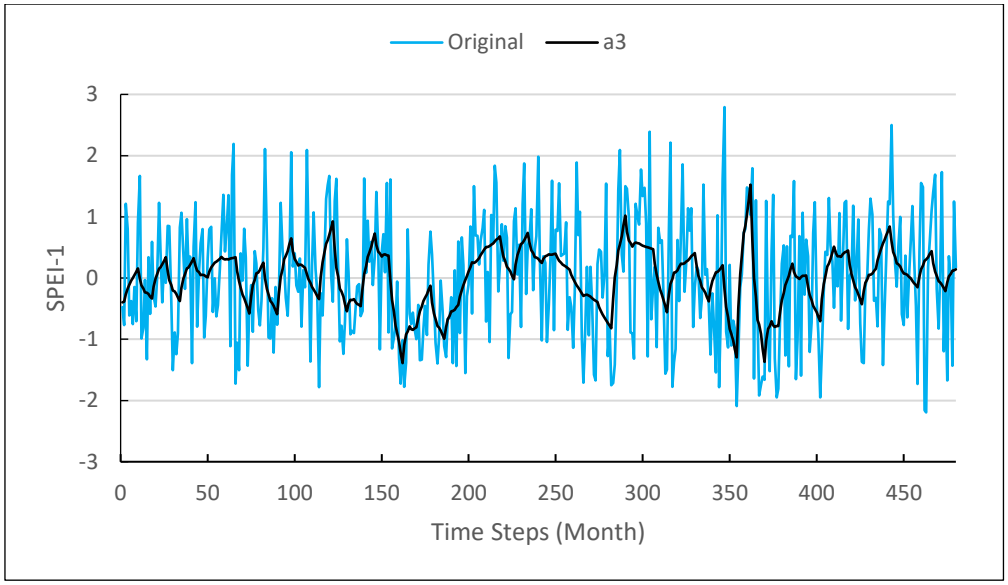
Original
a3
SPEI-1
3
2
1
0
-1
-2
-3
0
50
100
150
200
250
300
350
400
450
Time Steps (Month)

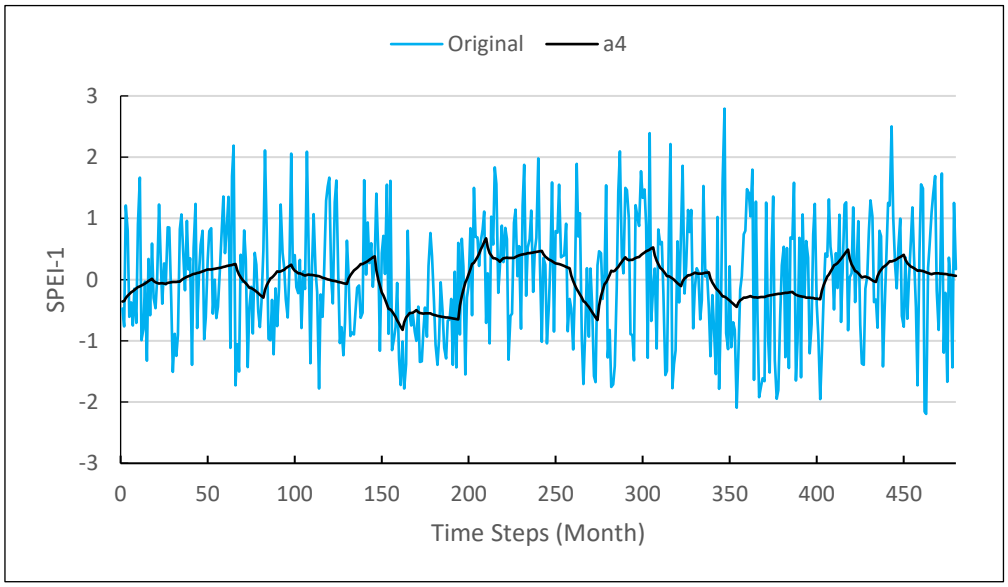
Original
a4
SPEI-1
3
2
1
0
-1
-2
-3
0
50
100
150
200
250
300
350
400
450
Time Steps (Month)

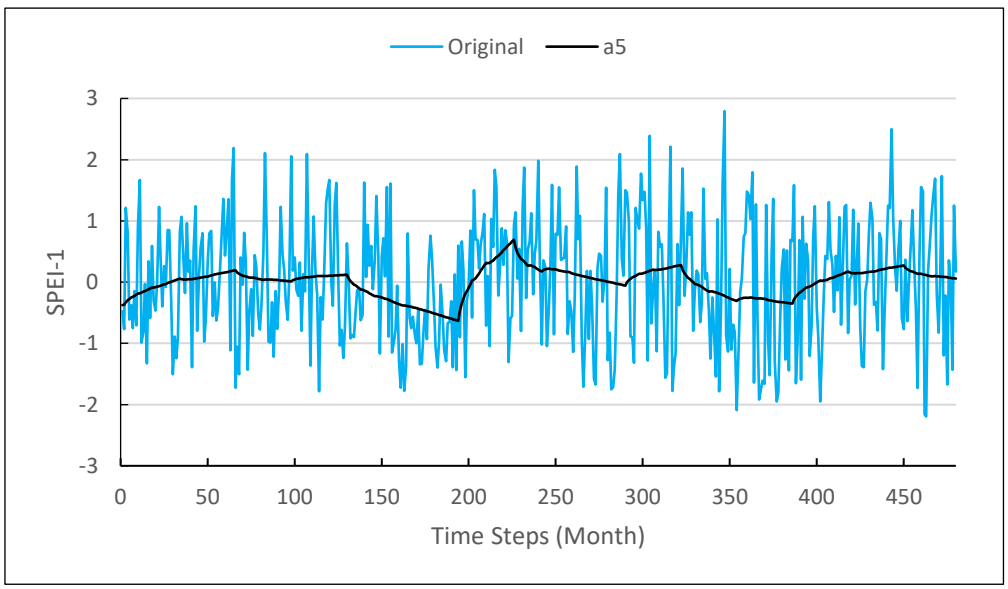
Original
a5
SPEI-1
3
2
1
0
-1
-2
-3
0
50
100
150
200
250
300
350
400
450
Time Steps (Month)

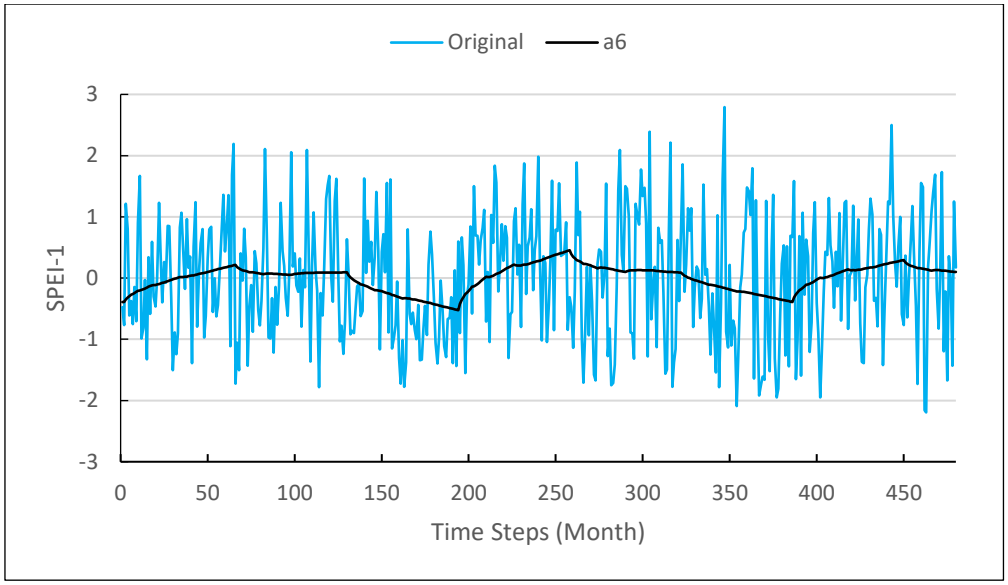
Original
a6
SPEI-1
3
2
1
0
-1
-2
-3
0
50
100
150
200
250
300
350
400
450
Time Steps (Month)

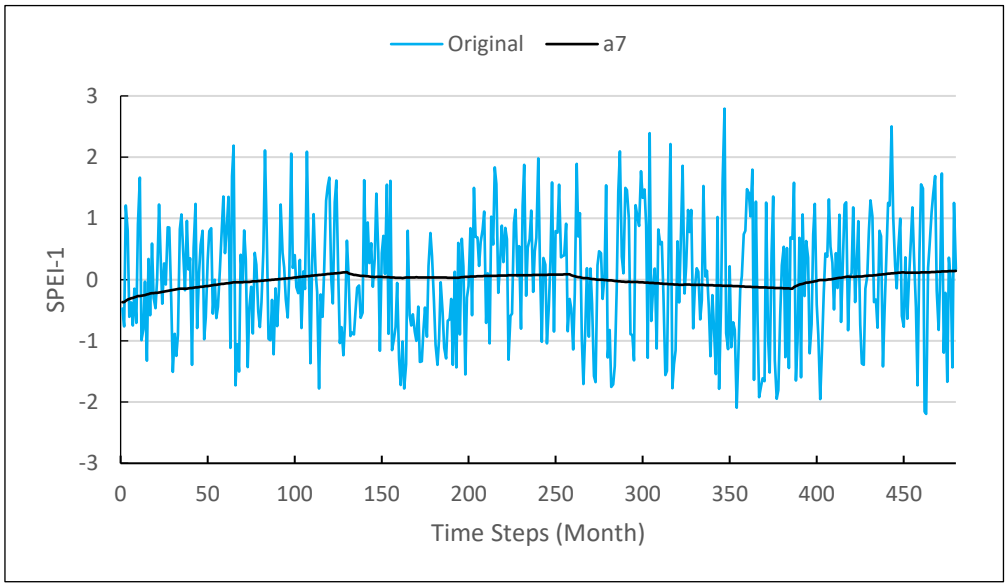
Original
a7
SPEI-1
3
2
1
0
-1
-2
-3
0
50
100
150
200
250
300
350
400
450
Time Steps (Month)

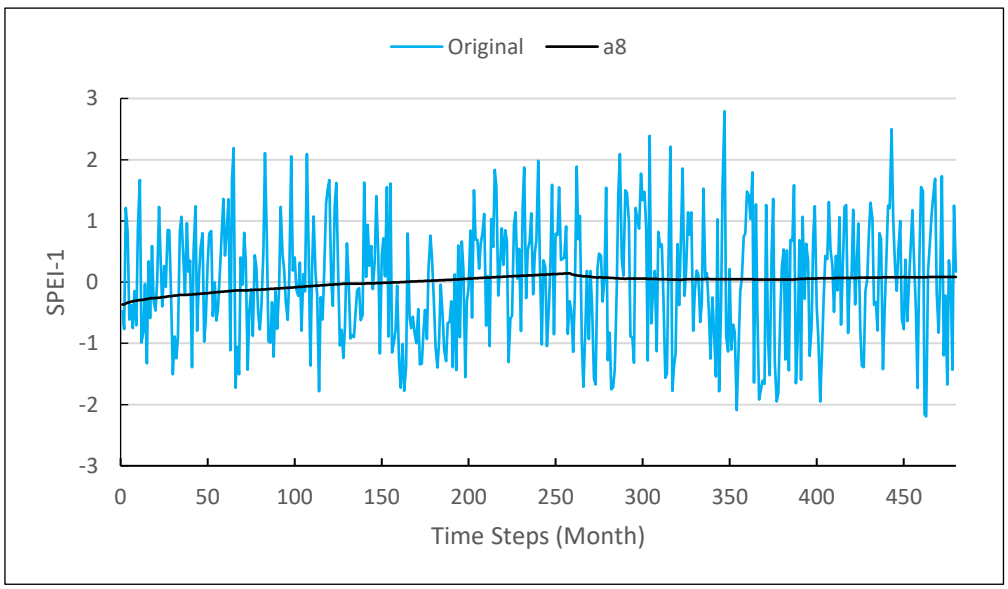
Original
a8
SPEI-1
3
2
1
0
-1
-2
-3
0
50
100
150
200
250
300
350
400
450
Time Steps (Month)

APPENDIX A5

(SPEI-3, s2917001)

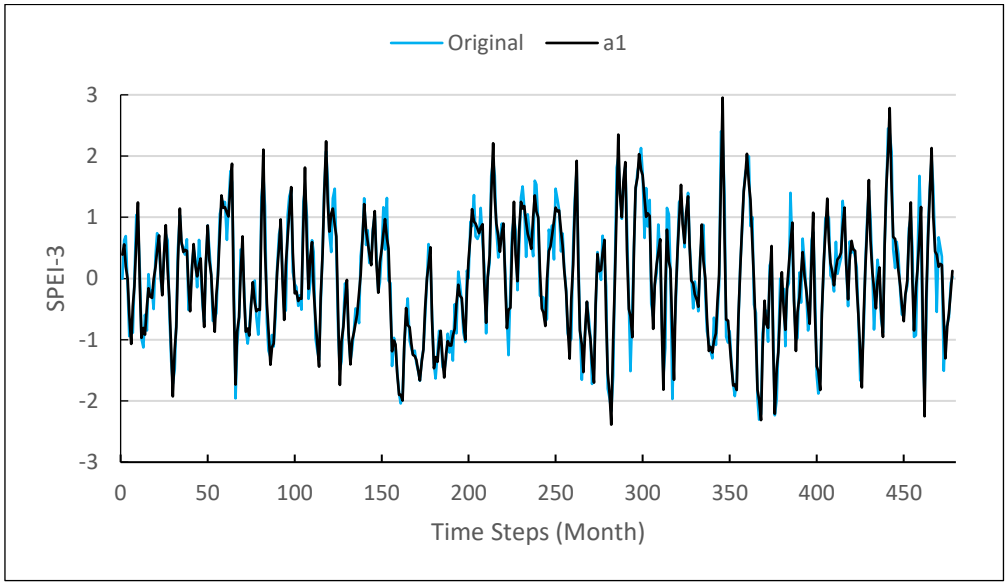

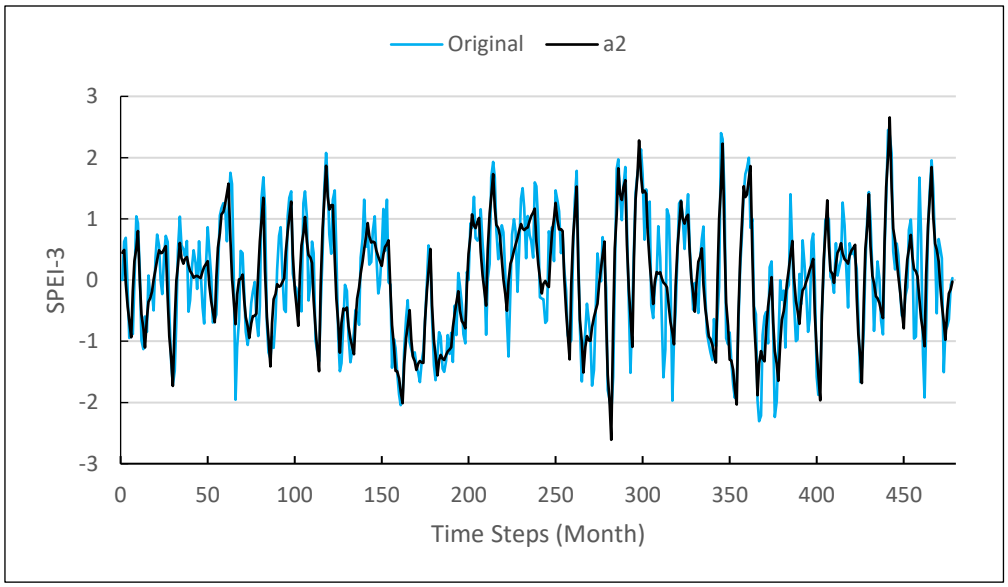

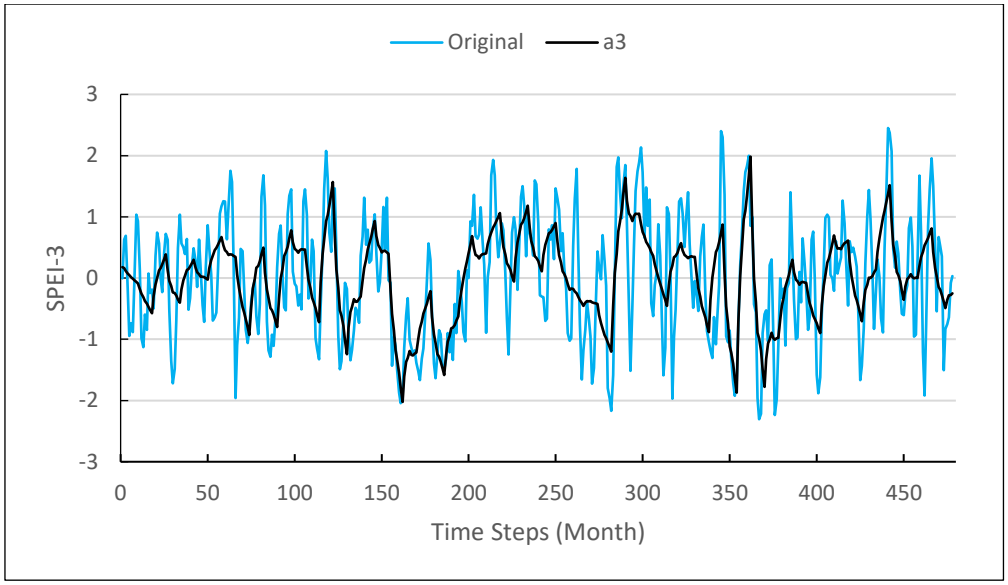
Original
a3
SPEI-3
3
2
1
0
-1
-2
-3
0
50
100
150
200
250
300
350
400
450
Time Steps (Month)

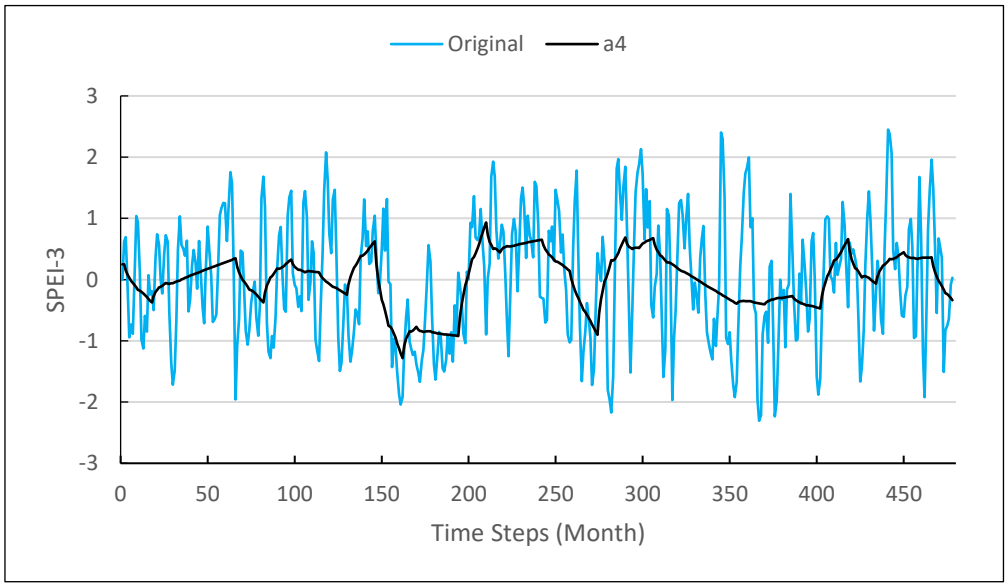
Original
a4
SPEI-3
3
2
1
0
-1
-2
-3
0
50
100
150
200
250
300
350
400
450
Time Steps (Month)

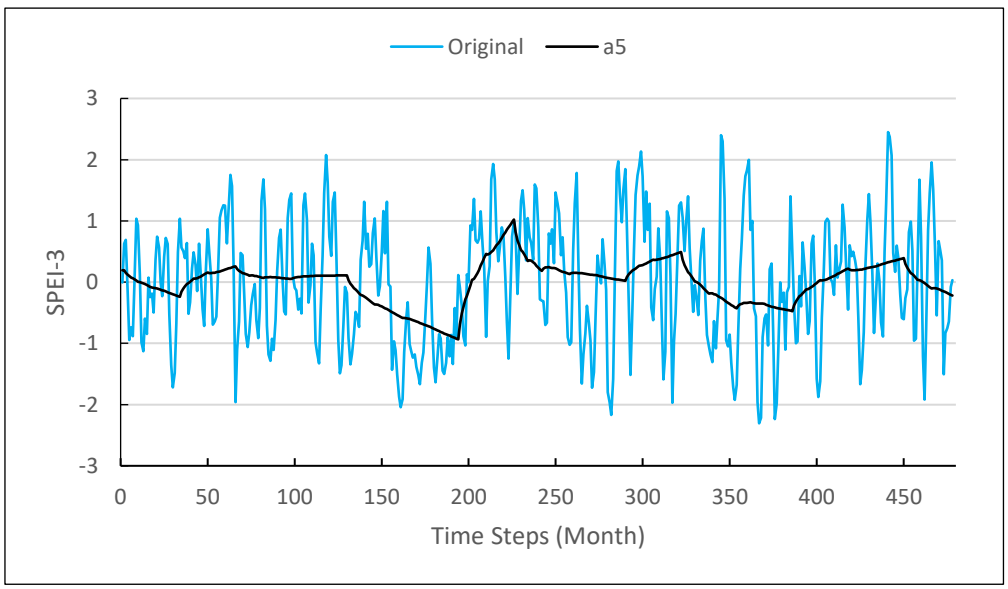
Original
a5
SPEI-3
3
2
1
0
-1
-2
-3
0
50
100
150
200
250
300
350
400
450
Time Steps (Month)

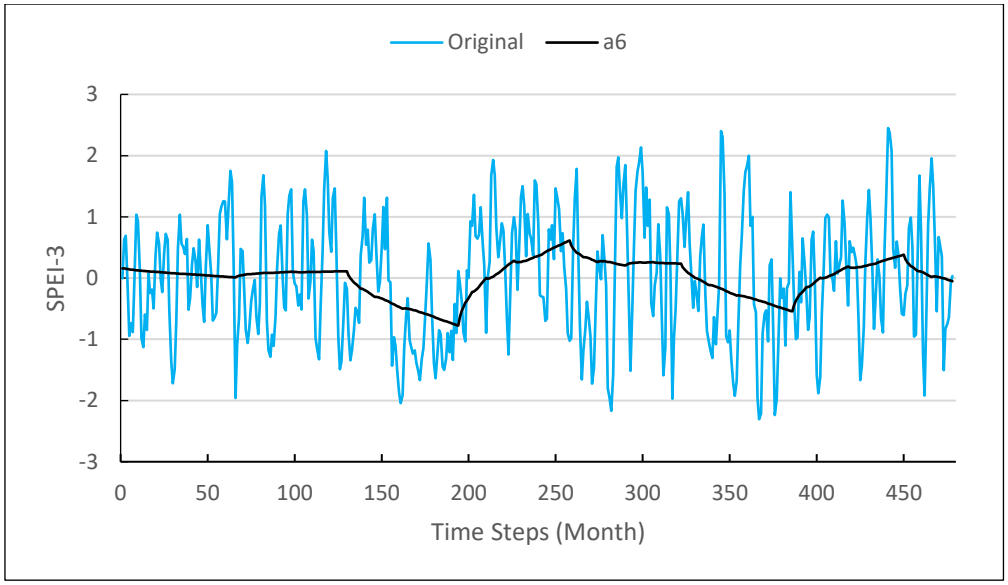
Original
a6
SPEI-3
3
2
1
0
-1
-2
-3
0
50
100
150
200
250
300
350
400
450
Time Steps (Month)

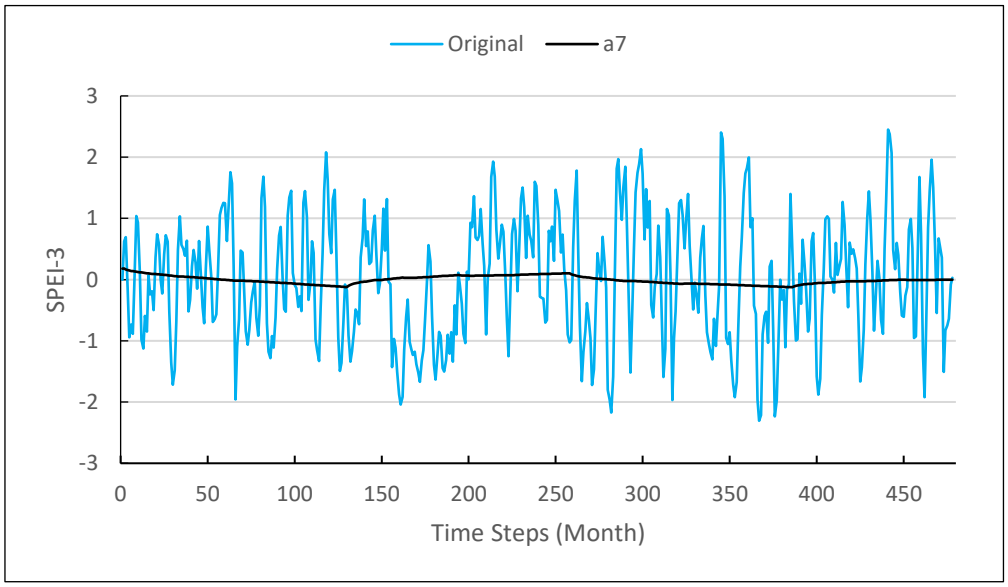
Original
a7
SPEI-3
3
2
1
0
-1
-2
-3
0
50
100
150
200
250
300
350
400
450
Time Steps (Month)

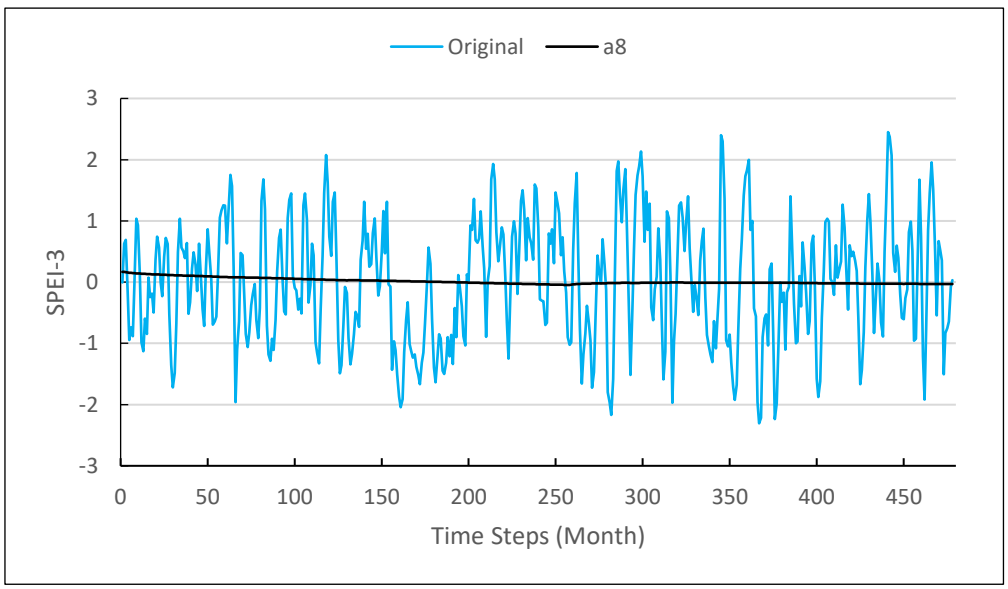
Original
a8
SPEI-3
3
2
1
0
-1
-2
-3
0
50
100
150
200
250
300
350
400
450
Time Steps (Month)

APPENDIX A6

(SPEI-6, s2917001)

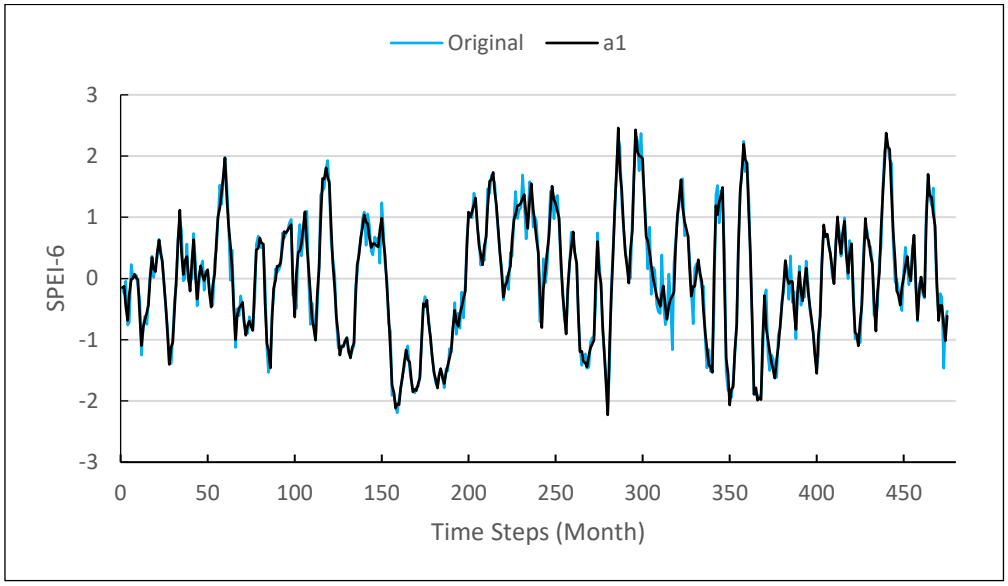

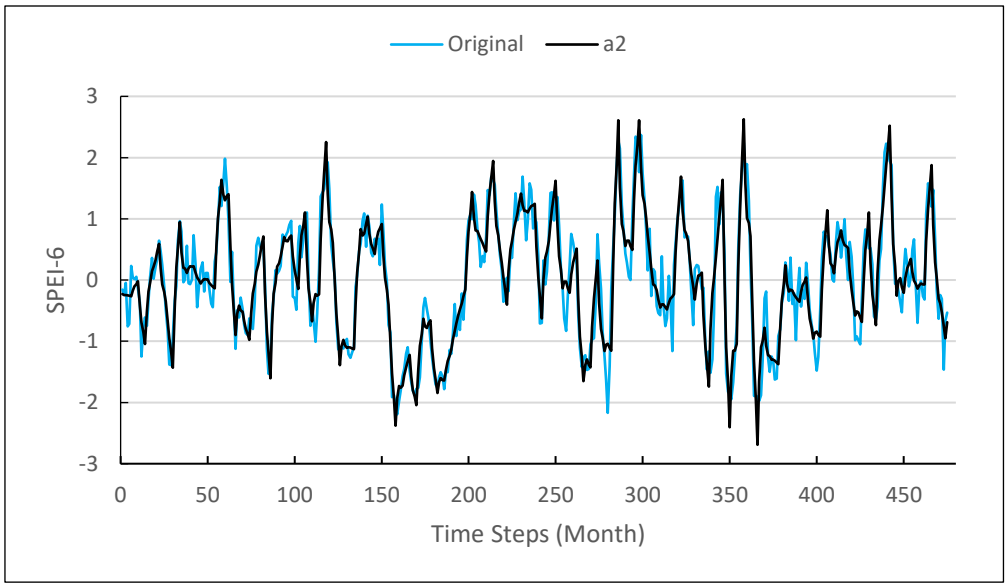

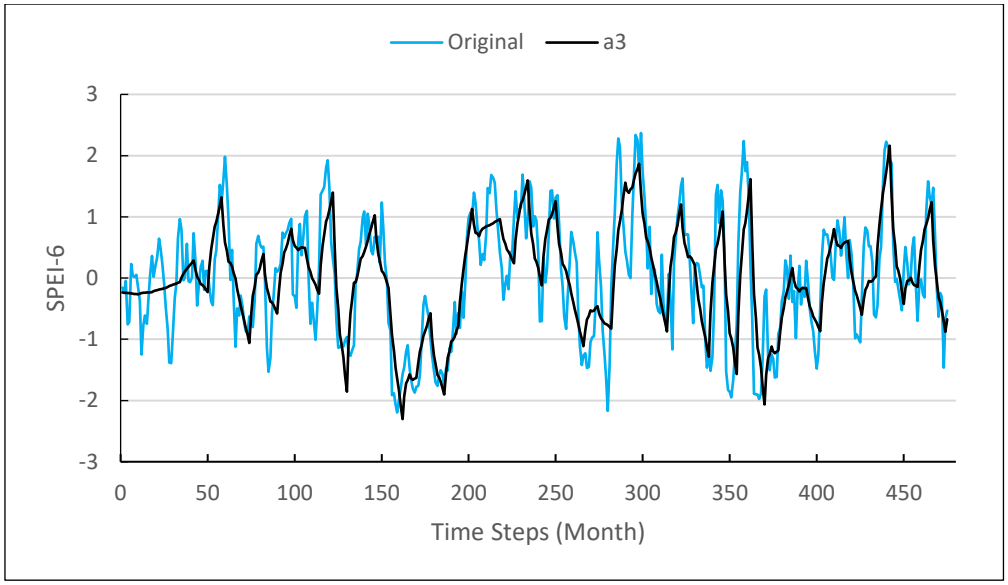
Original
a3
SPEI-6
3
2
1
0
-1
-2
-3
0
50
100
150
200
250
300
350
400
450
Time Steps (Month)

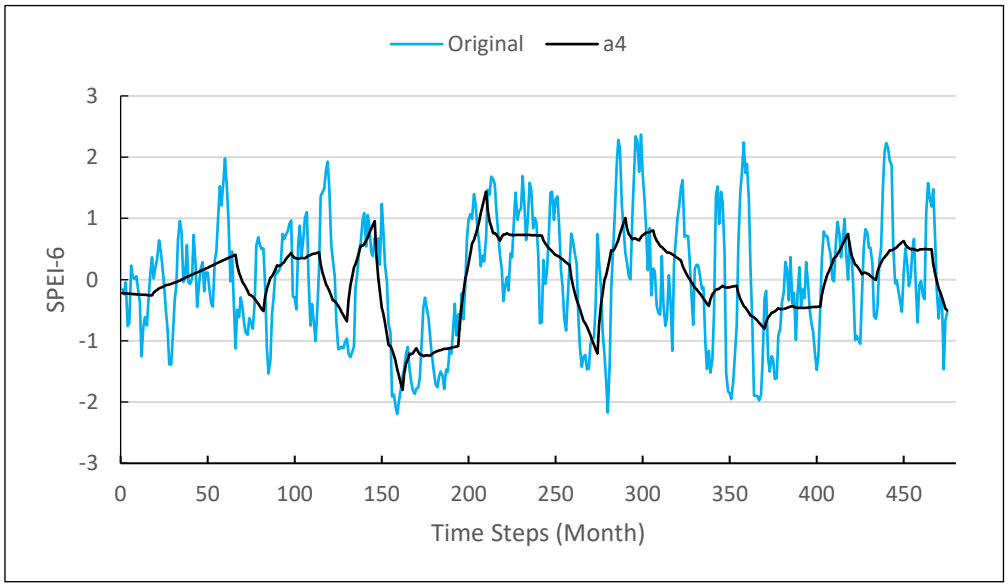
Original
a4
SPEI-6
3
2
1
0
-1
-2
-3
0
50
100
150
200
250
300
350
400
450
Time Steps (Month)

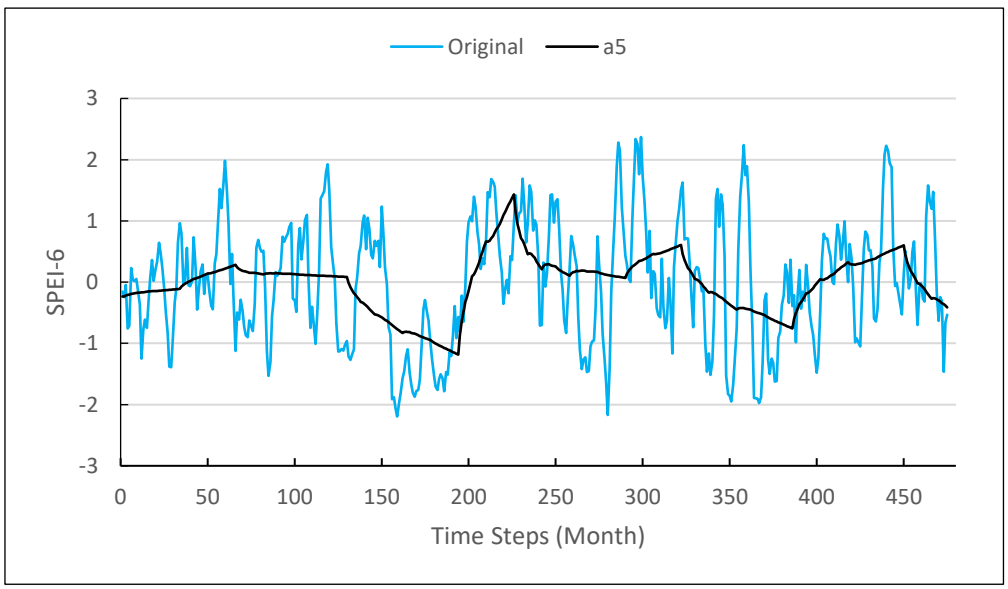
Original
a5
SPEI-6
3
2
1
0
-1
-2
-3
0
50
100
150
200
250
300
350
400
450
Time Steps (Month)

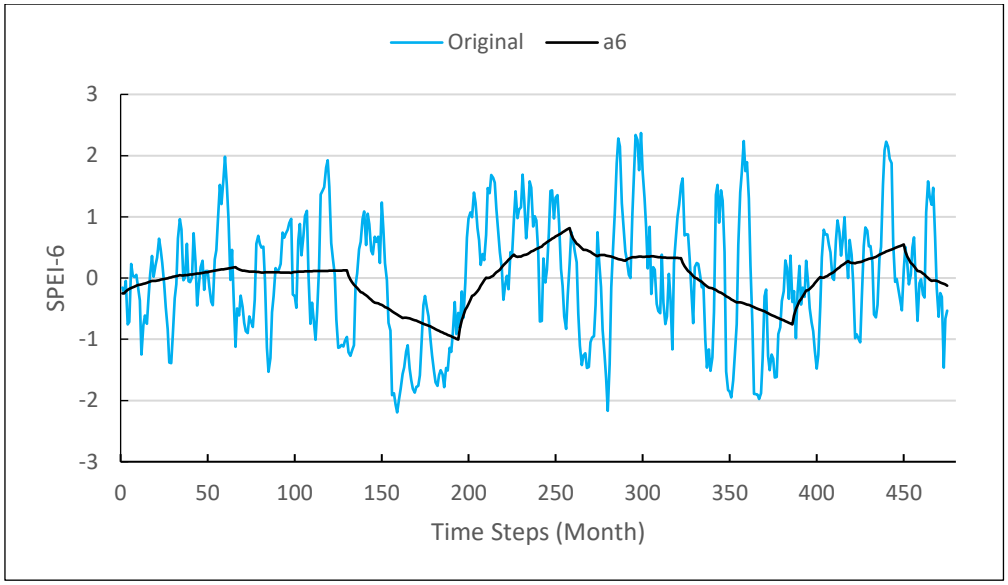
Original
a6
SPEI-6
3
2
1
0
-1
-2
-3
0
50
100
150
200
250
300
350
400
450
Time Steps (Month)

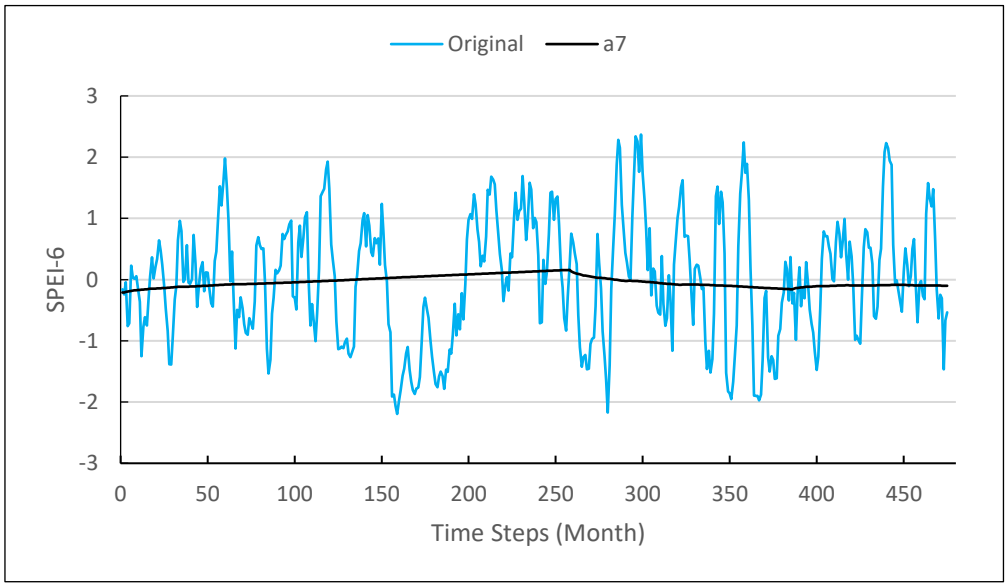
Original
a7
SPEI-6
3
2
1
0
-1
-2
-3
0
50
100
150
200
250
300
350
400
450
Time Steps (Month)

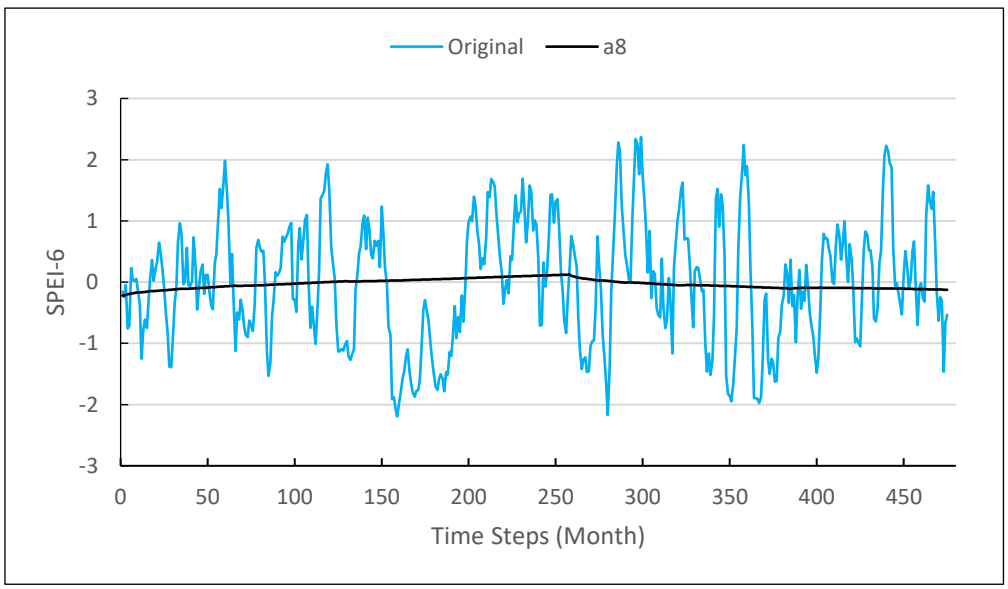
Original
a8
SPEI-6
3
2
1
0
-1
-2
-3
0
50
100
150
200
250
300
350
400
450
Time Steps (Month)

APPENDIX B1

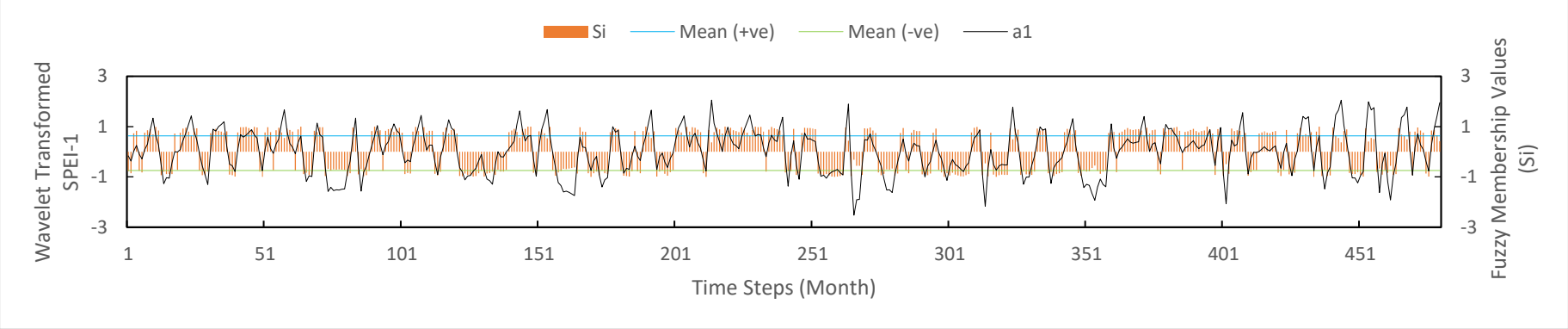

Figure B1.1: Fuzzy Membership Values of Wavelet Transformed SPEI-1 (a1) for station s2815001

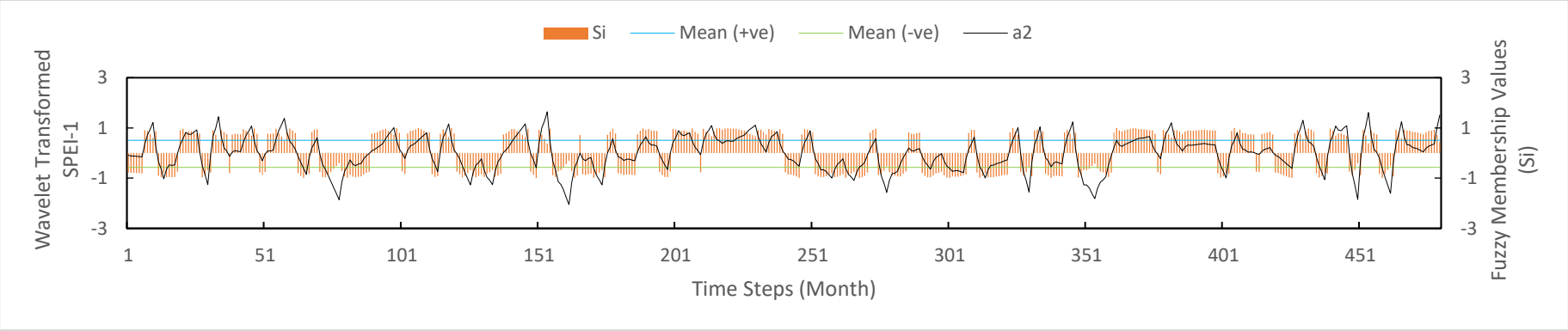

Figure B1.2: Fuzzy Membership Values of Wavelet Transformed SPEI-1 (a2) for station s2815001

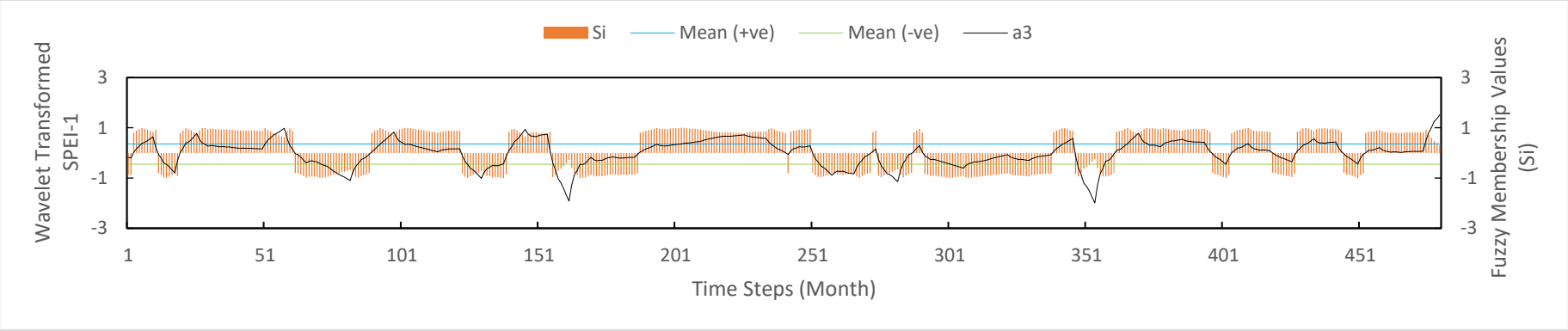

Figure B1.3: Fuzzy Membership Values of Wavelet Transformed SPEI-1 (a3) for station s2815001

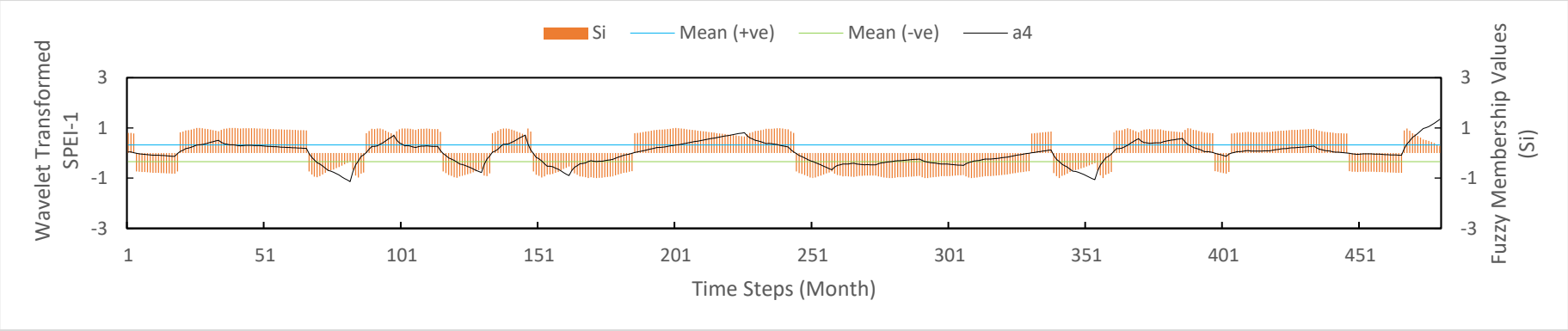

Figure B1.4: Fuzzy Membership Values of Wavelet Transformed SPEI-1 (a4) for station s2815001

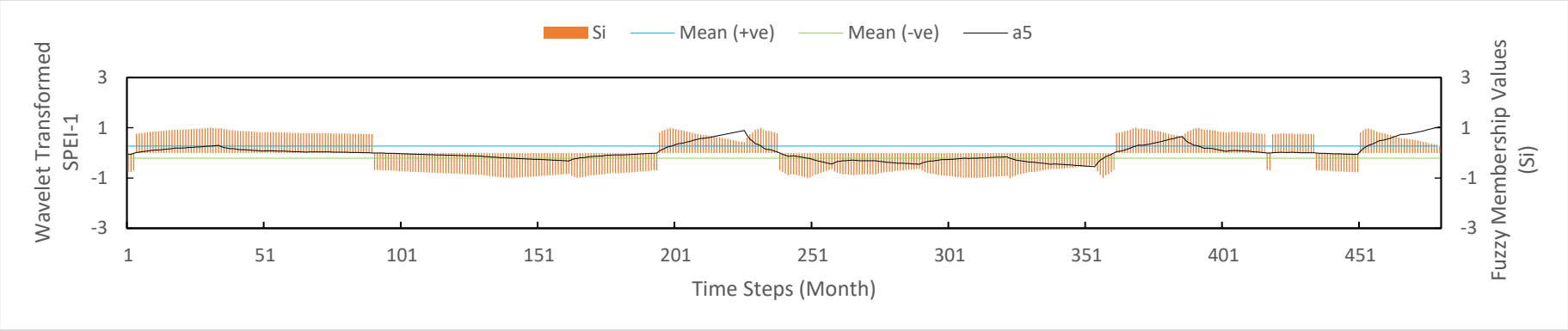

Figure B1.5: Fuzzy Membership Values of Wavelet Transformed SPEI-1 (a5) for station s2815001

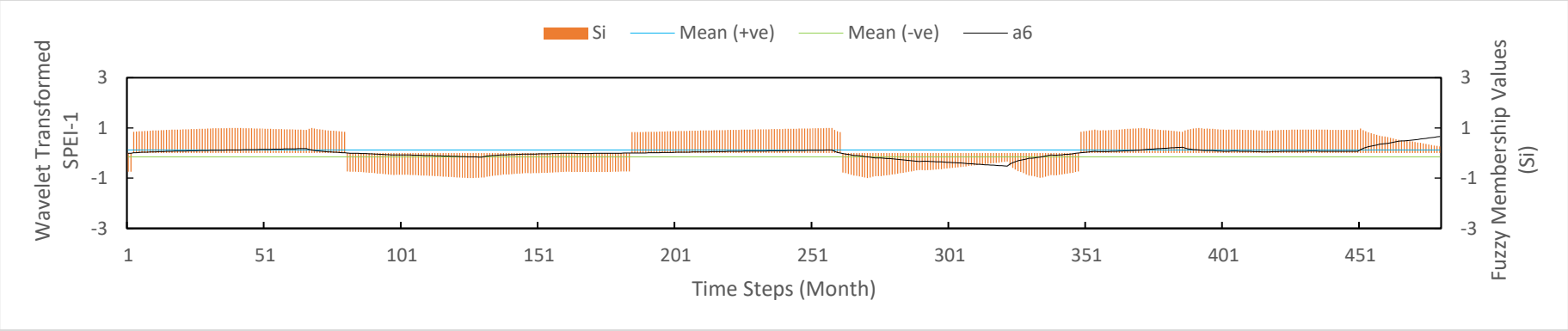

Figure B1.6: Fuzzy Membership Values of Wavelet Transformed SPEI-1 (a6) for station s2815001

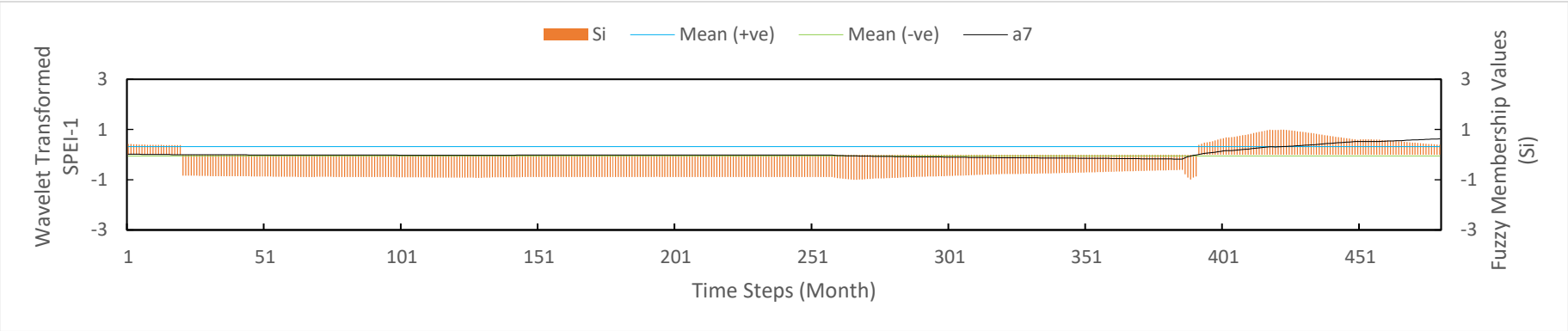

Figure B1.7: Fuzzy Membership Values of Wavelet Transformed SPEI-1 (a7) for station s2815001

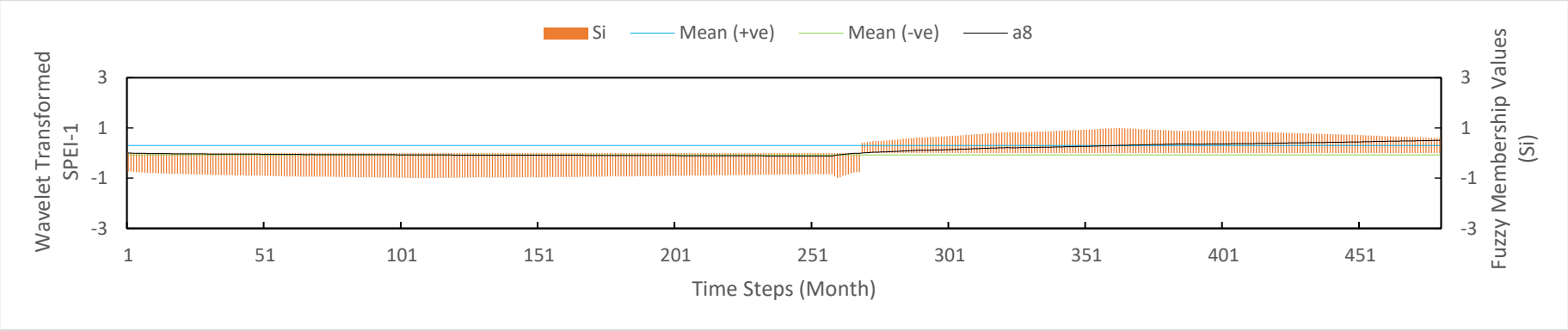

Figure B1.8: Fuzzy Membership Values of Wavelet Transformed SPEI-1 (a8) for station s2815001

APPENDIX B2

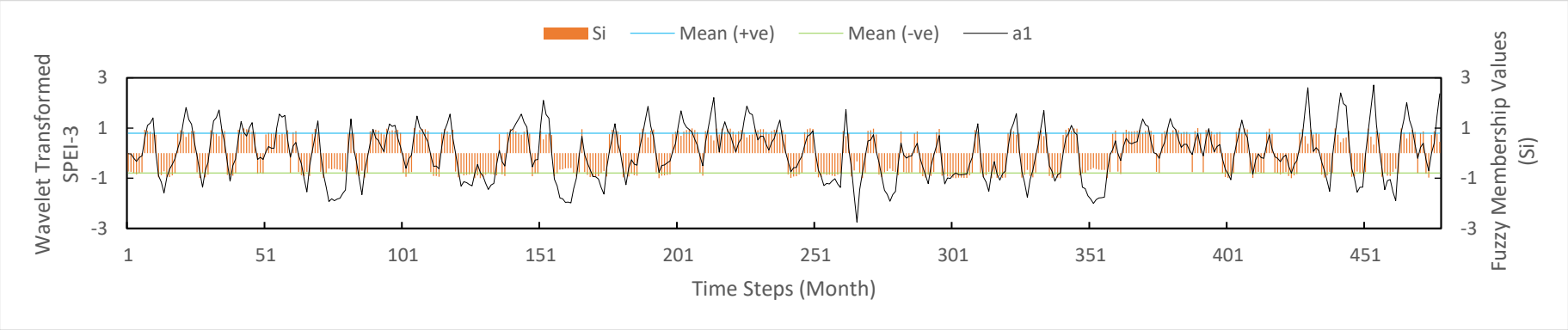

Figure B2.1: Fuzzy Membership Values of Wavelet Transformed SPEI-3 (a1) for station s2815001

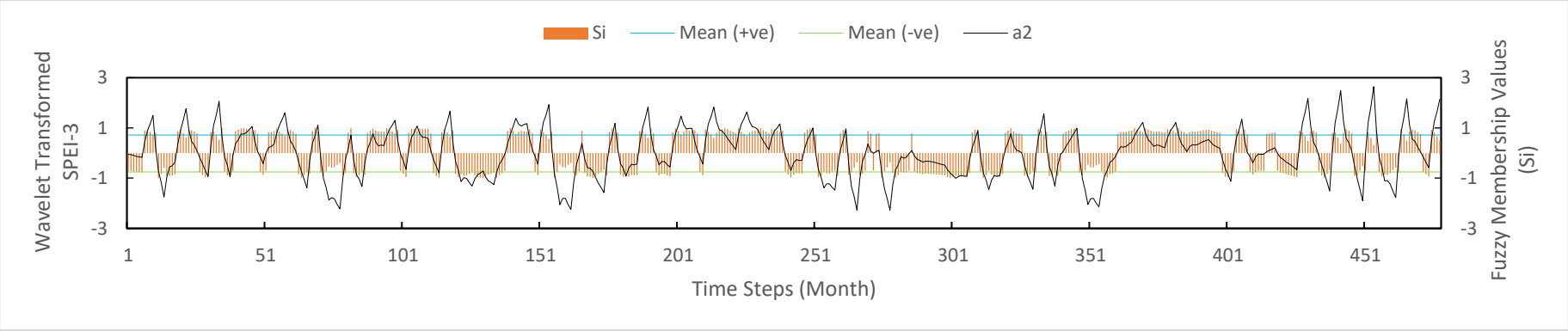

Figure B2.2: Fuzzy Membership Values of Wavelet Transformed SPEI-3 (a2) for station s2815001

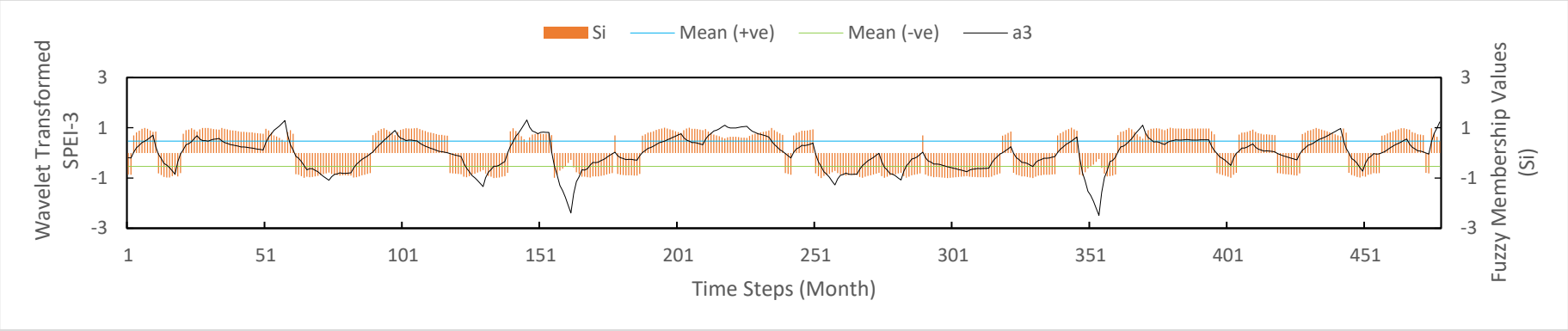

Figure B2.3: Fuzzy Membership Values of Wavelet Transformed SPEI-3 (a3) for station s2815001

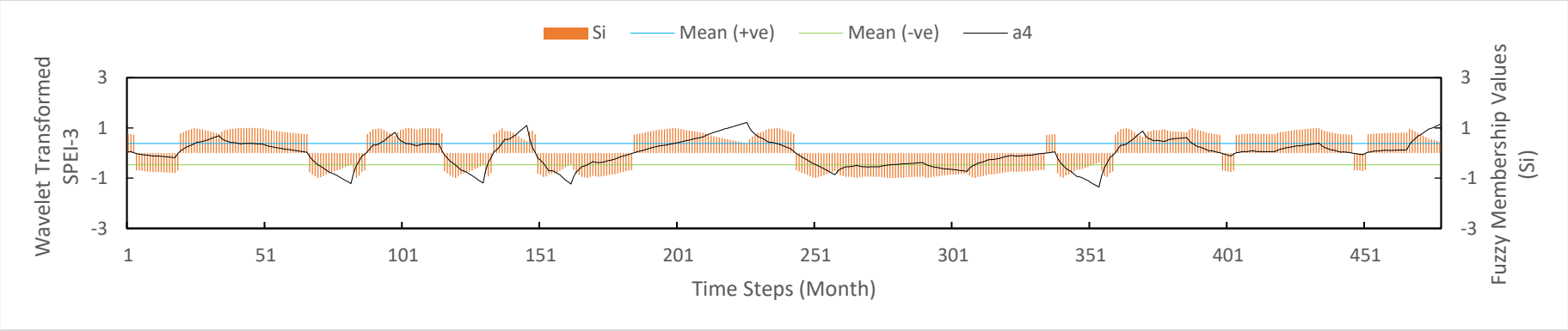

Figure B2.4: Fuzzy Membership Values of Wavelet Transformed SPEI-3 (a4) for station s2815001

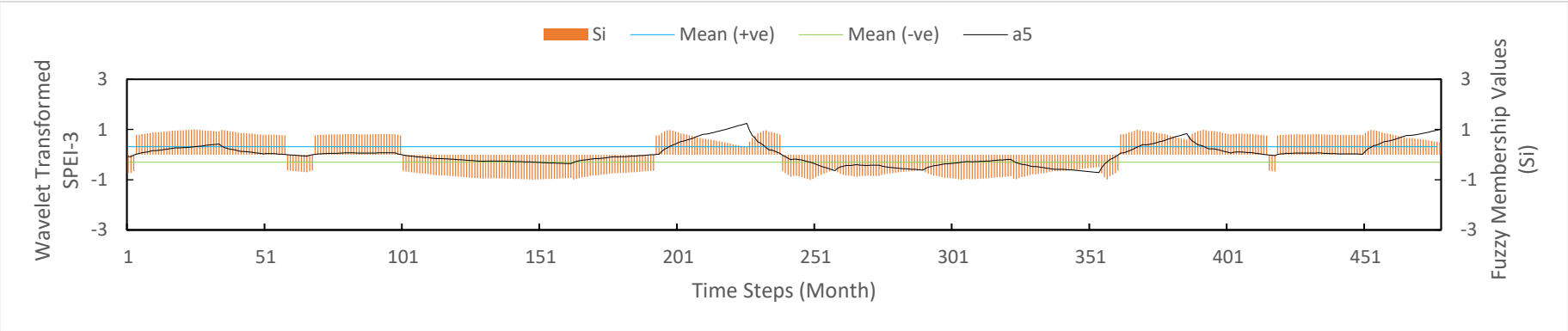

Figure B2.5: Fuzzy Membership Values of Wavelet Transformed SPEI-3 (a5) for station s2815001

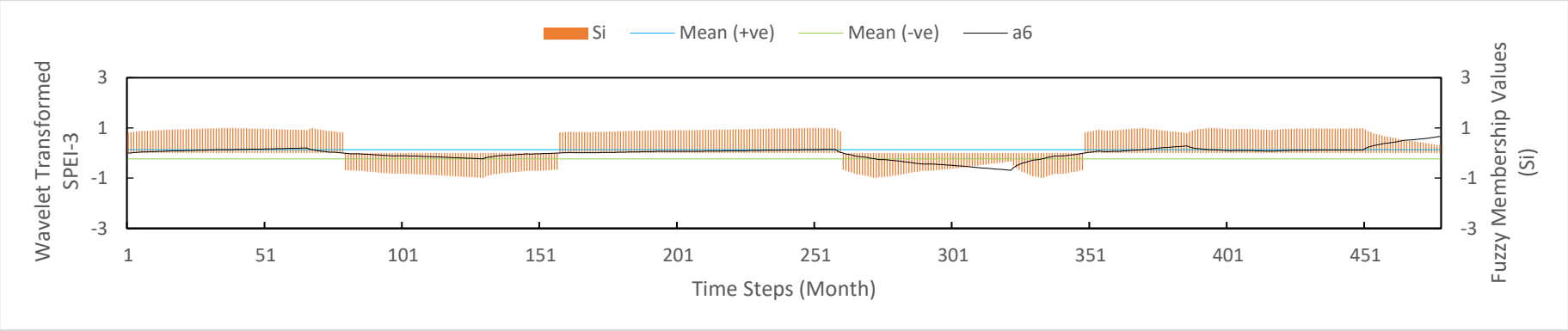

Figure B2.6: Fuzzy Membership Values of Wavelet Transformed SPEI-3 (a6) for station s2815001

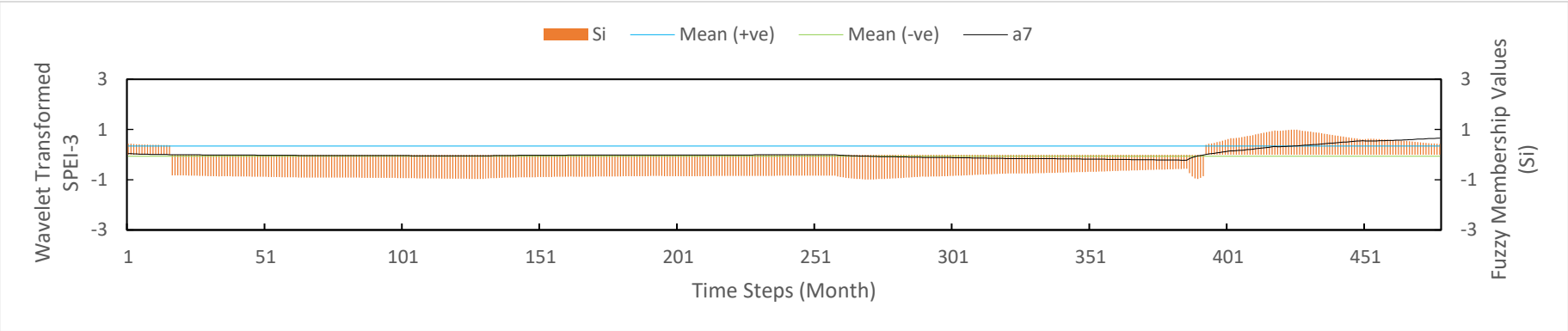

Figure B2.7: Fuzzy Membership Values of Wavelet Transformed SPEI-3 (a7) for station s2815001

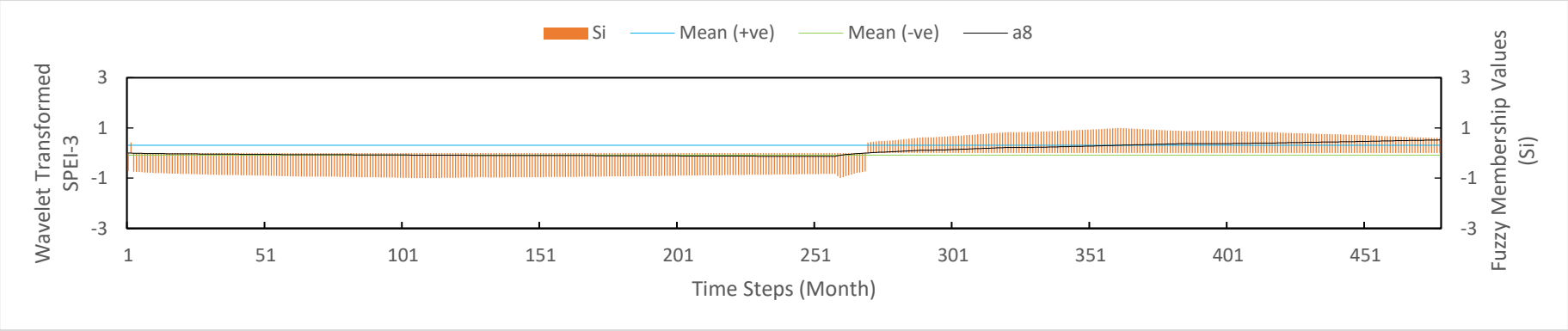

Figure B2.8: Fuzzy Membership Values of Wavelet Transformed SPEI-3 (a8) for station s2815001

APPENDIX B3

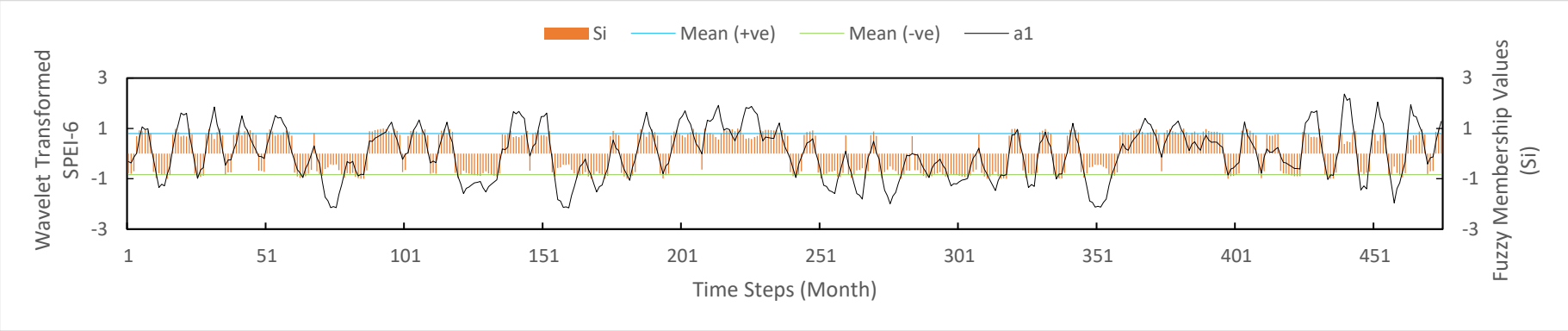

Figure B3.1: Fuzzy Membership Values of Wavelet Transformed SPEI-6 (a1) for station s2815001

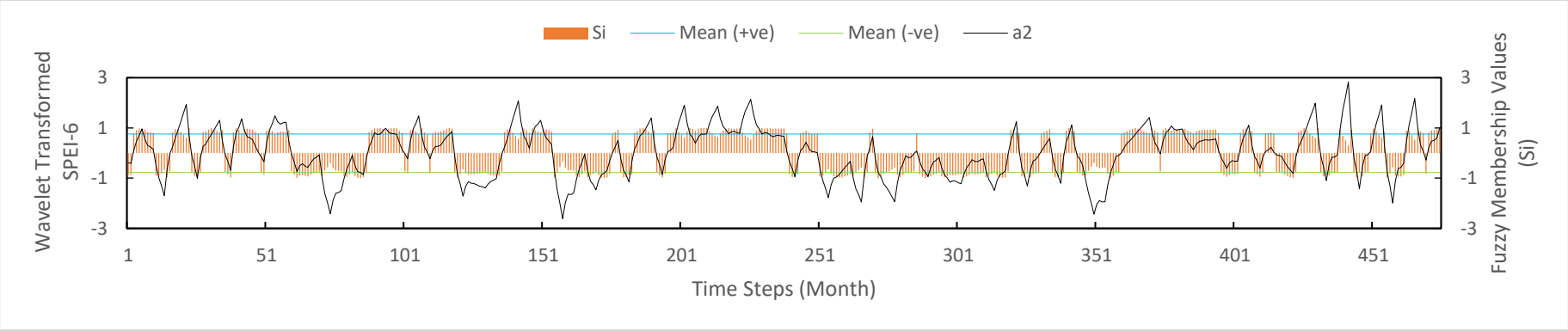

Figure B3.2: Fuzzy Membership Values of Wavelet Transformed SPEI-6 (a2) for station s2815001

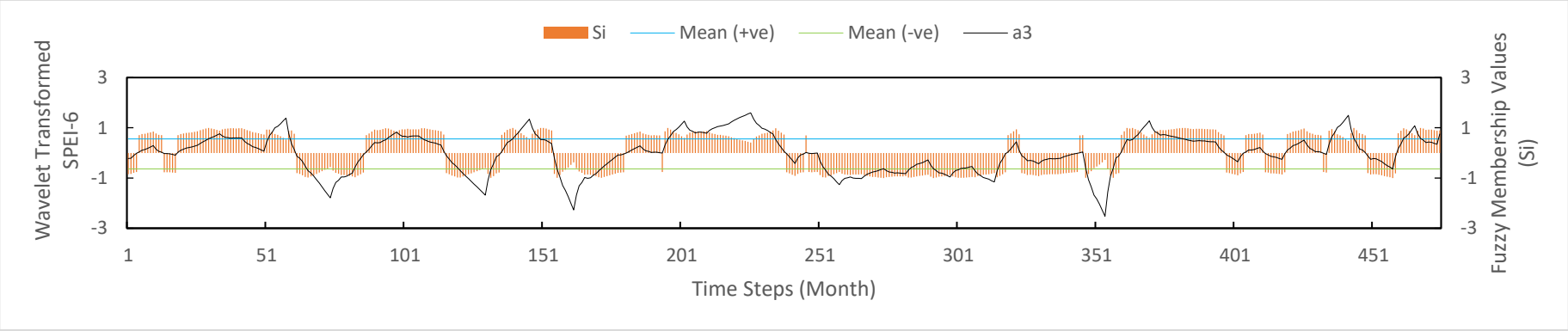

Figure B3.3: Fuzzy Membership Values of Wavelet Transformed SPEI-6 (a3) for station s2815001

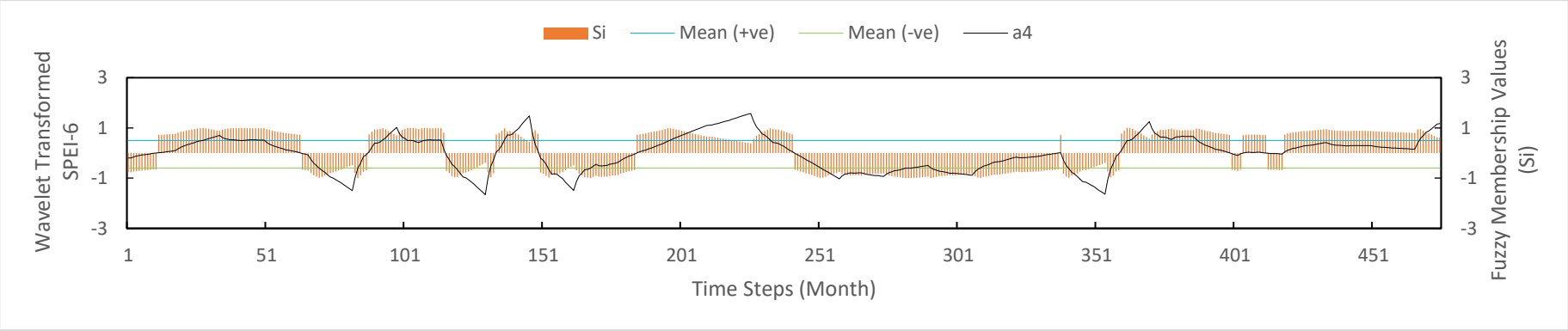

Figure B3.4: Fuzzy Membership Values of Wavelet Transformed SPEI-6 (a4) for station s2815001

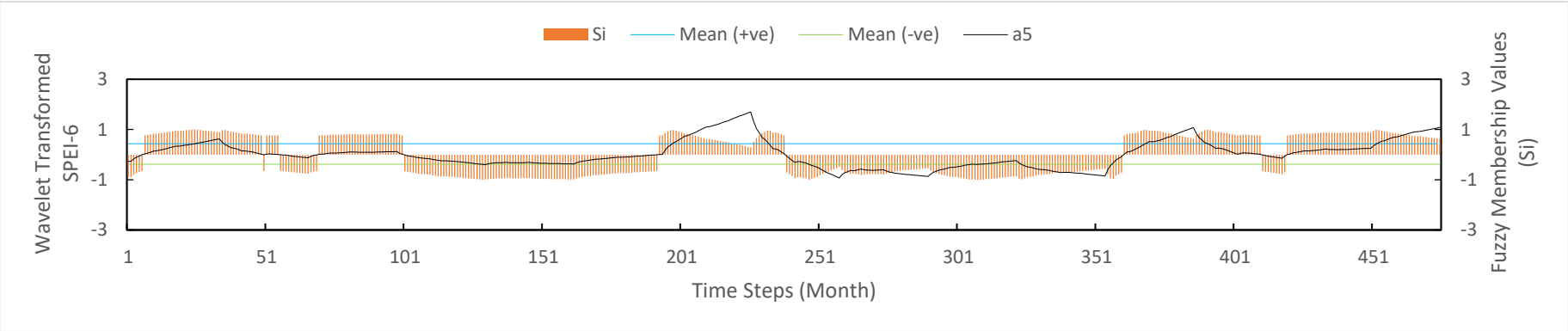

Figure B3.5: Fuzzy Membership Values of Wavelet Transformed SPEI-6 (a5) for station s2815001

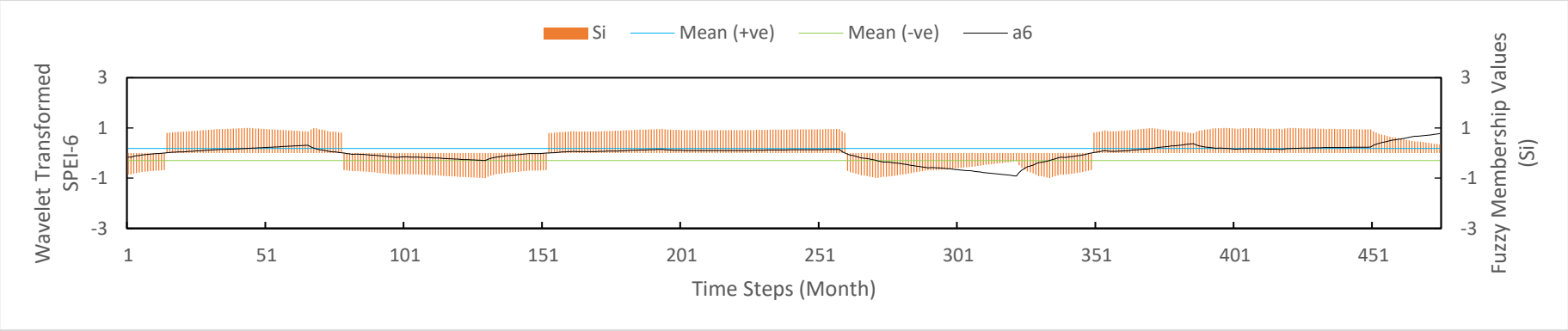

Figure B3.6: Fuzzy Membership Values of Wavelet Transformed SPEI-6 (a6) for station s2815001

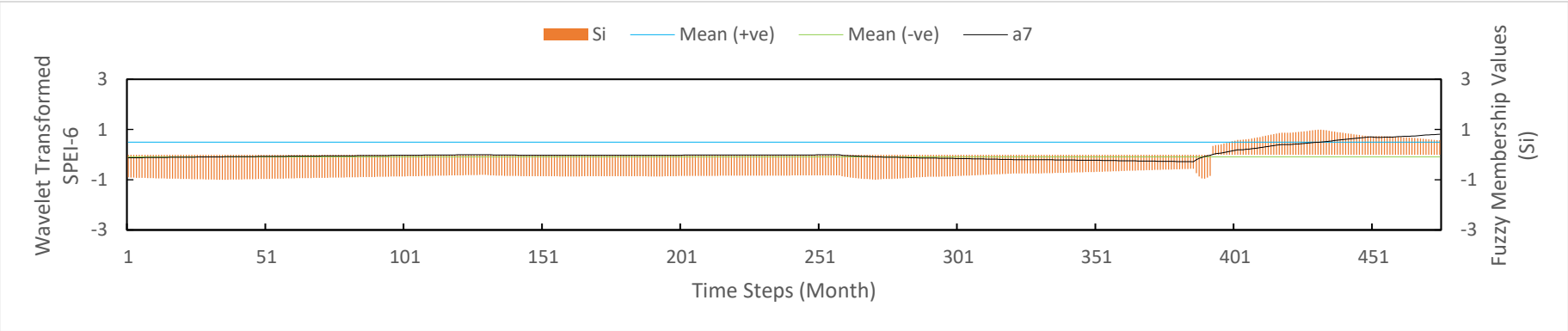

Figure B3.7: Fuzzy Membership Values of Wavelet Transformed SPEI-6 (a7) for station s2815001

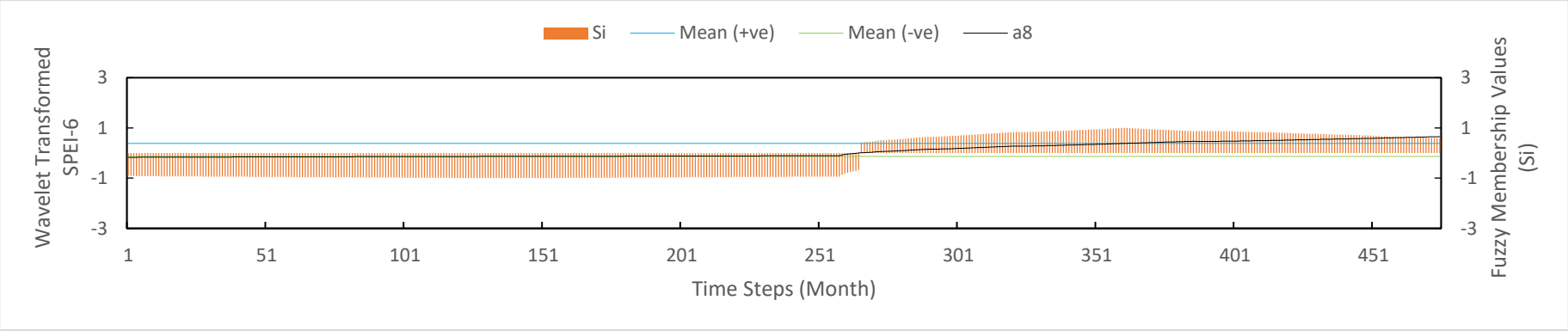

Figure B3.8: Fuzzy Membership Values of Wavelet Transformed SPEI-6 (a8) for station s2815001

APPENDIX B4

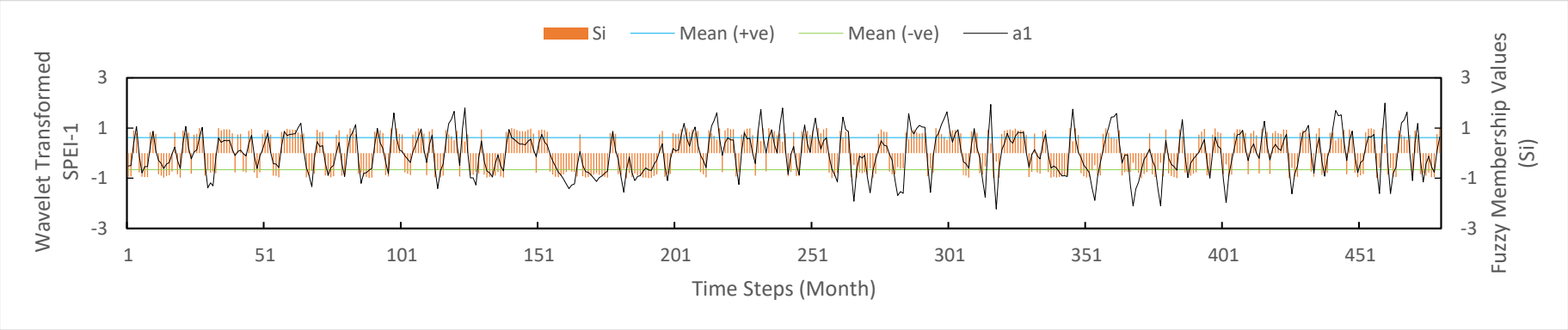

Figure B4.1: Fuzzy Membership Values of Wavelet Transformed SPEI-1 (a1) for station s2917001

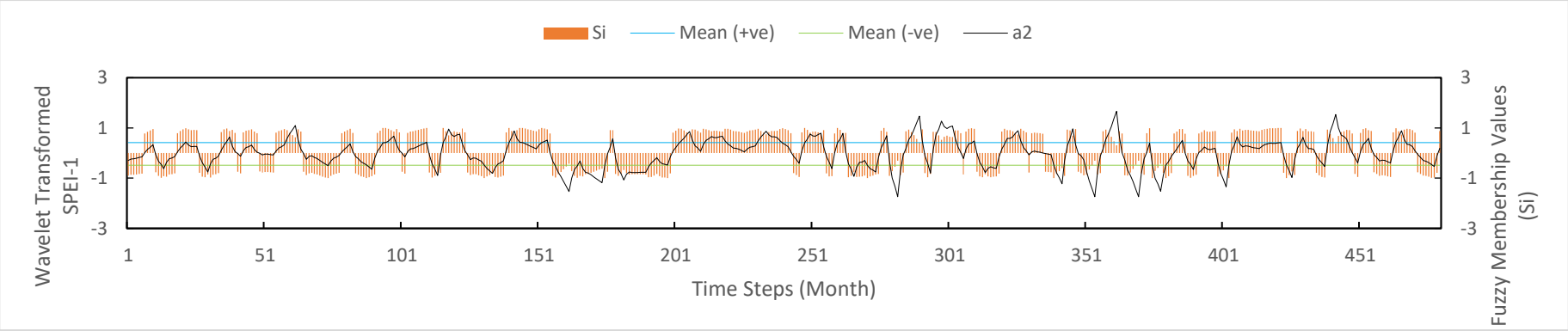

Figure B4.2: Fuzzy Membership Values of Wavelet Transformed SPEI-1 (a2) for station s2917001

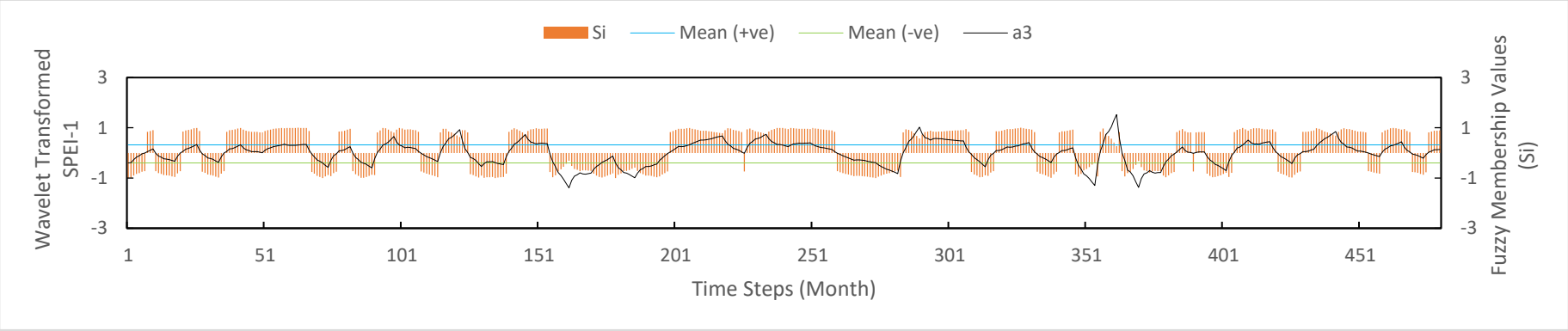

Figure B4.3: Fuzzy Membership Values of Wavelet Transformed SPEI-1 (a3) for station s2917001

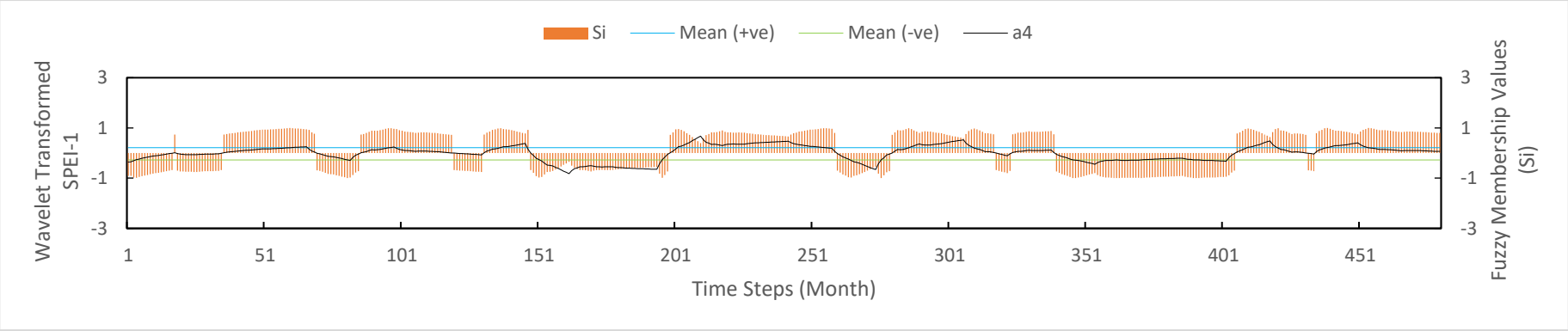

Figure B4.4: Fuzzy Membership Values of Wavelet Transformed SPEI-1 (a4) for station s2917001

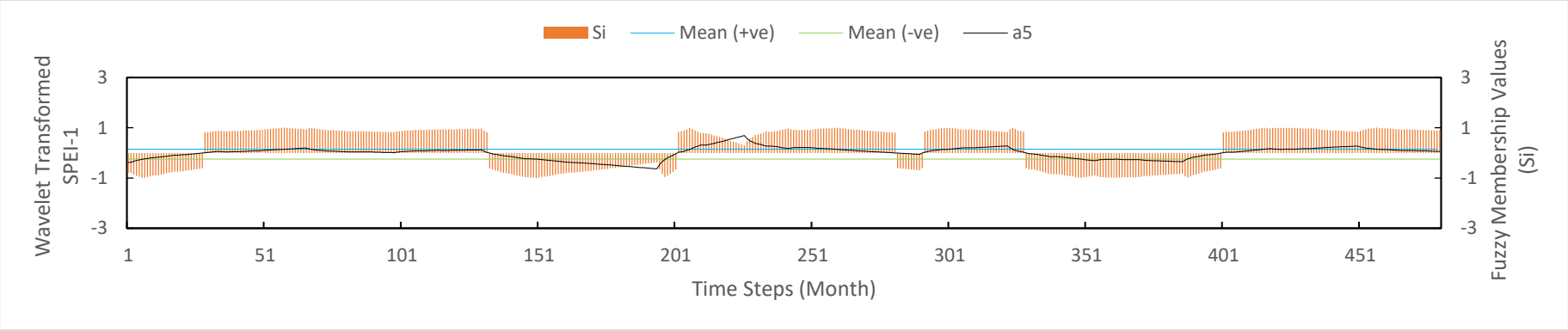

Figure B4.5: Fuzzy Membership Values of Wavelet Transformed SPEI-1 (a5) for station s2917001

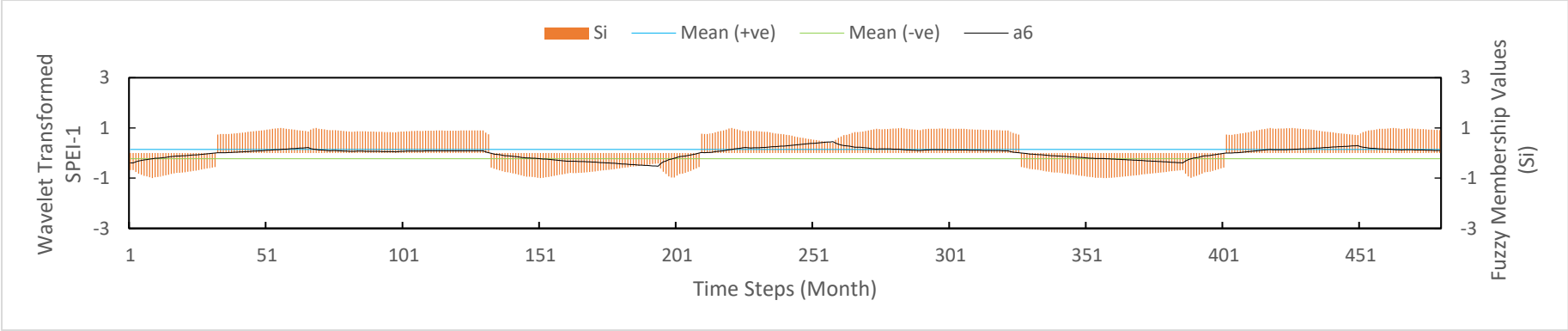

Figure B4.6: Fuzzy Membership Values of Wavelet Transformed SPEI-1 (a6) for station s2917001

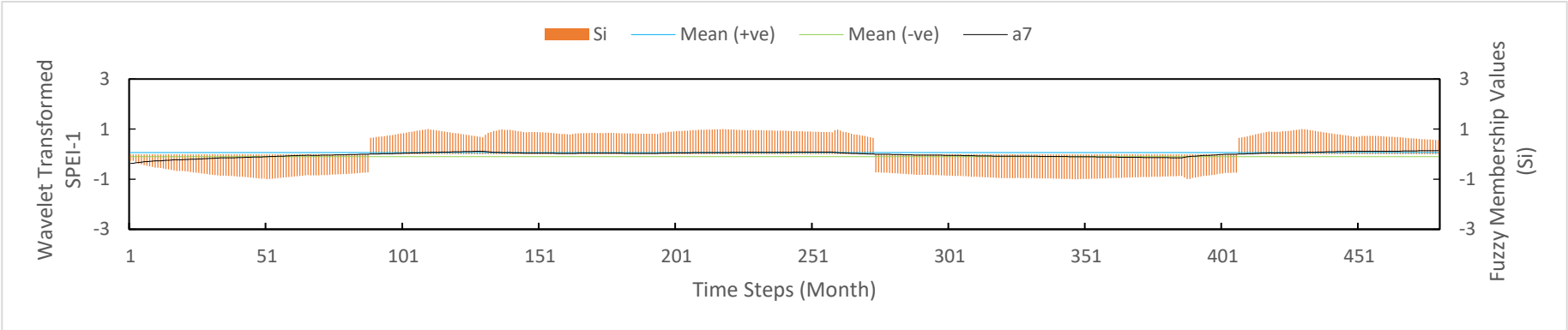

Figure B4.7: Fuzzy Membership Values of Wavelet Transformed SPEI-1 (a7) for station s2917001

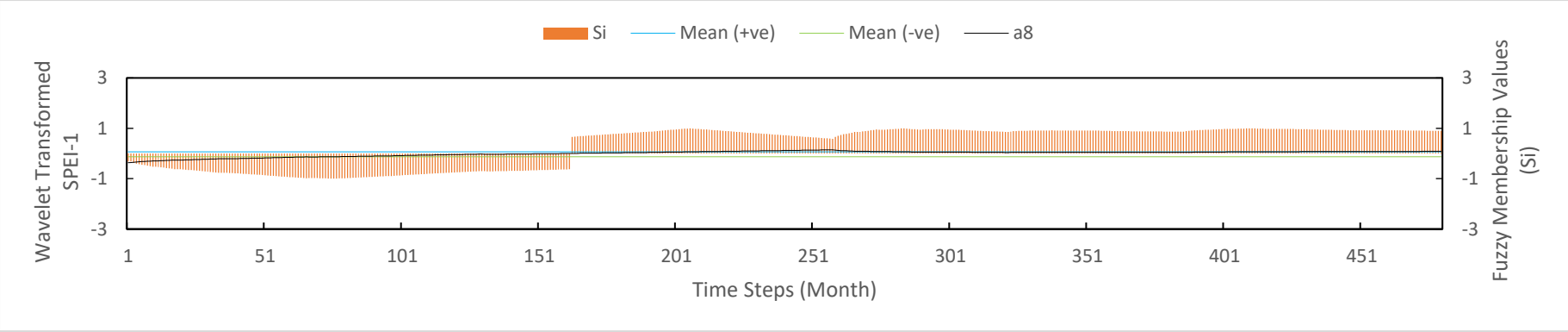

Figure B4.8: Fuzzy Membership Values of Wavelet Transformed SPEI-1 (a8) for station s2917001

APPENDIX B5

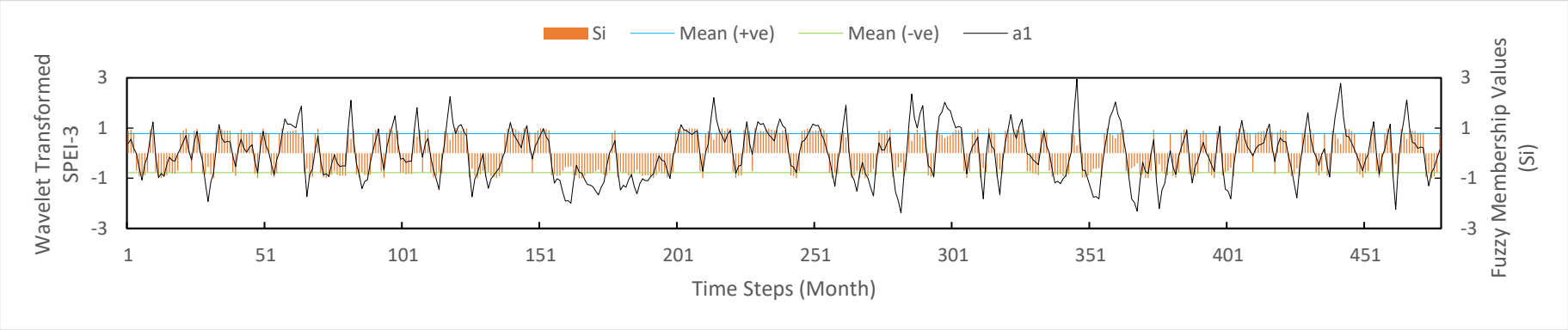

Figure B5.1: Fuzzy Membership Values of Wavelet Transformed SPEI-3 (a1) for station s2917001

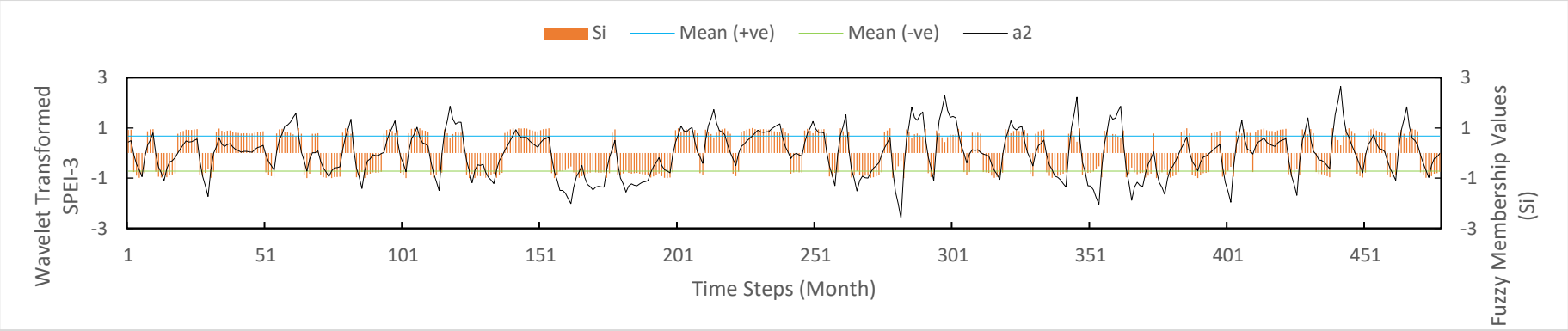

Figure B5.2: Fuzzy Membership Values of Wavelet Transformed SPEI-3 (a2) for station s2917001

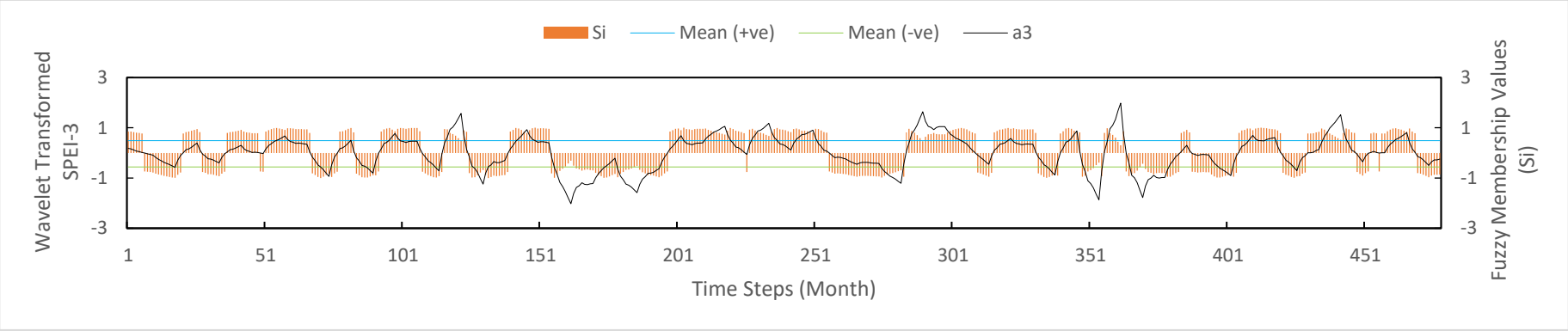

Figure B5.3: Fuzzy Membership Values of Wavelet Transformed SPEI-3 (a3) for station s2917001

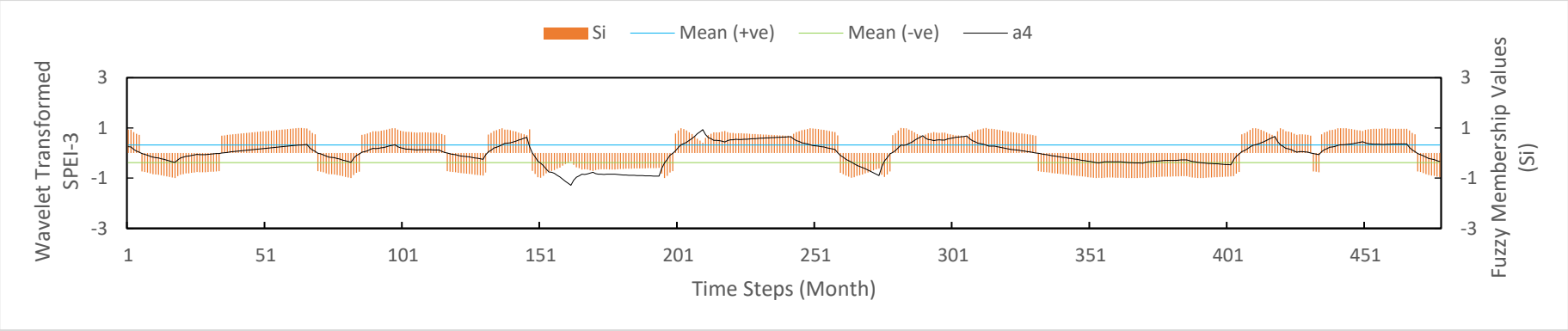

Figure B5.4: Fuzzy Membership Values of Wavelet Transformed SPEI-3 (a4) for station s2917001

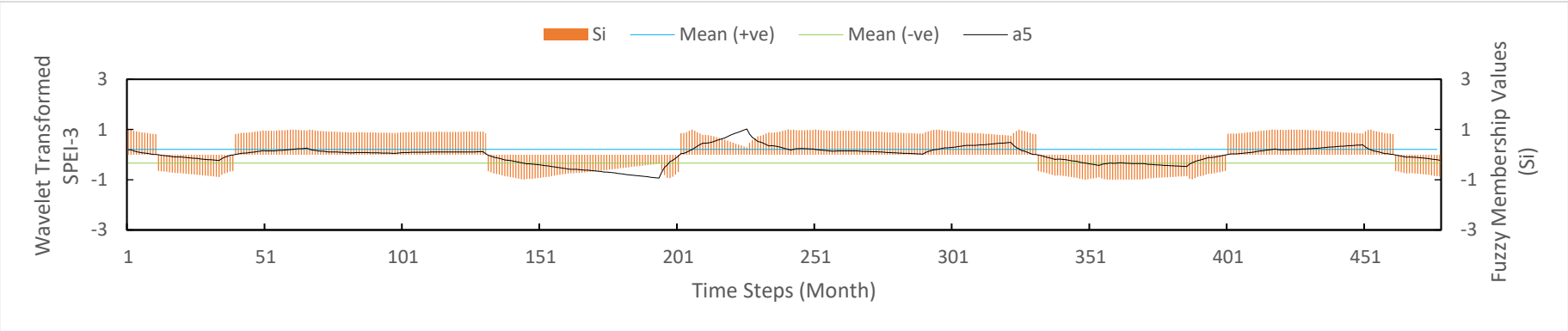

Figure B5.5: Fuzzy Membership Values of Wavelet Transformed SPEI-3 (a5) for station s2917001

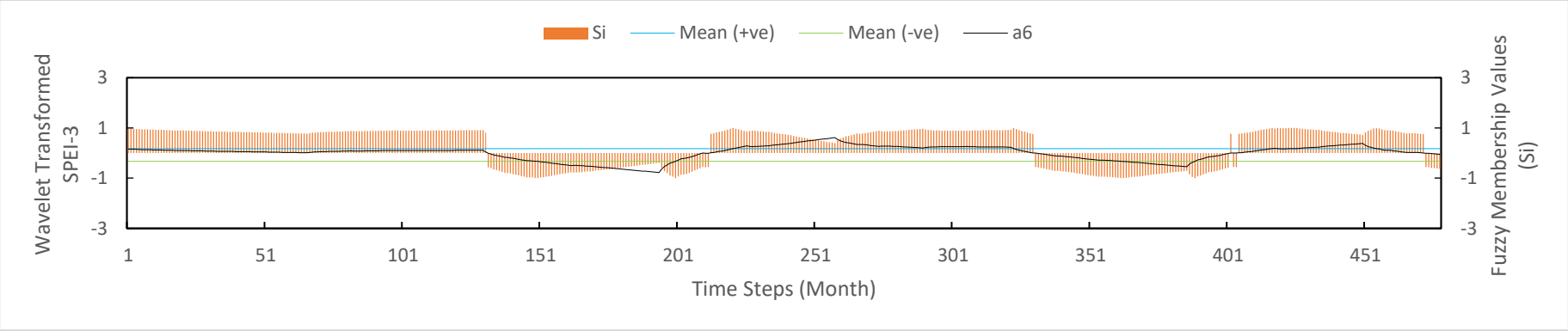

Figure B5.6: Fuzzy Membership Values of Wavelet Transformed SPEI-3 (a6) for station s2917001

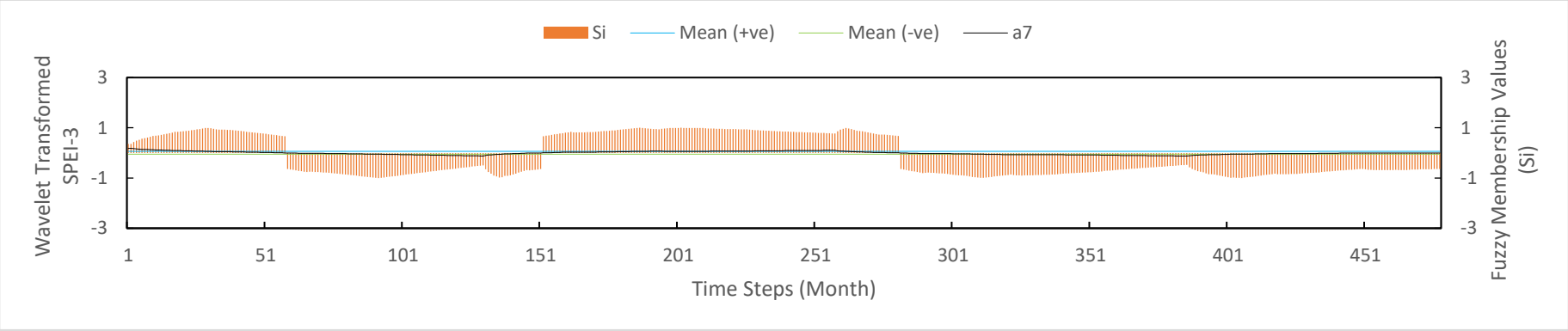

Figure B5.7: Fuzzy Membership Values of Wavelet Transformed SPEI-3 (a7) for station s2917001

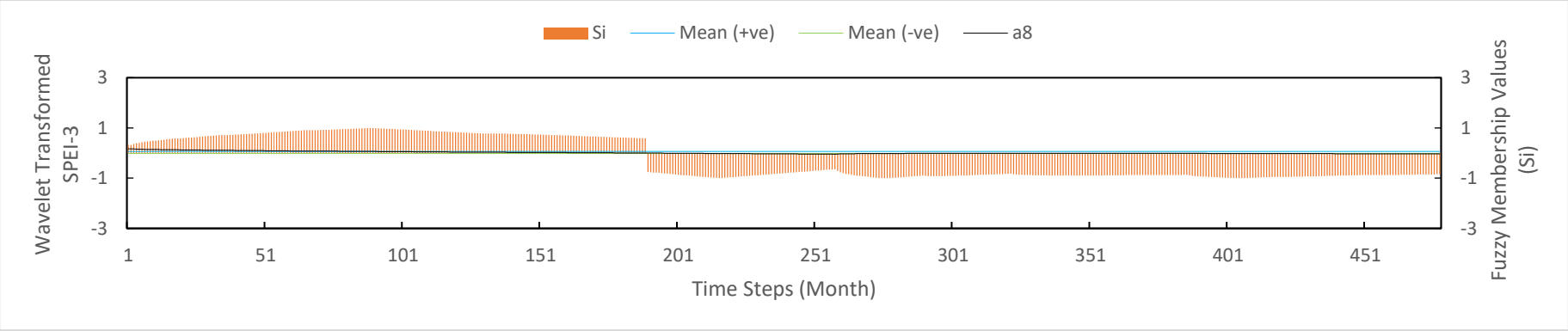

Figure B5.8: Fuzzy Membership Values of Wavelet Transformed SPEI-3 (a8) for station s2917001

APPENDIX B6

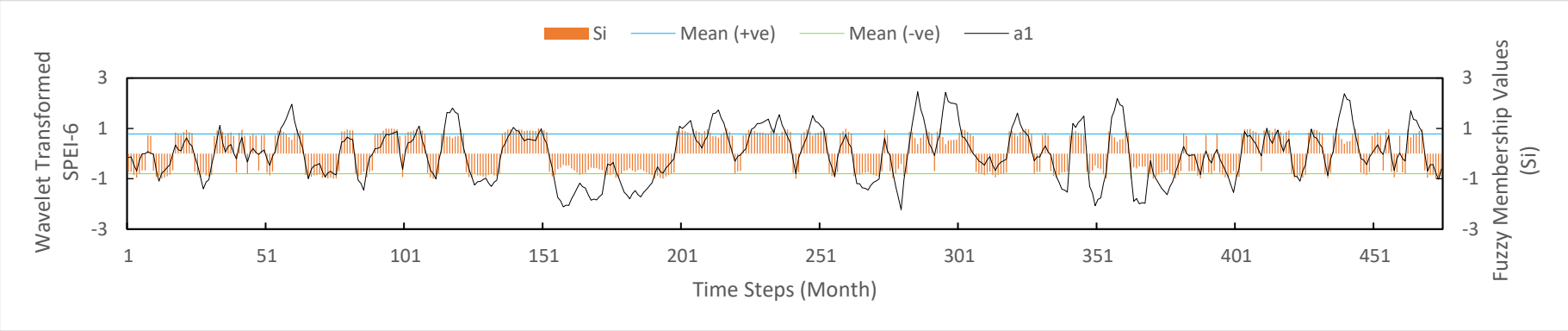

Figure B6.1: Fuzzy Membership Values of Wavelet Transformed SPEI-6 (a1) for station s2917001

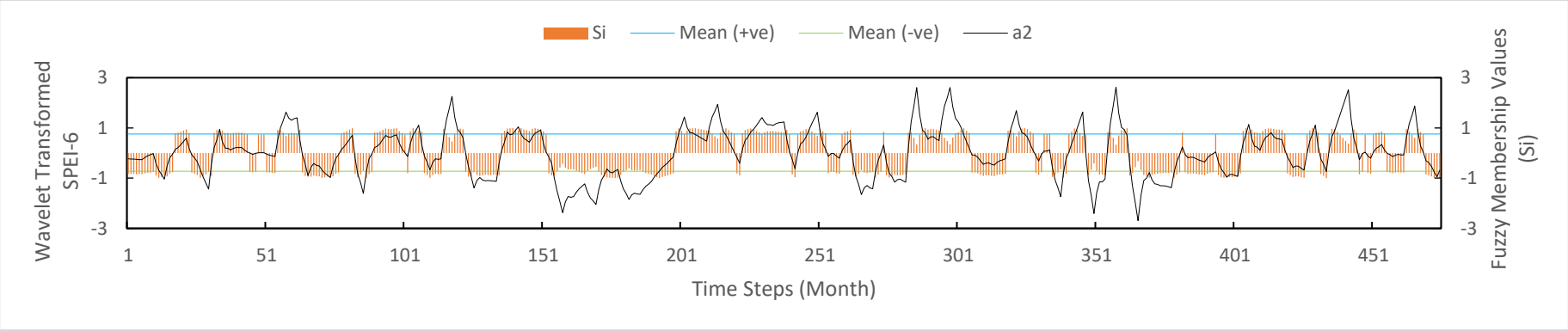

Figure B6.2: Fuzzy Membership Values of Wavelet Transformed SPEI-6 (a2) for station s2917001

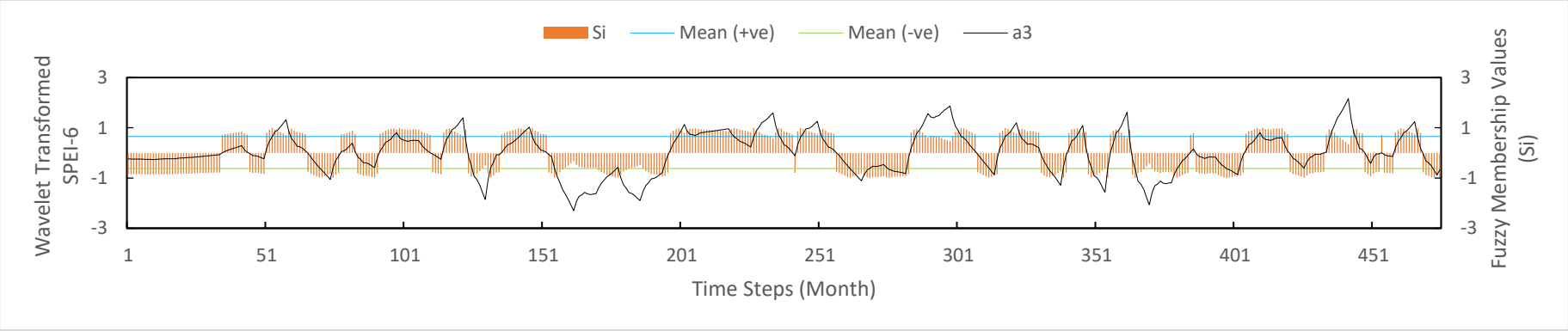

Figure B6.3: Fuzzy Membership Values of Wavelet Transformed SPEI-6 (a3) for station s2917001

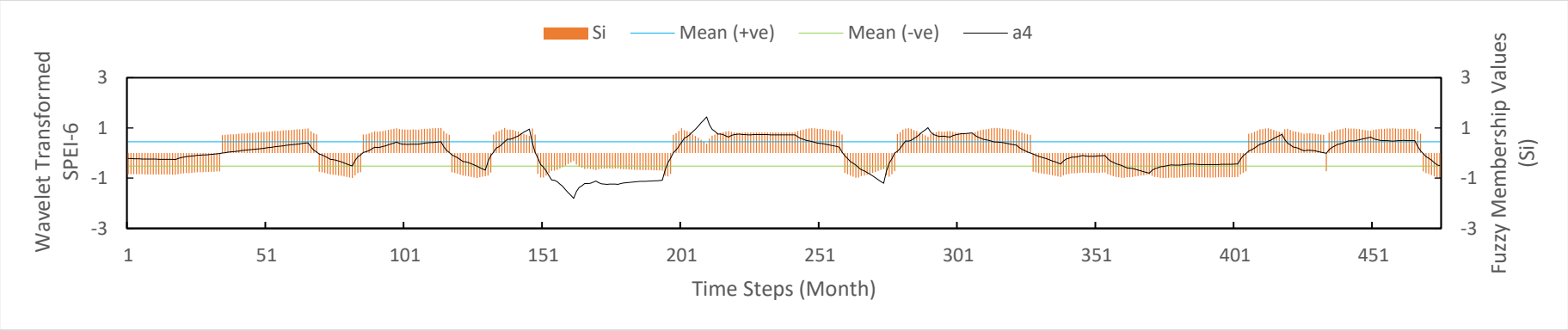

Figure B6.4: Fuzzy Membership Values of Wavelet Transformed SPEI-6 (a4) for station s2917001

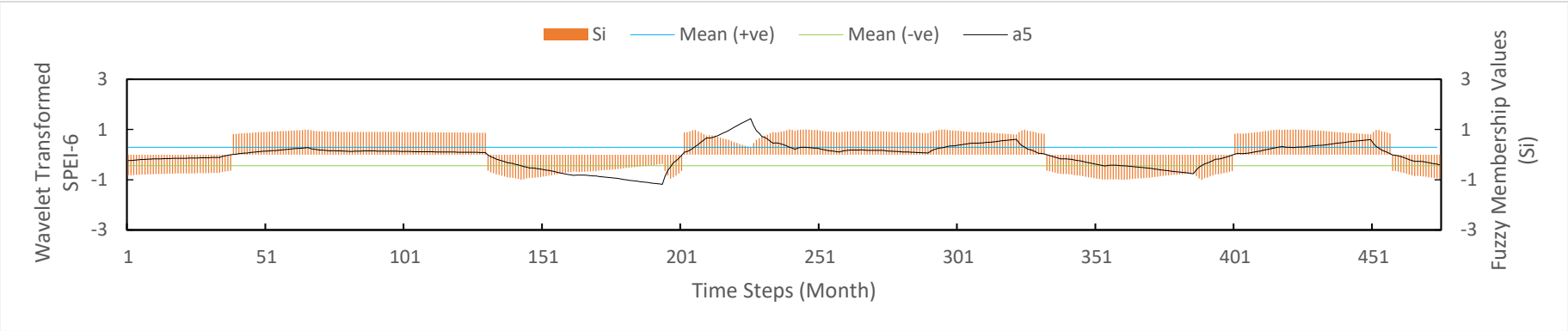

Figure B6.5: Fuzzy Membership Values of Wavelet Transformed SPEI-6 (a5) for station s2917001

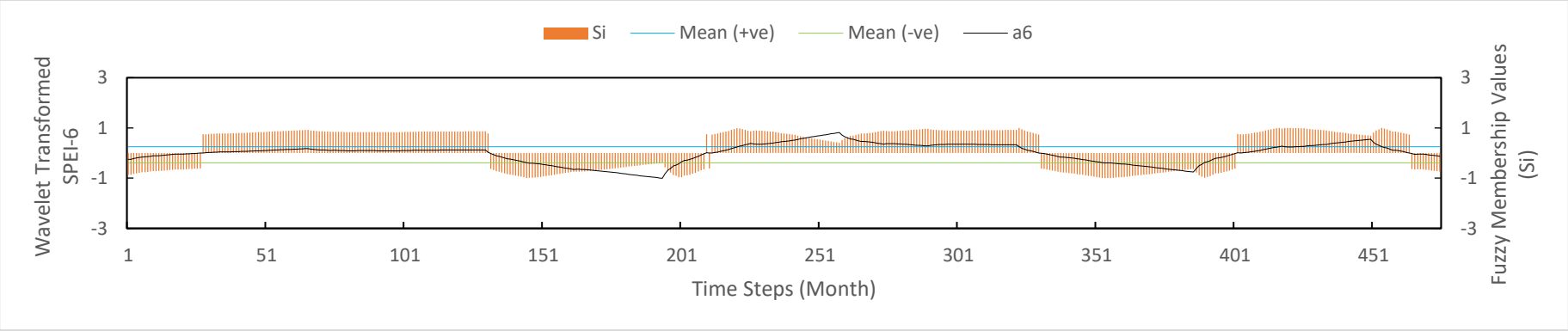

Figure B6.6: Fuzzy Membership Values of Wavelet Transformed SPEI-6 (a6) for station s2917001

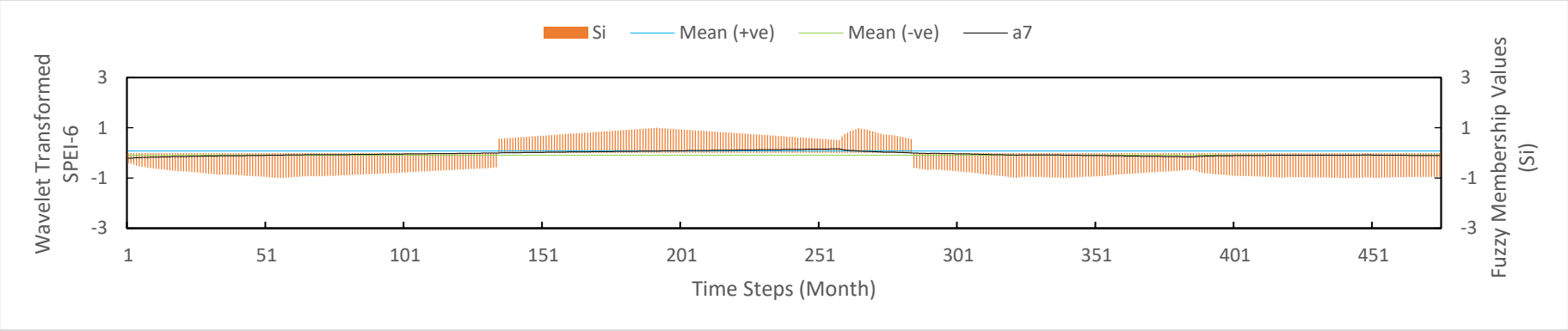

Figure B6.7: Fuzzy Membership Values of Wavelet Transformed SPEI-6 (a7) for station s2917001

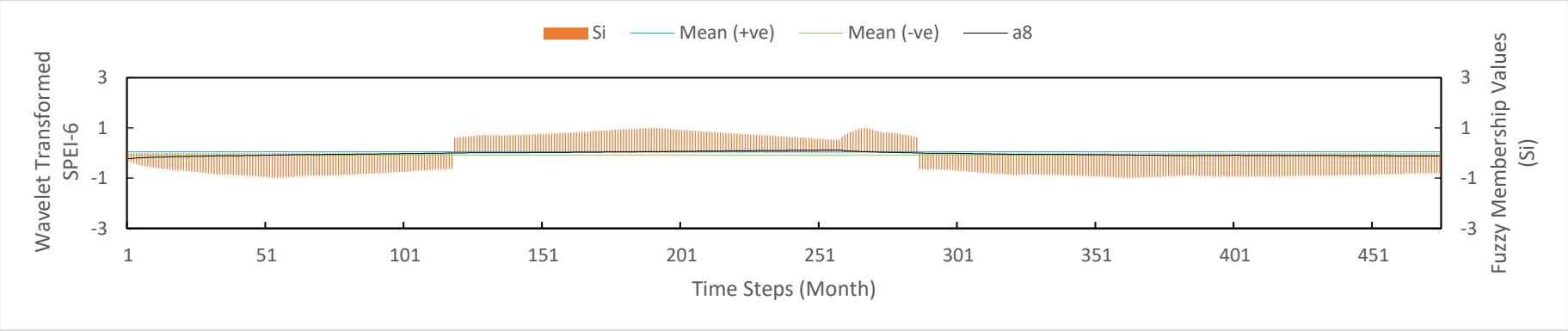

Figure B6.8: Fuzzy Membership Values of Wavelet Transformed SPEI-6 (a8) for station s2917001

APPENDIX C

Table C1: Model Performance in MAE, RMSE and Bias for station s2815001 (Training)

Lead Time	Time Scales	Models	W1			W2			W3			W4			W5			W6			W7			W8		
			MAE	RMSE	Bias	MAE	RMSE	Bias	MAE	RMSE	Bias	MAE	RMSE	Bias	MAE	RMSE	Bias	MAE	RMSE	Bias	MAE	RMSE	Bias	MAE	RMSE	Bias
1-Month	SPEI-1	W-BS-SVR	**0.074**	**0.090**	**-0.040**	0.075	0.092	-0.049	0.119	0.141	0.011	0.185	0.221	-0.038	0.257	0.304	-0.030	0.501	0.593	-0.051	0.352	0.417	-0.026	0.461	0.546	-0.032
		M-W-FSVR	0.145	0.171	-0.038	0.107	0.135	-0.038	0.160	0.205	-0.031	0.168	0.198	-0.086	0.161	0.188	-0.048	**0.044**	**0.057**	**0.025**	0.556	0.655	0.016	0.810	0.958	-0.022
		W-W-FSVR	**0.075**	**0.090**	**-0.037**	0.119	0.143	-0.057	0.152	0.184	-0.080	0.184	0.220	-0.064	0.245	0.290	-0.032	0.156	0.185	0.024	0.553	0.653	-0.002	0.970	1.148	0.041
	SPEI-3	W-BS-SVR	0.106	0.125	-0.024	**0.030**	**0.037**	**-0.016**	0.074	0.090	-0.019	0.153	0.189	-0.067	0.104	0.125	-0.005	0.276	0.332	-0.005	0.200	0.242	-0.024	0.281	0.340	-0.032
		M-W-FSVR	0.086	0.102	-0.014	**0.031**	**0.037**	**0.024**	0.053	0.066	-0.022	0.148	0.184	-0.118	0.178	0.218	-0.076	0.252	0.302	0.004	1.027	1.235	0.054	0.741	0.891	0.014
		W-W-FSVR	0.080	0.096	-0.010	**0.016**	**0.019**	**0.015**	0.050	0.062	-0.034	0.142	0.175	-0.120	0.191	0.234	-0.067	0.225	0.269	0.008	0.823	0.991	0.057	0.907	1.094	0.083
	SPEI-6	W-BS-SVR	**0.006**	**0.007**	**-0.002**	0.020	0.021	-0.020	0.060	0.072	0.006	0.057	0.068	0.005	0.102	0.123	-0.024	0.174	0.211	-0.034	0.183	0.220	0.014	0.278	0.335	-0.010
		M-W-FSVR	0.052	0.063	0.007	0.042	0.052	-0.030	0.046	0.057	-0.017	**0.012**	**0.015**	**0.008**	0.055	0.072	-0.009	0.122	0.143	0.049	0.954	1.155	0.046	0.642	0.758	-0.205
		W-W-FSVR	0.049	0.059	0.003	**0.012**	**0.014**	**0.005**	0.027	0.033	-0.001	0.046	0.057	-0.023	0.082	0.101	-0.038	0.113	0.136	0.031	0.751	0.905	0.011	0.897	1.082	0.055
3-Month	SPEI-1	W-BS-SVR	0.386	0.457	0.001	**0.138**	**0.163**	**0.011**	0.206	0.244	-0.031	0.168	0.199	-0.019	0.236	0.281	-0.050	0.566	0.670	-0.009	0.441	0.522	-0.025	0.322	0.382	-0.033
		M-W-FSVR	0.679	0.803	-0.030	0.355	0.425	-0.072	**0.099**	**0.117**	**0.002**	0.176	0.206	-0.079	0.223	0.263	-0.050	0.141	0.168	-0.050	0.678	0.800	0.008	0.935	1.108	0.011
		W-W-FSVR	0.694	0.822	-0.002	0.297	0.352	-0.014	**0.084**	**0.100**	**-0.062**	0.152	0.182	-0.045	0.158	0.190	-0.058	0.156	0.185	0.017	0.590	0.699	0.007	0.982	1.163	0.043
	SPEI-3	W-BS-SVR	0.232	0.277	0.032	0.144	0.172	0.024	0.192	0.234	-0.054	0.194	0.238	-0.067	**0.086**	**0.106**	**-0.044**	0.187	0.224	0.001	0.321	0.388	-0.036	0.275	0.331	-0.030
		M-W-FSVR	0.593	0.712	0.019	0.448	0.534	-0.022	0.171	0.202	-0.075	**0.076**	**0.084**	**-0.076**	0.137	0.170	-0.097	0.331	0.394	0.019	0.950	1.142	0.067	0.839	1.009	0.015
		W-W-FSVR	0.586	0.704	0.018	0.448	0.537	0.006	**0.050**	**0.058**	**-0.050**	0.096	0.119	-0.073	0.144	0.179	-0.081	0.196	0.235	-0.008	0.763	0.918	0.060	0.900	1.083	0.052
	SPEI-6	W-BS-SVR	0.064	0.077	0.019	0.098	0.117	0.046	0.059	0.071	0.015	**0.045**	**0.054**	**0.007**	0.064	0.077	-0.004	0.187	0.224	0.035	0.191	0.230	-0.010	0.315	0.380	-0.019
		M-W-FSVR	0.396	0.469	-0.021	0.307	0.368	0.002	0.081	0.097	0.000	**0.030**	**0.035**	**-0.014**	0.061	0.074	-0.041	0.075	0.093	0.045	0.985	1.190	0.037	0.660	0.776	-0.187
		W-W-FSVR	0.402	0.484	0.010	0.291	0.352	0.040	0.053	0.065	0.012	0.024	0.029	0.008	0.050	0.060	-0.026	**0.019**	**0.023**	**-0.011**	0.848	1.022	0.012	0.923	1.113	0.065
6-Month	SPEI-1	W-BS-SVR	0.479	0.567	-0.014	0.630	0.747	-0.033	0.497	0.590	-0.045	**0.261**	**0.309**	**-0.006**	0.364	0.433	-0.067	0.356	0.423	-0.030	0.529	0.627	0.017	0.437	0.517	-0.021
		M-W-FSVR	0.864	1.026	0.003	0.913	1.078	0.014	0.580	0.682	0.037	**0.116**	**0.135**	**-0.039**	0.136	0.145	-0.034	0.249	0.294	0.053	0.562	0.664	0.001	0.680	0.805	-0.085
		W-W-FSVR	0.835	0.990	0.028	0.918	1.087	-0.020	0.485	0.575	-0.038	0.164	0.195	-0.028	**0.106**	**0.125**	**-0.024**	0.166	0.197	0.037	0.518	0.614	-0.006	0.898	1.064	0.017
	SPEI-3	W-BS-SVR	0.377	0.450	0.055	0.359	0.428	0.100	0.405	0.486	0.001	**0.113**	**0.140**	**-0.080**	0.136	0.165	-0.025	0.366	0.439	0.000	0.388	0.468	-0.040	0.379	0.456	-0.019
		M-W-FSVR	0.928	1.120	0.058	0.935	1.133	0.074	0.438	0.527	0.015	**0.081**	**0.101**	**-0.079**	0.150	0.158	-0.050	0.354	0.423	0.021	0.790	0.948	0.053	0.763	0.920	-0.006
		W-W-FSVR	0.923	1.113	0.089	0.940	1.132	0.063	0.370	0.443	-0.013	0.076	0.084	-0.076	**0.057**	**0.071**	**-0.036**	0.305	0.366	0.001	0.747	0.899	0.045	0.759	0.913	0.043
	SPEI-6	W-BS-SVR	0.483	0.579	0.055	0.303	0.363	0.030	0.122	0.147	-0.006	**0.053**	**0.065**	**-0.040**	0.114	0.137	0.002	0.256	0.308	0.019	0.248	0.298	0.009	0.279	0.335	0.003
		M-W-FSVR	0.693	0.834	0.053	0.642	0.771	0.023	0.258	0.319	0.030	0.131	0.174	-0.021	**0.046**	**0.057**	**-0.040**	0.105	0.128	-0.029	0.953	1.153	0.039	0.584	0.696	-0.212
		W-W-FSVR	0.713	0.858	0.044	0.648	0.781	0.044	0.224	0.269	-0.019	0.068	0.083	-0.050	0.037	0.044	-0.032	**0.033**	**0.034**	**0.033**	0.721	0.867	0.018	0.812	0.978	0.039

Table C2: Model Performance in MAE, RMSE and Bias for station s2815001 (Validation)

Lead Time	Time Scales		W1			W2			W3			W4			W5			W6			W7			W8		
			MAE	RMSE	Bias	MAE	RMSE	Bias	MAE	RMSE	Bias	MAE	RMSE	Bias	MAE	RMSE	Bias	MAE	RMSE	Bias	MAE	RMSE	Bias	MAE	RMSE	Bias
1-Month	SPEI-1	W-BS-SVR	**0.090**	**0.104**	**-0.026**	0.108	0.104	-0.041	0.152	0.174	0.024	0.233	0.267	-0.018	0.325	0.372	-0.002	0.635	0.726	0.005	0.447	0.511	0.013	0.586	0.670	0.019
		M-W-FSVR	0.183	0.213	-0.058	0.135	0.161	-0.022	0.205	0.249	-0.002	0.199	0.229	-0.078	0.198	0.223	-0.042	**0.054**	**0.067**	**0.014**	0.705	0.802	-0.037	1.032	1.186	-0.124
		W-W-FSVR	**0.090**	**0.104**	**-0.025**	0.143	0.167	-0.044	0.181	0.213	-0.065	0.227	0.262	-0.044	0.310	0.355	-0.005	0.199	0.229	0.041	0.704	0.805	-0.063	1.234	1.411	-0.066
	SPEI-3	W-BS-SVR	0.134	0.155	-0.036	**0.039**	**0.045**	**-0.011**	0.097	0.114	-0.004	0.201	0.232	-0.037	0.137	0.163	0.016	0.364	0.434	0.050	0.264	0.313	0.016	0.371	0.440	0.024
		M-W-FSVR	0.117	0.140	-0.037	**0.037**	**0.047**	**0.030**	0.072	0.085	0.014	0.180	0.205	-0.099	0.233	0.268	-0.044	0.354	0.419	0.082	1.341	1.593	-0.129	1.036	1.225	-0.207
		W-W-FSVR	0.117	0.140	-0.037	**0.018**	**0.021**	**0.013**	0.063	0.072	-0.026	0.168	0.193	-0.099	0.250	0.292	-0.030	0.296	0.353	0.053	1.085	1.289	-0.107	1.196	1.420	-0.098
	SPEI-6	W-BS-SVR	**0.008**	**0.009**	**0.001**	0.022	0.024	-0.022	0.083	0.095	0.030	0.078	0.090	0.028	0.136	0.152	0.017	0.234	0.263	0.037	0.253	0.289	0.089	0.381	0.432	0.104
		M-W-FSVR	0.074	0.082	-0.014	0.057	0.069	-0.043	0.062	0.069	0.001	**0.016**	**0.019**	**0.012**	0.063	0.076	-0.024	0.168	0.198	0.094	1.286	1.466	-0.345	0.895	1.045	-0.443
		W-W-FSVR	0.067	0.076	-0.017	**0.016**	**0.019**	**0.010**	0.037	0.042	0.010	0.058	0.065	-0.005	0.105	0.117	-0.006	0.155	0.182	0.076	1.034	1.173	-0.299	1.230	1.390	-0.314
3-Month	SPEI-1	W-BS-SVR	0.503	0.572	0.049	**0.180**	**0.205**	**0.028**	0.266	0.302	-0.006	0.218	0.247	0.002	0.304	0.346	-0.021	0.737	0.837	0.061	0.573	0.651	0.030	0.417	0.474	0.006
		M-W-FSVR	0.888	1.009	-0.120	0.463	0.539	-0.134	**0.129**	**0.147**	**-0.012**	0.216	0.244	-0.065	0.281	0.315	-0.038	0.182	0.211	-0.067	0.879	0.996	-0.067	1.221	1.386	-0.106
		W-W-FSVR	0.906	1.029	-0.087	0.388	0.441	-0.050	**0.086**	**0.106**	**-0.068**	0.194	0.221	-0.027	0.200	0.229	-0.039	0.204	0.233	0.036	0.770	0.874	-0.065	1.278	1.451	-0.078
	SPEI-3	W-BS-SVR	0.303	0.365	0.073	0.188	0.227	0.050	0.256	0.297	-0.020	0.259	0.299	-0.033	**0.114**	**0.129**	**-0.030**	0.247	0.293	0.034	0.426	0.503	0.021	0.364	0.430	0.019
		M-W-FSVR	0.799	0.945	-0.107	0.613	0.726	-0.136	0.221	0.271	-0.109	**0.070**	**0.082**	**-0.068**	0.176	0.195	-0.095	0.454	0.538	0.105	1.249	1.473	-0.082	1.167	1.376	-0.220
		W-W-FSVR	0.774	0.919	-0.086	0.591	0.703	-0.073	**0.058**	**0.066**	**-0.058**	0.119	0.136	-0.059	0.190	0.215	-0.058	0.259	0.307	0.026	1.010	1.194	-0.076	1.191	1.410	-0.107
	SPEI-6	W-BS-SVR	0.082	0.099	0.039	0.122	0.152	0.075	0.076	0.091	0.034	**0.058**	**0.068**	**0.021**	0.082	0.095	0.016	0.241	0.287	0.095	0.247	0.286	0.051	0.408	0.472	0.083
		M-W-FSVR	0.530	0.611	-0.152	0.419	0.481	-0.102	0.109	0.125	-0.027	**0.035**	**0.041**	**-0.016**	0.067	0.085	-0.053	0.100	0.066	0.100	1.259	1.467	-0.277	0.885	1.046	-0.400
		W-W-FSVR	0.521	0.604	-0.120	0.374	0.431	-0.054	0.068	0.078	-0.006	0.031	0.037	0.015	0.062	0.077	-0.040	**0.025**	**0.031**	**-0.019**	1.101	1.277	-0.263	1.194	1.380	-0.234
6-Month	SPEI-1	W-BS-SVR	0.641	0.730	0.118	0.842	0.958	0.140	0.663	0.753	0.092	**0.350**	**0.398**	**0.066**	0.481	0.545	0.033	0.475	0.540	0.068	0.711	0.812	0.163	0.584	0.664	0.099
		M-W-FSVR	1.163	1.328	-0.239	1.218	1.385	-0.231	0.766	0.864	-0.111	**0.140**	**0.158**	**-0.025**	0.160	0.174	-0.038	0.340	0.390	0.123	0.749	0.850	-0.146	0.932	1.065	-0.284
		W-W-FSVR	1.118	1.273	-0.202	1.233	1.407	-0.273	0.653	0.748	-0.172	0.217	0.246	0.017	**0.137**	**0.158**	**-0.015**	0.224	0.259	0.082	0.696	0.794	-0.149	1.204	1.371	-0.230
	SPEI-3	W-BS-SVR	0.666	0.793	0.202	0.696	0.835	0.260	0.362	0.429	0.100	**0.162**	**0.189**	**0.015**	0.284	0.330	0.028	0.394	0.468	0.106	0.432	0.506	0.068	0.352	0.413	0.062
		M-W-FSVR	1.289	1.517	-0.304	1.306	1.535	-0.302	0.609	0.718	-0.156	**0.094**	**0.113**	**-0.058**	0.164	0.171	-0.063	0.500	0.591	0.172	1.064	1.244	-0.181	1.111	1.302	-0.382
		W-W-FSVR	1.259	1.481	-0.236	1.282	1.513	-0.268	0.506	0.601	-0.142	0.073	0.083	-0.018	**0.067**	**0.081**	**-0.066**	0.416	0.494	0.108	1.019	1.203	-0.218	1.035	1.222	-0.224
	SPEI-6	W-BS-SVR	0.642	0.749	0.262	0.402	0.468	0.160	0.161	0.185	0.047	**0.068**	**0.084**	**-0.059**	0.151	0.174	0.051	0.341	0.396	0.130	0.329	0.380	0.116	0.369	0.426	0.123
		M-W-FSVR	0.918	1.046	-0.248	0.849	0.973	-0.254	0.329	0.376	-0.070	0.172	0.210	-0.071	**0.059**	**0.067**	**-0.012**	0.140	0.168	-0.073	1.242	1.435	-0.363	0.770	0.919	-0.443
		W-W-FSVR	0.938	1.075	-0.263	0.853	0.977	-0.235	0.298	0.346	-0.115	0.089	0.109	-0.073	0.046	0.056	-0.043	**0.035**	**0.036**	**0.035**	0.952	1.094	-0.292	1.071	1.228	-0.311

Table C3: Model Performance in MAE, RMSE and Bias for station s2917001 (Training)

Lead Time	Time Scales	Models	W1			W2			W3			W4			W5			W6			W7			W8		
			MAE	RMSE	Bias	MAE	RMSE	Bias	MAE	RMSE	Bias	MAE	RMSE	Bias	MAE	RMSE	Bias	MAE	RMSE	Bias	MAE	RMSE	Bias	MAE	RMSE	Bias
1-Month	SPEI-1	W-BS-SVR	0.176	0.210	-0.005	**0.091**	**0.114**	**-0.048**	0.152	0.183	-0.047	0.285	0.340	-0.013	0.389	0.464	-0.007	0.323	0.385	-0.008	0.591	0.707	-0.037	0.647	0.772	-0.018
		M-W-FSVR	0.121	0.143	0.035	**0.048**	**0.057**	**0.002**	0.095	0.114	-0.018	0.132	0.159	-0.056	0.126	0.149	-0.008	0.183	0.217	-0.023	0.701	0.846	-0.007	0.802	0.966	0.007
		W-W-FSVR	**0.035**	**0.044**	**-0.028**	0.163	0.197	-0.052	0.148	0.178	-0.021	0.180	0.217	-0.036	0.282	0.336	0.000	0.176	0.210	-0.009	0.465	0.555	0.012	0.556	0.664	0.029
	SPEI-3	W-BS-SVR	0.043	0.051	-0.003	**0.038**	**0.045**	**0.015**	0.052	0.062	0.020	0.188	0.225	0.002	0.211	0.253	0.001	0.236	0.281	0.020	0.314	0.376	-0.040	0.385	0.461	0.007
		M-W-FSVR	0.099	0.117	-0.024	**0.037**	**0.050**	**0.017**	0.041	0.054	-0.029	0.106	0.131	-0.019	0.088	0.118	-0.011	0.076	0.092	0.014	0.233	0.281	0.010	0.511	0.608	-0.047
		W-W-FSVR	0.078	0.093	-0.013	**0.033**	**0.034**	**0.033**	0.046	0.050	-0.026	0.124	0.148	-0.020	0.171	0.204	0.001	0.149	0.178	0.031	0.272	0.325	-0.005	1.325	1.585	0.070
	SPEI-6	W-BS-SVR	0.014	0.016	-0.013	**0.013**	**0.016**	**-0.007**	0.059	0.071	0.004	0.089	0.109	-0.035	0.115	0.140	-0.003	0.186	0.225	-0.001	0.171	0.207	0.015	0.202	0.243	0.035
		M-W-FSVR	0.054	0.064	-0.021	0.033	0.041	-0.019	0.043	0.059	0.022	**0.019**	**0.025**	**-0.016**	0.102	0.129	0.013	0.145	0.191	0.029	0.155	0.189	0.053	0.162	0.207	0.043
		W-W-FSVR	0.045	0.055	-0.019	**0.011**	**0.014**	**-0.007**	0.049	0.060	0.001	0.095	0.115	-0.014	0.051	0.052	0.051	0.047	0.052	0.047	0.208	0.253	0.033	0.329	0.399	0.011
3-Month	SPEI-1	W-BS-SVR	0.864	1.034	-0.025	0.280	0.335	-0.015	**0.245**	**0.294**	**-0.027**	0.391	0.468	-0.030	0.469	0.561	0.003	0.322	0.386	-0.027	0.491	0.587	-0.001	0.460	0.551	-0.017
		M-W-FSVR	0.821	0.984	-0.006	0.302	0.357	0.027	0.092	0.106	-0.002	0.168	0.202	-0.042	0.222	0.266	-0.023	**0.077**	**0.092**	**-0.015**	0.820	0.991	-0.014	0.792	0.958	-0.012
		W-W-FSVR	0.812	0.972	0.008	0.273	0.326	-0.010	**0.036**	**0.046**	**-0.024**	0.121	0.146	-0.046	0.204	0.244	-0.020	0.188	0.225	-0.013	0.459	0.550	0.013	0.572	0.686	0.032
	SPEI-3	W-BS-SVR	0.503	0.603	-0.039	0.274	0.328	-0.005	0.141	0.169	0.028	0.195	0.233	-0.013	**0.118**	**0.143**	**-0.040**	0.314	0.376	0.003	0.384	0.460	-0.052	0.397	0.475	0.033
		M-W-FSVR	0.662	0.792	-0.002	0.437	0.522	0.033	0.208	0.246	-0.027	0.081	0.097	-0.034	**0.048**	**0.064**	**-0.037**	0.057	0.070	0.011	0.391	0.471	0.021	0.522	0.622	-0.048
		W-W-FSVR	0.651	0.778	-0.017	0.425	0.509	0.018	0.140	0.167	-0.022	0.103	0.124	-0.017	0.071	0.087	-0.043	**0.031**	**0.037**	**-0.020**	0.225	0.269	-0.010	1.328	1.590	0.084
	SPEI-6	W-BS-SVR	0.159	0.194	-0.032	0.130	0.157	-0.005	0.117	0.140	0.021	**0.067**	**0.082**	**-0.026**	0.125	0.150	0.025	0.217	0.263	-0.004	0.206	0.249	-0.003	0.270	0.324	0.048
		M-W-FSVR	0.281	0.340	-0.016	0.264	0.316	-0.055	0.121	0.145	-0.009	0.106	0.128	0.010	**0.025**	**0.031**	**0.015**	0.151	0.204	0.043	0.065	0.086	0.047	0.148	0.185	0.025
		W-W-FSVR	0.319	0.385	-0.016	0.253	0.305	-0.035	0.114	0.137	-0.021	0.098	0.118	0.000	**0.015**	**0.017**	**0.015**	0.093	0.115	0.056	0.145	0.178	0.044	0.286	0.345	0.006
6-Month	SPEI-1	W-BS-SVR	0.636	0.760	0.009	0.620	0.742	-0.028	0.467	0.558	-0.024	**0.375**	**0.450**	**-0.042**	0.423	0.506	-0.026	0.722	0.866	-0.077	0.451	0.540	-0.022	0.536	0.641	-0.010
		M-W-FSVR	0.755	0.896	0.017	0.989	1.189	-0.023	0.486	0.589	-0.023	0.100	0.130	-0.053	0.218	0.272	-0.014	**0.082**	**0.099**	**0.014**	0.724	0.878	0.024	0.858	1.038	0.006
		W-W-FSVR	0.697	0.833	-0.007	0.921	1.101	0.038	0.458	0.548	0.018	**0.073**	**0.089**	**-0.034**	0.193	0.233	-0.037	0.088	0.107	-0.030	0.526	0.629	0.020	0.536	0.643	0.040
	SPEI-3	W-BS-SVR	1.233	1.529	-0.025	0.796	0.951	0.047	0.407	0.486	0.030	**0.249**	**0.297**	**0.019**	0.264	0.315	-0.011	0.368	0.439	0.056	0.446	0.532	0.025	0.440	0.525	0.035
		M-W-FSVR	0.796	0.949	0.056	0.918	1.095	-0.007	0.511	0.610	-0.004	0.098	0.082	-0.003	**0.051**	**0.064**	**-0.037**	0.146	0.161	0.012	0.406	0.494	0.027	0.432	0.517	-0.034
		W-W-FSVR	0.738	0.882	0.018	0.841	1.005	0.022	0.475	0.568	0.055	0.063	0.076	-0.007	**0.048**	**0.061**	**-0.001**	0.143	0.171	0.047	0.090	0.111	0.047	1.341	1.603	0.084
	SPEI-6	W-BS-SVR	0.518	0.625	0.026	0.398	0.481	-0.006	0.311	0.376	0.009	**0.094**	**0.115**	**-0.015**	0.128	0.155	0.006	0.261	0.317	-0.031	0.265	0.321	-0.025	0.355	0.430	-0.009
		M-W-FSVR	0.730	0.899	0.021	0.696	0.855	-0.005	0.439	0.538	-0.029	**0.056**	**0.070**	**0.011**	0.157	0.188	0.031	0.198	0.262	0.053	0.092	0.113	0.066	0.133	0.169	0.043
		W-W-FSVR	0.731	0.887	0.061	0.670	0.811	0.035	0.467	0.564	0.005	**0.039**	**0.047**	**0.031**	0.156	0.189	0.009	0.087	0.107	0.054	0.136	0.168	0.066	0.258	0.314	0.032

Table C4: Model Performance in MAE, RMSE and Bias for station s2917001 (Validation)

Lead Time	Time Scales		W1			W2			W3			W4			W5			W6			W7			W8		
			MAE	RMSE	Bias	MAE	RMSE	Bias	MAE	RMSE	Bias	MAE	RMSE	Bias	MAE	RMSE	Bias	MAE	RMSE	Bias	MAE	RMSE	Bias	MAE	RMSE	Bias
1-Month	SPEI-1	W-BS-SVR	0.193	0.234	0.032	**0.087**	**0.112**	**-0.029**	0.158	0.197	-0.016	0.312	0.379	0.046	0.427	0.519	0.074	0.354	0.430	0.060	0.645	0.785	0.086	0.709	0.861	0.117
		M-W-FSVR	0.127	0.157	0.015	**0.050**	**0.062**	**-0.007**	0.101	0.124	0.003	0.141	0.180	-0.048	0.137	0.169	0.009	0.199	0.248	-0.002	0.772	0.936	-0.183	0.883	1.070	-0.184
		W-W-FSVR	**0.035**	**0.046**	**-0.026**	0.169	0.211	-0.019	0.160	0.195	0.010	0.192	0.236	0.001	0.310	0.376	0.058	0.193	0.234	0.028	0.510	0.619	-0.085	0.608	0.739	-0.087
	SPEI-3	W-BS-SVR	0.044	0.054	0.012	**0.042**	**0.053**	**0.028**	0.058	0.072	0.038	0.198	0.244	0.070	0.222	0.273	0.077	0.251	0.310	0.105	0.321	0.395	0.073	0.406	0.500	0.146
		M-W-FSVR	0.110	0.137	-0.060	**0.033**	**0.040**	**-0.014**	0.043	0.047	-0.023	0.091	0.114	0.005	0.072	0.103	0.000	0.084	0.110	-0.006	0.258	0.328	-0.085	0.583	0.743	-0.256
		W-W-FSVR	0.084	0.104	-0.041	0.036	0.037	0.044	**0.030**	**0.031**	**0.030**	0.125	0.155	0.025	0.180	0.221	0.063	0.162	0.201	0.085	0.287	0.353	-0.103	1.377	1.694	-0.410
	SPEI-6	W-BS-SVR	0.010	0.012	-0.008	**0.010**	**0.012**	**0.000**	0.052	0.071	0.038	0.070	0.088	0.015	0.099	0.135	0.066	0.161	0.218	0.109	0.153	0.209	0.116	0.186	0.253	0.152
		M-W-FSVR	0.057	0.076	-0.053	0.036	0.044	-0.035	0.065	0.089	0.057	**0.022**	**0.027**	**-0.021**	0.120	0.170	-0.058	0.178	0.254	-0.087	0.183	0.252	0.162	0.145	0.187	0.074
		W-W-FSVR	0.047	0.061	-0.044	**0.013**	**0.016**	**-0.010**	0.043	0.058	0.030	0.079	0.105	0.042	0.046	0.047	0.046	0.058	0.061	0.058	0.174	0.230	-0.090	0.283	0.383	-0.184
3-Month	SPEI-1	W-BS-SVR	0.934	1.149	0.193	0.301	0.371	0.056	**0.261**	**0.323**	**0.035**	0.419	0.517	0.069	0.510	0.627	0.122	0.344	0.425	0.054	0.533	0.655	0.123	0.497	0.612	0.099
		M-W-FSVR	0.893	1.097	-0.219	0.325	0.403	-0.028	0.099	0.117	-0.018	0.173	0.218	-0.003	0.237	0.293	0.030	**0.083**	**0.101**	**-0.028**	0.896	1.097	-0.255	0.864	1.058	-0.251
		W-W-FSVR	0.881	1.083	-0.197	0.299	0.366	-0.079	**0.052**	**0.064**	**-0.010**	0.120	0.153	-0.016	0.217	0.269	0.031	0.202	0.249	0.034	0.497	0.611	-0.103	0.616	0.759	-0.113
	SPEI-3	W-BS-SVR	0.529	0.645	0.138	0.292	0.356	0.092	0.156	0.191	0.077	0.205	0.250	0.056	**0.116**	**0.144**	**0.000**	0.337	0.410	0.114	0.399	0.486	0.082	0.431	0.526	0.173
		M-W-FSVR	0.704	0.857	-0.234	0.439	0.529	-0.110	0.243	0.304	-0.107	0.071	0.086	-0.012	**0.051**	**0.072**	**0.039**	0.062	0.077	0.005	0.444	0.559	-0.131	0.614	0.772	-0.251
		W-W-FSVR	0.699	0.852	-0.246	0.451	0.549	-0.132	0.153	0.188	-0.071	0.106	0.130	0.019	0.065	0.081	-0.021	**0.033**	**0.042**	**-0.032**	0.242	0.295	-0.089	1.400	1.707	-0.384
	SPEI-6	W-BS-SVR	0.132	0.172	0.054	0.109	0.149	0.066	0.103	0.145	0.084	**0.055**	**0.068**	**0.004**	0.112	0.157	0.092	0.183	0.252	0.115	0.174	0.239	0.109	0.239	0.335	0.193
		M-W-FSVR	0.247	0.343	-0.173	0.260	0.359	-0.208	0.089	0.124	-0.064	0.098	0.136	0.071	**0.029**	**0.037**	**0.024**	0.190	0.251	-0.071	0.097	0.127	0.085	0.154	0.196	0.059
		W-W-FSVR	0.272	0.379	-0.190	0.221	0.310	-0.172	0.101	0.142	-0.082	0.082	0.114	0.053	**0.018**	**0.021**	**0.018**	0.074	0.086	0.011	0.119	0.151	-0.034	0.240	0.331	-0.150
6-Month	SPEI-1	W-BS-SVR	0.688	0.851	0.161	0.664	0.824	0.121	0.499	0.619	0.088	**0.396**	**0.494**	**0.048**	0.451	0.561	0.075	0.764	0.953	0.096	0.483	0.599	0.086	0.577	0.714	0.118
		M-W-FSVR	0.810	1.006	-0.130	1.077	1.326	-0.288	0.536	0.654	-0.180	0.086	0.123	-0.012	0.236	0.294	0.067	**0.084**	**0.105**	**-0.001**	0.782	0.966	-0.188	0.932	1.148	-0.244
		W-W-FSVR	0.753	0.931	-0.174	0.986	1.224	-0.182	0.491	0.609	-0.091	**0.072**	**0.091**	**-0.022**	0.201	0.253	0.009	0.089	0.113	-0.010	0.564	0.699	-0.106	0.571	0.710	-0.088
	SPEI-3	W-BS-SVR	0.742	0.911	0.260	0.845	1.039	0.306	0.432	0.532	0.162	**0.265**	**0.326**	**0.100**	0.276	0.338	0.075	0.395	0.488	0.174	0.473	0.581	0.169	0.468	0.575	0.178
		M-W-FSVR	0.794	0.963	-0.183	0.981	1.208	-0.313	0.563	0.698	-0.182	0.089	0.110	0.025	**0.055**	**0.066**	**0.017**	0.056	0.078	-0.007	0.467	0.593	-0.127	0.510	0.647	-0.197
		W-W-FSVR	0.774	0.948	-0.222	0.881	1.080	-0.251	0.490	0.600	-0.099	0.066	0.080	0.014	**0.046**	**0.064**	**-0.037**	0.157	0.195	0.091	0.085	0.107	0.020	1.397	1.710	-0.352
	SPEI-6	W-BS-SVR	0.456	0.627	0.279	0.348	0.473	0.190	0.273	0.375	0.162	**0.079**	**0.103**	**0.029**	0.113	0.155	0.069	0.227	0.300	0.097	0.231	0.307	0.105	0.310	0.421	0.166
		M-W-FSVR	0.766	0.987	-0.369	0.739	0.958	-0.378	0.480	0.628	-0.265	**0.069**	**0.088**	**-0.005**	0.118	0.155	-0.037	0.234	0.286	-0.061	0.108	0.147	0.107	0.080	0.125	0.006
		W-W-FSVR	0.639	0.850	-0.298	0.585	0.787	-0.295	0.408	0.555	-0.224	**0.047**	**0.056**	**0.046**	0.136	0.183	-0.068	0.073	0.085	0.016	0.116	0.139	0.004	0.225	0.297	-0.095

APPENDIX D

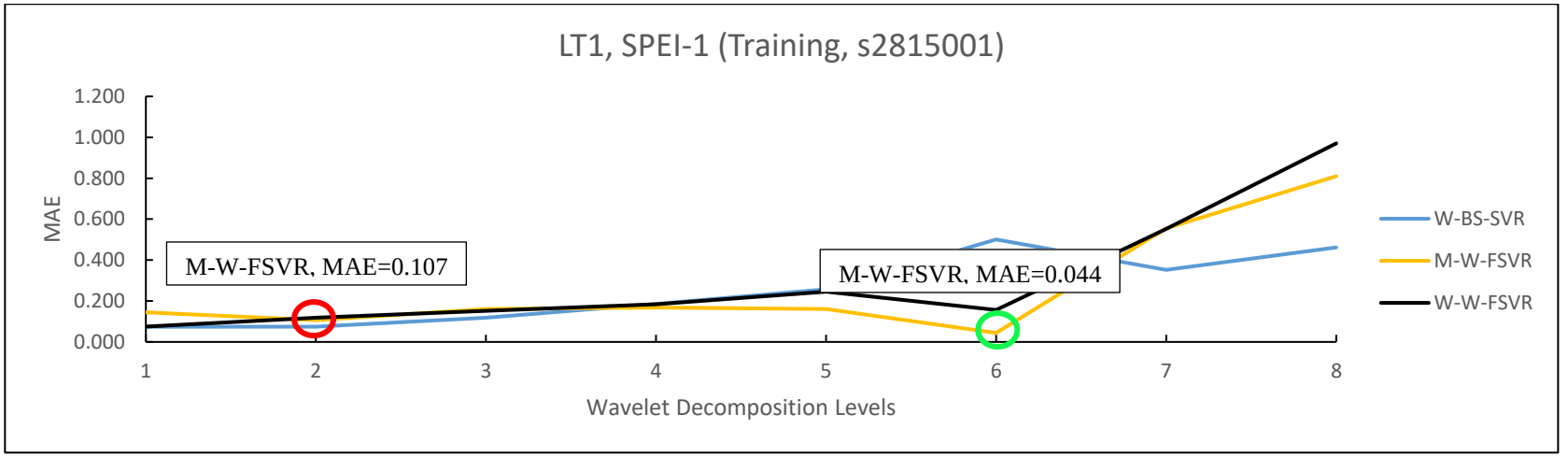
LT1, SPEI-1 (Training, s2815001)
MAE
1.200
1.000
0.800
0.600
0.400
0.200
0.000
M-W-FSVR, MAE=0.107
M-W-FSVR, MAE=0.044
1
2
3
4
5
6
7
8
Wavelet Decomposition Levels
W-BS-SVR
M-W-FSVR
W-W-FSVR

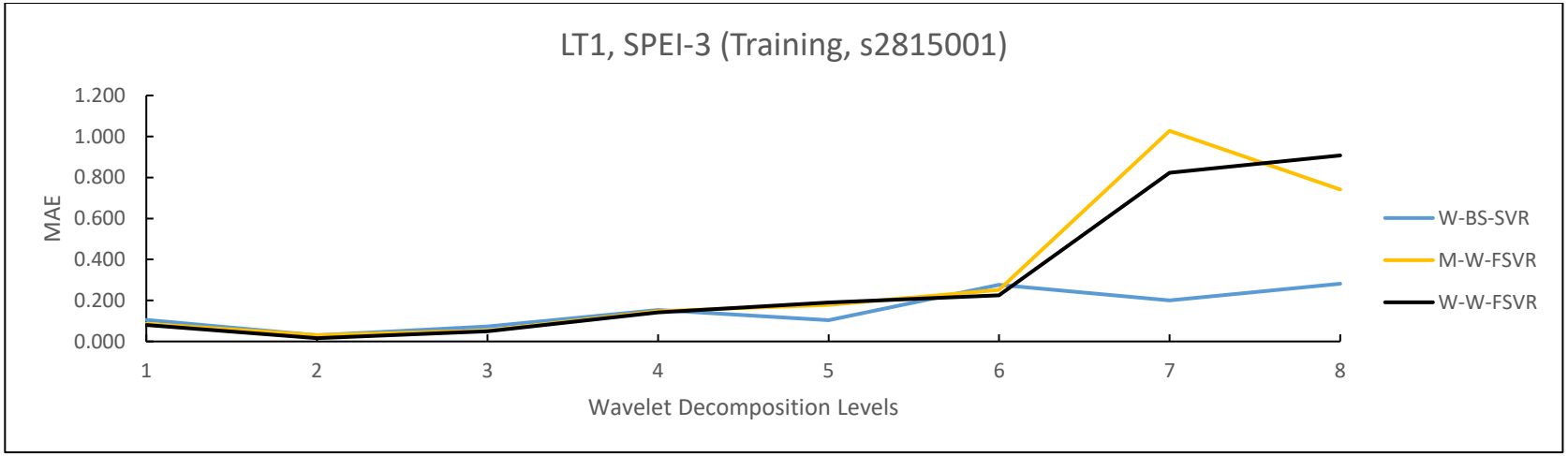
LT1, SPEI-3 (Training, s2815001)
MAE
1.200
1.000
0.800
0.600
0.400
0.200
0.000
1
2
3
4
5
6
7
8
Wavelet Decomposition Levels
W-BS-SVR
M-W-FSVR
W-W-FSVR

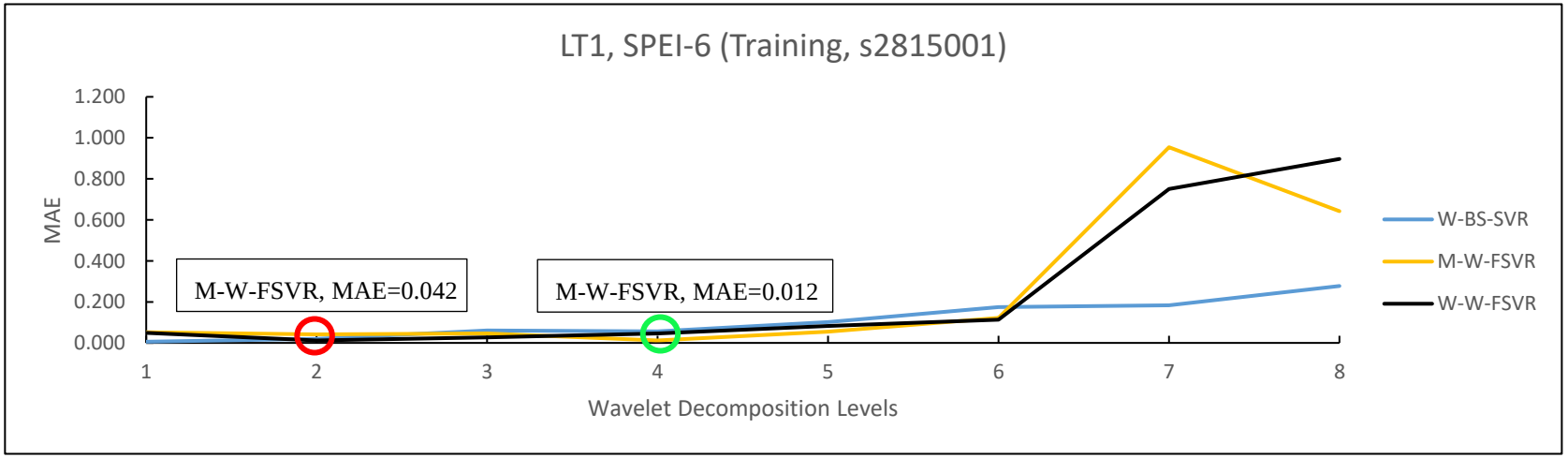
LT1, SPEI-6 (Training, s2815001)
MAE
1.200
1.000
0.800
0.600
0.400
0.200
0.000
M-W-FSVR, MAE=0.042
M-W-FSVR, MAE=0.012
1
2
3
4
5
6
7
8
Wavelet Decomposition Levels
W-BS-SVR
M-W-FSVR
W-W-FSVR

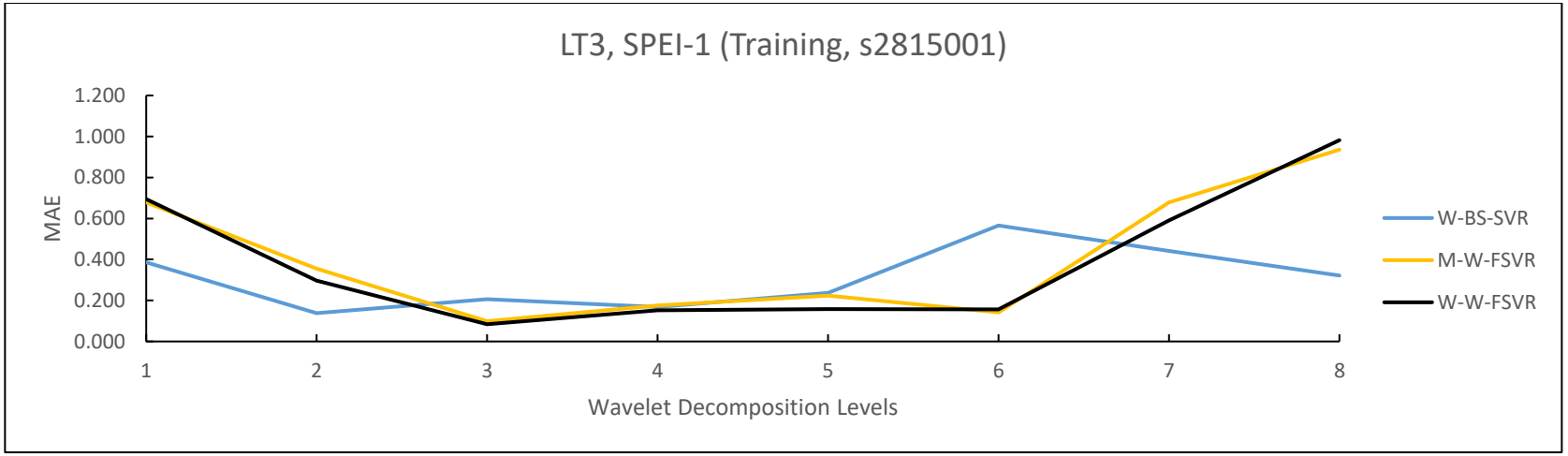
LT3, SPEI-1 (Training, s2815001)
MAE
1.200
1.000
0.800
0.600
0.400
0.200
0.000
1
2
3
4
5
6
7
8
Wavelet Decomposition Levels
W-BS-SVR
M-W-FSVR
W-W-FSVR

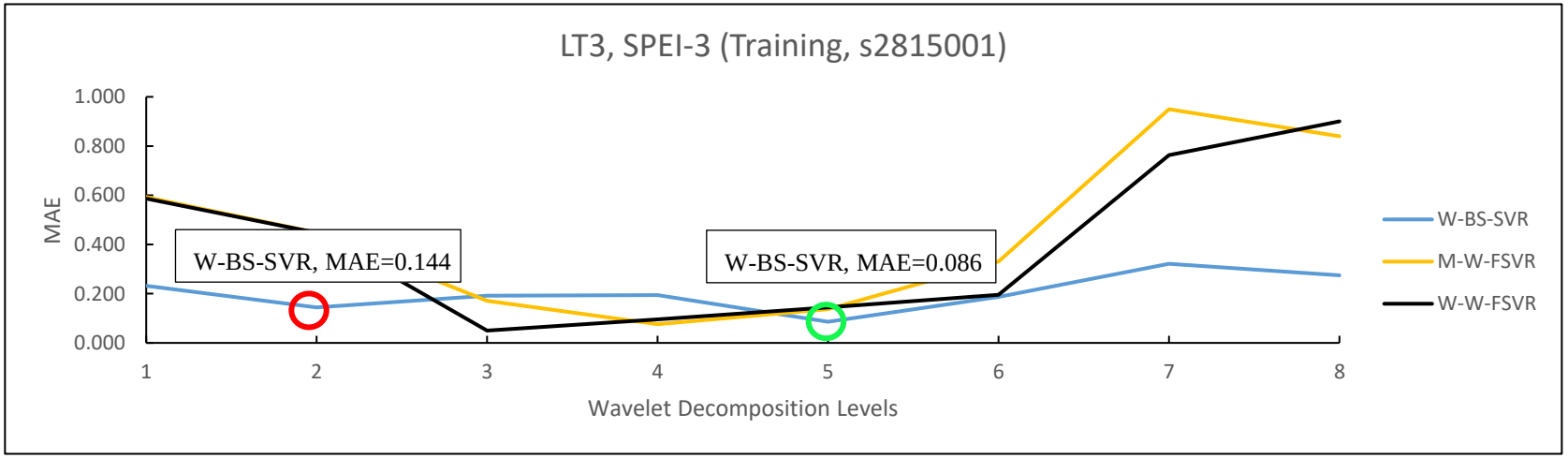
LT3, SPEI-3 (Training, s2815001)
MAE
1.000
0.800
0.600
0.400
0.200
0.000
W-BS-SVR, MAE=0.144
W-BS-SVR, MAE=0.086
1
2
3
4
5
6
7
8
Wavelet Decomposition Levels
W-BS-SVR
M-W-FSVR
W-W-FSVR

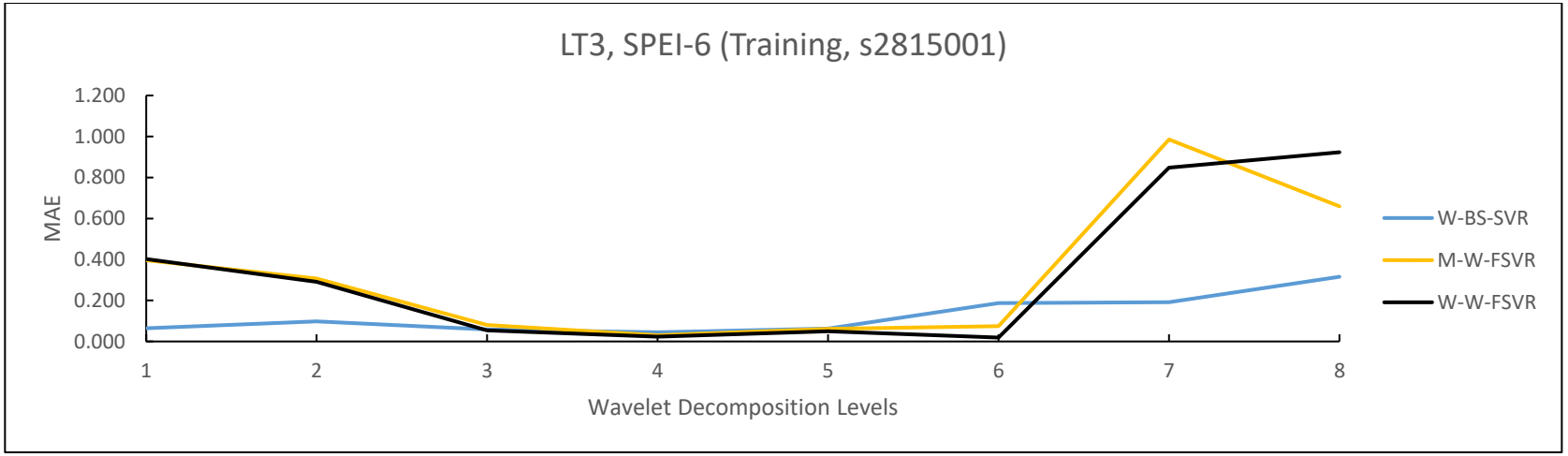
LT3, SPEI-6 (Training, s2815001)
MAE
1.200
1.000
0.800
0.600
0.400
0.200
0.000
1
2
3
4
5
6
7
8
Wavelet Decomposition Levels
W-BS-SVR
M-W-FSVR
W-W-FSVR

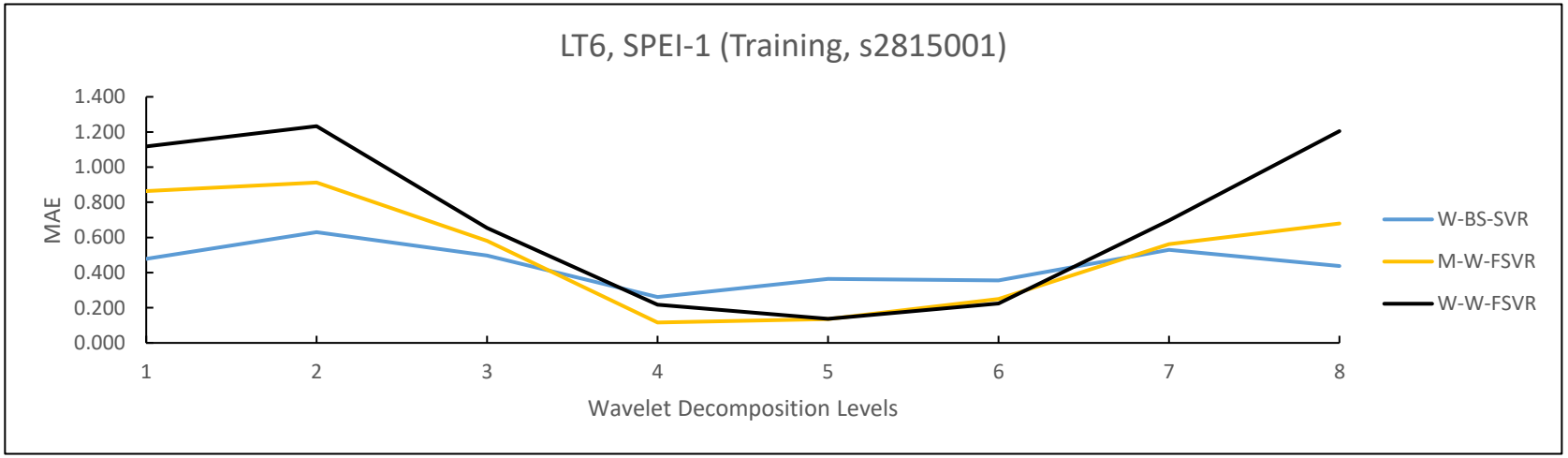
LT6, SPEI-1 (Training, s2815001)
MAE
1.400
1.200
1.000
0.800
0.600
0.400
0.200
0.000
1
2
3
4
5
6
7
8
Wavelet Decomposition Levels
W-BS-SVR
M-W-FSVR
W-W-FSVR

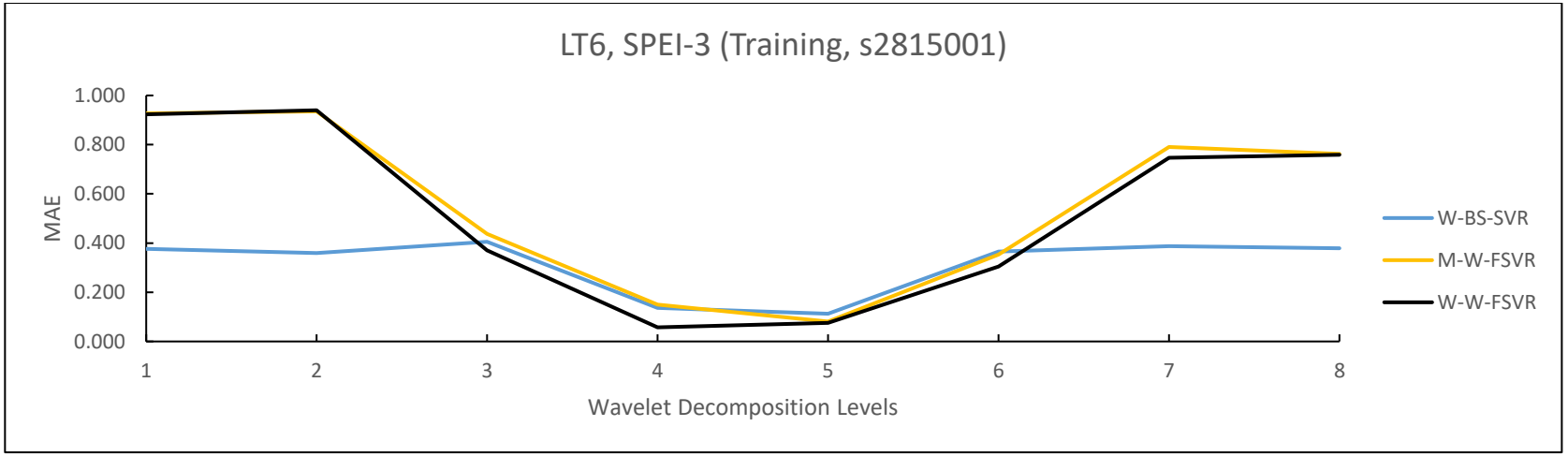
LT6, SPEI-3 (Training, s2815001)
MAE
1.000
0.800
0.600
0.400
0.200
0.000
1
2
3
4
5
6
7
8
Wavelet Decomposition Levels
W-BS-SVR
M-W-FSVR
W-W-FSVR

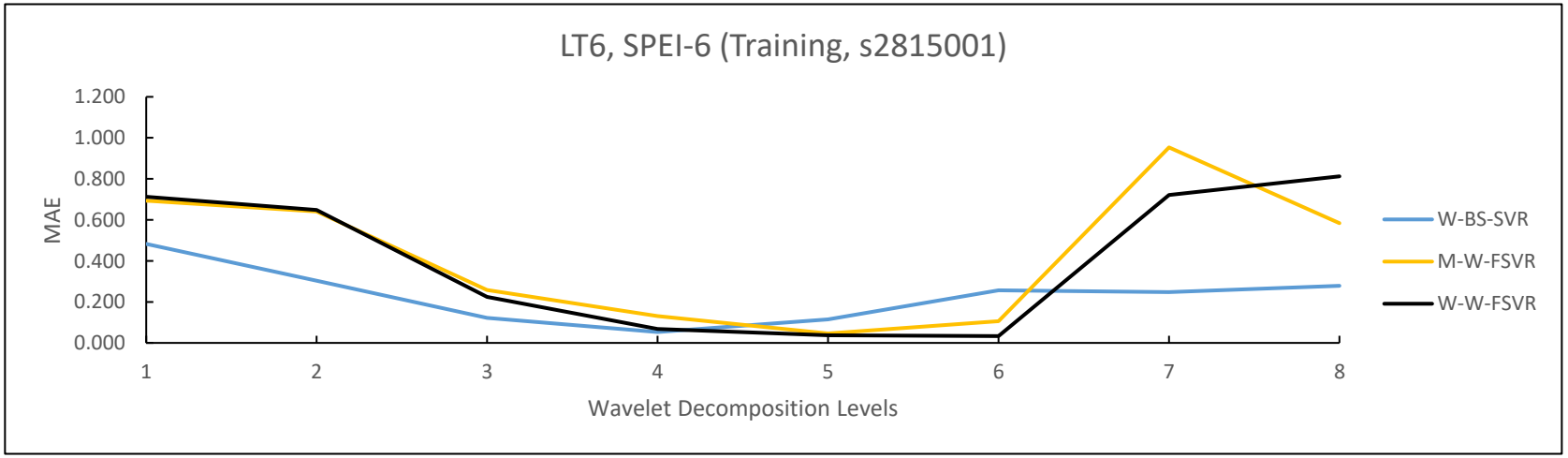
LT6, SPEI-6 (Training, s2815001)
MAE
1.200
1.000
0.800
0.600
0.400
0.200
0.000
1
2
3
4
5
6
7
8
Wavelet Decomposition Levels
W-BS-SVR
M-W-FSVR
W-W-FSVR

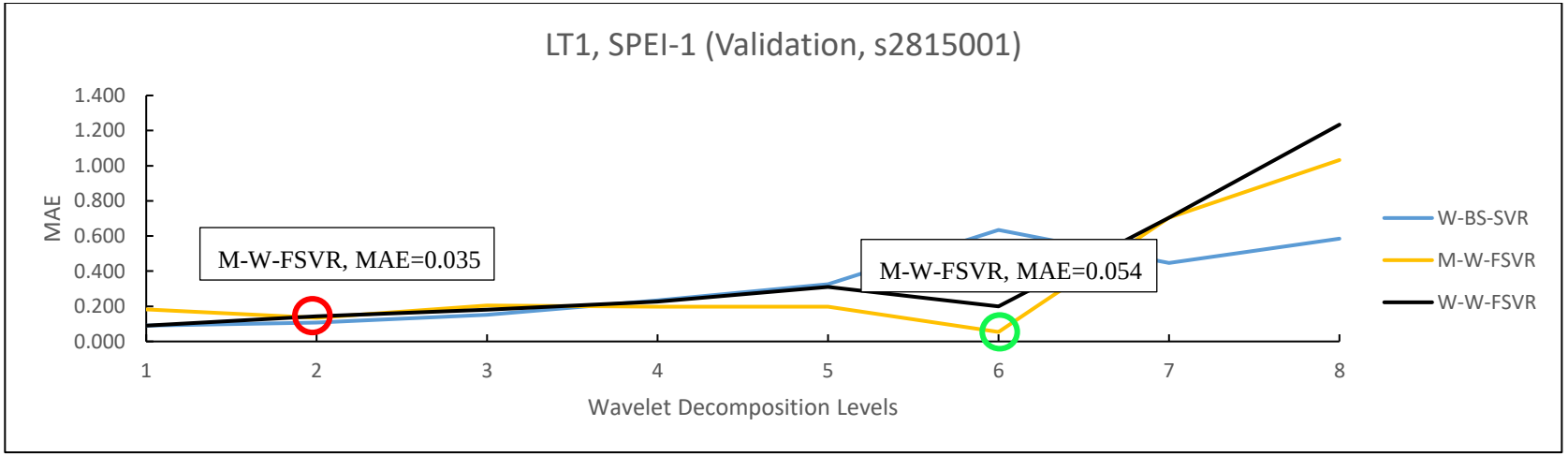
LT1, SPEI-1 (Validation, s2815001)
MAE
1.400
1.200
1.000
0.800
0.600
0.400
0.200
0.000
M-W-FSVR, MAE=0.035
M-W-FSVR, MAE=0.054
1
2
3
4
5
6
7
8
Wavelet Decomposition Levels
W-BS-SVR
M-W-FSVR
W-W-FSVR

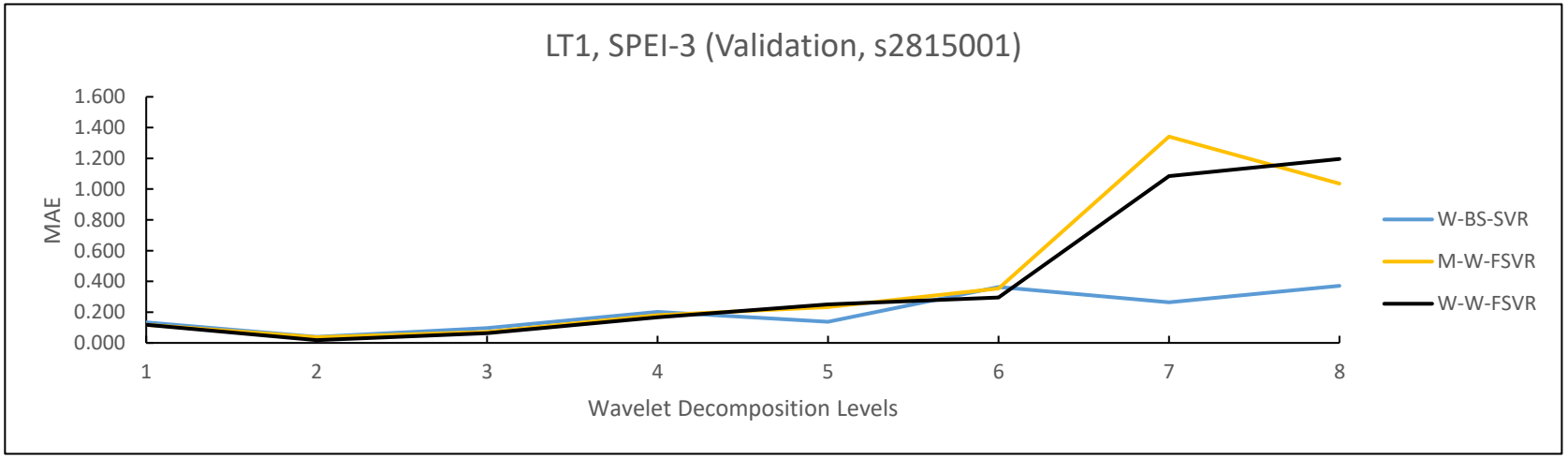
LT1, SPEI-3 (Validation, s2815001)
MAE
1.600
1.400
1.200
1.000
0.800
0.600
0.400
0.200
0.000
1
2
3
4
5
6
7
8
Wavelet Decomposition Levels
W-BS-SVR
M-W-FSVR
W-W-FSVR

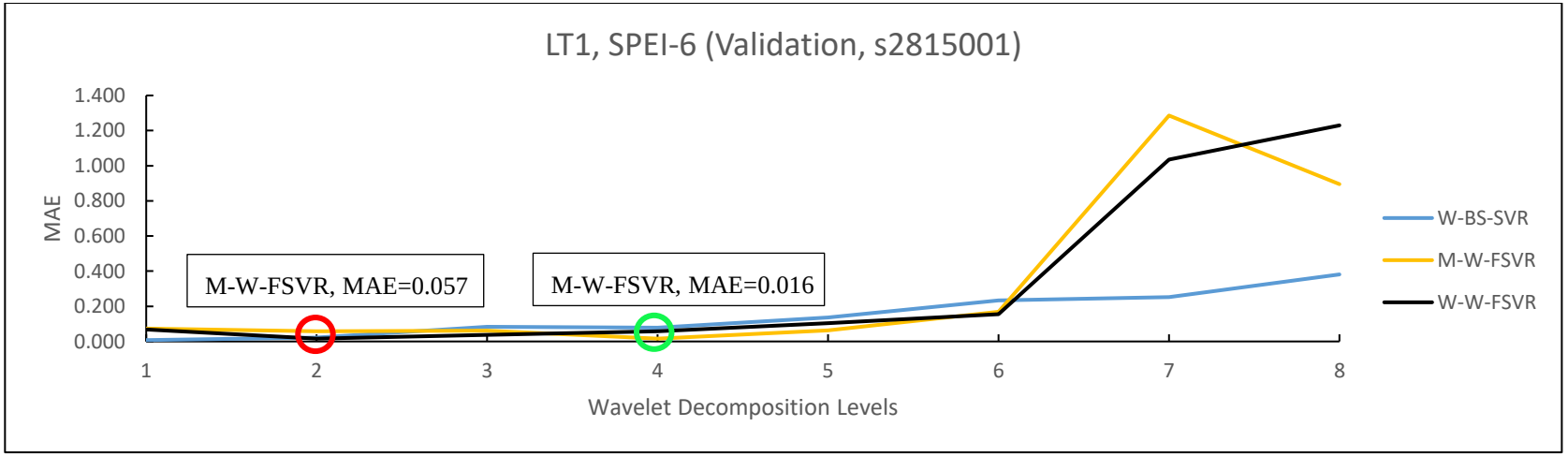
LT1, SPEI-6 (Validation, s2815001)
MAE
1.400
1.200
1.000
0.800
0.600
0.400
0.200
0.000
M-W-FSVR, MAE=0.057
M-W-FSVR, MAE=0.016
1
2
3
4
5
6
7
8
Wavelet Decomposition Levels
W-BS-SVR
M-W-FSVR
W-W-FSVR

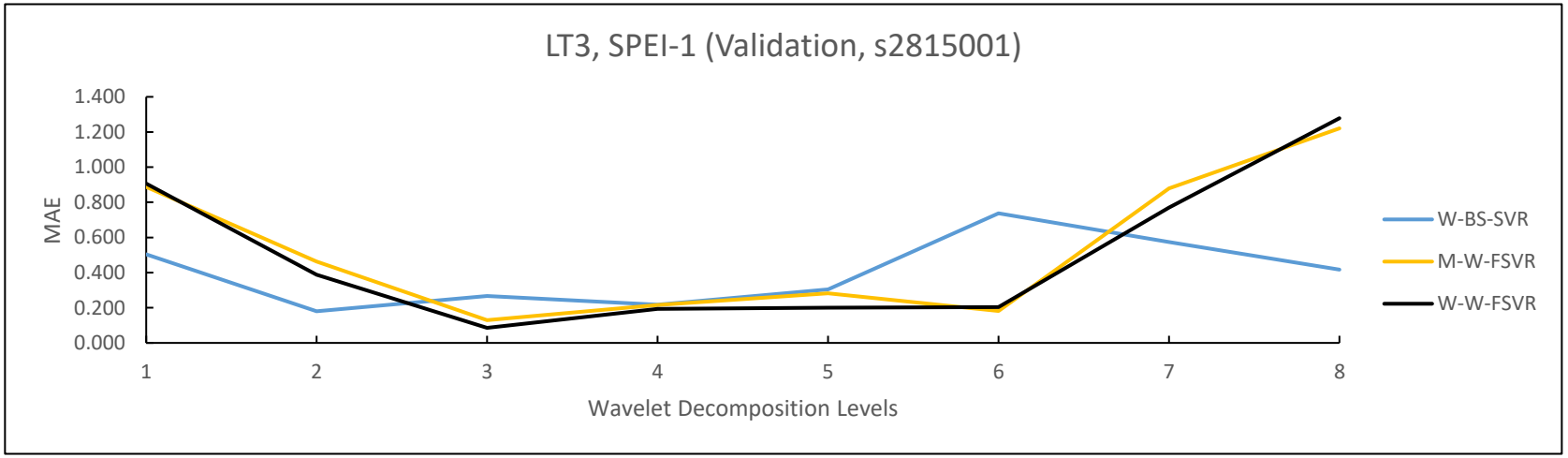
LT3, SPEI-1 (Validation, s2815001)
MAE
1.400
1.200
1.000
0.800
0.600
0.400
0.200
0.000
1
2
3
4
5
6
7
8
Wavelet Decomposition Levels
W-BS-SVR
M-W-FSVR
W-W-FSVR

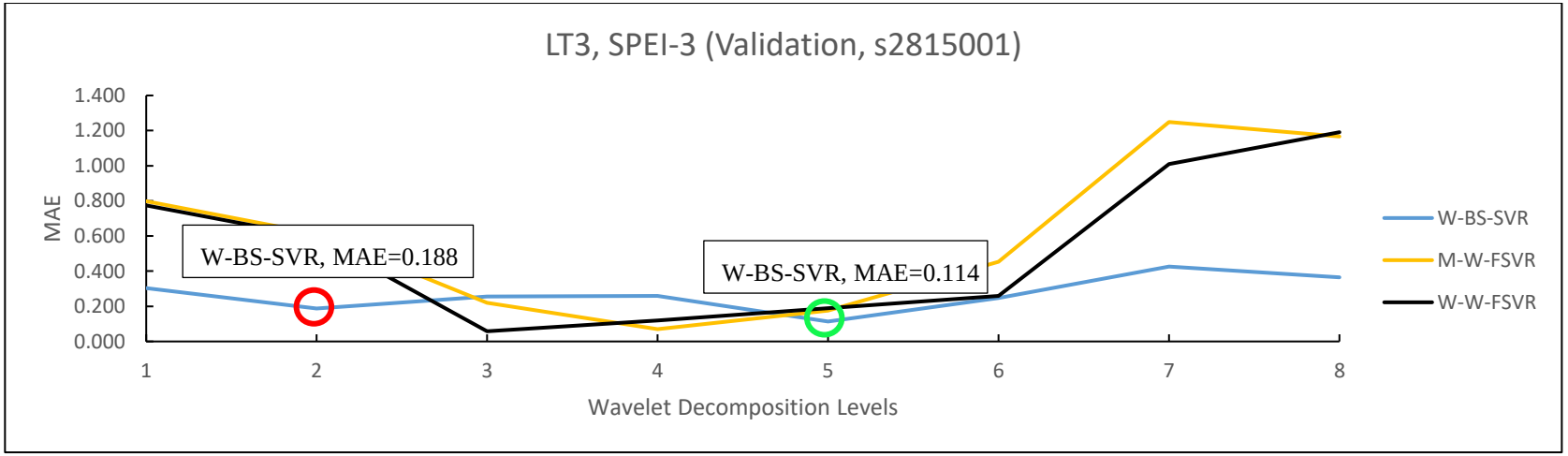
LT3, SPEI-3 (Validation, s2815001)
MAE
1.400
1.200
1.000
0.800
0.600
0.400
0.200
0.000
1
2
3
4
5
6
7
8
Wavelet Decomposition Levels
W-BS-SVR, MAE=0.188
W-BS-SVR, MAE=0.114
W-BS-SVR
M-W-FSVR
W-W-FSVR

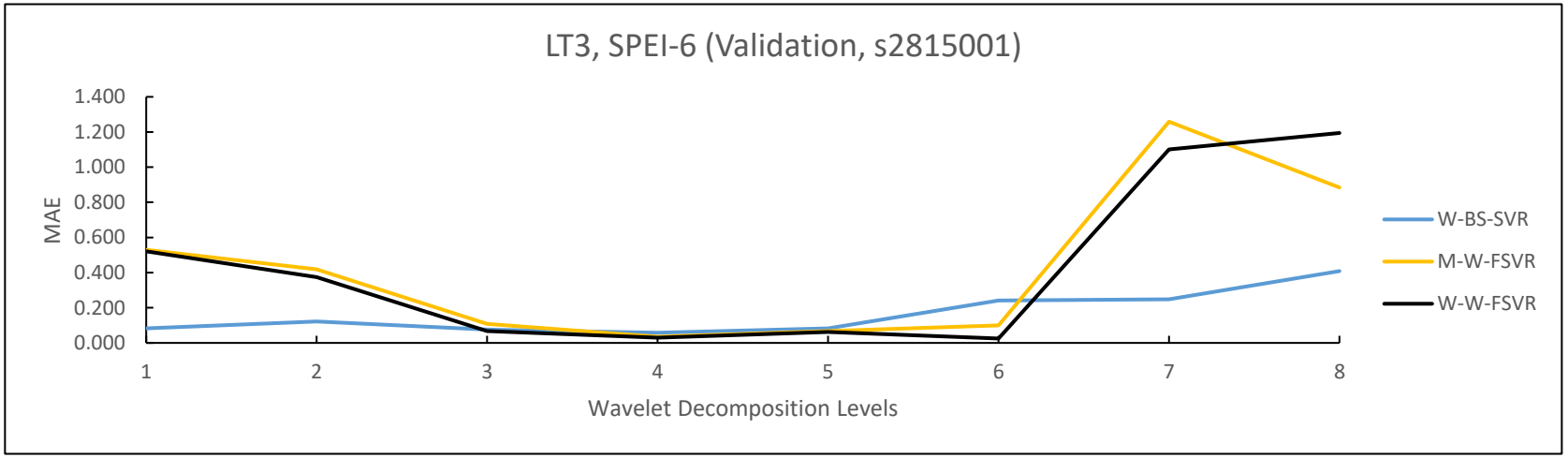
LT3, SPEI-6 (Validation, s2815001)
MAE
1.400
1.200
1.000
0.800
0.600
0.400
0.200
0.000
1
2
3
4
5
6
7
8
Wavelet Decomposition Levels
W-BS-SVR
M-W-FSVR
W-W-FSVR

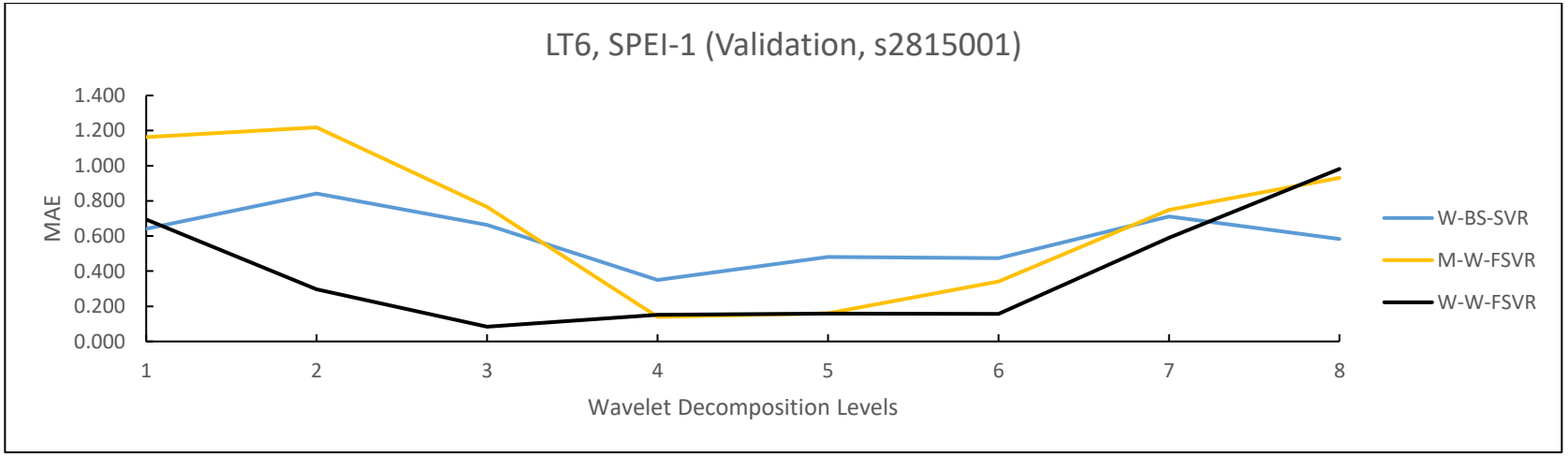
LT6, SPEI-1 (Validation, s2815001)
MAE
1.400
1.200
1.000
0.800
0.600
0.400
0.200
0.000
1
2
3
4
5
6
7
8
Wavelet Decomposition Levels
W-BS-SVR
M-W-FSVR
W-W-FSVR

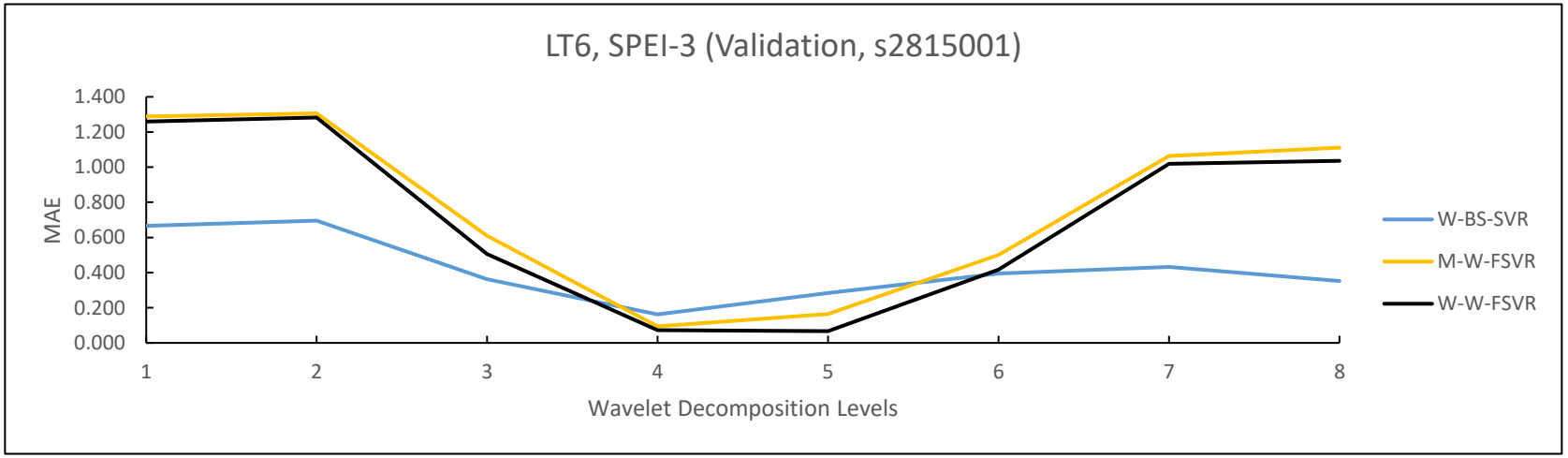
LT6, SPEI-3 (Validation, s2815001)
MAE
1.400
1.200
1.000
0.800
0.600
0.400
0.200
0.000
1
2
3
4
5
6
7
8
Wavelet Decomposition Levels
W-BS-SVR
M-W-FSVR
W-W-FSVR

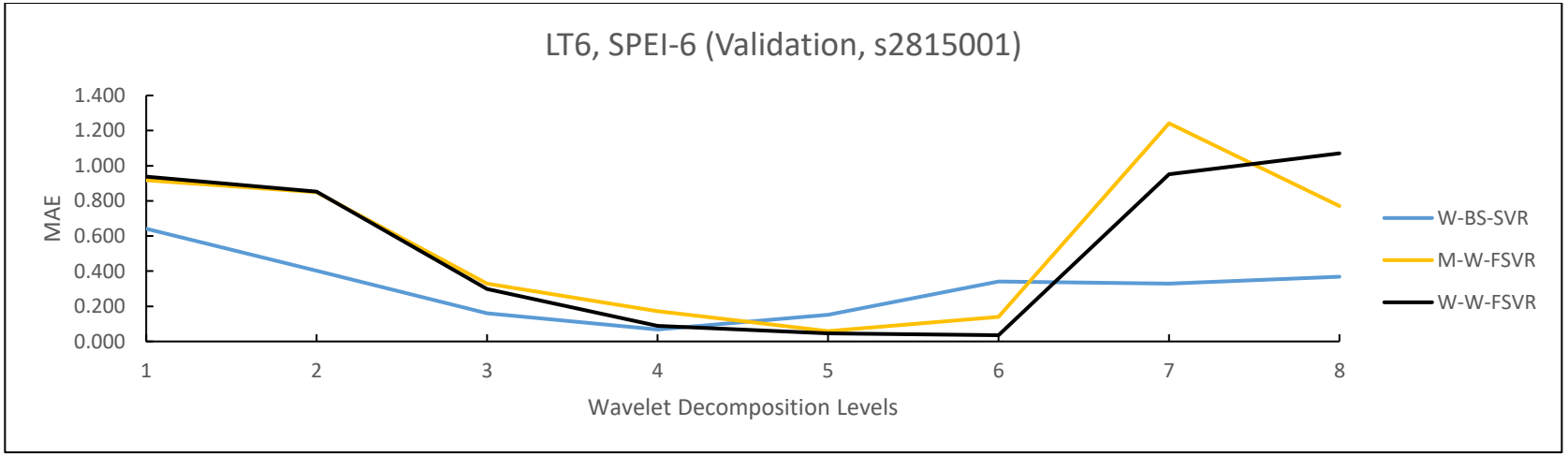
LT6, SPEI-6 (Validation, s2815001)
MAE
1.400
1.200
1.000
0.800
0.600
0.400
0.200
0.000
1
2
3
4
5
6
7
8
Wavelet Decomposition Levels
W-BS-SVR
M-W-FSVR
W-W-FSVR

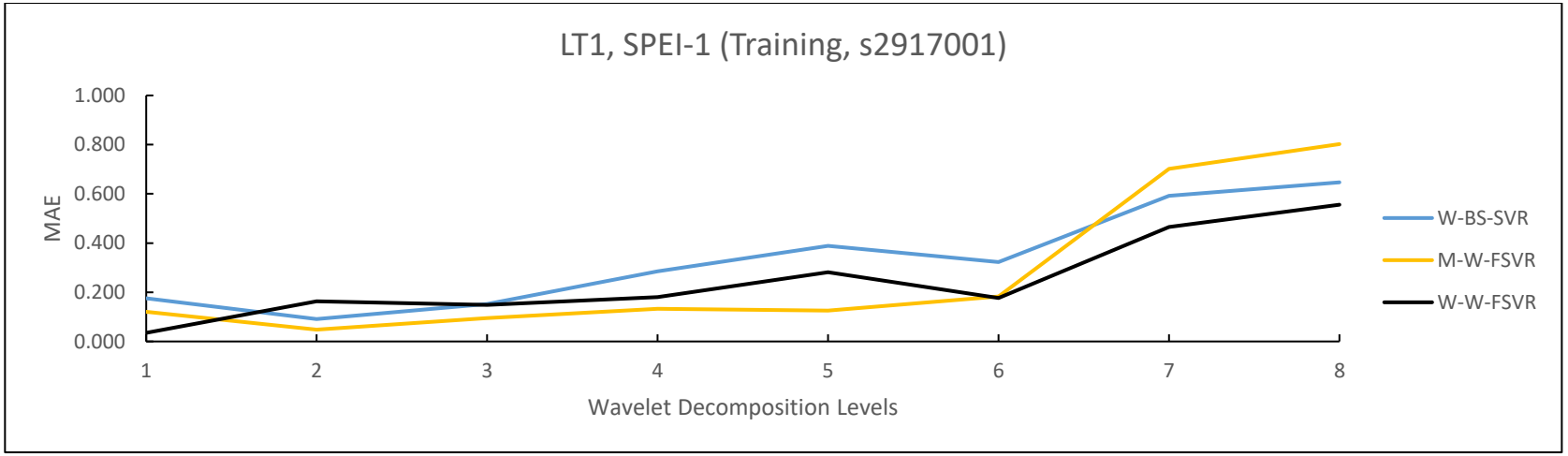
LT1, SPEI-1 (Training, s2917001)
MAE
1.000
0.800
0.600
0.400
0.200
0.000
1
2
3
4
5
6
7
8
Wavelet Decomposition Levels
W-BS-SVR
M-W-FSVR
W-W-FSVR

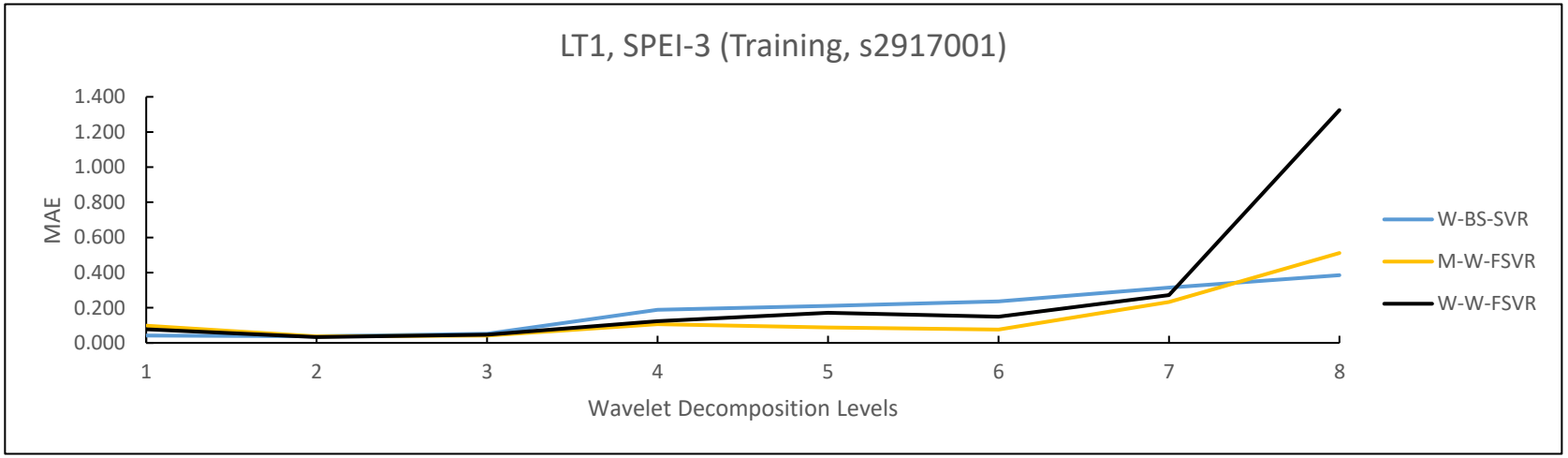
LT1, SPEI-3 (Training, s2917001)
MAE
1.400
1.200
1.000
0.800
0.600
0.400
0.200
0.000
1
2
3
4
5
6
7
8
Wavelet Decomposition Levels
W-BS-SVR
M-W-FSVR
W-W-FSVR

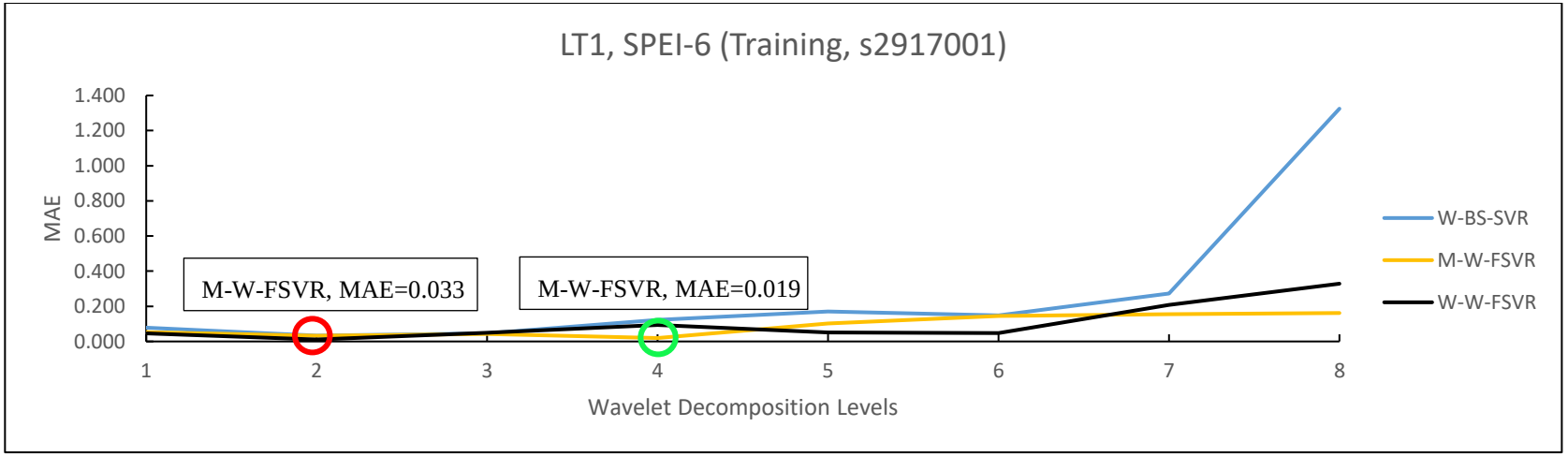
LT1, SPEI-6 (Training, s2917001)
MAE
1.400
1.200
1.000
0.800
0.600
0.400
0.200
0.000
1
2
3
4
5
6
7
8
Wavelet Decomposition Levels
M-W-FSVR, MAE=0.033
M-W-FSVR, MAE=0.019
W-BS-SVR
M-W-FSVR
W-W-FSVR

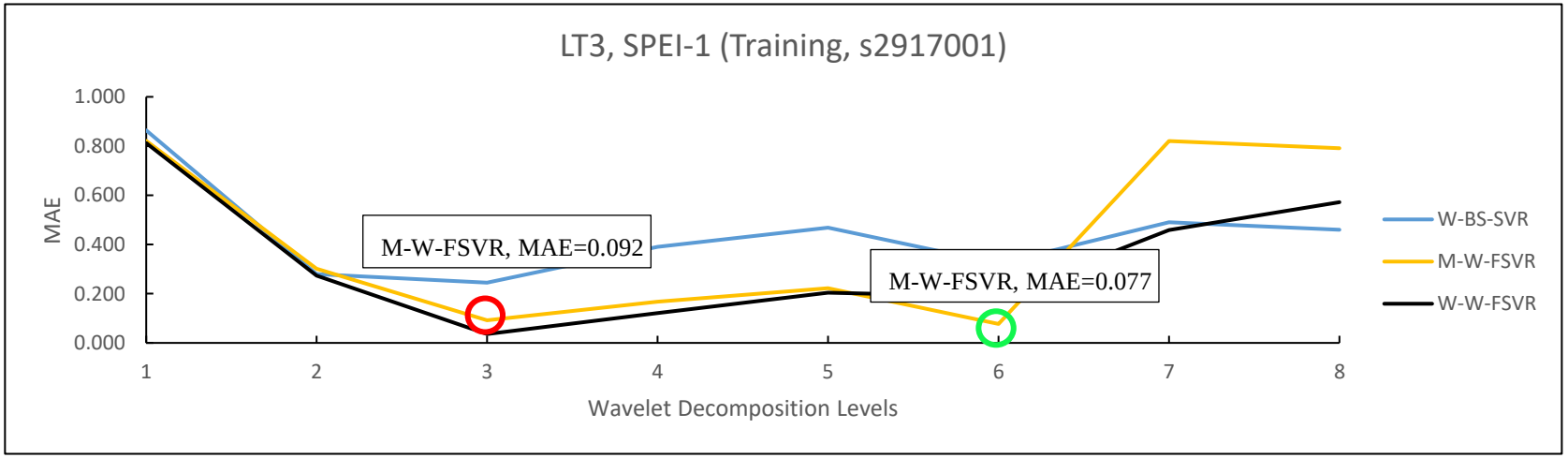
LT3, SPEI-1 (Training, s2917001)
MAE
1.000
0.800
0.600
0.400
0.200
0.000
1
2
3
4
5
6
7
8
Wavelet Decomposition Levels
M-W-FSVR, MAE=0.092
M-W-FSVR, MAE=0.077
W-BS-SVR
M-W-FSVR
W-W-FSVR

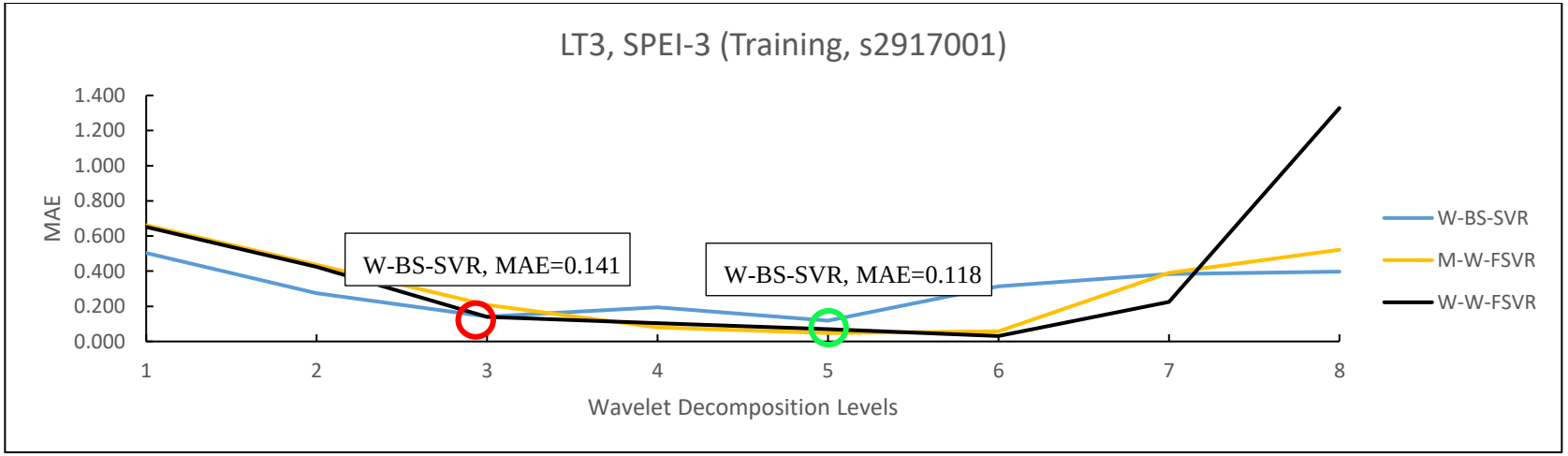
LT3, SPEI-3 (Training, s2917001)
MAE
1.400
1.200
1.000
0.800
0.600
0.400
0.200
0.000
W-BS-SVR, MAE=0.141
W-BS-SVR, MAE=0.118
1
2
3
4
5
6
7
8
Wavelet Decomposition Levels
W-BS-SVR
M-W-FSVR
W-W-FSVR

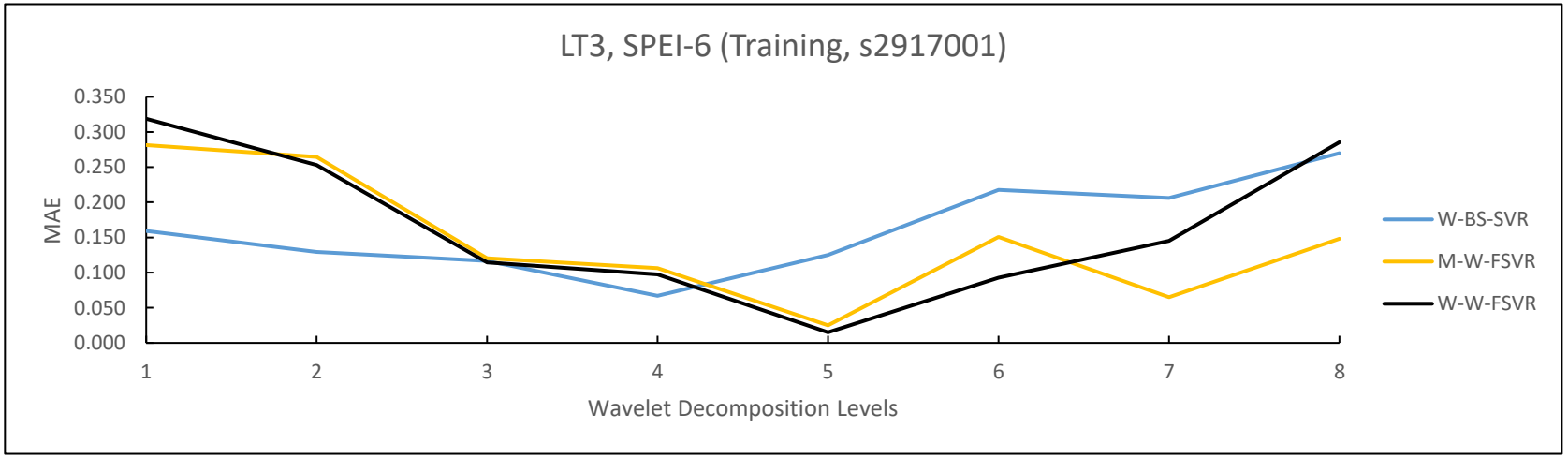
LT3, SPEI-6 (Training, s2917001)
MAE
0.350
0.300
0.250
0.200
0.150
0.100
0.050
0.000
1
2
3
4
5
6
7
8
Wavelet Decomposition Levels
W-BS-SVR
M-W-FSVR
W-W-FSVR

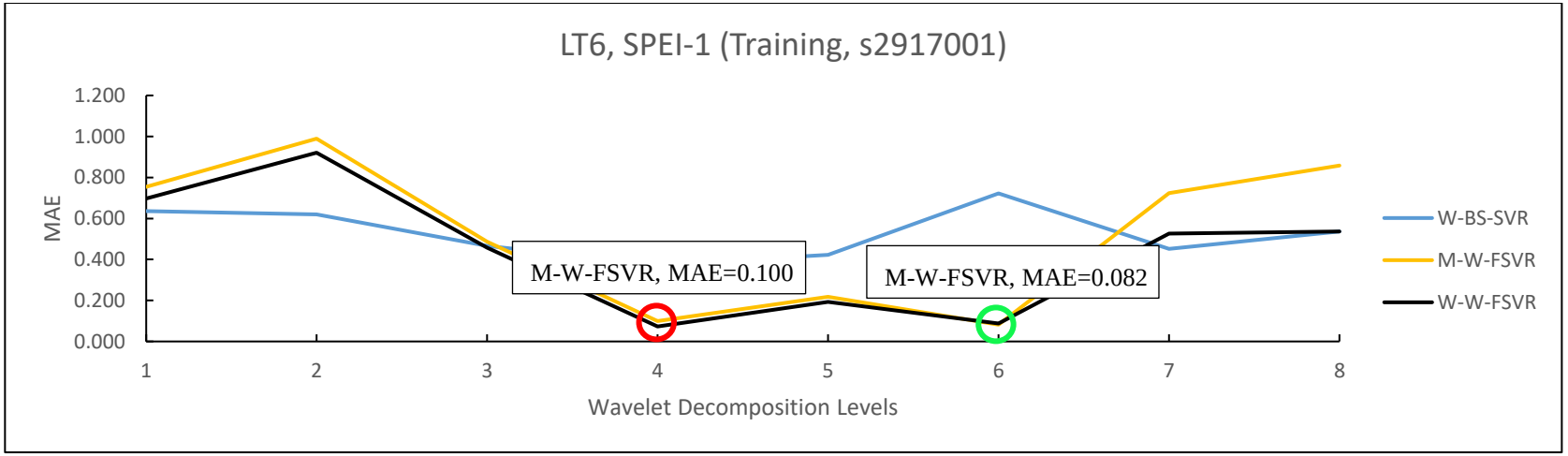
LT6, SPEI-1 (Training, s2917001)
MAE
1.200
1.000
0.800
0.600
0.400
0.200
0.000
1
2
3
4
5
6
7
8
Wavelet Decomposition Levels
M-W-FSVR, MAE=0.100
M-W-FSVR, MAE=0.082
W-BS-SVR
M-W-FSVR
W-W-FSVR

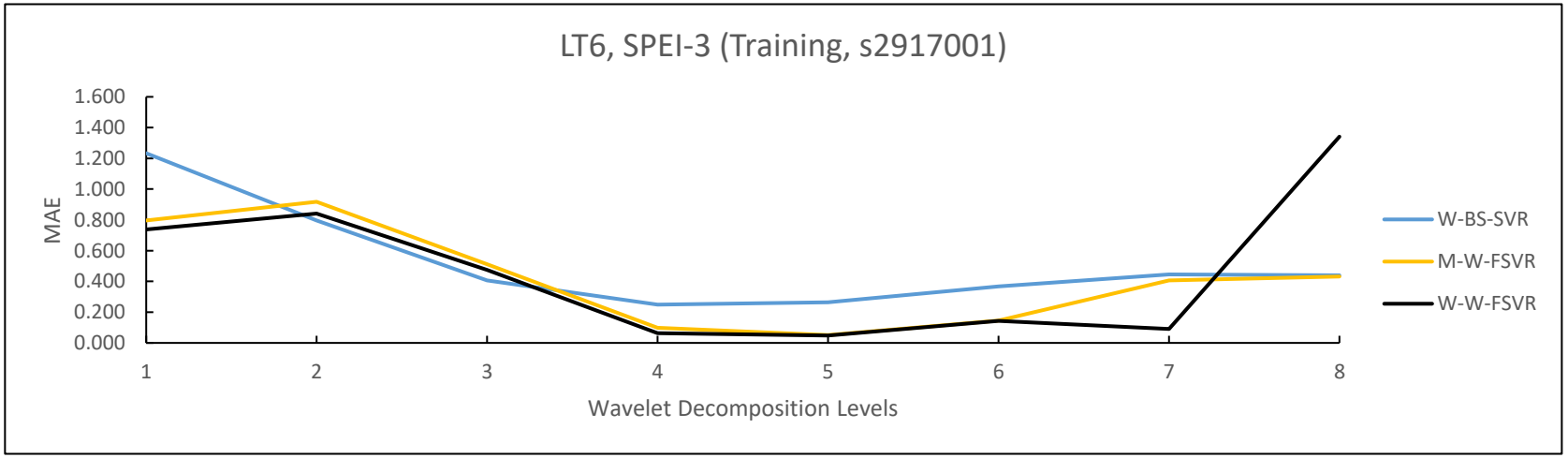
LT6, SPEI-3 (Training, s2917001)
MAE
1.600
1.400
1.200
1.000
0.800
0.600
0.400
0.200
0.000
1
2
3
4
5
6
7
8
Wavelet Decomposition Levels
W-BS-SVR
M-W-FSVR
W-W-FSVR

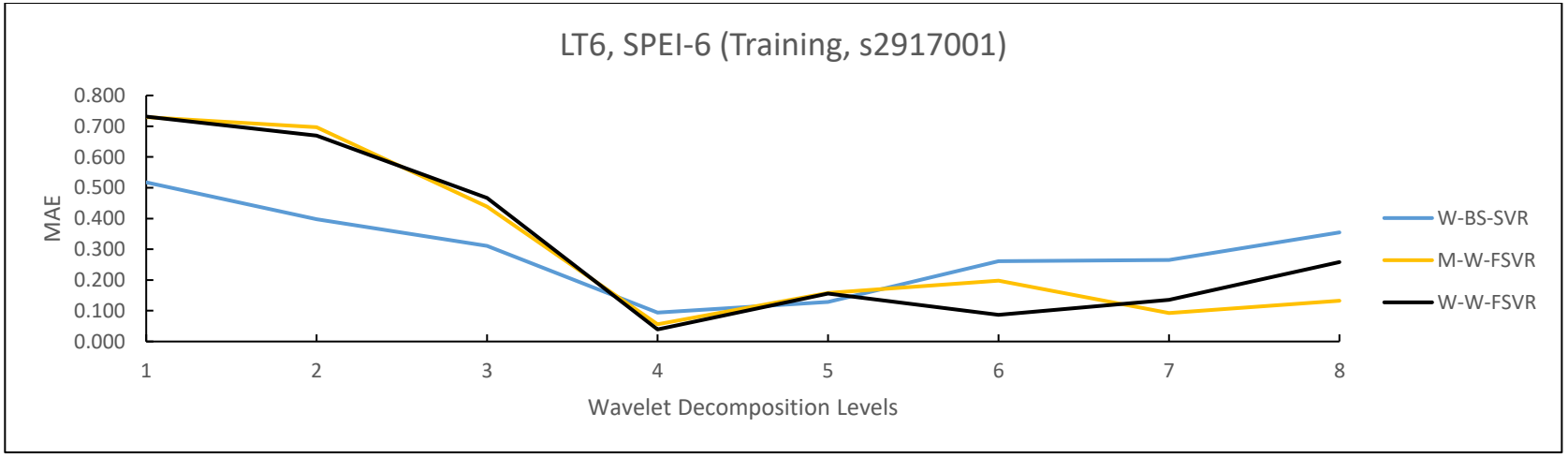
LT6, SPEI-6 (Training, s2917001)
MAE
0.800
0.700
0.600
0.500
0.400
0.300
0.200
0.100
0.000
1
2
3
4
5
6
7
8
Wavelet Decomposition Levels
W-BS-SVR
M-W-FSVR
W-W-FSVR

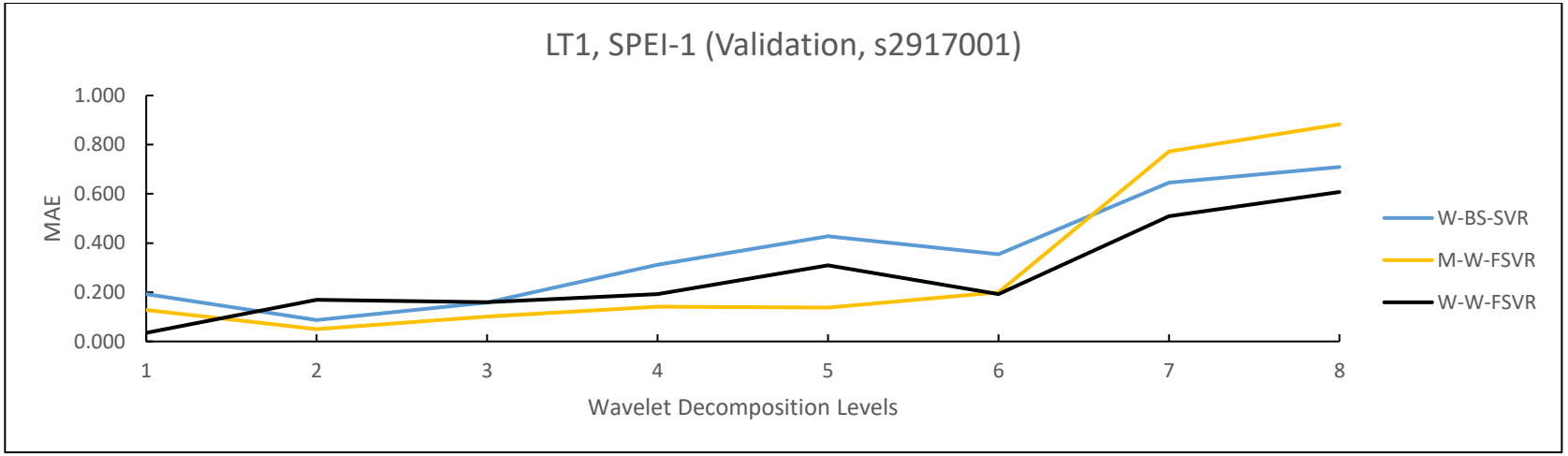
LT1, SPEI-1 (Validation, s2917001)
MAE
1.000
0.800
0.600
0.400
0.200
0.000
1
2
3
4
5
6
7
8
Wavelet Decomposition Levels
W-BS-SVR
M-W-FSVR
W-W-FSVR

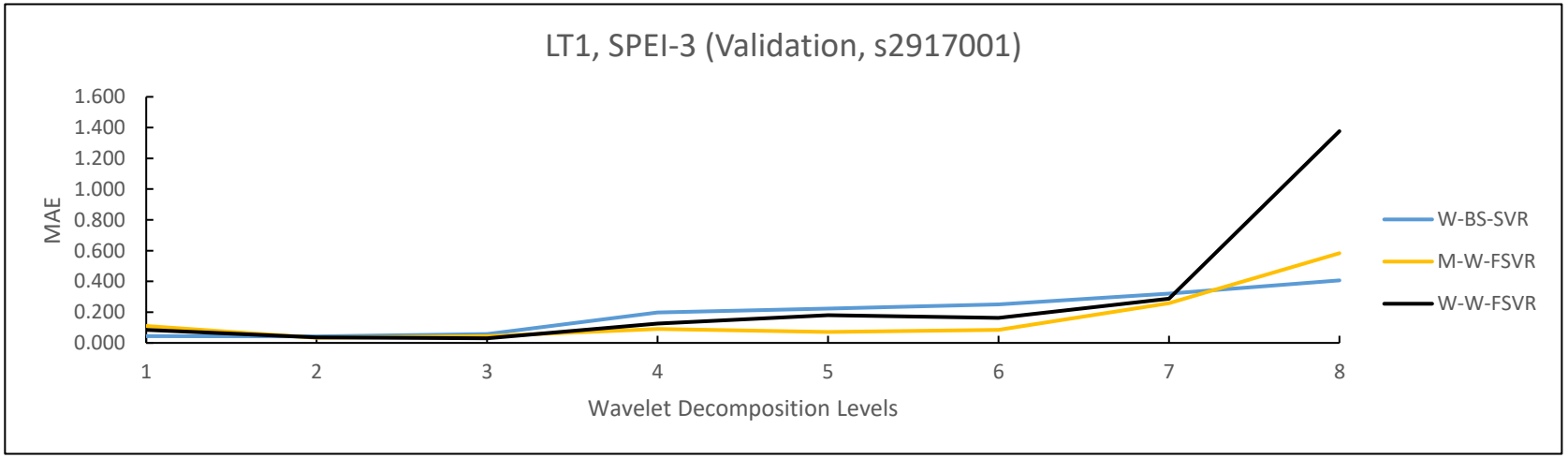
LT1, SPEI-3 (Validation, s2917001)
MAE
1.600
1.400
1.200
1.000
0.800
0.600
0.400
0.200
0.000
1
2
3
4
5
6
7
8
Wavelet Decomposition Levels
W-BS-SVR
M-W-FSVR
W-W-FSVR

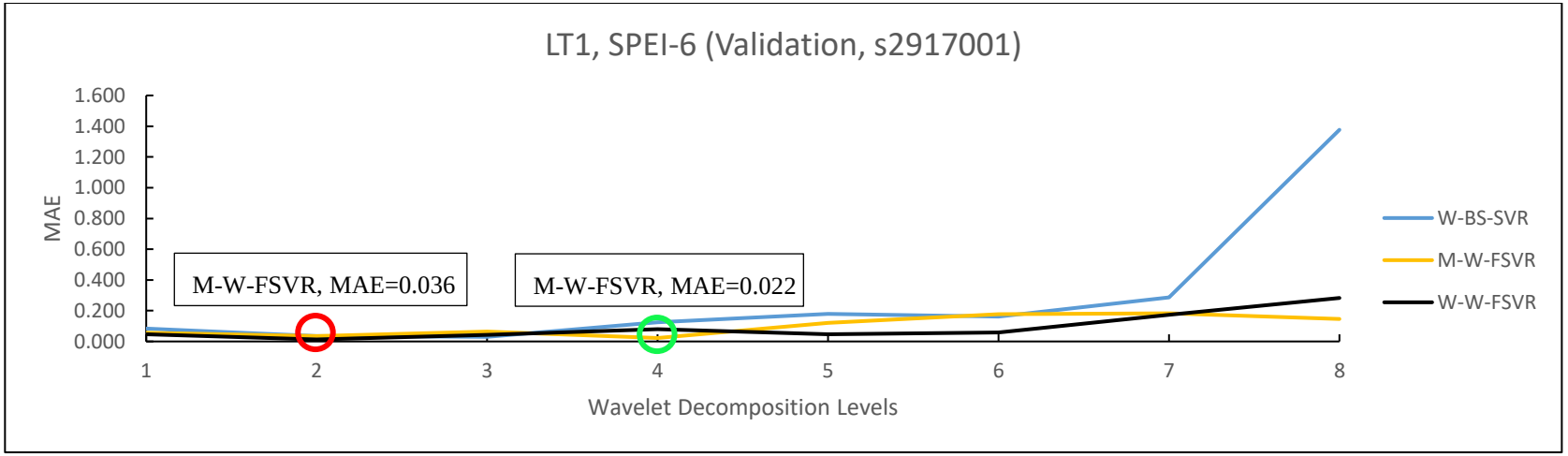
LT1, SPEI-6 (Validation, s2917001)
MAE
1.600
1.400
1.200
1.000
0.800
0.600
0.400
0.200
0.000
M-W-FSVR, MAE=0.036
M-W-FSVR, MAE=0.022
1
2
3
4
5
6
7
8
Wavelet Decomposition Levels
W-BS-SVR
M-W-FSVR
W-W-FSVR

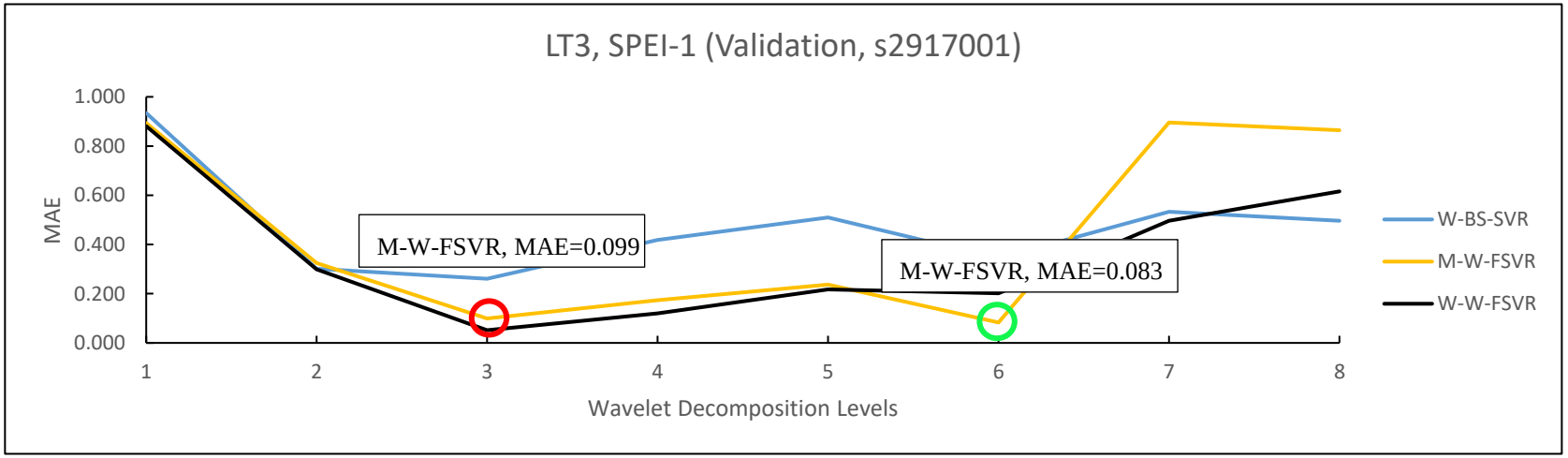
LT3, SPEI-1 (Validation, s2917001)
MAE
1.000
0.800
0.600
0.400
0.200
0.000
M-W-FSVR, MAE=0.099
M-W-FSVR, MAE=0.083
1
2
3
4
5
6
7
8
Wavelet Decomposition Levels
W-BS-SVR
M-W-FSVR
W-W-FSVR

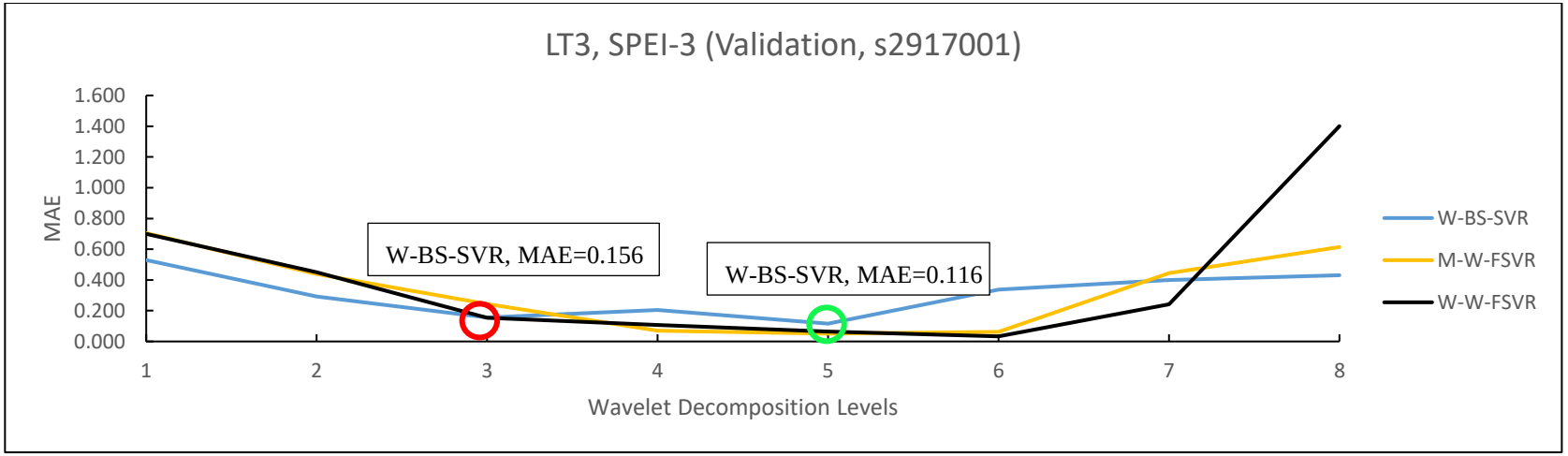
LT3, SPEI-3 (Validation, s2917001)
MAE
1.600
1.400
1.200
1.000
0.800
0.600
0.400
0.200
0.000
W-BS-SVR, MAE=0.156
W-BS-SVR, MAE=0.116
1
2
3
4
5
6
7
8
Wavelet Decomposition Levels
W-BS-SVR
M-W-FSVR
W-W-FSVR

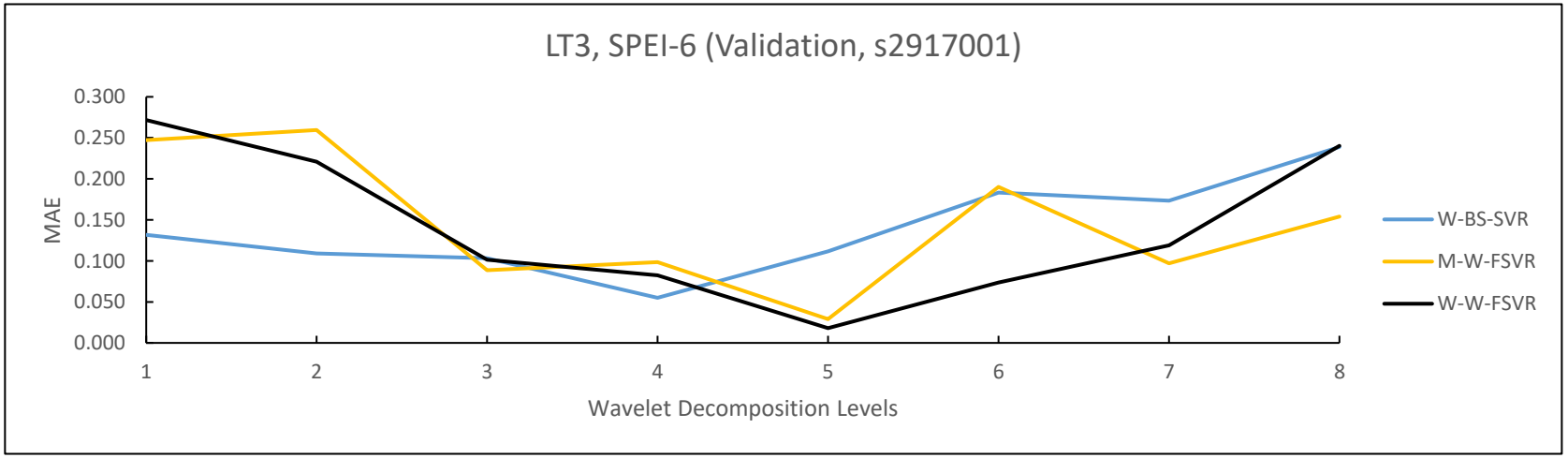
LT3, SPEI-6 (Validation, s2917001)
MAE
0.300
0.250
0.200
0.150
0.100
0.050
0.000
1
2
3
4
5
6
7
8
Wavelet Decomposition Levels
W-BS-SVR
M-W-FSVR
W-W-FSVR

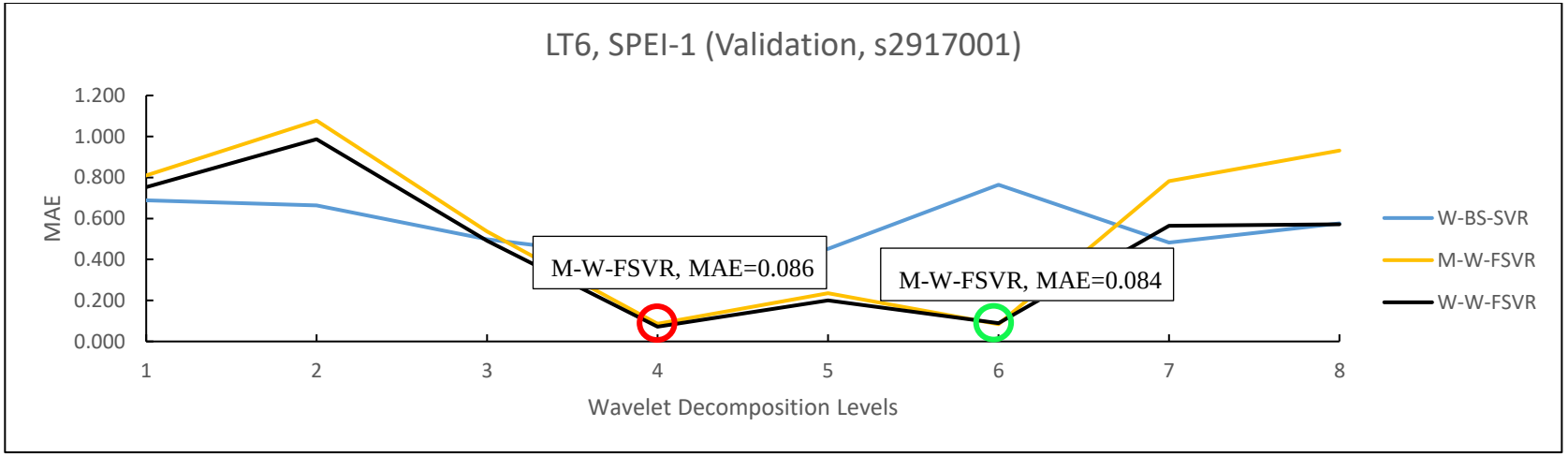
LT6, SPEI-1 (Validation, s2917001)
MAE
1.200
1.000
0.800
0.600
0.400
0.200
0.000
1
2
3
4
5
6
7
8
Wavelet Decomposition Levels
M-W-FSVR, MAE=0.086
M-W-FSVR, MAE=0.084
W-BS-SVR
M-W-FSVR
W-W-FSVR

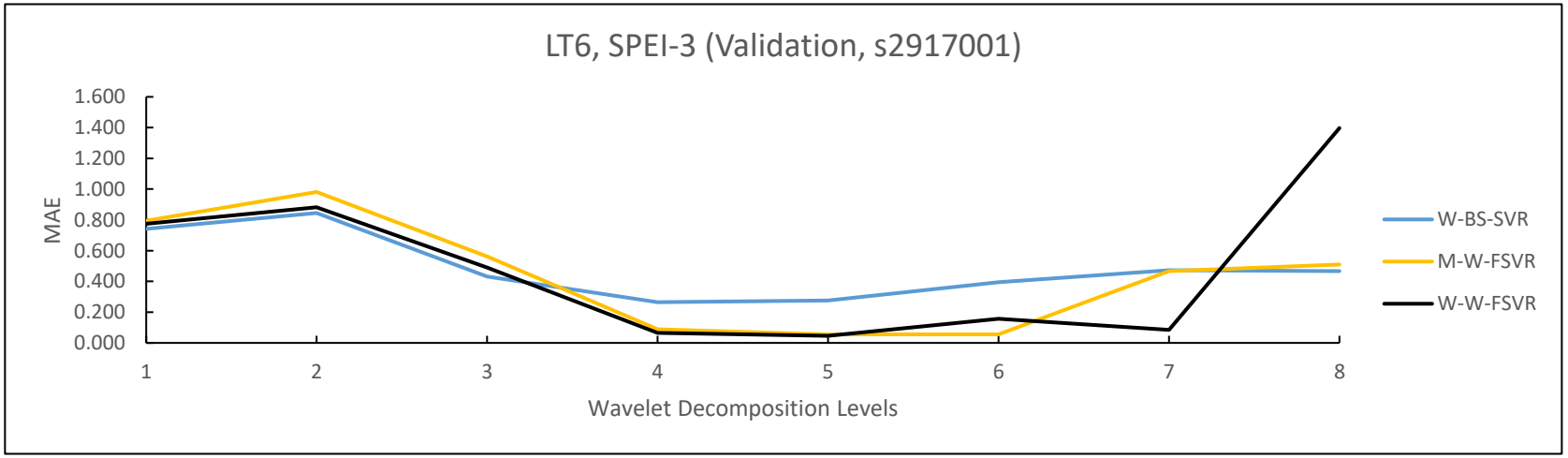
LT6, SPEI-3 (Validation, s2917001)
MAE
1.600
1.400
1.200
1.000
0.800
0.600
0.400
0.200
0.000
1
2
3
4
5
6
7
8
Wavelet Decomposition Levels
W-BS-SVR
M-W-FSVR
W-W-FSVR

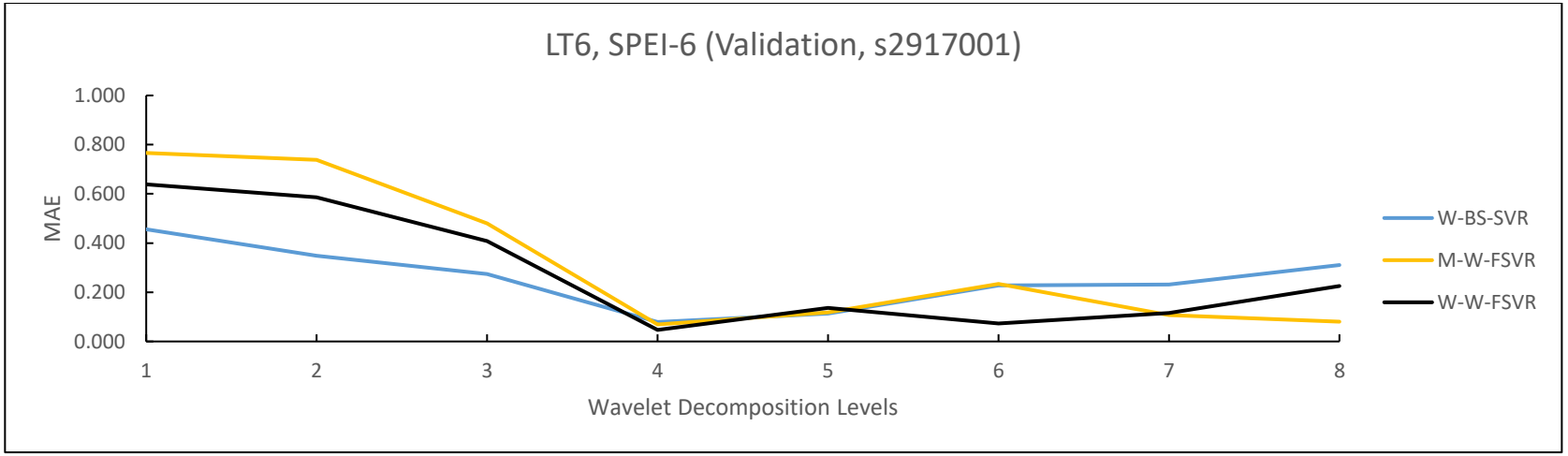
LT6, SPEI-6 (Validation, s2917001)
1.000
0.800
0.600
0.400
0.200
0.000
MAE
1
2
3
4
5
6
7
8
Wavelet Decomposition Levels
W-BS-SVR
M-W-FSVR
W-W-FSVR

APPENDIX E

List of Publications

1. Fung, K.F., Huang, Y.F. and Koo, C.H., 2018. Drought Prediction Using W-SVR and W-BS-SVR for Langat River Basin. *Arabian Journal of Geosciences.* (Manuscript Accepted)

2. Fung, K.F., Huang, Y.F. and Koo, C.H., 2018. SVR-based Machine Learning Approaches for Drought Prediction: Case Study of the Langat River Basin, Malaysia. *Natural Hazards.* (Under Review)

3. Fung, K.F., Huang, Y.F., Koo, C.H. and Soh, Y.W., 2018. Drought Forecasting: A Review of Modeling Approaches 2007 – 2017. *Journal of Water and Climate Change.* (Submitted)